DEVELOPMENT OF AGGREGATION-INDUCED EMISSION PHOTOSENSITIZERS AS ANTIPLANKTONIC AND ANTIBIOFILM AGENTS

HUNG CHEUNG HIN

PhD

The Hong Kong Polytechnic University

2025

The Hong Kong Polytechnic University

Department of Applied Biology and Chemical Technology

Development of Aggregation-Induced Emission Photosensitizers as Antiplanktonic and Antibiofilm Agents

Hung Cheung Hin

A thesis submitted in partial fulfilment of the requirements for the degree of Doctor of Philosophy

June 2025

Certificate of Originality

I hereby declare that this thesis is my own work and that, to the best of my knowledge and belief, it reproduces no material previously published or written, nor material that has been accepted for the award of any other degree or diploma, except where due acknowledgement has been made in the text.

Signature:

Name of Student: Hung Cheung Hin

Abstract

Bacterial infection has always been a clinical challenge to humans. One of the biggest challenges is that bacteria can encase in self-produced extracellular polymeric substances (EPS) to form biofilms. Bacteria encased in biofilms are difficult to kill due to their tolerance to high concentrations of antibiotics that can normally kill planktonic bacteria. With the emergence of antimicrobial resistance (AMR), traditional antibiotics are losing their effectiveness in treating bacterial infections. To cope with this situation, alternative antibacterial strategies, including photodynamic therapy (PDT), have been developed. PDT utilizes a photosensitizer (PS) to generate reactive oxygen species (ROS) under light irradiation. These ROS can damage essential biological components in bacteria without generating AMR. Recently, aggregation-induced emission (AIE) PSs have gained popularity for antibacterial PDT because of their ability to prevent aggregation-caused quenching (ACQ) and enhance ROS generation upon target binding. Despite significant efforts invested over the last decade, AIE PSs with both good antibiofilm activity and biocompatibility remain rare.

In this thesis, novel AIE PSs have been developed for antiplanktonic and antibiofilm applications. A water-soluble and bacterial targeting AIE PS, TPA-1, which is a triphenylamine derivative, has been designed and synthesized. TPA-1 has minimal cytotoxicity towards human cells with and without light irradiation. Additionally, TPA-1 exhibits intrinsic antibacterial activity. Without light irradiation, TPA-1 acts as a narrow-spectrum antibacterial agent, eradicating *S. aureus* and preventing their biofilm formation. Upon light irradiation, TPA-1 effectively eradicates planktonic and biofilm *S. aureus* and *P. aeruginosa*. The therapeutic efficacy of TPA-1 has also been assessed with *in vivo* mice models. Furthermore, the intrinsic antibacterial activity of TPA-1 was improved through structural modifications. Among the modified AIE PSs, TPA-C3-C6 was shown to be the most active AIE PS against *S. aureus* and *P. aeruginosa*, even without light irradiation, while maintaining relatively low cytotoxicity. The

combined effects of PDT and the intrinsic antibacterial activity of TPA-C3-C6 enhance the antibiofilm activity and prevent biofilm recurrence.

Acknowledgements

I would like to give my sincere gratitude to Prof. Kwok-Yin Wong for his supervision and support throughout my PhD studies. His experience and knowledge in research have always provided me with valuable insights. Without his guidance, it would be impossible to complete this study.

I would like to extend my thanks to Prof. Wing-Leung Wong and Prof. Ge Ding for their guidance during the initial stage of this project.

I am also grateful to Dr. Yong Wang, Dr. Zhiguang Liang, and Mr. Weile Yin for teaching me organic synthesis. I appreciate the advice from Dr. Yu Wai Chen on my thesis and presentations, as well as the assistance from Dr. Kang Ding with SEM experiments and from Mr. Ka Hin Chan with cytotoxicity assays. Special thanks go to Dr. Ho-Wing Man, Dr. Xiandi Zhang, Dr. Wing-Lam Cheong, Dr. Yik-Hong Fung and other past colleagues for their support during my studies. I would like to express my deep gratitude to all my labmates who have helped me overcome the difficulties in my studies, especially Dr. Wai-Po Kong, Dr. Ruo-Lan Du and Dr. Yuanyuan Zheng.

Finally, I would like to express my deepest gratitude to my parents and friends for their encouragement and support during my PhD journey.

Thank you to everyone who has helped me throughout my studies in one way or another.

Table of Contents

List of Abbreviations

A. baumannii	*Acinetobacter baumannii*
ACQ	Aggregation-caused quenching
AIE	Aggregation-induced emission
AMR	Antimicrobial resistance
aPDT	Antibacterial photodynamic therapy
BODIPY	Boron dipyrromethene
BTRC	BODIPY^{TM} TR cadaverine
CaMHB	Mueller Hinton broth 2 cation adjusted
CC_{50}	50% Cytotoxicity concentration
Ce6	Chlorin e6
cLogP	Calculated partition coefficient
DEP	Differentially expressed protein
DHR123	Dihydrorhodamine 123
DIC	Differential interference contrast
Disc3(5)	3,3'-Dipropylthiadicarbocyanine Iodide
E. coli	*Escherichia coli*
E. faecalis	*Enterococcus faecalis*
eDNA	Extracellular DNA
EPS	Extracellular polymeric substances
GDP	Gross domestic product
GO	Gene ontology
HC_{50}	50% Haemolytic concentration
HOMO	Highest occupied molecular orbital
HPF	Hydroxyphenyl fluorescein
KEGG	Kyoto Encyclopedia of Genes and Genomes
LB	Lysogeny broth
LogP	Partition coefficient
LPS	Lipopolysaccharide
LTA	Lipoteichoic acid
LUMO	Lowest unoccupied molecular orbital
MHB	Mueller Hinton broth
MIC	Minimum inhibitory concentration
MRSA	Methicillin-resistant *Staphylococcus aureus*
MS	Mass spectrometry
NIR	Near-infrared region
P. aeruginosa	*Pseudomonas aeruginosa*
PBS	Phosphate-buffered saline
PDT	Photodynamic therapy

PS	Photosensitizer
qRT-PCR	Real-time quantitative reverse transcription PCR
ROS	Reactive oxygen species
S. aureus	*Staphylococcus aureus*
S. mutans	*Streptococcus mutans*
S. typhimurium	*Salmonella typhimurium*
SEM	Scanning electron microscopy
SOSG	Singlet oxygen sensor green
TCA	Tricarboxylic acid
Tris	Tris(hydroxymethyl)aminomethane
TSB	Tryptic soy broth
WTA	Wall teichoic acid

Chapter I

Introduction

1.1 Current Obstacles in Treating Bacterial Infections

Bacterial infection has always been a severe challenge to human health. The discovery of penicillin in 1928 provided us with a weapon to combat bacteria. Following the "golden age" of antibiotics, other classes of antibacterial agents such as tetracyclines, aminoglycosides and quinolones, have been discovered and quickly introduced into clinical settings. These antibiotics, discovered decades ago, remain some of the most effective drugs for treating bacterial infections.[1-3] However, the inappropriate use of antibiotics has accelerated the emergence of antimicrobial resistance (AMR). A recently published study estimated that AMR could cause 8.22 million associated deaths in 2050 if no intervention is made.[4] In addition, AMR could reduce the global gross domestic product (GDP) by more than 1 trillion US dollars annually after 2030.[5]

1.2 Bacterial Biofilm

Apart from AMR, many bacteria can form biofilms, in which the bacteria are enclosed in self-produced extracellular polymeric substances (EPS).[6] EPS mainly consist of polysaccharides, proteins, lipids and extracellular DNA (eDNA).[7] These molecules can protect the bacteria from the host immune system and antibiotics.[6, 7] Compared to freely moving planktonic bacteria, bacteria in the biofilm can be 1000 times more resistant to antibiotics.[8, 9]

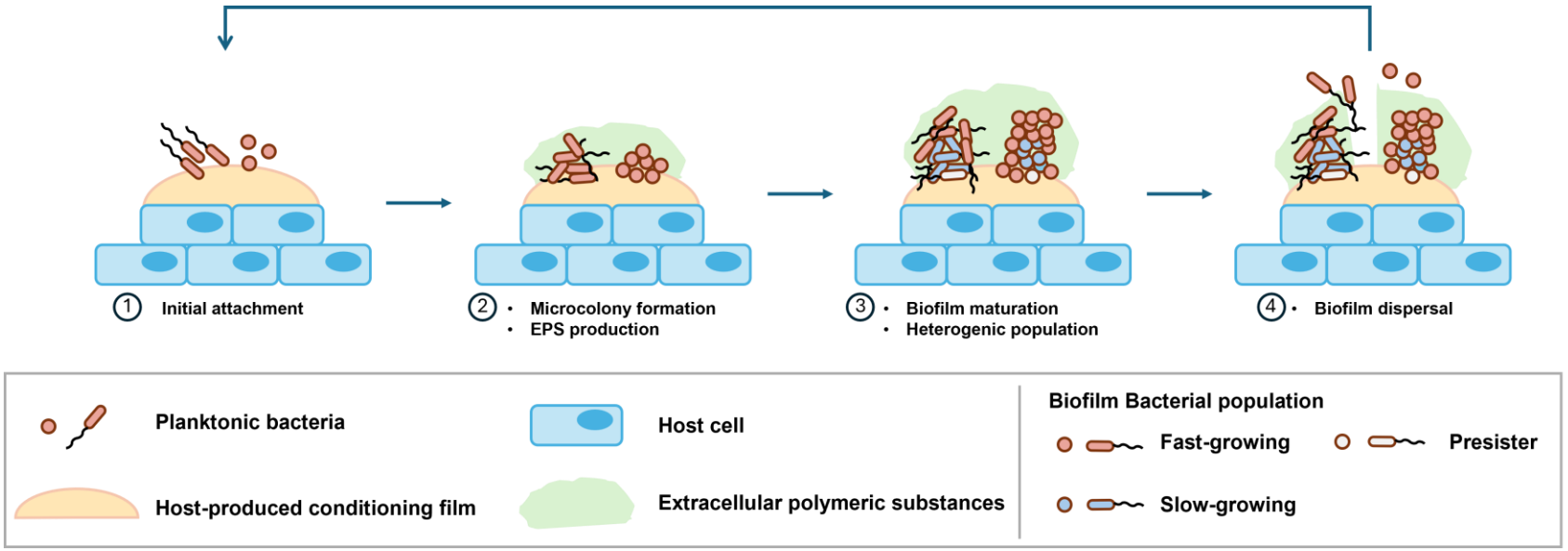

Figure 1.1. Biofilm growth cycle. This illustration has been recreated based on the reference.[10]

The formation of bacterial biofilm is illustrated in **Figure 1.1**. The biofilm cycle starts with the attachment of planktonic bacteria to a biotic or abiotic surface. Biotic surfaces, like mammalian tissue, are usually covered with conditioning film that contains host macromolecules.[10] This conditioning film can facilitate the binding of bacteria to the surface. In tissue infection, bacteria can attach to viscous mucus and damaged tissue to form aggregates.[11, 12] The aggregated cells then multiply and initiate the production of EPS, forming a microcolony. At this stage, bacteria can also utilize the DNA from damaged host cells to construct the biofilm matrix.[13, 14] Upon biofilm maturation, the number of bacteria is significantly increased, as well as the complexity of the biofilm matrix, creating a microenvironment with gradients of nutrients and oxygen.[15] Depending on the location of the bacteria, they will show different physiological properties that will allow them to adapt to changes in the microenvironment. Bacteria near the surface can freely access oxygen and nutrients, so they are fast-growing cells, similar to planktonic bacteria.[16] In contrast, bacteria in the deeper layer are slow-growing or even metabolically inactive, which are called persister cells, due to limited resources.[17] Lastly, a mature biofilm can undergo detachment to release individual bacterial cells or small portions of the biofilm. This detachment can be actively performed by bacteria or as a response to environmental stress.[10] The dispersed bacteria or biofilm can attach to other locations, leading to another biofilm cycle.

1.2.1 Biofilm Tolerance to Antimicrobials

Biofilm tolerance to antimicrobials refers to the ability of bacteria in a biofilm to survive high concentrations of antimicrobials that are lethal to their planktonic counterparts. There are three major mechanisms that contribute to antimicrobial tolerance: penetration barrier caused by biofilm matrix, adaptive responses, and metabolic heterogeneity.[6, 10]

The penetration barrier is provided by the self-produced EPS from the bacteria. For example, negatively charged components, like polysaccharides and eDNA, can slow down the diffusion of positively charged antibiotics, such as aminoglycosides and polymyxins.[18, 19] The barrier can also directly restrict the penetration of cefotaxime and vancomycin in *S. aureus* biofilm.[20] Apart from limiting access to antibiotics, this penetration barrier creates an antibiotic gradient, allowing bacteria in the biofilm that are exposed to a sub-lethal dosage of antibiotics to activate specific responses.[6, 10] For instance, *P. aeruginosa* biofilm treated with a subinhibitory concentration of imipenem showed an increase in alginate production and biofilm volume.[21]

Additionally, nutrient and oxygen limitations can activate adaptive responses, such as the stringent response and SOS response, in bacteria inside the biofilm. The activation of these responses can help bacteria cope with the accumulation of reactive oxygen species during cell metabolism by overproducing antioxidants and activating DNA repair mechanisms.[22-24] Bacteria that activate these responses showed tolerance against fluoroquinolones and other antibiotics that kill bacteria by increasing oxidative stress.[22]

Regarding metabolic heterogeneity, biofilm consists of a subpopulation of fast-growing bacteria at the biofilm surface and a subpopulation of slow-growing or metabolically inactive bacteria inside the biofilm.[10, 15] These two subpopulations use different strategies to resist antibiotics. Fast-growing bacteria can undergo adaptation by activating specific antibiotic resistance mechanisms. For example, upon exposure to colistin, the bacteria at the surface of *P. aeruginosa* biofilm showed an increase in expression of the efflux pump and underwent modification of lipopolysaccharides to reduce the binding affinity towards colistin.[16] In addition, limited oxygen and nutrients in the inner layers of biofilm induce the formation of slow-growing bacteria and persister cells. Persister cells are metabolically inactive bacteria that can survive under various environmental stresses, such as starvation and exposure to antibiotics.[25, 26] Until now, researchers have been unable to clearly distinguish between slow-

growing bacteria and persister cells as they exhibit similar phenotypic properties.[25] Nonetheless, both contribute greatly to biofilm tolerance. One of their tolerance strategies is to downregulate the tricarboxylic acid (TCA) cycle, which can limit the production of reactive oxygen species.[27] Additionally, toxin-antitoxin modules are activated in persister cells.[28] Toxins are proteins that can inhibit the replication and translation of bacteria, while antitoxins counteract the activity of these toxins.[29] The activation of toxin-antitoxin modules often leads to the accumulation of toxins in bacteria, further reducing the synthesis of antibiotic target proteins.[10, 30]

With the above tolerance mechanisms, it is difficult to completely remove bacteria in the biofilm without using a high dosage of antibiotics. Studies also showed that biofilm-related infections were the major cause of chronic and recurrent wounds.[31-33] Together with the emergence of AMR, traditional antibiotics are rapidly losing their effectiveness in treating bacterial infections. Therefore, there is a pressing need to develop new strategies for treating bacterial infections.

1.3 Antibacterial Photodynamic Therapy

Antibacterial photodynamic therapy (aPDT) has gained increasing interest in recent years. aPDT uses non-toxic photosensitizers (PSs) that can be excited by light irradiation to generate toxic reactive oxygen species (ROS). Like other living organisms, bacteria have defence systems against oxidative stress. For example, bacteria can remove superoxide anion and hydrogen peroxide by producing superoxide dismutase and catalase.[34] However, not all ROS, especially hydroxyl radical and singlet oxygen, can be effectively removed by bacteria. These ROS can still destroy essential biological components of the bacteria and eventually lead to cell death. [35-39] One of the biggest advantages of aPDT is that it can overcome antibiotic resistance. Since antibiotics are usually specific to a single target, bacteria can easily generate resistance by point mutation of the corresponding targets.[40] In contrast, aPDT generates ROS that can disrupt multiple targets simultaneously, making it difficult for bacteria to accumulate

enough mutations to resist the treatment. Hence, bacteria can hardly develop resistance against aPDT.[41, 42] In addition to avoiding the emergence of AMR, aPDT also offers the advantages of non-invasive treatment, broad-spectrum antibacterial effects and rapid eradication of bacteria in minutes.[1, 43, 44]

1.3.1 The Mechanisms of Photodynamic Therapy

The photophysical process by which a PS generates ROS is shown in **Figure 1.2**. Upon appropriate light irradiation, the PS will transfer from the singlet ground state (S_0) to the singlet excited state (S_1). The excited PS in the S_1 state can return to the ground state through the emission of a photon (fluorescence) or by non-radiative decay. Additionally, the PS can undergo intersystem crossing, which involves the transfer from the S_1 state to the triplet excited state (T_1). PSs at the T_1 state can relax to the ground state by phosphorescence or, more importantly, the generation of ROS. There are two major ROS generation mechanisms, which are through electron transfer (Type I) to generate radicals and energy transfer (Type II) to generate singlet oxygen. [45, 46]

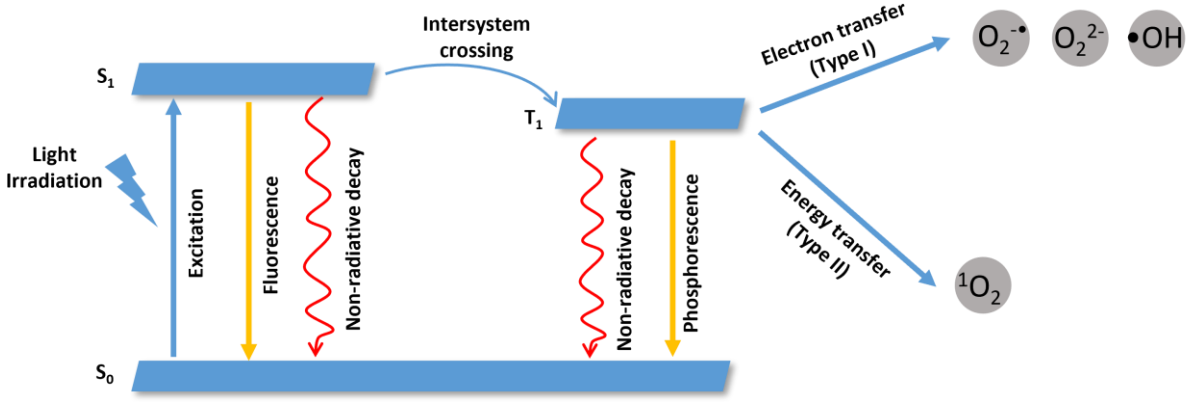

Figure 1.2. The Jablonski diagram shows the two ROS generation mechanisms of a PS.

1.3.2 Type I ROS Generation

For the Type I mechanism, the first free radical, superoxide anion ($O_2^{\bullet-}$), is generated from molecular oxygen by capturing an electron from a PS in the triplet excited state (PS^*) (**Equation (1)**) or with the help of a reducing agent, such as NADH and NADPH (**Equation (2)-(3)**).[47]

$$PS^* + O_2 \rightarrow PS^{\bullet+} + O_2^{\bullet-} \quad \textbf{(1)}$$

$$2PS^* + NAD(P)H \rightarrow 2PS^{\bullet-} + NAD(P)^+ + H^+ \quad \textbf{(2)}$$

$$PS^{\bullet-} + O_2 \rightarrow PS + O_2^{\bullet-} \quad \textbf{(3)}$$

The superoxide anion can undergo disproportionation to form hydrogen peroxide (H_2O_2). This process is often catalyzed by superoxide dismutase in biological systems or through one electron reduction of the superoxide anion (**Equation (4)**).[47]

$$2O_2^{\bullet-} + 2H^+ \rightarrow O_2 + H_2O_2 \quad \textbf{(4)}$$

Hydrogen peroxide can then interact with superoxide anion to form strongly oxidizing hydroxyl radical (•OH) (**Equation (5)**). If the lifetime of triplet excited PS is long enough, it can also interact with hydrogen peroxide to generate a hydroxyl radical (**Equation (6)**).[48]

$$H_2O_2 + O_2^{\bullet-} \rightarrow O_2 + OH^- + \bullet OH \quad \textbf{(5)}$$

$$H_2O_2 + PS^* \rightarrow H_2O_2^{\bullet-} + PS^{\bullet+} \rightarrow H_2O + PS^{\bullet} + \bullet OH \quad \textbf{(6)}$$

The hydroxyl radicals generated through the Type I mechanism are capable of oxidising enzymes, lipids, and DNA.[46] For example, hydroxyl radicals can interact with phospholipids

in the bacterial membrane, forming lipid peroxides. The formation of lipid peroxides can disrupt the packing efficiency of the bacterial membrane, affecting membrane integrity and may further cause leakage of cellular components.[43, 49]

1.3.3 Type II ROS Generation

For the Type II mechanism, the triplet excited PS with light irradiation returns to the ground state by transferring the energy to a triplet ground state of molecular oxygen ($^3O_2$), leading to the formation of singlet oxygen ($^1O_2^*$) (**Equation (7)**).[47]

$$PS^* + {}^3O_2 \rightarrow PS + {}^1O_2^* \quad \textbf{(7)}$$

Singlet oxygen is highly reactive and can effectively oxidize nearby lipids, amino acids, DNA, and RNA, disrupting normal cell function and eventually causing cell death.[50] For instance, singlet oxygen can cause DNA strand breakage and mutation in bacterial cells.[51] G:C to T:A transversions were the most observed DNA transversions in a singlet oxygen-damaged plasmid after overnight amplification in an *E.coli* strain.[51]

1.4 A Brief Review on Organic Antibacterial PSs

The efficiency of aPDT is highly dependent on the properties of the PSs. An effective antibacterial PS should be selective towards bacteria, have efficient ROS generation under long-wavelength irradiation, and be non-toxic to human cells. Although inorganic PSs, such as carbon dots, titanium oxide and copper sulfide, have a remarkable ROS generation ability and photostability, their toxicity and difficulty in metabolism limit their bioapplications.[52, 53] On the other hand, organic PSs are relatively less toxic than inorganic PSs as they can often be metabolized by human cells.[1] Hence, organic PSs can potentially treat bacterial infections *in vivo*. In this section, several types of common and recently developed antibacterial organic PSs are reviewed.

1.4.1 Xanthenes

Xanthenes are cyclic molecules that contain three aromatic rings and one oxygen atom in the middle ring (**Figure 1.3**). They are often used as fluorescent probes for bioimaging due to their high quantum yield and low toxicity.[43] The common xanthene PSs are halogenated derivatives of fluorescein, such as Rose Bengal and Erythrosine B, which have absorption ranging from 500 nm to 550 nm. Under green light irradiation, Rose Bengal and Erythrosine B were able to eradicate *S. aureus* and *S. typhimurium*.[54]

Xanthenes have been widely incorporated into various materials for aPDT.[55, 56] For example, Wu *et al.* have designed a pH-sensitive nanoparticle, RB@PMB@GA, to eliminate Gram-negative biofilm bacteria.[57] Rose Bengal was first mixed with dopamine to form RB-PDA nanoparticles, which were then coated with polymyxin B and gluconic acid to form RB@PMB@GA. The decoration of polymyxin B on the nanoparticles helps to increase the specificity towards Gram-negative bacteria, and the gluconic acid controls the surface charge of the nanoparticle under different pH environments.

Apart from functionalizing the traditional xanthene PSs, researchers have also developed new xanthenes with improved ROS generation and extended absorption into the near-infrared region (NIR). For example, an iodinated xanthene-cyanine PS, I_2-XCy, has been developed with an absorption maximum at 680 nm.[58] I_2-XCy has infused two iodine atoms into Xcy, which enhances the phototoxicity against *S. aureus* upon 660 nm light irradiation.

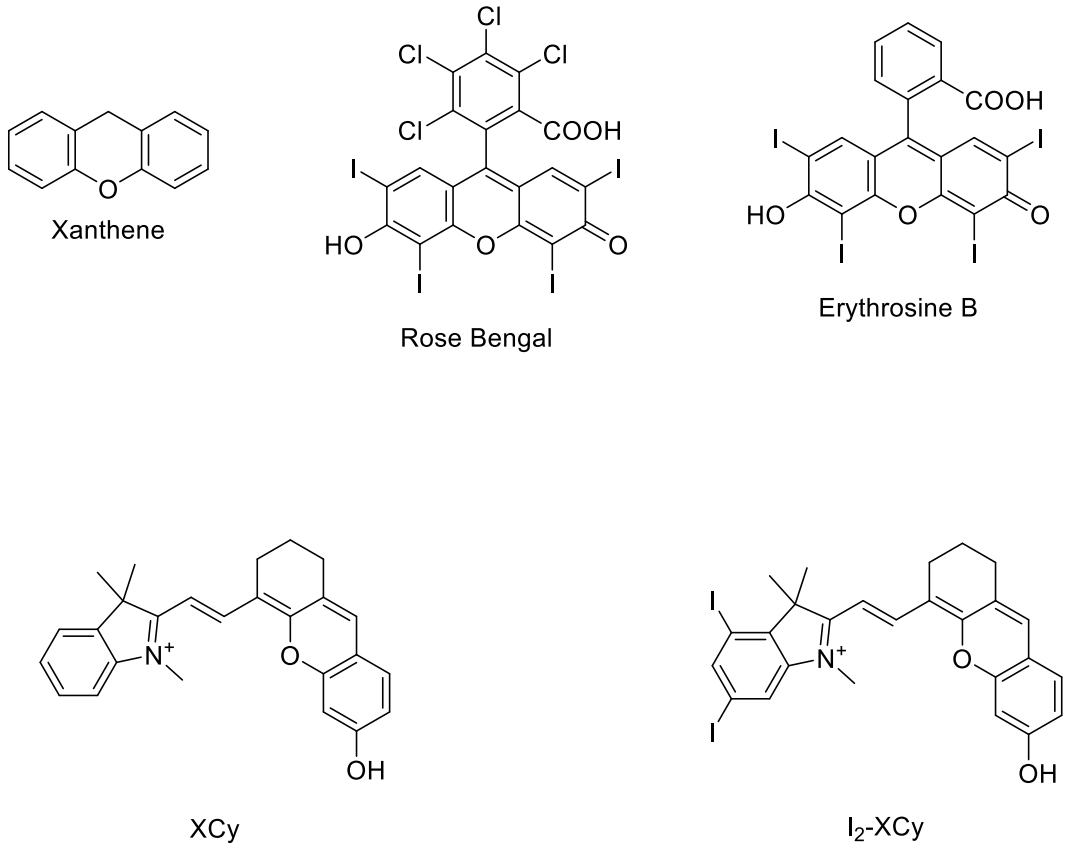

Figure 1.3. Examples of xanthene PSs

1.4.2 BODIPYs

Apart from xanthenes, boron dipyrromethene (BODIPY) is another type of commonly used PS due to its great photostability (**Figure 1.4**).[59] BODIPY typically absorbs around 500 nm. The absorption of BODIPY can also shift towards the NIR region with the infusion of heavy atoms such as selenium and iodine.[60] One of the major drawbacks of BODIPY PSs is the poor water solubility, which can cause precipitation in body fluids. Therefore, attempts have been made to improve the water solubility of BODIPY PSs by introducing cationic or hydrophilic groups to the structure. For example, Dai *et al.* designed a water-soluble BODIPY copolymer with galactose and quaternary ammonium groups named P(ATA-C4)-*r*-GAL-I2.[61] The galactose polymer helps to increase the water-solubility and the quaternary ammonium groups guide the polymer towards bacteria through electrostatic interactions. Upon white light irradiation, P(ATA-C4)-*r*-GA-I2 is able to eradicate *S. aureus* and *P. aeruginosa*.

In addition, Xie's group developed a guanidine-attached BODIPY PS, LIBDP, to treat bacterial infections. LIBDP, upon green light irradiation, can generate ROS and eradicate *S. aureus* in the biofilm.[62] The ROS generated can also oxidize the guanidine group to form nitric oxide, which enhances the antibacterial activity and promotes wound healing.[63] Moreover, the inclusion of cationic pyridine at the meso-position of the BODIPY core is a common modification found in BODIPY PSs. Lin *et al.* have studied the effects of the pyridinium cation orientation on the antibacterial activities of the PSs.[64] They found that compound 3c, which has the positively charged nitrogen at the meta-position, exhibited minimal aggregation and improved antibacterial activity upon light irradiation compared to the para- and ortho-position. To further enhance the binding to bacteria, a BODIPY PS (IBDPPy-PBA) with cationic pyridine and phenylboronic acid was designed.[65] Boronic acids have been commonly used for sugar recognition as they can bind with the adjacent hydroxyl groups on sugars, forming boronate esters.[66] Since teichoic acids in Gram-positive bacteria and lipopolysaccharides in

Gram-negative bacteria are composed of multiple sugars, IBDPPy-PBA can target these components through the phenylboronic motif. Additionally, the cationic pyridine group can also bind with negative charges on bacterial surfaces. Upon green light irradiation, IBDPPy-PBA can eradicate *S. aureus* and *E. coli* in the biofilms.

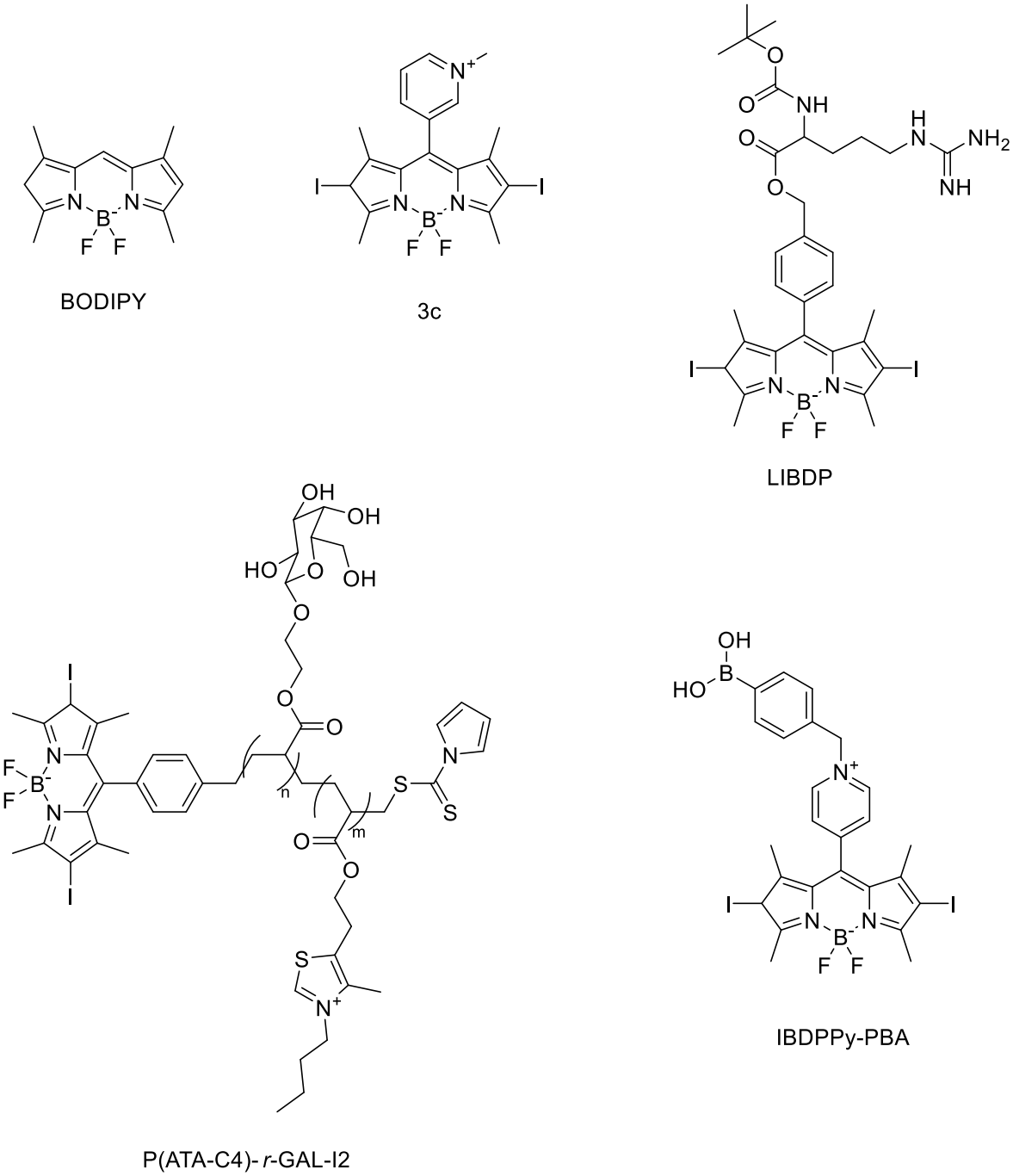

Figure 1.4. Examples of BODIPY PSs.

1.4.3 Porphyrins

Porphyrins are macrocyclic molecules that are composed of four pyrroles linked by methine bridges. (**Figure 1.5**). They are commonly found in nature, such as in chlorophylls and heme, and they often exhibit low cytotoxicity and are easily metabolized in the human body.[1] Porphyrin PSs are one of the most commonly used antibacterial PSs due to their great quantum yield and efficient Type II ROS generation.[1, 43] Similar to other antibacterial PSs, the affinity of porphyrins towards bacteria can be increased by introducing positively charged cationic groups. TMPyP was the first porphyrin PS used for antibacterial purposes. When exposed to visible light irradiation, TMPyP can eradicate *E. coli*, *E. seriolicida and V. anguillarum*.[67] In 2022, Hao *et al.* further investigated the antibacterial effects of TMPyP on aerobic and facultative anaerobic bacteria.[68] Interestingly, TMPyP can be reduced by some facultative anaerobic bacteria, including *E. coli*, *S. typhimurium* and *E. faecalis*. These bacteria had a redox potential lower than or close to that of TMPyP. The reduced form of TMPyP, called Phlorin, had good photothermal conversion upon 730 nm irradiation. Depending on the type of bacteria, TMPyP can eradicate them by generating ROS or heat upon light irradiation.

Zhang's group has also designed a zwitterion porphyrin PS (ZMP).[69] The zwitterion property of ZMP improved its water solubility. Upon 410 nm light irradiation, ZMP can oxidize colored chromogen and eradicate biofilm *S. mutans*. Later, the same group developed Ga-CHP, which has iron-blocking antibacterial activity.[70] During infection, bacteria rely on the host's heme (iron protoporphyrin IX) as an iron source. Since the molecular structure of Ga-CHP is similar to that of heme, Ga-CHP can be taken by the bacteria. The chemical properties of Ga^{3+} are very similar to Fe^{3+} but Ga^{3+} cannot be reduced to Ga^{2+} under physiological conditions.[71] Therefore, the redox cycle for several iron-involved enzymes will be disrupted. Hence, Ga-CHP can kill drug-resistant *S. aureus*, *A. baumannii* and *P. aeruginosa* even without light

irradiation. Moreover, the iron-blocking activity of Ga-CHP and PDT upon 410 nm irradiation had synergistic effects against *S. aureus* and *E. coli*.

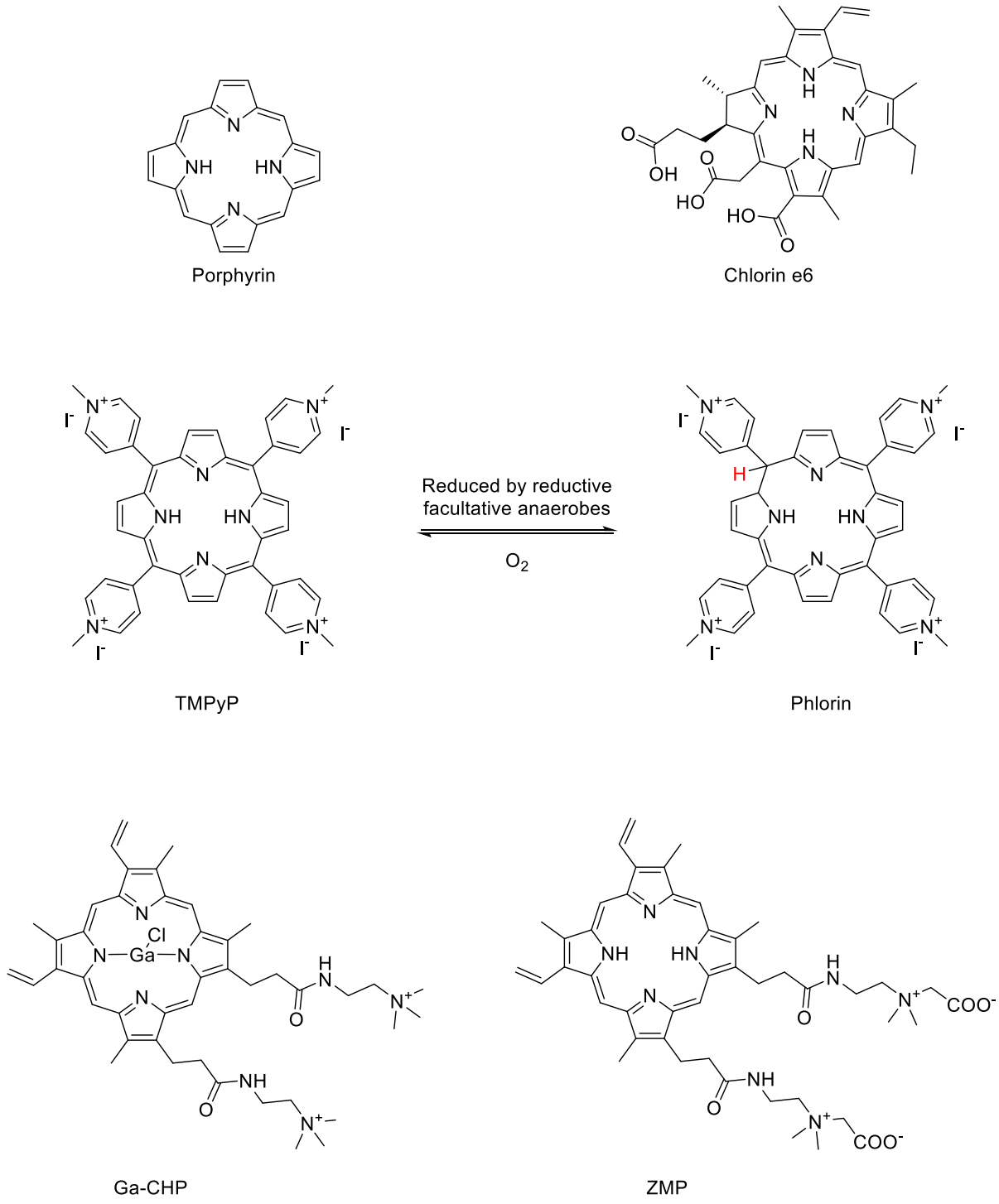

Figure 1.5. Examples of porphyrin PSs.

1.4.4 Phthalocyanines

Phthalocyanines are aromatic heterocyclic PSs that are closely related to porphyrins.[72] They consist of four isoindoles linked by nitrogen bridges (**Figure 1.6**). With the benzene moieties infused into the isoindole, phthalocyanines can be excited by longer wavelengths of light (around 600-700 nm) compared to porphyrins, enabling them to work effectively in deeper layers of tissue.[73] Phthalocyanines have gained significant attention for their development into antibacterial PSs due to their high ROS quantum yield, good photostability and low dark toxicity.[74]

However, traditional phthalocyanines have large planar and hydrophobic structures, which result in low water solubility and a tendency to aggregate in aqueous environments, thereby limiting their efficiency in PDT. To address this problem, researchers have attached hydrophilic substituents to phthalocyanines to improve their water solubility. Cationization is a commonly used modification that enhances the water solubility of phthalocyanines and increases their binding affinity towards bacteria. For instance, Fan *et al.* designed a cationic phthalocyanine, 7b, with four positively charged morpholiums attached to its α positions.[75] Compared to its neutral counterpart 7a, 7b shows improved water solubility and ROS generation in water. With 680 nm light irradiation, 7b was able to eradicate over 90% of *C. albicans* at 1.12 μM and *E. coli* at 0.47 μM through the combination of photodynamic and photothermal effects. Apart from cationization, Ng's group have conjugated an antimicrobial peptide (AMP), Bac, with zinc(II) phthalocyanine to enhance water solubility and bacterial selectivity.[76] Moreover, the combination of AMP and the ROS generated by phthalocyanine under light irradiation resulted in synergistic antibacterial activity. With >610 nm light irradiation, the minimum inhibitory concentration (MIC) of AMP-conjugated phthalocyanine against *S. aureus* and *E. coli* are 0.5 μM and 4 μM, respectively.

Apart from cationization, crafting phthalocyanines into nanoparticles is another popular strategy to increase their biocompatibility. Wang *et al*. reported a phthalocyanine nanoparticle, NanoPcN, which is created by attaching a 3-(dimethylamino) phenoxy group to zinc(II) phthalocyanine to facilitate self-assembly in water.[77] Under 655 nm light irradiation, NanoPcN exhibits good photodynamic and photothermal activities against *S. aureus* and *E. coli*. Additionally, Ding's group developed a phenyl boronic acid-substituted zinc(II) phthalocyanine and ciprofloxacin co-assembled nanoparticle, BAPc-CIP.[78] Upon incubation with bacterial cells, the boronic acid groups on the phthalocyanine interact with the bacterial cell wall, resulting in the disassembly of the nanoparticle and the release of ciprofloxacin. The synergistic antibacterial activity of ciprofloxacin, combined with the ROS generated by phthalocyanine, eradicated planktonic *S. aureus* and *E. coli*, and inhibited their biofilm formation.

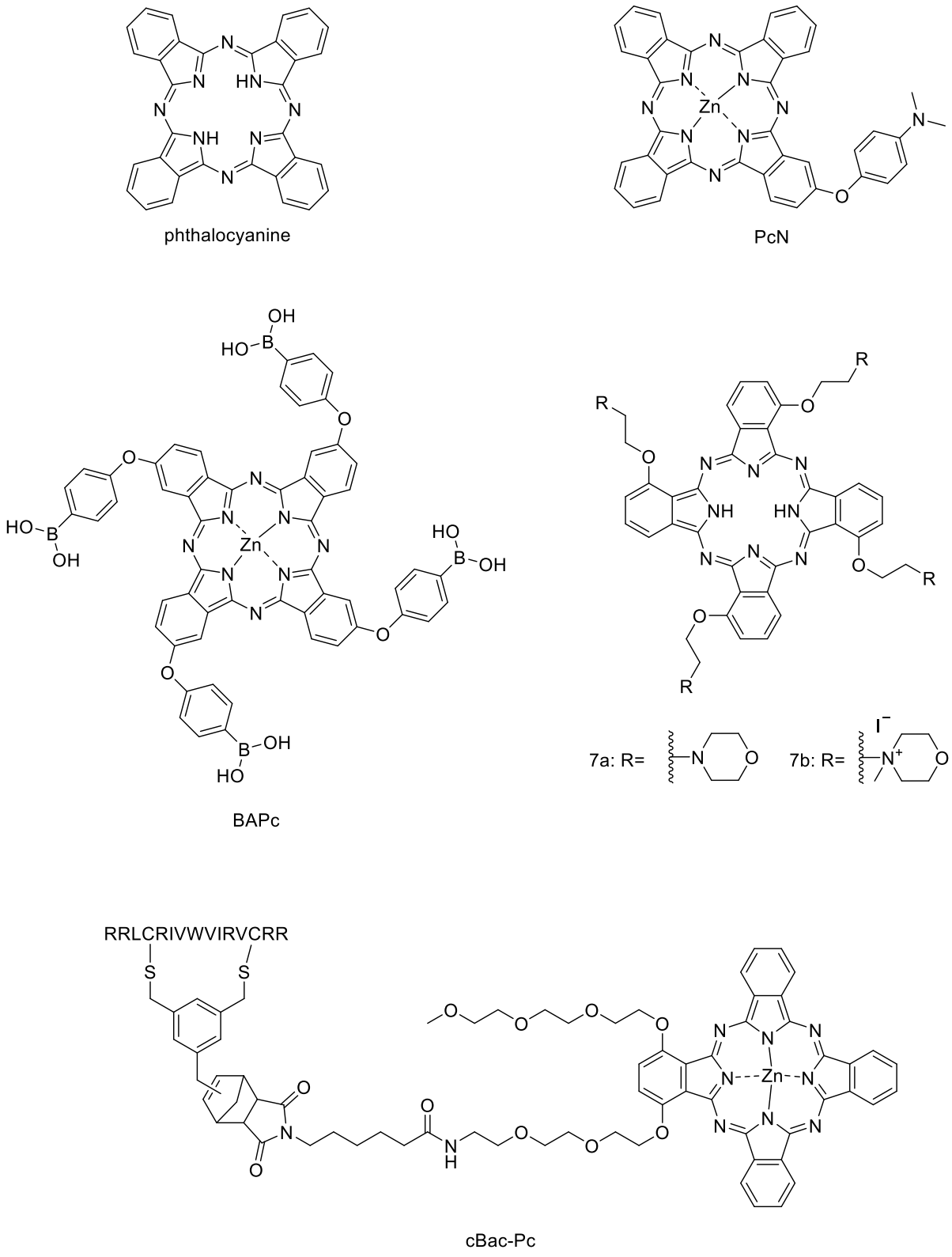

Figure 1.6. Examples of phthalocyanine photosensitizers.

1.4.5 Aggregation-Induced Emission (AIE) PSs

In 2001, Tang's group proposed the idea of aggregation-induced emission (AIE).[79] AIE refers to the phenomenon in which molecules show minimal or no fluorescence in the soluble state but emit intense fluorescent signals once they are in the aggregation state.[80] These molecules can also be called AIE luminogens (AIEgens). Typically, AIEgens contain an extensive conjugate system and a propeller-like structure in which large conjugation groups are connected to the core motif through single bonds (**Figure 1.7a**). In the soluble state, the conjugation groups can freely rotate and help dissipate the energy of the excited AIEgens through intramolecular motions. When AIEgens are in an aggregation state, the intramolecular motions are inhibited by intermolecular stacking and interactions. The propeller structure also prevents perfect π-π stacking. Hence, the energy in excited AIEgens will be released in other forms, including radiative decay and the generation of ROS through intersystem crossing. The enhancement of ROS generation by aggregation is sometimes referred to as the aggregation-induced generation of ROS (AIG-ROS).[81, 82]

Based on the properties of AIE, multiple AIE PSs have been designed for antibacterial purposes. For example, Liu's group developed a bacteria-metabolizable AIE PS, TPEPy-D-Ala, to eradicate intracellular bacteria.[83] D-alanine is an essential amino acid used by bacteria to construct their cell wall, while it is not commonly metabolized by human cells. TPEPy-D-Ala contains a D-alanine motif, which can be internalized by bacteria. Once TPEPy-D-Ala is incorporated into the cell wall, the intramolecular movement will be restricted by the surrounding cell wall molecules, causing an increase in fluorescence emissions. TPEPy-D-Ala can also label bacteria inside macrophages. Upon white light irradiation, TPEPy-D-Ala can eradicate intracellular methicillin-resistant *S. aureus* (MRSA) while causing minimal toxicity to the host cell.

Moreover, Liu *et al.* reported an AIE PS, CTBZPyI, with improved ROS generation through cationization.[84] The cationization of the pyridine group increased the HOMO-LUMO separation. Thus, it can lower the energy gap between singlet and triplet states, further facilitating the intersystem crossing. The pyridinium cation on CTBZPyI can also enhance bacterial binding and provide moderate dark toxicity towards MRSA. Upon light irradiation, CTBZPyI can promote the healing of MRSA-infected wounds. A similar cationization strategy has also been applied to the design of DMMA-SCPI, which has photodynamic activity towards *S. aureus* and *E. coli*.[85] Besides, Lee *et al*. studied the effect of the hydrophobicity of the cationic AIE PSs on bacterial binding activity.[86] Their results showed that hydrophilic AIE PS, TTVP-Am (clogP = 0.14), had better Gram-positive and Gram-negative bacteria labelling ability than hydrophobic AIE PS, TTVP-Nap (clogP = 8.2). This finding indicates that, in addition to the net charge of the PS, structural hydrophobicity also plays a significant role in PS-bacteria interactions.

a

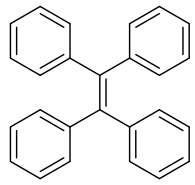

Tetraphenylethylene

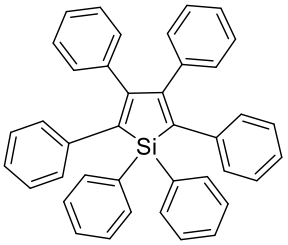

Hexaphenylsiole

b

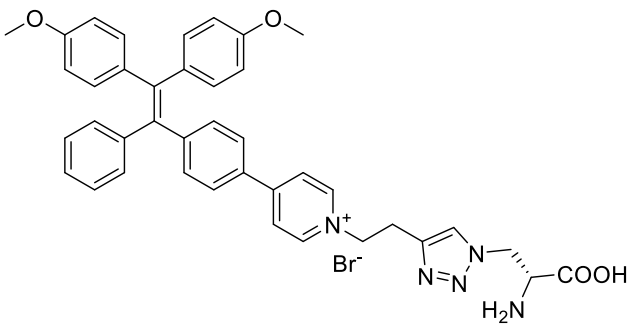

TPEPy-D-Ala

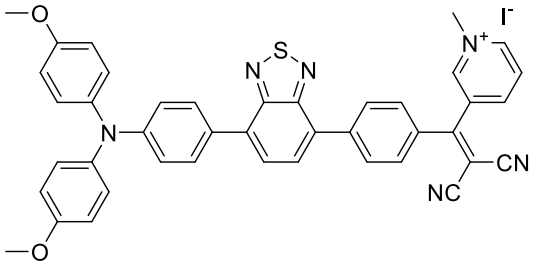

CTBZPyl

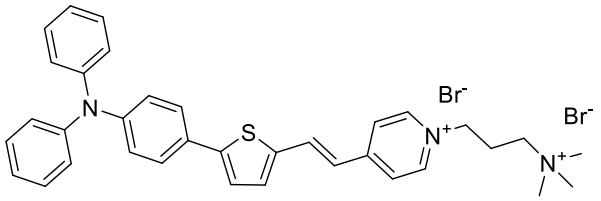

TTVP-Am

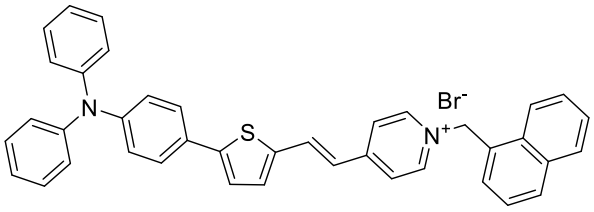

TTVP-Nap

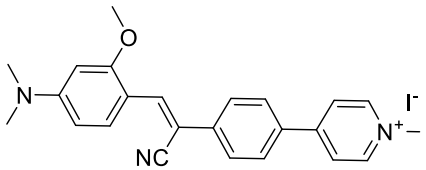

DMMA-SCPI

Figure 1.7. (a) Two typical structures of AIEgens. (B) Examples of AIE PSs.

Table 1.1. Summary of some of the previously reported PSs.

Type	Compound name	Antibacterial activity			Cytotoxicity		
		Strain	-L	+L	Cell line	-L	+L
			Bacteria reduction %, compound concentration			Cell Viability %, compound concentration	
Xanthenes	Rose Bengal[54]	SA	N/A	> 99.9%, 25 nM		N/A	
		Biofilm SA		> 99.9%, 250 μM			
		ST		> 99.9%, 75 μM			
		Biofilm ST		> 99.9%, 50 μM			
	Erythrosine B[54]	SA	N/A	> 99.9%, 500 nM		N/A	
		Biofilm SA		> 99.9%, 500 μM			
		ST		>99%, 75 μM			
		Biofilm ST		No effect, ≤ 1 mM			
	RB@PMB @GA[57]	PA	>99.9%, 256 μM	>99.9%,4 μM	L929	>50%, 256 μM	>50%, 256 μM
		Biofilm PA	No effect at 256 μM	60-80%, 256 μM			
	I_2-XCy[58]	SA	No effect ≤ 10 μM	98.9 %, 1 μM		N/A	
BODIPY	P(ATA-C4)-*r*-GAL-I2[61]	Biofilm BA	N/A	> 70%, 22 μg/mL	A549	No effect, ≤ 4 mg/mL	N/A
		Biofilm SA					
		Biofilm PA					
		Biofilm EC					
	LIBDP[62]	SA	MIC: 10 μg/mL	MIC: 0.3 μg/mL	L929	> 80%, 20 μg/mL	< 20%, ≥ 5 μg/mL
		EC	No effect, ≤15 μg/mL	No effect, ≤ 0.5 μg/mL	NIH 3T3	No effect, ≤ 20 μg/mL	

	3c[64]	SA	No effect, ≤ 5 μM	MIC: 0.63 μM	HaCaT	No effect, ≤ 20 μM	< 25%, ≥ 20 μg/mL
		EC	No effect, ≤ 10 μM	MIC: 1.25 μM			
		CA	No effect, ≤ 2 μM	MIC: 0.63 μM			
		MRSA	No effect, ≤ 1.25 μM	MIC: 0.63 μM			
	IBDPPy-PBA[65]	SA	No effect, ≤ 0.3 μM	MIC: 0.3 μM	L929	No effect, ≤ 30 μg/mL	N/A
		Biofilm SA	> 40%, 30 μM	> 80 %, 30 μM			
		EC	No effect, ≤ 3 μM	MIC: 3 μM	NIH 3T3	No effect, ≤ 30 μg/mL	
		Biofilm EC	No effect, ≤ 2 μM	> 80%, 2 μM			
Porphyrins	TMPyP[68]	BS	No effect, ≤ 0.1 mM	> 99.9%, 0.1 mM	NCM460	< 50%, ≥ 0.2 mM	N/A
		PA					
		SA					
		EC		> 99%, 0.1 mM			
		ST					
	ZMP[69]	SA	MIC: 12.5 μM	MIC: 1.6 μM	NIH 3T3	> 90%, 100 μM	N/A
		SM	No effect, ≤ 12.5 μM	> 90%, 12.5 μM			
		Biofilm SM	> 30%, 500 μM	> 80%, 500 μM			
	Ga-CHP[70]	SA	> 99.9%, 12.5 μM	> 99.9%, 1.6 μM	NIH 3T3	> 80%, 100 μM	N/A
		EC	> 99.9%, 25 μM	> 99.9%, 6.3 μM			
Phthalocyanines	7b[75]	CA	No effect, ≤ 35 μM	> 90 %, 1.12 μM		N/A	
		EC	N/A	> 90%, 0.47 μM			
	cBac-Pc[76]	SA	~ 50%, 0.5 μM	MIC: 0.5 μM	Raw 264.7	> 70%, 50 μM	< 10%, 50 μM
		MRSA	~ 50%, 1 μM	MIC: 1 μM			

		EC	~ 90%, 4 μM	MIC: 4 μM			
		MDR EC	~ 90%, 4 μM	MIC: 4 μM			
	PcN[77]	SA	No effect, ≤ 50 nM	> 99.9 %, 50 nM	L929	> 90% 5 μM	N/A
		MRSA	No effect, ≤ 50 nM	> 90 %, 50 nM			
		EC	No effect, ≤ 5 μM	> 90%, 5 μM			
		ESBL EC	No effect, ≤ 10 μM	> 90%, 5 μM			
	BAPc-CIP[78]	SA	< 50 %, 5 μM	> 90%, 5 μM	L929	N/A	> 80%, 5 μM
		EC	< 50 %, 5 μM	> 90%, 5 μM	HaCat	N/A	> 80%, 5 μM
AIE	TPEPy-D-Ala[83]	MRSA	N/A	> 95%, 10 μM	Raw 264.7	> 80%, 100 μM	> 40%, 100 μM
		Intracellular MRSA		> 90%, 20 μM			
		EC		> 95%, 10 μM			
		Intracellular EC		> 80 %, 20 μM			
	CTBZPyI[84]	MRSA	> 80%, 2 μM	> 99.8%, 2μM		N/A	
	DMMA-SCPI[85]	SA	>50%, 20 μM	> 99.9%, 10 μM	LO2	<20%, 50 μM	<20%, 50 μM
		EC	No effect, ≤ 20 μM	> 97%, 20 μM	NIH 3T3	> 80%, 20 μM	> 80%, 20 μM
	TTVP-Am[86]	SA	No effect, ≤ 1 μM	> 90%, 1 μM		N/A	
		EC	No effect, ≤ 10 μM	> 40%, 10 μM			

Strain: PA, *P. aeruginosa*; SA, *S. aureus*; BA, *B. amyloliquefaciens*; ML, *M. luteus*; SF, *S. flexneri*; EC, *E. coli*; MDR EC, multidrug-resistant *E. coli*; ESBL EC, extended-spectrum β-lactamase-producing *E. coil*; CA, C. albicans; MRSA, methicillin-resistant *S. aureus*; BS, *B. subtilis*; ST, *S. typhimurium*; SM, *S. mutans*. MIC: Minimum inhibitory concentration, in which no bacterial growth was observed after overnight incubation. N/A: Data not available. -L: Without light irradiation. +L: With light irradiation.

1.5 AIE PS as A Promising Class of Antibacterial PS

Traditional PSs, such as porphyrins and xanthenes, have large planar structures. This property can easily cause aggregation-caused quenching (ACQ), which could happen during a decrease in solubility in an aqueous environment, upon binding to targets and accumulation in infected tissue.[87] ACQ can allow efficient nonradiative decay of singlet (S_1 to S_0) and triplet excitons (T_1 to S_0) through intermolecular interactions, such as π-π stacking, often leading to loss in fluorescent signals and reduction in ROS generation.[88, 89] Hence, it can limit the antibacterial PDT efficiency of traditional PSs. In contrast, the twisted structures of AIE PSs prevent sufficient π-π stacking and help avoid ACQ. In addition, the restriction of intramolecular motions in the aggregation state causes an increase in fluorescence and ROS generation, thereby enhancing PDT efficiency.[90] Such unique features of AIE PSs make them a promising class of target-mediated aggregation formation antibacterial PS.

1.6 Limitations of Currently Developed Antibacterial PSs

Over the last decade, tremendous effort has been invested in developing antibacterial PSs. Most of the reported PSs showed excellent performance against planktonic bacteria; however, only a few have been proven to be effective against bacterial biofilms.[91-93] Since 65-80% of infections are related to biofilms, there remains an urgent need to develop effective antibiofilm PSs.[94] Among different types of PSs, AIE PSs are one of the popular antibacterial candidates due to their ability to avoid ACQ. However, common AIE PSs exhibit poor water solubility because of their extensive hydrophobic structures, which leads to the formation of aggregates in aqueous environments, including biological fluids.[95] These aggregates can accumulate in cells and cause cytotoxicity, which limits the bioapplication of AIE PSs. Moreover, one of the weaknesses of PSs is that their antibacterial activity will be lost once the light source is removed. This could allow for the regrowth of bacteria and biofilms in the dark if bacterial eradication

is incomplete.[96] Therefore, designing a PS with intrinsic antibacterial activity could potentially improve the overall therapeutic effect.

1.7 Thesis Objectives and Aims

This thesis developed AIE PSs that serve as antiplanktonic and antibiofilm agents. The water solubility, antibacterial activity, and cytotoxicity of the AIE PSs are improved through structural design and modifications. The antiplanktonic and antibiofilm activities of the AIE PSs, both with and without light irradiation, were tested against Gram-positive *S. aureus* and Gram-negative *P. aeruginosa*. These two bacteria were chosen as the model strains due to their ability to form robust biofilms *in vitro* and their clinical importance. In addition, the detailed antibacterial mechanisms of the designed AIE PSs are investigated. The therapeutic efficiency of the selected AIE PS was also assessed through *in vivo* mice models. Overall, the research presented in this thesis aims to explore the potential of incorporating intrinsic antibacterial activity into a PS, providing insight into the development of new PSs to overcome the challenges posed by bacterial biofilms and AMR.

Chapter II

Design of An Aggregation-Induced Emission Photosensitizer with Antiplanktonic Properties

2.1 Introduction

Most of the reported antibacterial AIE PSs are not water-soluble due to the hydrophobicity of the common AIE structures, such as triphenylamine and tetraphenylethylene.[97, 98] These sparingly water-soluble PSs aggregate in aqueous biological fluid and may induce cytotoxicity.[95, 99-105] Although some AIE PSs were crafted into positively charged nanoparticles with good water dispersion, these positively charged nanoparticles still tend to accumulate in human cells, causing toxicity in the dark and during PDT.[106-108] Designing a water-soluble AIE PS could help minimize the cytotoxic effects and various water-solubilizing groups have been utilized to improve the water solubility of AIE PSs.[87, 109-111]Moreover, only a few antibacterial AIE PSs have good antibacterial effects on both planktonic Gram-positive and Gram-negative bacteria.[99, 112-114] In this regard, an AIE PS with good water solubility and broad-spectrum antibacterial effect is still highly desirable.

In this chapter, the design and synthesis of a novel water-soluble AIE PS, TPA-1, is reported. Assessments on ROS generation abilities, bacterial targeting abilities and antiplanktonic activities of TPA-1 have also been conducted. Without light irradiation, TPA-1 can effectively eradicate planktonic *S. aureus* through targeting multiple bacterial components. In particular, TPA-1 inhibits the supercoiling activity of *S. aureus* DNA gyrase, a property that is not commonly reported by other antibacterial PSs.[84, 114-120] Mass spectrometry (MS)-based proteomic analysis was also conducted to further reveal the antibacterial mechanisms of TPA-1. Upon light irradiation, TPA-1 is capable of generating type I and type II ROS and shows good PDT effects on both planktonic Gram-positive *S. aureus* and Gram-negative *P. aeruginosa* by inducing membrane damage.

The work presented in this chapter was published in the Journal of Medicinal Chemistry, titled "A Water-Soluble Aggregation-Induced Emission Photosensitizer with Intrinsic Antibacterial Activity as an Antiplanktonic and Antibiofilm Therapeutic Agent" by **Hung, C. -H.**, et al.

2.2 Materials and Methods

2.2.1 Materials and Instruments

4-Bromo-4',4''-dimethoxytriphenylamine, 1,3-dibromopropane, 4-bromo-1-butyne, bromoethane, 2-methylbenzothiazole, 5-Formyl-2-thienylboronic acid, trimethylamine, and zinc phthalocyanine were purchased from TCI. Boron tribromide and [1,1'-bis(diphenylphosphino)ferrocene]dichloropalladium(II) were purchased from Aladdin. Dulbecco's Modified Eagle Medium (DMEM), fetal bovine serum (FBS) and penicillin-streptomycin (10000 U/mL) solution, phosphate-buffered saline (PBS), and trypsin were purchased from Gibco^{TM}. SYTO 9, hydroxyphenyl fluorescein (HPF), dihydrorhodamine 123 (DHR123), singlet oxygen sensor green (SOSG), and BODIPY^{TM}-TR-cadaverine were purchased from Invitrogen^{TM}. 3,3-Dipropylthiadicarbocyanine iodide (Disc3(5)), crystal violet, LB Miller, agar, D-(+)-glucose, LTA from *S. aureus* and LPS from *P. aeruginosa* were purchased from Sigma-Aldrich. Mueller Hinton Broth (MHB) and Tryptic Soy Broth (TSB) were purchased from BD^{TM}. All chemical reagents and solvents were directly used without further purification. *Staphylococcus aureus* (ATCC 29213), methicillin-resistant *Staphylococcus aureus* (BAA 41 and ATCC 43300), *Pseudomonas aeruginosa* (ATCC 27853) and human foreskin fibroblast (HFF-1) cells were obtained from American Type Culture Collection (ATCC). MTT assays were performed using the MTT assay kit from ThermoFisher Scientific.

A Bruker Advance-III 400 MHZ FT-NMR system was used to record the ^{1}H and ^{13}C NMR spectra of the compounds. High-resolution mass spectra were acquired on an Agilent 6540 Quadrupole-TOF LC/MS. UV-visible absorption spectra were obtained from an Agilent Technologies Cary 8454 UV-Vis spectrometer. Fluorescence spectra were obtained on an Agilent Technologies Cary Eclipse Fluorescence Spectrophotometer. A TECAN Infinite M1000 PRO microplate reader was used to perform assays requiring fluorescence intensity

measurements. Cytotoxicity, crystal violet staining assays, and cell components leakage assays were conducted on a BMG Labtech CLARIOstar microplate reader. Fluorescence images were taken using a Nikon Eclipse Ti2-E Live-cell Fluorescence Imaging System. SEM images were obtained from a Tescan MAIA3 scanning electron microscope. The photodynamic properties of the compounds were studied using a CEL-HXF300-T3 xenon light system from CEAulight, equipped with a 420-780 nm UV-visible cut filter and a 600 nm band-pass filter. The clogP values of the compounds were obtained using the integrated function in ChemDraw. The graphs related to biological assays were plotted using GraphPad Prism 8. All HFF-1 cells used in this study were obtained from Mr. Ka Hin Chan.

2.2.2 Synthesis of Compound 1

4-Bromo-4',4''-dimethoxytriphenylamine (0.8 g, 2 mmol) was dissolved in dichloromethane (DCM, 15 mL) and purged with nitrogen. Boron tribromide (6 mmol) was slowly added to the solution at 0℃. The reaction was then allowed to stir at room temperature overnight. The reaction was quenched with ice water (2 mL). After the addition of water, some deep blue solids were formed in the solution. DCM (100 mL) was added in several portions to wash the solids. The organic layer was then filtered, washed with water (30 mL, 3 times), brine (30 mL), and dried with sodium sulphate. The sodium sulphate was removed by filtration, and the filtrate was evaporated under vacuum to obtain crude Compound 1 as a green oil. The crude Compound 1 was directly used to synthesize Compound 2 without further purification.

2.2.3 Synthesis of Compound 2

Crude Compound 1 (0.7 g, 2 mmol) was dissolved in dimethylformamide (DMF, 5 mL) with 1,3-dibromopropane (7.93 g, 40 mmol). Caesium carbonate (1.99 g, 6.2 mmol) was then added to the solution. The reaction was stirred overnight at room temperature. Upon completion of the reaction, ethyl acetate (80 mL) was added to the solution. The organic solution was washed

with water (30 mL, 3 times), brine (30 mL) and dried over sodium sulphate. The solution was concentrated and purified by column chromatography (hexane:ethyl acetate = 20:1) to obtain Compound 2 as a colourless oil (0.45 g, 38% yield).^{1}H NMR (400 MHz, $CDCl_3$) δ= 7.29 (d, *J* = 7.92 Hz, 2H), 7.08 (d, *J* = 8.04 Hz, 4H), 6.90-6.85 (m, 6H), 4.12 (t, *J* = 5.28 Hz, 4H), 3.65 (t, *J* = 6.2 Hz, 4H), 2.38-2.32 ppm (m, 4H). ^{13}C NMR (100 MHz, $CDCl_3$) δ= 155.2, 147.9, 140.8, 131.9, 126.6, 122.2, 115.6, 112.6, 65.6, 32.5, 30.3 ppm. HRMS (ESI) *m/z* calcd for $C_{24}H_{24}Br_3NO_2^+$: 596.9337 $[M]^+$; found: 596.9328.

2.2.4 Synthesis of Compound 3

Compound 2 (0.45 g, 0.75 mmol) and 5-formyl-2-thienylboronic acid (0.24 g, 1.5 mmol) were dissolved in degassed methanol:toluene (30 mL, 2:3) with potassium carbonate (0.52 g, 3.75 mmol) and Pd(dppf)Cl_2 (27 mg, 0.035 mmol). The reaction was purged with nitrogen and heated to reflux overnight. Then, the solvent was evaporated, and the remaining mixture was redissolved in DCM (100 mL). The mixture was washed with water (30 mL, 3 times) and brine (30 mL). The organic layer was dried with sodium sulphate and purified with column chromatography (hexane:ethyl acetate = 10:1) to obtain Compound 3 as a yellow oil (0.2g, 42% yield). ^{1}H NMR (400 MHz, $CDCl_3$) δ= 9.82 (s, 1H), 7.67 (d, *J* = 2.76 Hz, 1H), 7.45 (d, *J* = 7.8 Hz, 2H), 7.25 (d, *J* = 0.8 Hz, 1H), 7.08 (d, *J* = 7.72 Hz, 4H), 6.91-6.85 (m, 6H), 4.09 (t, *J* = 5.12 Hz, 4H), 3.61 (t, *J* = 6 Hz, 4H), 2.31 ppm (m, 4H). ^{13}C NMR (100 MHz, $CDCl_3$) δ= 182.6, 155.6, 155.0, 149.9, 140.8, 140.1, 137.9, 127.2, 127.2, 124.4, 122.4, 119.5, 115.5, 65.6, 32.4, 30.1 ppm. HRMS (ESI) *m/z* calcd for $C_{29}H_{27}Br_2NO_3S^+$: 629.0058 $[M]^+$; found 629.0068.

2.2.5 Synthesis of Compound 4

Compound 3 (0.2g, 0.32 mmol) was dissolved in tetrahydrofuran (THF, 5 mL). The solution was then cooled to -78℃ under nitrogen. A large excess of trimethylamine (in THF) was slowly added to the solution. The reaction was stirred at -78℃ for an hour and stirred at room temperature for three days. The reaction progress was monitored by a mass spectrometer (Waters QDa mass detector). Upon completion of the reaction, the mixture was centrifuged, and the supernatant was discarded. The remaining yellow solid was then washed with THF (40 mL, 4 times) to yield Compound 4 (0.18 g, 76% yield) as a yellow solid. ^{1}H NMR (400 MHz, CD_3OD) δ= 9.80 (s, 1H), 7.85, (d, *J* = 2.64 Hz, 1H), 7.54 (d, *J* = 7.88 Hz, 2H), 7.42 (d, *J* = 2.76 Hz, 1H), 7.07 (d, *J* = 8.04 Hz, 4H), 6.95 (d, *J* = 7.88 Hz, 4H), 6.85 (d, *J* = 7.88 Hz, 2H), 4.12 (t, *J* = 5.12 Hz, 4H), 3.62 (t, *J* = 7.92 Hz, 4H), 3.22 (s, 18H), 2.35-2.28 ppm (m, 4H). ^{13}C NMR (100 MHz, CD_3OD) δ= 184.6, 157.0, 156.3, 151.4, 142.1, 141.8, 140.4, 128.5, 128.3, 125.8, 124.1, 120.5, 116.8, 66.1, 65.6, 53.7, 24.4 ppm. HRMS (ESI) *m/z* calcd for $C_{35}H_{45}N_3O_3S^{2+}$ 293.6586 $[M-2Br]^{2+}$; found 293.6590.

2.2.6 Synthesis of M1

2-Methylbenzothiazole (0.5 g, 3.36 mmol) and 4-bromo-1-butyne (2.23 g,16.78 mmol) were added to a pressure tube with 2 mL acetonitrile. The reaction was heated to 110℃ overnight. After the reaction mixture was cooled to room temperature, diethyl ether (10 mL) was added. The precipitate was filtered and redissolved in water (10 mL). The solution was then washed with DCM until no starting materials were observed on the TLC plate. The aqueous layer was then concentrated, and THF was added for precipitation. The solid was filtered and washed with THF to obtain M1 (0.24 g, 25% yield) as a white solid. ^{1}H NMR (400 MHz, CD_3OD) δ= 8.35-8.31 (m, 2H), 7.95-7.91 (m, 1H), 7.86-7.82 (m, 1H), 5.03 (t, *J* = 6.56 Hz, 2H), 3.34 (s, 3H), 3.06-3.02 (m, 2H), 2.51 ppm (t, *J* = 2.64 Hz, 1H). ^{13}C NMR (100 MHz, CD_3OD) δ= 179.4,

142.4, 131.1, 130.6, 129.9, 125.5, 118.1, 79.5, 74.3, 19.1, 17.8 ppm. HRMS (ESI) *m/z* calcd for $C_{12}H_{12}NS^+$ 202.0685 $[M\text{-}Br]^+$; found 202.0700.

2.2.7 Synthesis of M2

M2 was synthesized similarly to M1 while replacing 4-bromo-1-butyne with bromoethane. M2 was obtained as a white solid (0.3 g, 35% yield). ^{1}H NMR (400 MHz, DMSO-d_6) δ= 8.47 (d, *J* = 8.12 Hz, 1H), 8.35 (d, *J* = 8.4 Hz, 1H), 7.89 (t, *J* = 7.48 Hz, 1H), 7.80 (t, *J* = 7.64 Hz, 1H), 4.80-4.75 (m, 2H), 3.22 (s, 3H), 1.45 (t, *J* = 7.08 Hz, 3H). ^{13}C NMR (100 MHz, CD_3OD) δ= 177.8, 142.3, 131.1, 130.9, 129.8, 125.4, 117.8, 46.4, 13.7. HRMS (ESI) *m/z* calcd for $C_{10}H_{12}NS^+$ 178.0685 $[M\text{-}Br]^+$; found 178.0692.

2.2.8 Synthesis of TPA-1

Compound 4 (0.1 g, 0.13 mmol), M1 (73 mg, 0.26 mmol), and a catalytic amount of potassium carbonate (9 mg) were dissolved in absolute ethanol (15 mL). The reaction was heated to reflux under nitrogen for 24 hours. The reaction was then concentrated, filtered, and purified by preparative HPLC using a C18 column with acetonitrile (0.1% TFA) and water (0.1% TFA) as the gradient mobile phase. The eluent was concentrated and freeze-dried to get TPA-1 (40 mg, 30% yield) as a dark purple solid. ^{1}H NMR (400 MHz, CD_3OD) δ= 8.37 (d, *J* = 15.12 Hz, 1H), 8.21 (d, *J* = 8.08 Hz, 1H), 8.16 (d, *J* = 8.48, 1H), 7.84 (t, *J* = 7.56 Hz, 1H), 7.77-7.74 (m, 2H), 7.61-7.58 (m, 3H), 7.47 (d, *J* = 4.04, 1H), 7.11 (d, *J* = 8.84, 4H), 6.97 (d, *J* = 8.88 Hz, 4H), 6.87 (d, *J* = 8.76, 2H), 5.06 (t, *J* = 6.12 Hz, 2H), 4.12 (t, *J* = 5.56 Hz, 4H), 3.62-3.58 (m, 4H), 3.20 (s, 18H), 3.01-2.98 (m, 2H), 2.48 (t, *J* = 2.4 Hz, 1H), 2.34-2.28 ppm (m, 4H). ^{13}C NMR (100 MHz, CD_3OD) δ= 173.7, 157.2, 156.0, 151.6,143.2, 142.6, 141.6, 139.6, 138.5, 130.8, 129.6, 129.0, 128.6, 128.3, 125.2, 124.9, 120.3, 117.3, 116.7, 110.5, 79.7, 74.4, 66.0, 65.5, 53.7, 53.6, 53.6, 24.4, 19.4 ppm. HRMS (ESI) *m/z* calcd for $C_{47}H_{55}N_4O_2S_2^{3+}$ 257.1250 $[M\text{-}3Br]^{3+}$; found 257.1263.

2.2.9 Synthesis of TPA-0

TPA-0 was synthesized similarly to TPA-1 by replacing M1 with M2. TPA-0 was obtained as a dark purple solid (50 mg, 39% yield). ^{1}H NMR (400 MHz, CD_3OD) δ= 8.35 (d, *J* = 15.12, 1H), 8.19 (d, *J* = 8.04, 1H), 8.13 (d, *J* = 8.52, 1H), 7.84 (t, *J* = 7.52, 1H), 7.77-7.72 (m 2H), 7.58 (d, *J* = 8.76 Hz, 2H), 7.47-7.42 (m, 2H), 7.11 (d, *J* = 8.88 Hz, 4H), 6.97 (d, *J* = 8.92, 4H), 6.85 (d, *J* = 8.8, 2H), 4.93-4.84 (m, 2H), 4.13 (t, *J* = 5.56 Hz, 4H), 3.62-3.58 (m, 4H), 3.21 (s, 18H), 2.35-2.28 (m, 4H), 1.58 ppm (t, *J* = 7.2 Hz, 3H). ^{13}C NMR (100 MHz, CD_3OD) δ= 172.2, 157.2, 155.8, 151.6, 143.6, 142.5, 141.6, 139.5, 139.1, 138.3, 130.9, 129.5, 129.4, 128.6, 125.6, 125.1, 124.9, 120.2, 109.4, 66.0, 65.5, 53.7, 53.6, 53.6, 24.4, 14.2 ppm. HRMS (ESI) *m/z* calcd for $C_{45}H_{55}N_4O_2S_2^{3+}$ 249.1250 $[M\text{-}3Br]^{3+}$; found 249.1262.

2.2.10 Synthesis of Compound 5

4-Bromo-4',4''-dimethoxytriphenylamine (0.25 g, 0.65 mmol), 5-formyl-2-thienylboronic acid (0.2 g, 1.3 mmol), $Pd(dppf)Cl_2$ (24 mg, 0.033 mmol) and potassium carbonate (0.45 g, 3.25 mmol) were added to a mixture of degassed methanol:toluene (1:1). The mixture was refluxed under nitrogen overnight. The solvent was then evaporated, and the solid was redissolved in DCM (100 mL). The mixture was washed with water (30 mL, 3 times), brine (30 mL) and dried with sodium sulphate. Then, the mixture was concentrated and purified by column chromatography (hexane:ethyl acetate = 5:1) to obtain Compound 5 (190 mg, 70% yield) as an orange solid. ^{1}H NMR (400 MHz, $CDCl_3$) δ= 9.83 (s, 1H), 7.68 (d, *J* = 2.84 Hz, 1H), 7.46, (d, *J* = 7.68, 2H), 7.25 (d, *J* = 7.92, 1H), 7.09 (d, *J* = 7.72, 4H), 6.91-6.85 (m, 6H), 3.81 ppm (s, 6H). ^{13}C NMR (100 MHz, $CDCl_3$) δ= 182.6, 156.5, 155.1, 150.0, 140.8, 139.9, 137.9, 127.2, 127.2, 124.2, 122.3, 119.3, 114.9, 55.5 ppm. HRMS (ESI) *m/z* calcd for $C_{25}H_{21}NO_3S^{+}$ 415.1242 $[M]^{+}$; found 415.1238.

2.2.11 Synthesis of TPA-NC-1

Compound 5, M2, and a catalytic amount of potassium carbonate (9 mg) were dissolved in absolute ethanol. The reaction was purged with nitrogen and refluxed for 24 hours. The mixture was concentrated and purified by column chromatography (DCM:methanol = 10:1) to obtain TPA-NC-1 as a black solid (40 mg, 25% yield). ^{1}H NMR (400 MHz, DMSO-d_6) δ= 8.44-8.38 (m, 2H), 8.23 (d, *J* = 8.48 Hz, 1H), 7.95 (d, *J* = 3.12 Hz, 1H), 7.83 (t, *J* = 7.56 Hz, 1H), 7.74 (t, *J* = 7.6 Hz, 1H), 7.61-7.55 (m, 4H), 7.12 (d, *J* = 8.28 Hz, 4H), 6.97 (d, *J* = 7.72 Hz, 4H), 6.76 (d, *J* = 8.16 Hz, 2H), 4.91-4.86 (m, 2H), 3.76 (s, 6H), 1.44 ppm (t, *J* = 6.84 Hz, 3H). ^{13}C NMR (100 MHz, CD_3OD) δ= 172.3, 158.5, 156.2, 151.9, 143.7, 142.5, 141.0, 139.7, 138.2, 130.8, 129.5, 129.4, 128.7, 128.2, 125.2, 125.0, 124.9, 119.9, 117.0, 116.1, 109.2, 56.0, 45.4, 14.2 ppm. HRMS (ESI) *m/z* calcd for $C_{35}H_{31}N_2O_2S_2^+$ 575.1822 $[M\text{-}Br]^+$; found 575.1833.

A summary of the synthesis of TPA compounds is given in **Scheme 2.1**.

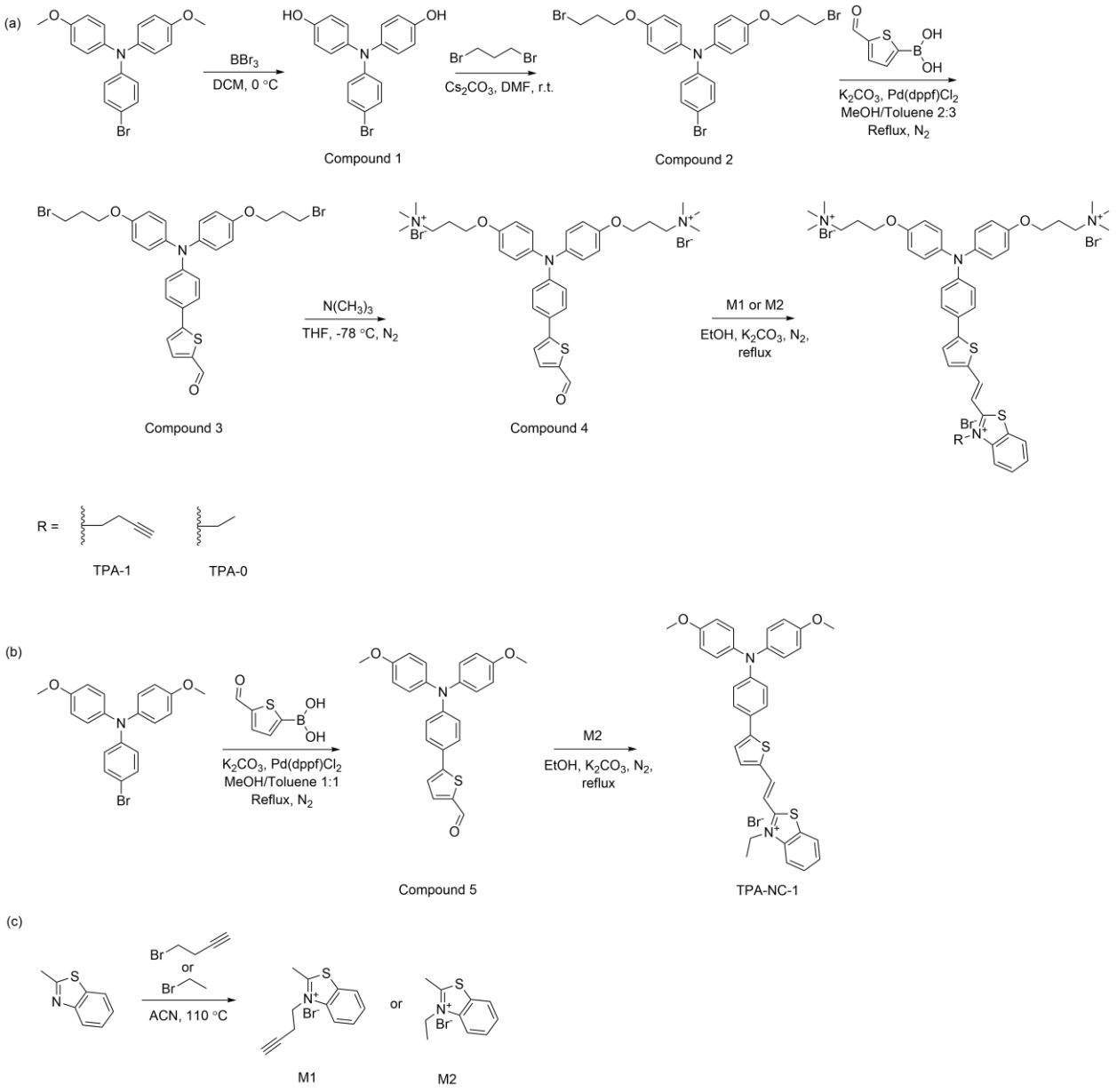

Scheme 2.1. Synthetic route of (a) TPA-1 or TPA-0, (b) TPA-NC-1 and (c) M1 or M2

2.2.12 LogP Values of TPA Compounds

The LogP values of TPA compounds were obtained according to a previously reported method.[121] 1-Octanol was first pre-saturated with water. Equal volumes and concentrations of TPA-NC-1, TPA-0 and TPA-1 were added to a 1-octanol:water (1:1) mixture and vortexed for 1 minute. The mixture was then centrifuged for 5 minutes at 13500 rpm. After that, the absorptions of the compounds in 1-octanol and water phases were measured. The concentrations of the compound in both phases were calculated using the absorption calibration curve of the corresponding compound. LogP was obtained by the following formula: LogP = Log (concentration of the compound in 1-octanol/concentration of the compound in water).

2.2.13 LTA and LPS Binding Assay

LTA and LPS stock solutions (1 mg/mL) were prepared in water. A BODIPY^{TM}-TR-cadaverine stock solution (500 μM) was prepared in DMSO. In a 96-well plate, BODIPY^{TM}-TR-cadaverine (final working concentration = 5 μM) was first mixed with LTA (final working concentration = 5 μg/mL) or LPS (final working concentration = 10 μg/mL) in Tris buffer (50 mM, pH 7.4) and incubated in the dark for 15 minutes at room temperature. Then, TPA compounds (final working concentration = 10 μM) were added to the well. The mixture was further incubated for 30 minutes before the fluorescence intensities were recorded (excitation 580 nm, emission 620 nm) with a plate reader (TECAN Infinite M1000 PRO). The displacement percentage was calculated as $(F_{compound} - F_{buffer})/(F_{probe\ only} - F_{buffer}) \times 100$ % where $F_{compound}$ is the fluorescence intensity after the addition of compound, F_{buffer} is the fluorescence intensity after the addition of buffer as a negative control, and $F_{probe\ only}$ is the fluorescence intensity of BODIPY^{TM}-TR-cadaverine alone in buffer without LPS or LTA as a positive control. The experiments were at least triplicated.[122, 123]

2.2.14 Cytotoxicity Assay

The cytotoxicity of TPA-1, TPA-0, and TPA-NC-1 against HFF-1 cells was evaluated using the 3-(4,5-dimethylthiazol-2-yl)-2,5-diphenyltetrazolium bromide (MTT) assay kit from ThermoFisher Scientific. In general, HFF-1 cells (MEM, 10% FBS, 1% penicillin-streptomycin) were seeded in a 96-well plate with a density of 3000 cells/well overnight at 37℃ with 5% CO_2. The cells were then treated with different concentrations of compounds for 24 hours. MTT (10 μL, 5 mg/mL) was added to the medium, and the cells were further incubated for 3 hours. The medium was then replaced by DMSO (100 μL). After gently shaking the plate for 30 seconds, the optical density of the solutions at 570 nm was measured by a BMG Labtech CLARIOstar microplate reader. The cell viability was calculated as $(OD_{compound} - OD_{DMSO})/(OD_{medium} - OD_{DMSO}) \times 100\%$ where $OD_{compound}$, OD_{medium}, and OD_{DMSO} are the optical densities of the treated cell, non-treated cells, and DMSO at 570nm, respectively. The experiments were conducted in triplicate. The CC_{50} ± Standard Deviation (SD) values were calculated using GraphPad Prism 8.

2.2.15 Fluorescence Imaging of HFF-1 Cells

HFF-1 cells were seeded in confocal dishes at a cell density of 50,000 cells overnight at 37℃. TPA compounds (10 μM) were added to the medium and incubated with the cells for 20 minutes. The fluorescence images of the cells were then taken using a Nikon Eclipse Ti2-E Live-cell Fluorescence Imaging System with an excitation wavelength of 550 nm. The emission was collected from 590 nm to 670 nm (ET630/75m filter).

2.2.16 ROS Generation Assay

Commercial ROS detection probes (DHR123, HPF, SOSG) were used to evaluate the ROS generation abilities of TPA compounds. DHR123, HPF, and SOSG were used to detect non-specific ROS, hydroxyl radical, and singlet state oxygen, respectively. In general, DHR123 (5

μM), HPF (5 μM), or SOSG (5 μM) was mixed with 10 μM of TPA compounds in PBS. TPA-1 and TPA-0 were irradiated by 600 nm light (60 mW/cm^2) for 15 minutes. The change in fluorescence intensity of the mixture was recorded by a plate reader. The fluorescence intensity for DHR123 was recorded at 529 nm with an excitation wavelength of 507 nm. The fluorescence intensity for HPF was measured at an excitation wavelength of 490 nm with an emission wavelength of 515 nm. The fluorescence intensity for SOSG was recorded at 525 nm with an excitation wavelength of 504 nm. The experiments were performed in triplicate.

2.2.17 Fluorescence Imaging of Bacterial Cells

Overnight culture of *S. aureus* (ATCC 29213) or *P. aeruginosa* (ATCC 27853) in Tryptic Soy Broth (TSB) was diluted 100 times in fresh TSB and grown to OD = 1. The bacterial culture was diluted to 2 × 10^8 CFU/mL with PBS. TPA compounds (20 μM) were mixed with the bacteria and incubated for 20 minutes at 30℃. SYTO 9 (2.5 μM) was also used to stain the bacterial DNA. The bacteria (1 μL) were then immobilized on a 1.2 % agarose pad. The fluorescence images of the bacteria were captured using a Nikon Eclipse Ti2-E Live-cell Fluorescence Imaging System with an excitation wavelength of 490 nm (SYTO 9) and 550 nm (TPA-1). Emission was collected from 500 nm to 550 nm (ET525/50m filter) for SYTO9 and 590 nm to 670 nm (ET630/75m filter) for TPA-1.

2.2.18 Minimum Inhibitory Concentration (MIC) Assay

MIC assays of TPA-1 were conducted according to the broth microdilution methods described in the Clinical and Laboratory Standards Institute (CLSI) standard.[124] A single colony of *S. aureus* (ATCC 29213), methicillin-resistant *S. aureus* (BAA 41) or *P. aeruginosa* (ATCC 27853) on an LB agar plate was picked and suspended in Mueller-Hinton Broth (MHB). The bacterial culture was grown overnight at 37℃ for 16 to 18 hours. The bacterial culture was then diluted 100 times in fresh MHB and grown to the mid-log phase. Bacteria in the mid-log phase were

further diluted to 5 × 10^6 CFU/mL in Cation-Adjusted MHB (*S. aureus*) or MHB (*P. aeruginosa*). 10 μL of the diluted bacteria were added to a 96-well plate containing 90 μL of serially diluted TPA-1 in the corresponding medium. The plate was incubated overnight at 37℃ for 16 to 18 hours. The MICs of the TPA compounds are the concentrations at which no apparent bacteria were observed by the naked eye. Different concentrations of LTA were also added to examine the change in MIC values of TPA-1 against *S. aureus*. The experiments were triplicated.

2.2.19 Time-Kill Kinetics Against *S. aureus*

Similar to the MIC assay, the overnight culture of *S. aureus* incubated in the dark was diluted in fresh MHB and grown to the mid-log phase. The *S. aureus* was then diluted to 1 × 10^6 CFU/mL in Cation-Adjusted MHB. 2 mL of diluted *S. aureus* was transferred into a 15 mL culture tube. 2 × MIC or 4 × MIC of TPA-1 were added into the bacterial culture and incubated in the dark for 24 hours. 2 × MIC of vancomycin and PBS were taken as the positive and negative controls, respectively. At times 0, 0.5, 1, 2, 4, 6, 8, and 24 h, 20 μL of the bacterial culture was taken out. The bacteria were serially diluted, and the number of viable bacteria was recorded using the plate counting method. The experiments were conducted in triplicate.

2.2.20 Resistance Generation Assay on *S. aureus*

The MICs for TPA-1 and norfloxacin against *S. aureus* were first determined by the abovementioned method. The wells with 0.5 × MIC of compounds were transferred to 3 mL fresh MHB and incubated in the dark for 3-4 hours at 37℃. The bacteria were then used to conduct another MIC assay. The experiments were repeated for 20 days. The fold changes in the MIC values of the compounds were recorded. The experiments were performed in duplicate.

2.2.21 Bacterial Membrane Depolarization Assay on *S. aureus*

This assay was conducted according to a previous publication with minor changes.[125] Disc3(5) was used to evaluate the membrane depolarization ability of the TPA compounds. The overnight culture of *S. aureus* was diluted 100 times in fresh MHB and grown to the mid-log phase. The bacterial culture was centrifuged (3900 × g, 5 minutes) and washed with glucose-supplemented HEPES buffer (5 mM glucose, 5 mM HEPES, pH 7.4). The cell platelet was resuspended in glucose-supplemented HEPES buffer with the addition of 100 mM potassium chloride and diluted to 1×10^8 CFU/mL. Diluted bacteria (150 μL) were transferred to each well of a 96-well plate. Disc3(5) (8 μM, 50 μL) was mixed with the cells and incubated in the dark for 30 minutes. Before adding TPA compounds, the background fluorescence was measured for 2 minutes at 670 nm with an excitation wavelength of 622 nm. Then, 10 μL of TPA compounds were added to the wells. The fluorescence intensity at 670 was further recorded for 24 minutes. The experiments were performed in triplicate.

2.2.22 Scanning Electron Microscope (SEM) Imaging of Bacterial Cells

Regarding the intrinsic antibacterial abilities of TPA-1, *S. aureus* was prepared to the mid-log phase according to the method described in the MIC assay. The *S. aureus* was then diluted to 1×10^8 CFU/mL in Cation-Adjusted MHB. 4 × MIC, and 8 × MIC of TPA-1 was added into the bacterial culture and incubated for 3 hours at 37℃ in darkness. The cells were centrifuged (3900 × g, 5 minutes) and washed with PBS. 2.5 % Glutaraldehyde was used to fix the bacteria at 4℃ overnight. The fixed bacteria were then gradually dehydrated with 30%, 50%, 70%, 90%, and absolute ethanol. The samples were allowed to stand for 5 minutes in each dehydration step. After dehydration, the samples were resuspended in 10 μL absolute ethanol and dropped on silicon slides. The samples were air-dried and imaged by SEM (Tescan MAIA3).

To study the photodynamic eradication abilities of TPA-1 against planktonic bacteria, an overnight culture of *S. aureus* or *P. aeruginosa* in TSB was diluted 100 times in fresh TSB and regrown to OD = 1. The bacterial culture was diluted to 1×10^8 CFU/mL in PBS. TPA-1 (10 μM) was added to the cells and incubated for 20 minutes at 30℃ in darkness. Then, the bacteria were irradiated by 600 nm light (60 mW/cm^2) for 45 minutes. After irradiation, the sample was prepared for SEM imaging as described above.

2.2.23 DNA Binding Assay

The genomic DNA of *S. aureus* was extracted using the DNA extraction kit from Sigma-Aldrich. The extracted DNA was diluted to 10 μg/mL and mixed with different concentrations of TPA-1 or 5 μM of SYTOX Green. The mixtures were mixed with loading dye and loaded on a 0.8% agarose gel with DNA stain for electrophoresis (120 V, 40 minutes). The gel image was then observed and captured using a Bio-Rad ChemiDoc imaging system.

2.2.24 *S. aureus* DNA Gyrase Inhibition Assay

The assay was conducted using a *S. aureus* gyrase supercoiling assay kit from Inspiralis. In general, relaxed bacterial plasmid (pBR322), *S. aureus* gyrase and different concentrations of TPA-1 were mixed and incubated at 37℃ for 30 minutes. The mixtures were then quenched and subjected to electrophoresis (1% agarose gel, 75V, 2 hours). The gel image was captured with a Bio-Rad ChemiDoc imaging system.

2.2.25 Mass Spectrometry-Based Proteomic Study

Overnight culture of *S. aureus* was diluted 100 times in CaMHB and grown to OD = 0.8 to 1.0. The *S. aureus* was then diluted to 1×10^8 CFU/mL in CaMHB. The diluted bacteria culture with or without 2 × MIC of TPA-1 (6.25 μM) was incubated for 1 hour at 37℃. The bacterial culture without TPA-1 was used as a control. After incubation, the bacteria were collected by

centrifugation (3900 × g, 10 minutes). The proteomic samples were prepared from the bacterial cell pellets using an EasyPep™ MS Sample Prep Kit from Thermo Scientific™.

The tryptic digests (2 µL) were injected into a Dionex UltiMate 3000 RSLCnano (Thermo Scientific, USA). A trap-and-elute method was employed using a PepMap 7cm × 75 µm C18 column (Thermo Scientific, USA) and an Aurora 25cm × 75 µm C18 column with CSI emitter (IonOpticks, Australia), with a trapping flow rate of 50 µL/min for 2 min at 50 °C. The elution gradient was applied with water (Solvent A) and acetonitrile (Solvent B) in 0.1% formic acid as follows: 2% B in 0-2 min, 6-30% B in 2-79 min, 30-90% B in 79-82 min, 90% B in 82-87 min, and 2% B from 87-89 min, in a constant 300 nL/min flow rate. Eluted samples were then analysed by an Orbitrap Fusion Lumos Mass Spectrometer (Thermo Scientific, USA) using data-independent acquisition (DIA) in positive ion mode. The source parameters were 2600 V of capillary voltage with a capillary temperature of 300 °C. Full-scan MS spectra were acquired from 400 to 1500 m/z, with a resolution of 60,000 and an automatic gain control (AGC) target of 400,000. MS/MS was acquired using an Orbitrap as a mass analyzer with a mass resolution of 15,000 and a standard AGC target. Data analysis was done using Spectronaut (Version 19, Biognosys). Default directDIA+ workflow was used to search against the reviewed *S. aureus* (11,274 sequences; 8 December 2024) and P. *aeruginosa* (3,966 sequences, 31 October 2024) database from UniProt. Peptides search for Tryp-sin/P cleavages with a maximum allowance of 2 missed cleavages. Fixed modifications of carbamidomethyl on cysteine residues and variable modifications of oxidation on methylation resides are included. 0.01 False Discovery Rate (FDR) was applied for peptide identification.

Differentially expressed protein was defined as a p-value < 0.05 and Log_2(fold change) > 1 or <-1. GO enrichment analysis was conducted using the PANTHER Overrepresentation Test (Released 20240807) with Fisher's Exact as the significant test and Bonferroni correction for multiple testing.[126, 127] Enrichment results with a corrected p-value < 0.05 were considered

significant. *Staphylococcus aureus* (all genes in database) was used as the reference list for *S. aureus*. KEGG pathway enrichment analysis was conducted in RStudio using the clusterProfiler package.[128] The analysis was performed with an adjusted *p*-value cutoff = 0.05 and Bonferroni as the *p*-value-adjusted method. The differentially expressed proteins were searched against the KEGG organism sao for *S. aureus*.

2.2.26 Photodynamic Eradication Assay for Planktonic Bacteria

Overnight culture of *S. aureus* or *P. aeruginosa* was diluted 100 times in TSB and grown to OD = 1. The bacterial cultures were then diluted to 5×10^6 CFU/mL in PBS. TPA-1 (2 μM) was added to the diluted cultures and incubated in the dark for 20 minutes at 30℃. The bacterial cultures (200 μL) were transferred to the wells of a 96-well plate. The plate was irradiated at 600 nm light (60 mW/cm^2) for 45 minutes. Then, the bacterial cultures were serially diluted, and the number of viable bacteria was counted using the plate counting method. The experiments were performed in triplicate.

2.2.27 DNA and Protein Leakage Assay

Mid-log phase *S. aureus* and *P. aeruginosa* in TSB were prepared as described above. The bacteria were washed and resuspended in PBS to a final OD = 1. TPA-1 (10 μM) was added to the bacteria and incubated for 20 minutes at 30℃ in darkness. The bacteria were then irradiated by 600 nm light for 45 minutes. After treatments, the bacteria were centrifuged (3900 × g, 5 minutes), and the supernatant was transferred to a UV-transparent 96-well plate. The absorption at 260 nm (DNA) and 280 nm (protein) were recorded by a plate reader. The experiments were performed in triplicate.

2.2.28 Statistical Analysis

Experimental data were presented as the mean ± standard deviation (SD). Analysis was conducted using GraphPad Prism 8. Group comparisons were performed using one- or two-

way ANOVA followed by the Tukey posthoc test. A *p*-value less than 0.05 was taken as statistical significance ($p < 0.05$).

2.3 Results and Discussion

2.3.1 Molecular Design of Triphenylamine (TPA) Derivatives

TPA-NC-1 is an AIE PS that has been reported to have high ROS generation abilities, and its nanoparticles have been shown to be effective in killing breast cancer cells.[129] The structure of TPA-NC-1 can be divided into three fragments: a triphenylamine as an electron donor, a thiophene bridge, which can extend the π system of the structure, and a positively charged benzothiazolium as an electron acceptor (**Figure 2.1**). Combining these three fragments can form a donor-π-acceptor (D-π-A) system. PS with a D-π-A system can often promote intramolecular charge transfer and further lower the HOMO-LUMO gap, causing the absorption of the compound to redshift.[130] Additionally, triphenylamine is a typical molecule that can introduce AIE properties to the structure. The propeller structure of triphenylamine can prevent good intermolecular π-π stacking, thereby restraining fluorescence quenching in aggregates. Besides, the thiophene and the benzothiazolium moiety contain heavy atoms (sulphur), which allow more efficient intersystem crossing and improve ROS generation abilities.[129, 131, 132]

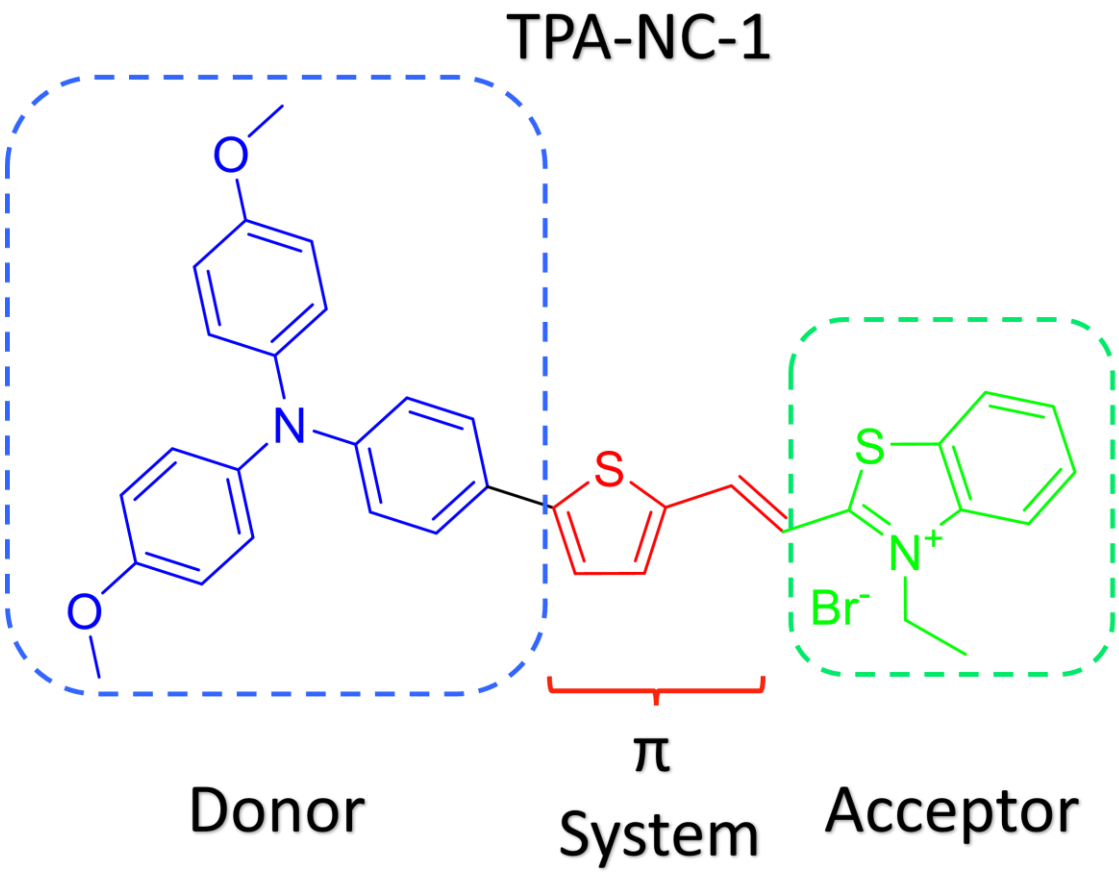

Figure 2.1 The chemical structure of TPA-NC-1.

However, like other AIE PS, TPA-NC-1 is insoluble in water and toxic to human cells. As shown in **Figure 2.2a**, the 50% cytotoxicity concentration (CC_{50}) of TPA-NC-1 against HFF-1 was as low as 7.8 ± 0.7 μM, indicating its high toxicity towards human cells. The fluorescence image of HFF-1 cells with TPA-NC-1 also showed that TPA-NC-1 can stain the HFF-1 cells (**Figure 2.2b**). Therefore, TPA-NC-1 cannot be used as an antibacterial PS directly. Further modifications have to be made in order to improve the water solubility and reduce cytotoxicity.

Based on the structure of TPA-NC-1, two novel derivatives, TPA-0 and TPA-1, have been designed and synthesized (**Figure 2.3a**). Two quaternary ammonium groups were first attached to the triphenylamine core of the TPA-NC-1 to improve its water solubility (TPA-0). Partition coefficient (LogP) was used to evaluate the water solubility of the compounds. LogP is the partition coefficient between 1-octanol and water (**Figure 2.3b**). A lower LogP value indicates that the molecule is more likely to dissolve in water than in 1-octanol, suggesting improved water solubility. The LogP value for TPA-NC-1 was 1.1, while the value for TPA-0 was -1.7, indicating that TPA-0 has better water solubility than TPA-NC-1.

Additionally, the introduction of quaternary ammonium groups on TPA-NC-1 reduced the cytotoxicity against human cells. The CC_{50} value for TPA-0 was 120 ± 20 μM, which was higher than that of TPA-NC-1 (**Figure 2.3c**). Besides, the binding affinity of TPA-0 on human cells was reduced since the fluorescence image of TPA-0-treated HFF-1 cells showed no observable fluorescence signal (**Figure 2.4**).

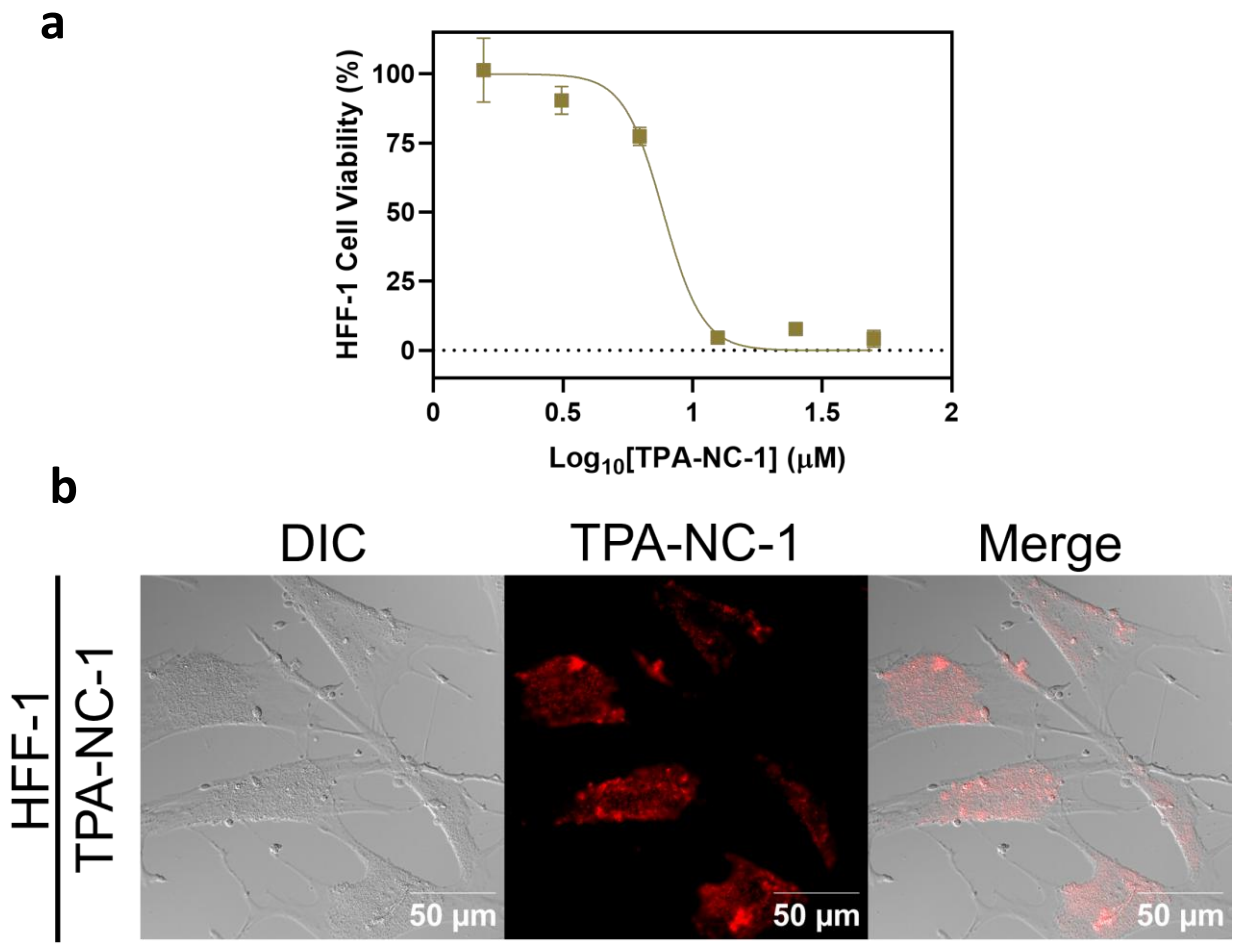

Figure 2.2. (a) Cell viability of HFF-1 cells treated with different concentrations of TPA-NC-1 for 24 hours in the dark. Data are presented as the mean ± SD, n = 3. (b) DIC and fluorescence image of HFF-1 cells after incubation with TPA-NC-1 (10 μM). DIC: Differential Interference Contrast. The excitation wavelength for TPA-NC-1 was 550 nm. The emission was collected from 590 nm to 670 nm (ET630/75m filter).

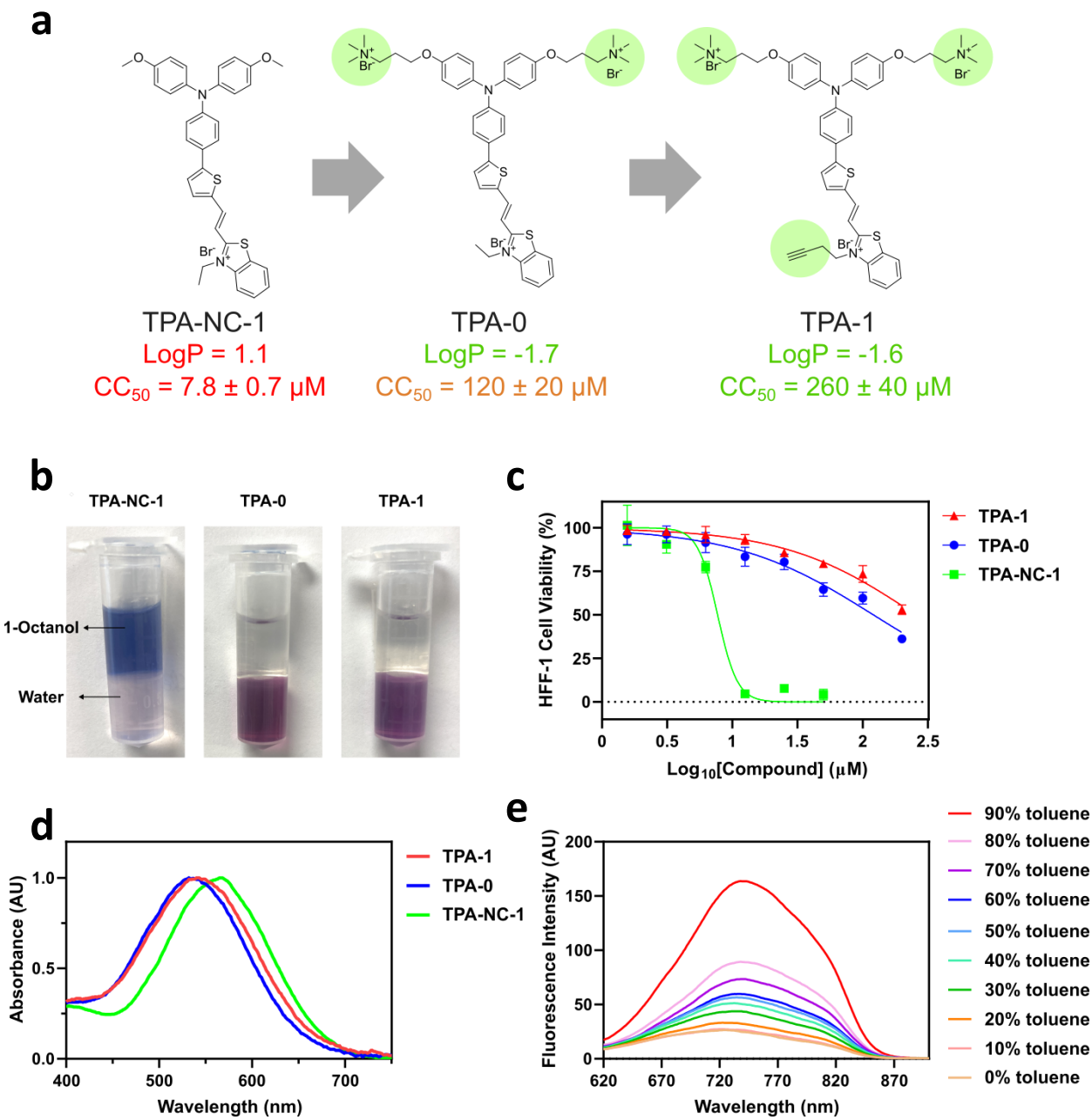

Figure 2.3. (a) Structural modifications of TPA compounds. (b) Photographs of TPA compounds in 1-octanol:water (1:1) mixture. (c) The viability of HFF-1 cells after incubation with different TPA compounds for 24 hours. Data are presented as the mean ± SD, n = 3 per group. (d) The normalized absorption spectrum of TPA compounds in water. (e) The fluorescence spectrum of TPA-1 in methanol with an increasing percentage of toluene. TPA-1 dissolves poorly in toluene. The fluorescence intensity of TPA-1 increased along with the concentration of toluene, indicating the AIE properties of TPA-1.

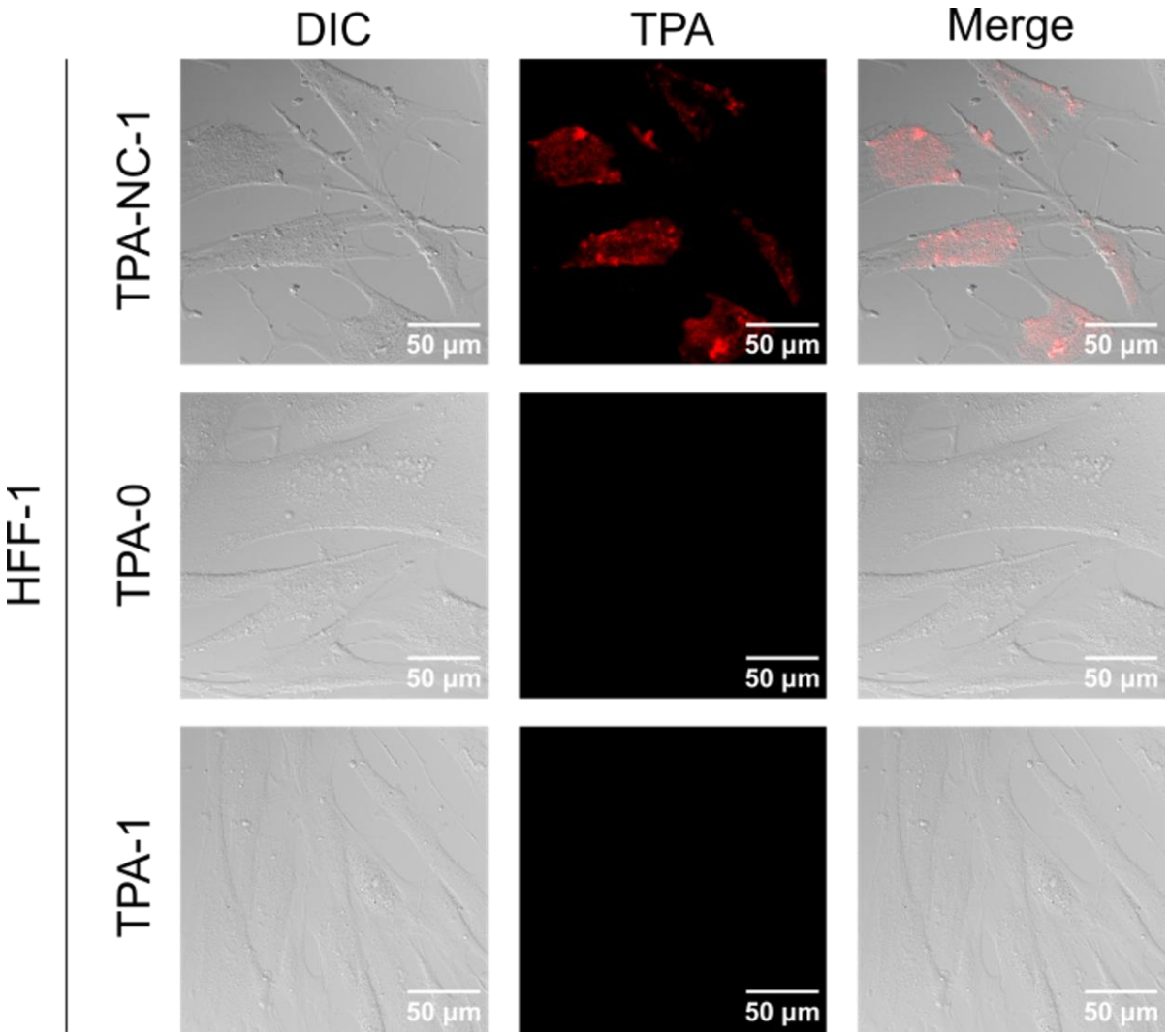

Figure 2.4. DIC and fluorescence image of HFF-1 cells after incubation with TPA-NC-1 (10 μM), TPA-0 (10 μM) or TPA-1 (10 μM). The excitation wavelength for TPA compounds was 550 nm. The emission was collected from 590 nm to 670 nm (ET630/75m filter).

Apart from improving water solubility and reducing cytotoxicity, the two quaternary ammonium groups were also designed to increase binding towards bacteria. The surface of the bacteria is negatively charged, which is mainly due to the presence of the anionic lipoteichoic acid (LTA) and wall teichoic acid (WTA) in the Gram-positive bacteria and lipopolysaccharide (LPS) in the Gram-negative bacteria (**Figure 2.5**). The addition of the positively charged quaternary ammonium groups was expected to increase the binding between the PS and these negatively charged molecules on the surface of the bacteria. A fluorescent dye, BODIPY™ TR Cadaverine (BTRC), was used to determine the binding between TPA compounds and LTA from *S. aureus* or LPS from *P. aeruginosa*.[122] The fluorescence signal of BRTC was initially quenched when binding with LTA or LPS. However, an intense fluorescence signal at 620 nm was generated if BRTC was displaced by LTA or LPS binding molecules (**Figure 2.6a**).[122, 123, 133] As shown in **Figure 2.6b**, TPA-0 displaced BTRC from *S. aureus* LTA and *P. aeruginosa* LPS more effectively than TPA-NC-1, suggesting that TPA-0 had a stronger binding affinity toward *S. aureus* LTA and *P. aeruginosa* LPS than TPA-NC-1. Therefore, the addition of quaternary ammonium groups can improve water solubility, reduce cytotoxicity and enhance the binding affinity towards bacteria.

Based on the structure of TPA-0, TPA-1 was synthesized by modifying the ethyl group on the benzothiazolium to 1-butyne. TPA-1 not only preserves the desirable properties of TPA-0, such as similar water solubility and LTA/LPS binding affinity (**Figure 2.3b, Figure 2.6b**), but also exhibits lower cytotoxicity. The CC_{50} of TPA-1 against HFF-1 cells was 260 ± 40 μM, which was higher than that of TPA-0 (**Figure 2.3c**). The ROS generation assays were conducted using commercial fluorescent probes for the detection of ROS. DHR123, HPF, and SOSG were used to detect non-specific ROS, hydroxyl radical (Type I), and singlet oxygen (Type II), respectively. After mixing TPA-1 or TPA-0 with the ROS detection probes, the fluorescence signals increased gradually with the irradiation time using 600 nm (60 mW/cm^2) light,

including both Type I and Type II ROS. (**Figure 2.7a**). In contrast, when incubating TPA-1 or TPA-0 with the ROS probes in the dark, only a minimal amount of fluorescence signal was generated (**Figure 2.7b**). These indicated that ROS generation from TPA-1 and TPA-0 was triggered by irradiation of 600 nm light. In addition, TPA-1 and TPA-0 had similar fluorescence intensities on DHR123 and SOSG, while TPA-1 showed a slightly higher fluorescence intensity on HPF than TPA-0. Overall, the modification of the ethyl group to 1-butyne has improved the properties of TPA-1. Given these enhanced properties, it is suggested that TPA-1 is a PS worthy of further study in its antibacterial performance.

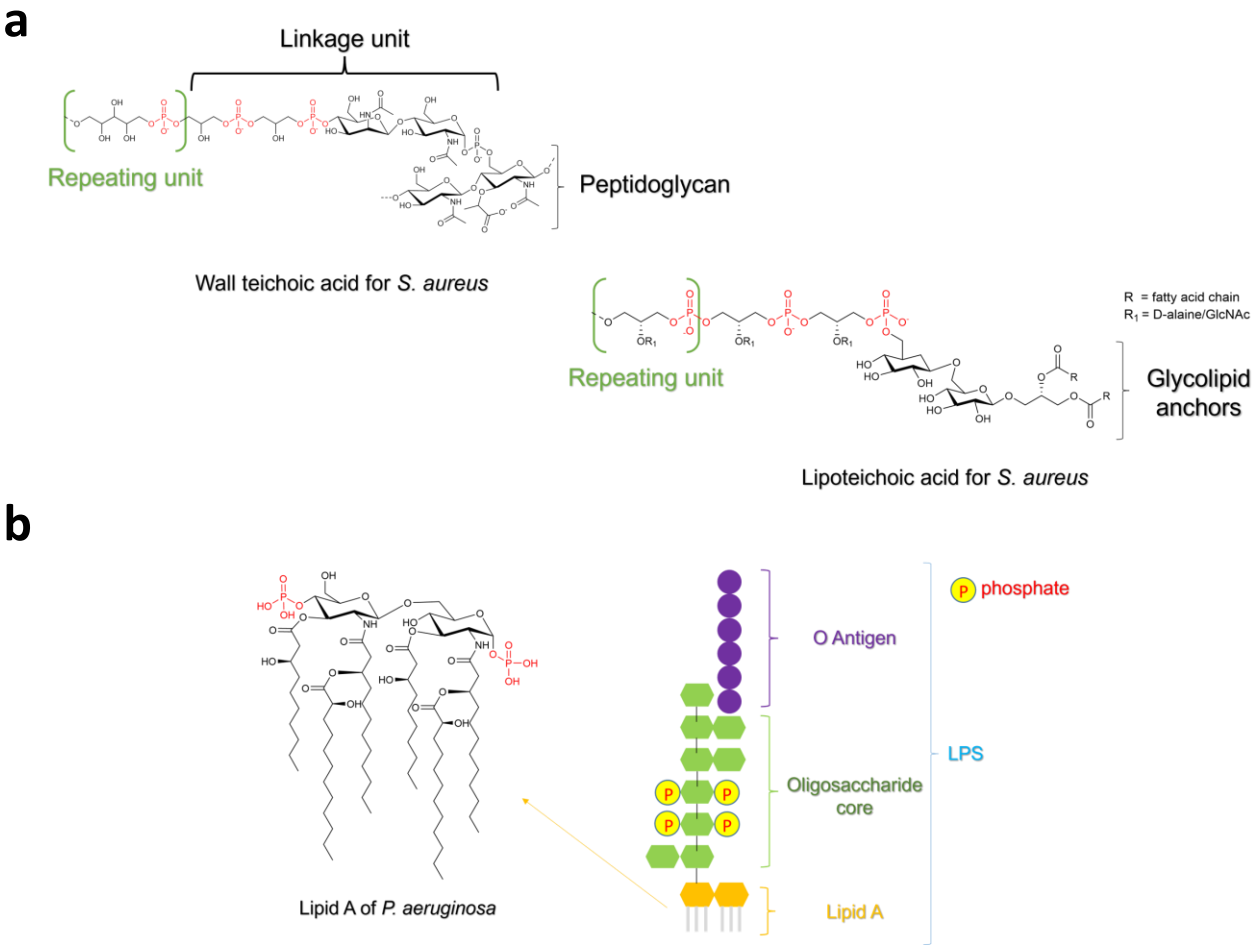

Figure 2.5. (a) The structure of wall teichoic acid (WTA) and lipoteichoic acid (LTA) of *S. aureus*. (b) An illustration of the lipopolysaccharide (LPS) of *P. aeruginosa.* The LPS contains three domains: lipid A, the oligosaccharide core, and the O-antigen. The charges on LPS are mainly derived from the phosphates and the acid groups in the lipid A head group and the oligosaccharide core.[134]

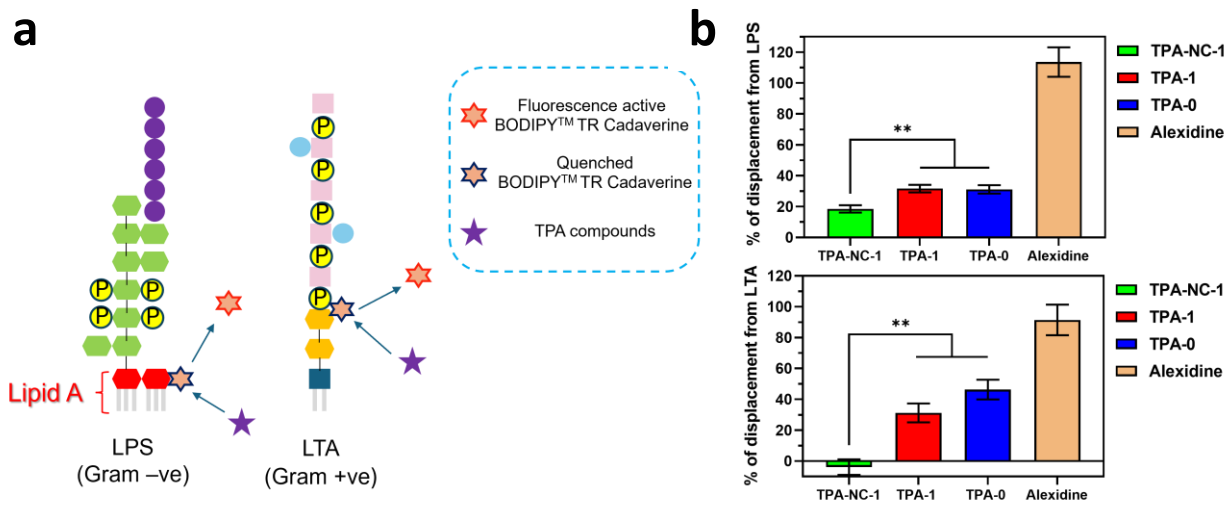

Figure 2.6. (a) Illustration of LTA/LPS binding assays using BODIPY^{TM} TR Cadaverine (BTRC). (b) The LTA/LPS binding assay results for TPA compounds (10 μM). Alexidine (10 μg/mL) was used as a positive control. Data are presented as the mean ± SD, n = 3 per group. ** p value < 0.01.

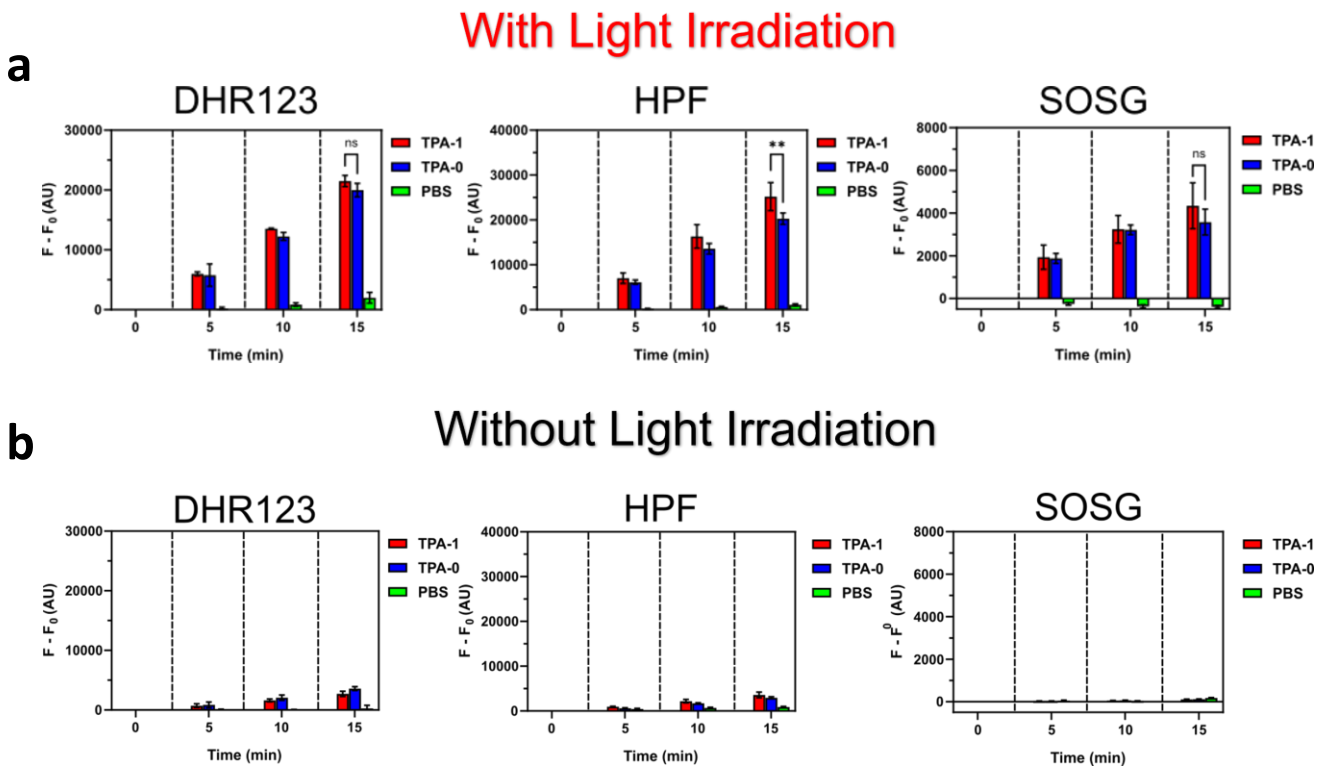

Figure 2.7. The ROS generation assay results of TPA-1 (10 μM) and TPA-0 (10 μM) (a) with or (b) without 600 nm light irradiation (60 mW/cm^2) for 0 to 15 minutes. PBS was used as the negative control. DHR123, HPF, and SOSG were used to detect non-specific ROS, hydroxyl radical, and singlet oxygen, respectively. Data are presented as the mean ± SD, n = 3 per group. ** p value < 0.01, ns (not significant) p value > 0.05.

2.3.2 Antiplanktonic Activities of TPA-1 without Light Irradiation

Fluorescence imaging was first used to validate the binding of TPA-1 towards bacteria. **Figure 2.8** shows that TPA-1 can label both Gram-positive *S. aureus* and Gram-negative *P. aeruginosa.*

The minimum inhibitory concentrations (MICs) of TPA-1 on *S. aureus* (ATCC 29213), MRSA (BAA 41) and *P. aeruginosa* (ATCC 27853) were first tested to see if TPA-1 has any intrinsic antibacterial activities (**Table 2.1**). Surprisingly, TPA-1 showed excellent antibacterial activity against *S. aureus* and methicillin-resistant *S. aureus* (MRSA), even without light irritation. The MIC values of TPA-1 against *S. aureus* and MRSA were both found to be 3.13 μM, while no inhibition on *P. aeruginosa* was observed at concentrations ≤ 100 μM (**Table 2.1**). Also, the time-kill kinetics of TPA-1 on *S. aureus* showed that 2 × MIC of TPA-1 can eradicate 10^5 CFU/mL of *S. aureus* in 2 hours, which is more rapid than 2 × MIC of vancomycin (**Figure 2.9**). The rapid killing rate of TPA-1 indicated a bactericidal killing mode (≥ 3 log reduction) on *S. aureus*. Additionally, the resistance development assay of TPA-1 on *S. aureus* was conducted to assess the antibacterial ability over different bacterial passages. In **Figure 2.10**, TPA-1 only showed a ≤ 2-fold increase in MIC value, whereas the antibiotic control, norfloxacin, had increased over 1000-fold after 20 days of consecutive treatments. These results indicated that the consecutive treatment of TPA-1 did not lead to the development of significant resistance in *S. aureus*. The great antibacterial activity of TPA-1 without light irradiation has prompted further investigation into its underlying antibacterial mechanisms.

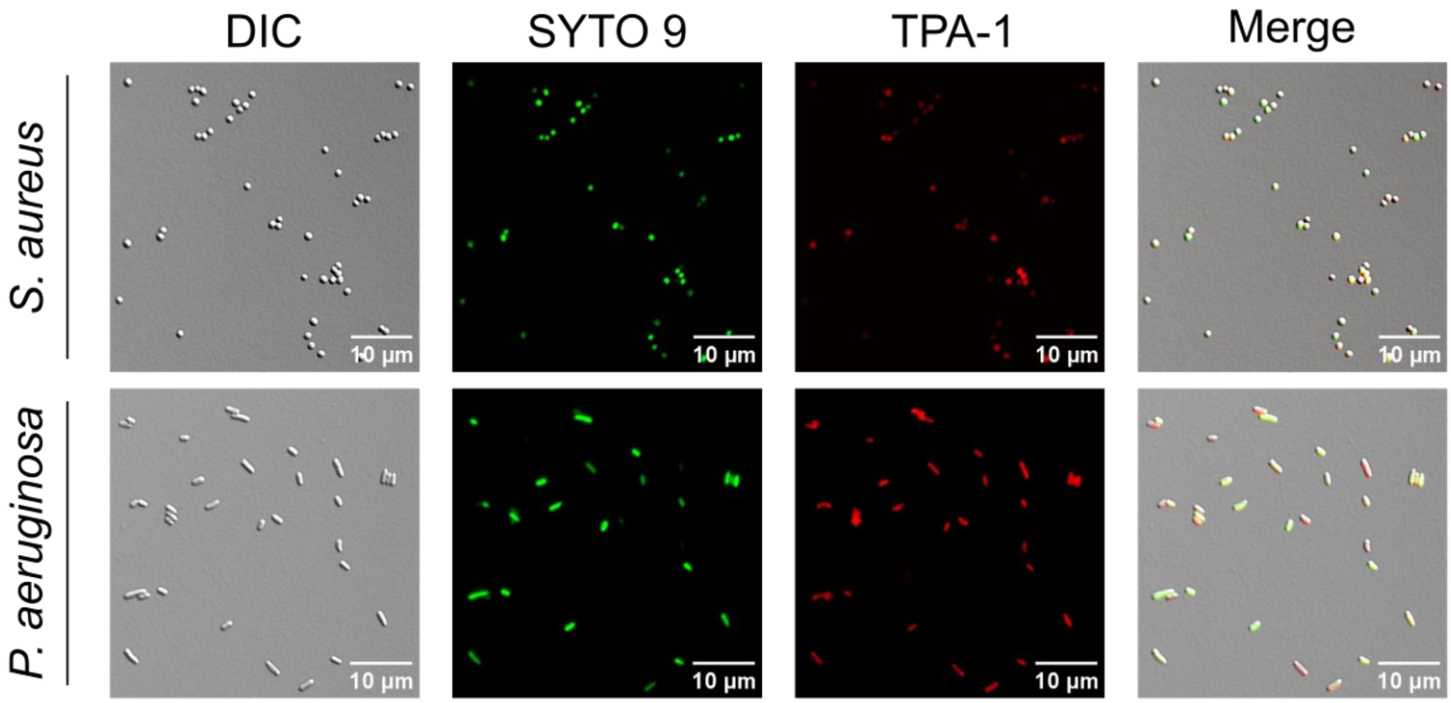

Figure 2.8. Fluorescence images of *S. aureus* and *P. aeruginosa* with SYTO 9 (2.5 μM) and TPA-1 (20 μM). SYTO 9 is a commercially available DNA stain. The excitation wavelengths for SYTO 9 and TPA-1 were 490 nm and 550 nm, respectively. The emissions for SYTO 9 and TPA-1 were collected from 500 nm to 550 nm (ET525/50m filter) and 590 nm to 670 nm (ET630/75m filter), respectively.

Table 2.1. The minimum inhibitory concentrations (MICs) of TPA-1 and control antibiotics on different bacteria.

Compound	*S. aureus* (ATCC 29213)	Methicillin-resistant *S. aureus* (BAA 41)	*P. aeruginosa* (ATCC 27853)
TPA-1	3.13 μM	3.13 μM	> 100 μM
Vancomycin	0.625 μM	0.625 μM	Not determined
Meropenem	0.313 μM	Not determined	2.5 μM

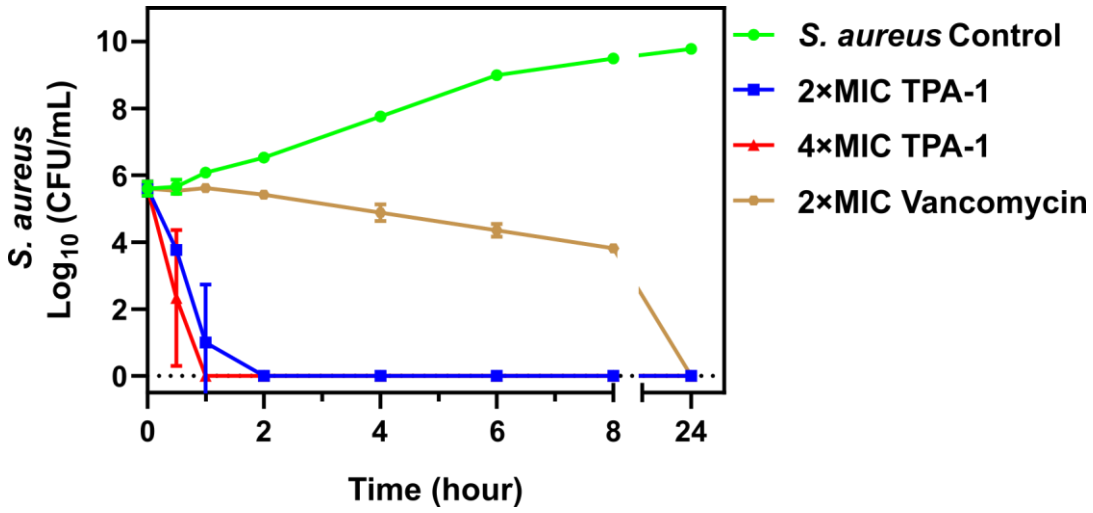

Figure 2.9. The time-kill kinetics of 2 × MIC TPA-1 (6.25 μM), 4 × MIC TPA-1 (12.5 μM), and 2 × MIC vancomycin (1.25 μM) against *S. aureus*. Data are presented as the mean ± SD, $n = 3$ per group.

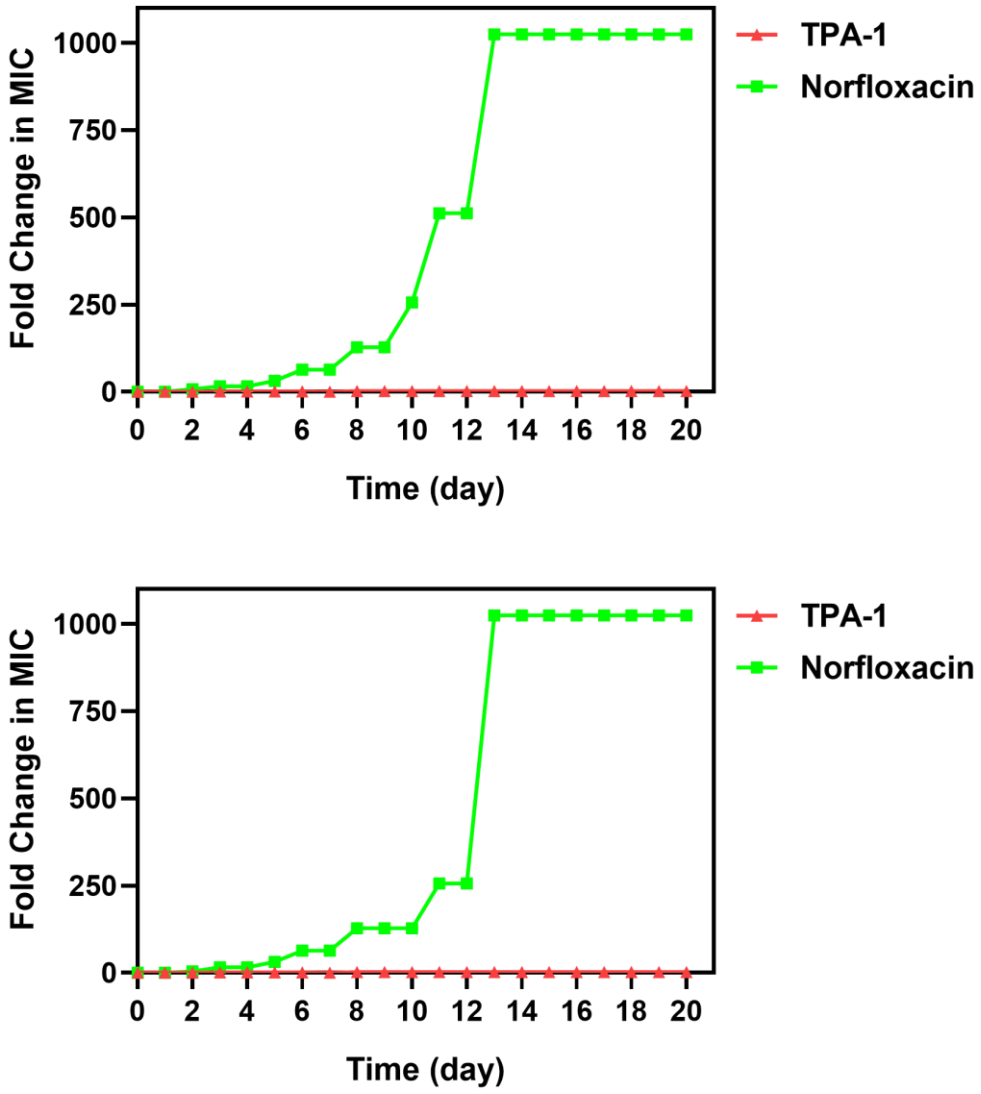

Figure 2.10. The two independent replicates of the resistance development assay results of TPA-1 and norfloxacin against *S. aureus* for 20 consecutive days.

2.3.3 Antibacterial Mechanisms of TPA-1 without Light Irradiation

The LTA binding assay showed that TPA-1 can bind to *S. aureus* LTA. Besides, the MIC value of TPA-1 against *S. aureus* increased upon the addition of *S. aureus* LTA (**Figure 2.11**). These results suggested that the binding of TPA-1 to LTA was important for its antibacterial effect.

Since *S. aureus* LTA is attached to the cytoplasmic membrane, it is logical to hypothesize that the positively charged TPA-1 might depolarize the *S. aureus* cell membrane and affect its integrity. To validate this idea, a membrane depolarization assay was conducted using Disc3(5), a cationic fluorescent dye with sufficient hydrophobicity that can accumulate in polarized cells.[135, 136] The fluorescence signal of Disc3(5) is quenched when it accumulates in polarized cells. If the cells are depolarized, the transmembrane potential drops toward zero, causing the release of Disc3(5) molecules from the cells and generating a fluorescence signal (**Figure 2.12**). From **Figure 2.13**, the addition of TPA-1 to a mixture of Disc3(5) and *S. aureus* caused an increase in the fluorescence signal of Disc3(5), suggesting the release of Disc3(5) from *S. aureus*. A higher concentration of TPA-1 also induced a more rapid increase in fluorescence. These findings indicated that TPA-1 could cause the depolarization of *S. aureus* membrane in a concentration-dependent manner.

In addition to examining membrane depolarization, scanning electron microscopy (SEM) was used to study the morphology of *S. aureus* after TPA-1 treatment. As shown in **Figure 2.14**, collapses of the cell envelope were found on the TPA-1-treated *S. aureus*, suggesting damage to the bacterial cell membrane.

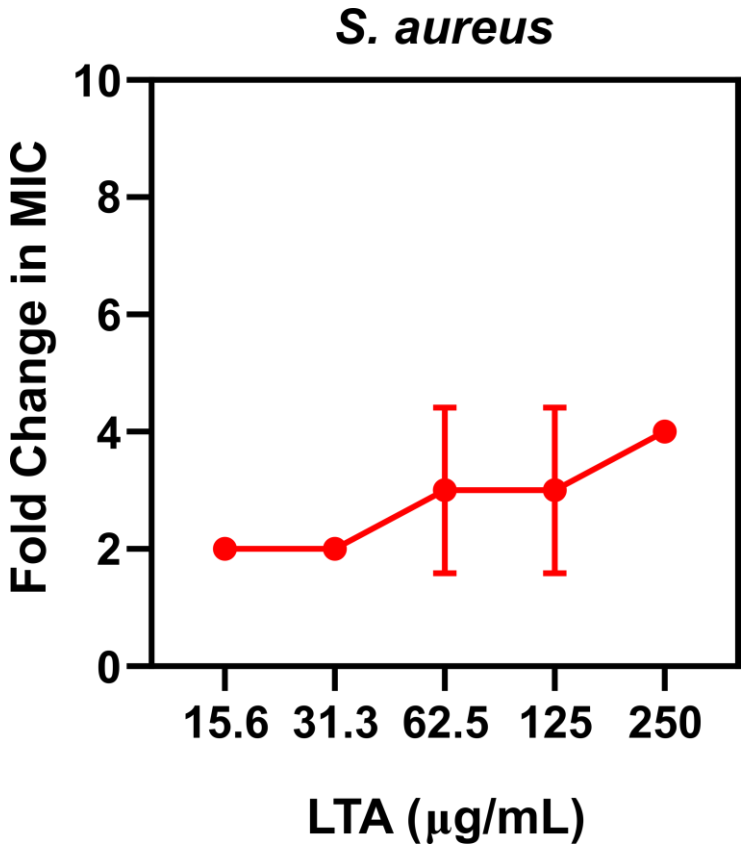

Figure 2.11. The fold change in MIC of TPA-1 after the addition of *S. aureus* LTA. Data are presented as the mean ± SD, $n = 2$.

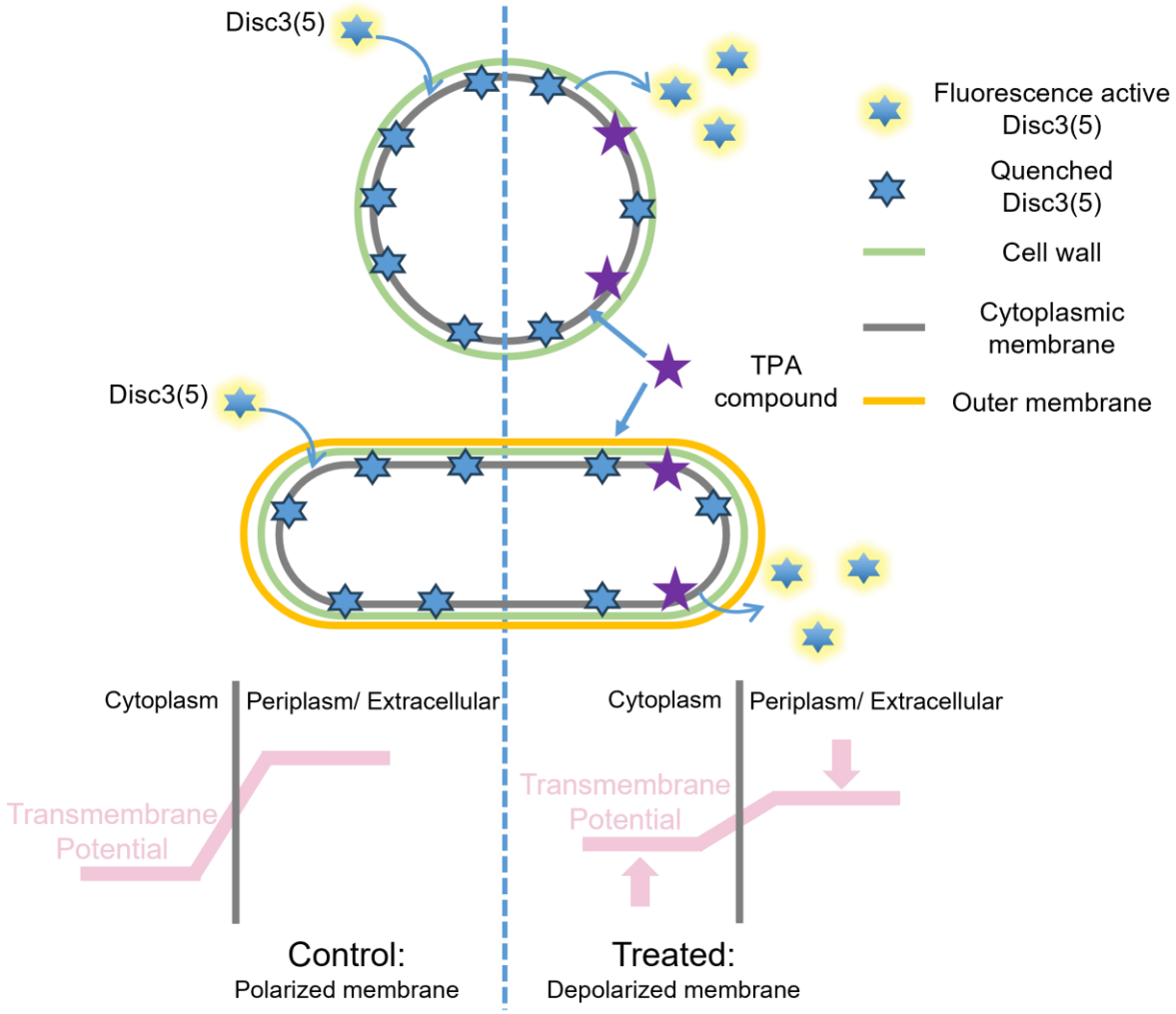

Figure 2.12. An illustration shows the principle of Disc3(5) assay.

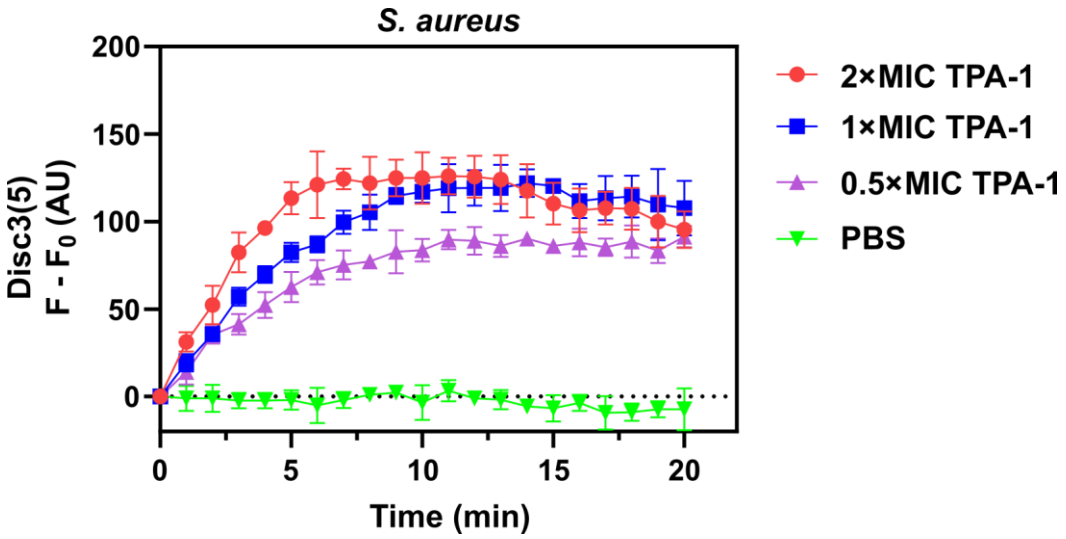

Figure 2.13. Membrane depolarization assay results of TPA-1 on *S. aureus* using Disc3(5). Data are presented as the mean ± SD, $n = 3$ per group.

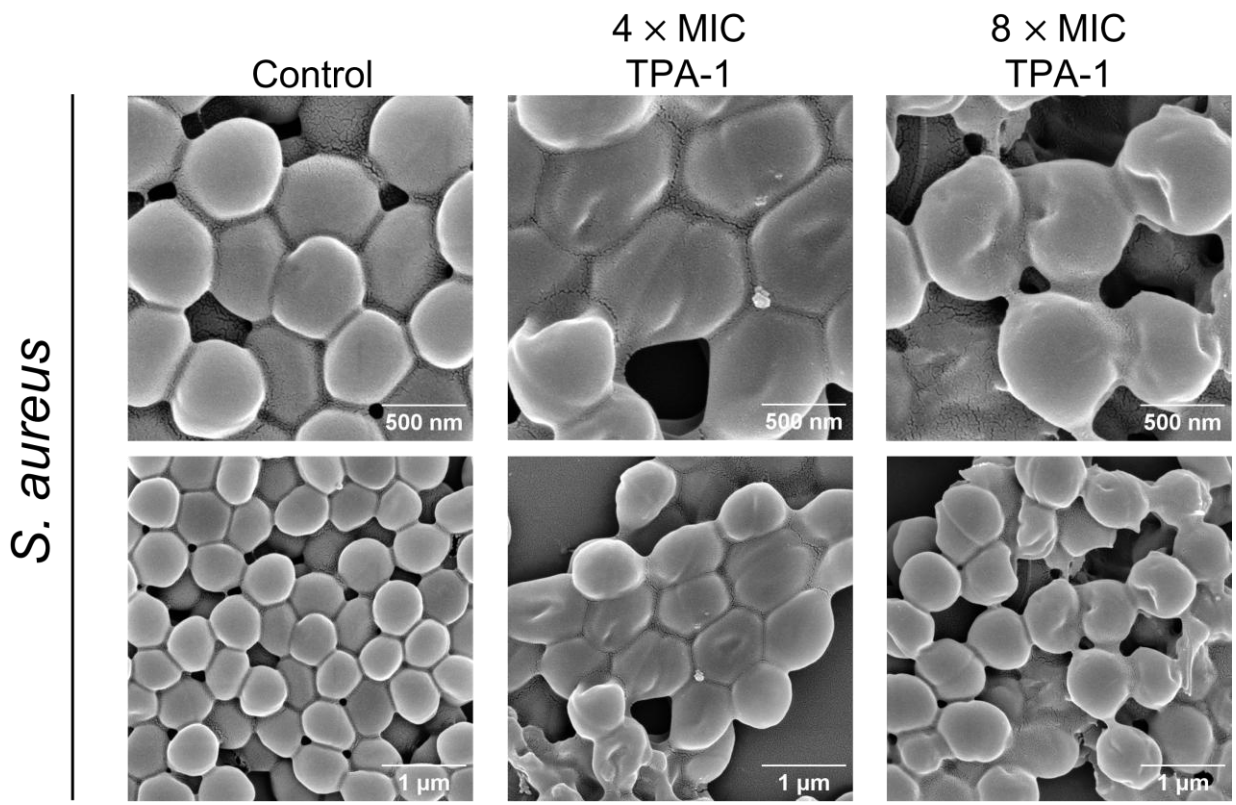

Figure 2.14. The SEM images of *S. aureus* incubated with 4 × MIC (12.5 μM) and 8 × MIC (25 μM) of TPA-1 for 3 hours in the dark.

Additionally, TPA-1 also showed binding affinity towards *S. aureus* genomic DNA. As shown in **Figure 2.15**, the DNA bands of the sample with the addition of 4 μM or 10 μM TPA-1 were upshifted. This phenomenon was also observed in the SYTOX Green positive control group. This shift in band position might result from an increase in the molecular weight and a decrease in the net negative charge of the DNA upon TPA-1 binding. Also, a decrease in band intensities of the DNA + TPA-1 samples was observed, likely due to the binding of TPA-1 to DNA, which hindered the binding of the DNA gel stain (SYBR Safe) to the DNA.

Furthermore, TPA-1 inhibited the negative supercoiling activity of *S. aureus* DNA gyrase. DNA gyrase is an enzyme that converts relaxed double-stranded DNA to negatively supercoiled DNA.[137] The negative supercoiling provides torsional strain to the DNA strand, which can lower the energy required for DNA double-strand separation.[138] Biological processes that are required for unwinding the DNA strand, such as DNA replication and transcription, are promoted by negative supercoiling.[139-141]. In the gel image (**Figure 2.16a**), the addition of *S. aureus* DNA gyrase to the relaxed DNA caused the DNA band to shift towards the bottom of the gel. This shift occurred because the supercoiled DNA has a higher charge density than the relaxed DNA. When TPA-1 was added to the enzyme reaction mixture, the intensity of the supercoiled DNA band decreased with increasing concentration of TPA-1. At 25 μM of TPA-1, the supercoiled DNA band disappeared, and the remaining DNA band resembled the negative control band containing only the substrate plasmid (pBR322) with 25 μM of TPA-1 (**Figure 2.16b**). These results indicated that TPA-1 could disrupt the DNA supercoiling process of *S. aureus* DNA gyrase.

In summary, even without light irradiation, TPA-1 can efficiently eradicate *S. aureus* by affecting the bacterial membrane integrity and inhibiting the DNA supercoiling process.

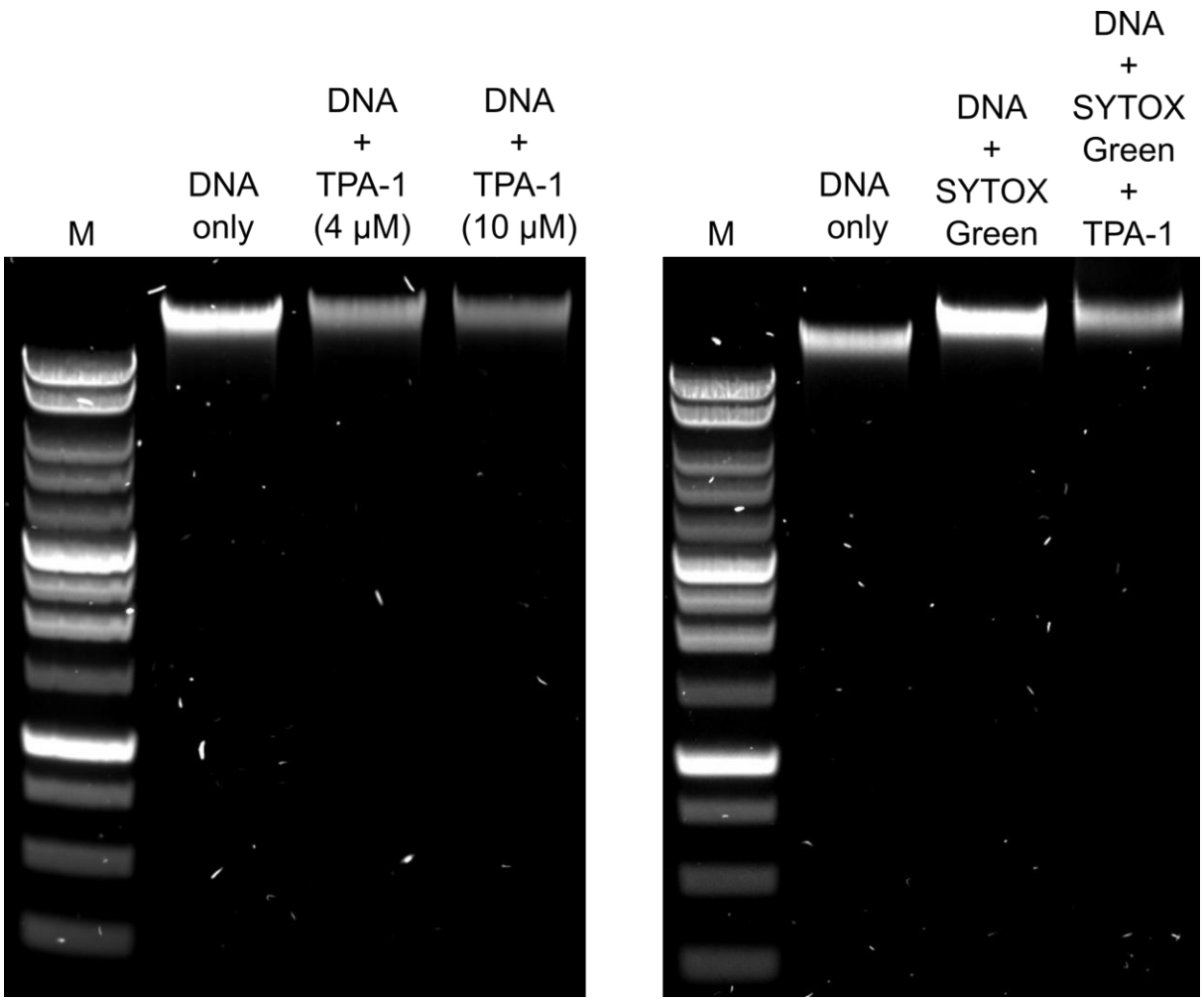

Figure 2.15. The DNA gel (0.8% agarose) images of TPA-1 or SYTOX Green mixed with genomic DNA of *S. aureus*. STYOX Green is a commercial DNA stain. M represented the DNA marker.

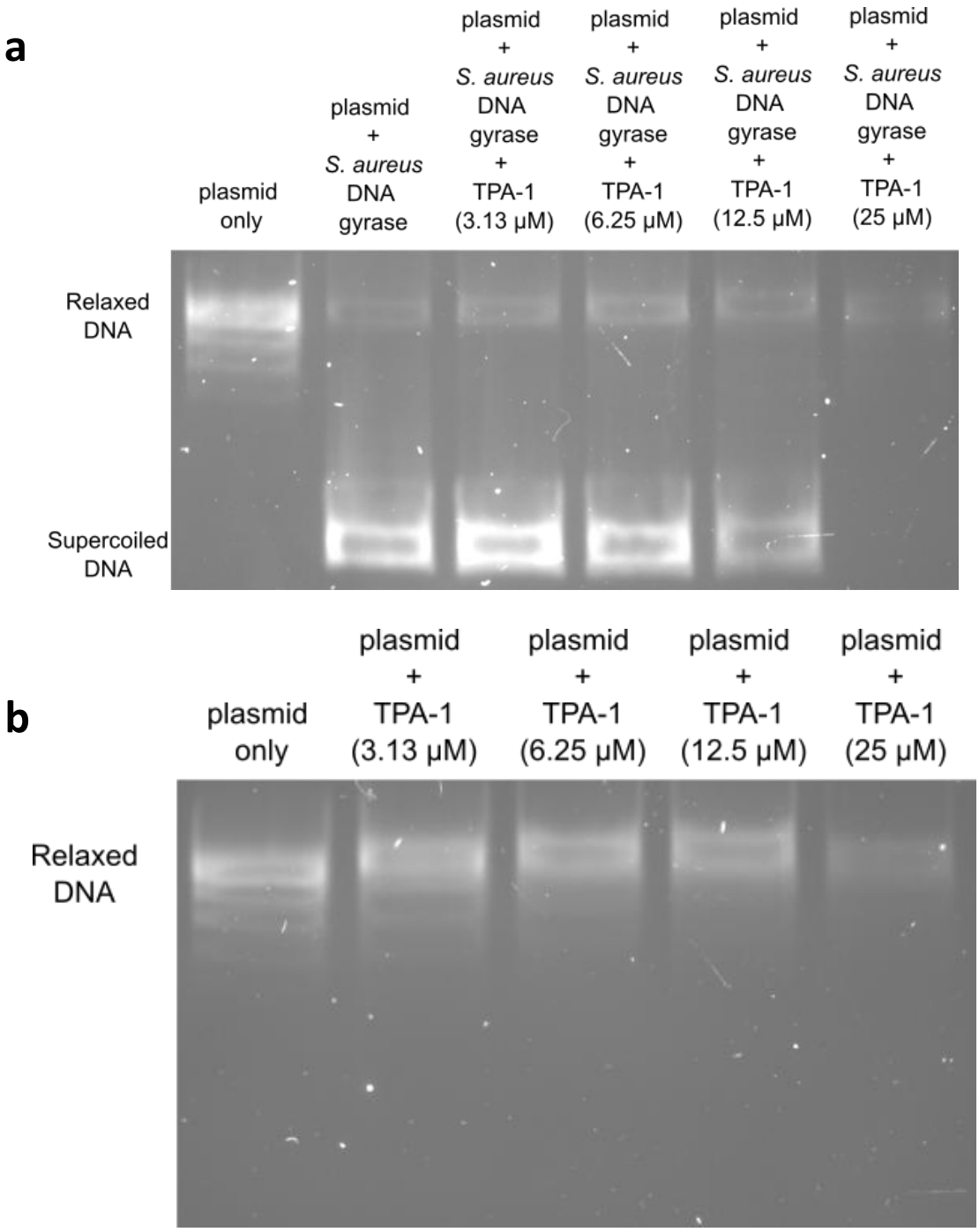

Figure 2.16. (a) The DNA gel (1% agarose) image showed the supercoiling inhibition activity of TPA-1. (b) The DNA gel (1% agarose) image of the substrate DNA in *S. aureus* DNA gyrase assay mixed with TPA-1.

2.3.4 Mass Spectrometry (MS)-Based Proteomic Study on TPA-1-Treated *S. aureus* without Light Irradiation

To further investigate the antibacterial effects of TPA-1 on *S. aureus* without light irradiation, mass spectrometry (MS)-based proteomic analysis was performed on *S. aureus* treated with 2 × MIC of TPA-1 for 1 hour in the dark (**Figure 2.17**). A total of 631 unique protein groups were identified, and 578 of them were considered as differentially expressed proteins (DEPs) based on *p*-value less than 0.05 and Log_2(Fold change) larger than 1 or less than -1. Among the DEPs, 524 proteins were downregulated, and 54 proteins were upregulated (**Figure 2.17a**). Gene ontology (GO) and Kyoto Encyclopedia of Genes and Genomes (KEGG) pathway enrichment analysis were then conducted on the genes corresponding to DEPs, using the PANTHER Classification System and the clusterProfiler package in RStudio.[126-128] The GO enrichment analysis categorized the DEPs into biological processes, molecular functions, and cellular components (**Figure 2.17b - Figure 2.17d**). The KEGG enrichment analysis also identified one major KEGG pathway (**Figure 2.17e**). Among all the GO and KEGG pathway terms, three biological processes, which included cytokinesis, peptidoglycan biosynthetic process, and tRNA aminoacylation for protein translation, were selected for further investigation as they are important for bacterial viability. The Log_2(Fold change) of the DEPs that are involved in these biological processes are shown in **Figure 2.17f**.

Cytokinesis and peptidoglycan synthesis are crucial biological processes during bacterial cell division and growth. All identified proteins in both processes were downregulated after one hour of treatment with 2 × MIC of TPA-1. For cytokinesis, the expression levels of FtsZ, FtsA, SepF, and DivlB were decreased. FtsZ is a tubulin-like protein that polymerizes at the midcell to form the Z ring at the beginning of bacterial cell division.[142] The Z ring will further act as a platform to recruit other division proteins for divisome assembly and guide septal cell wall synthesis.[143, 144] FtsA and SepF help the Z ring to anchor to the bacterial membrane while DivlB

accompanies the FtsW/PBP1 complex for cell constriction.[145-147] TPA-1 caused the downregulation of these proteins, which might interfere with the formation of the divisome and further inhibit cell division. In terms of peptidoglycan synthesis, several proteins related to peptidoglycan precursor synthesis, such as the Mur family proteins (MurB, MurC, MurD, MurF, MurG, and MurI), D-alanine ligase (ddl), and alanine racemase 1 (alr1), were downregulated, indicating that TPA-1 could also affect the cell wall synthesis of *S. aureus*.[148] Additionally, treatment with TPA-1 led to the downregulation of ten tRNA-ligases in *S. aureus*. tRNA-ligases are essential for protein translation as they catalyse the attachment of amino acids to the corresponding tRNA. The decrease in tRNA-ligase expression may result in poor translation efficiency. In summary, the proteomic study on planktonic *S. aureus* revealed that TPA-1 without light irradiation might affect cell division, cell wall synthesis, and translation efficiency in *S. aureus*.

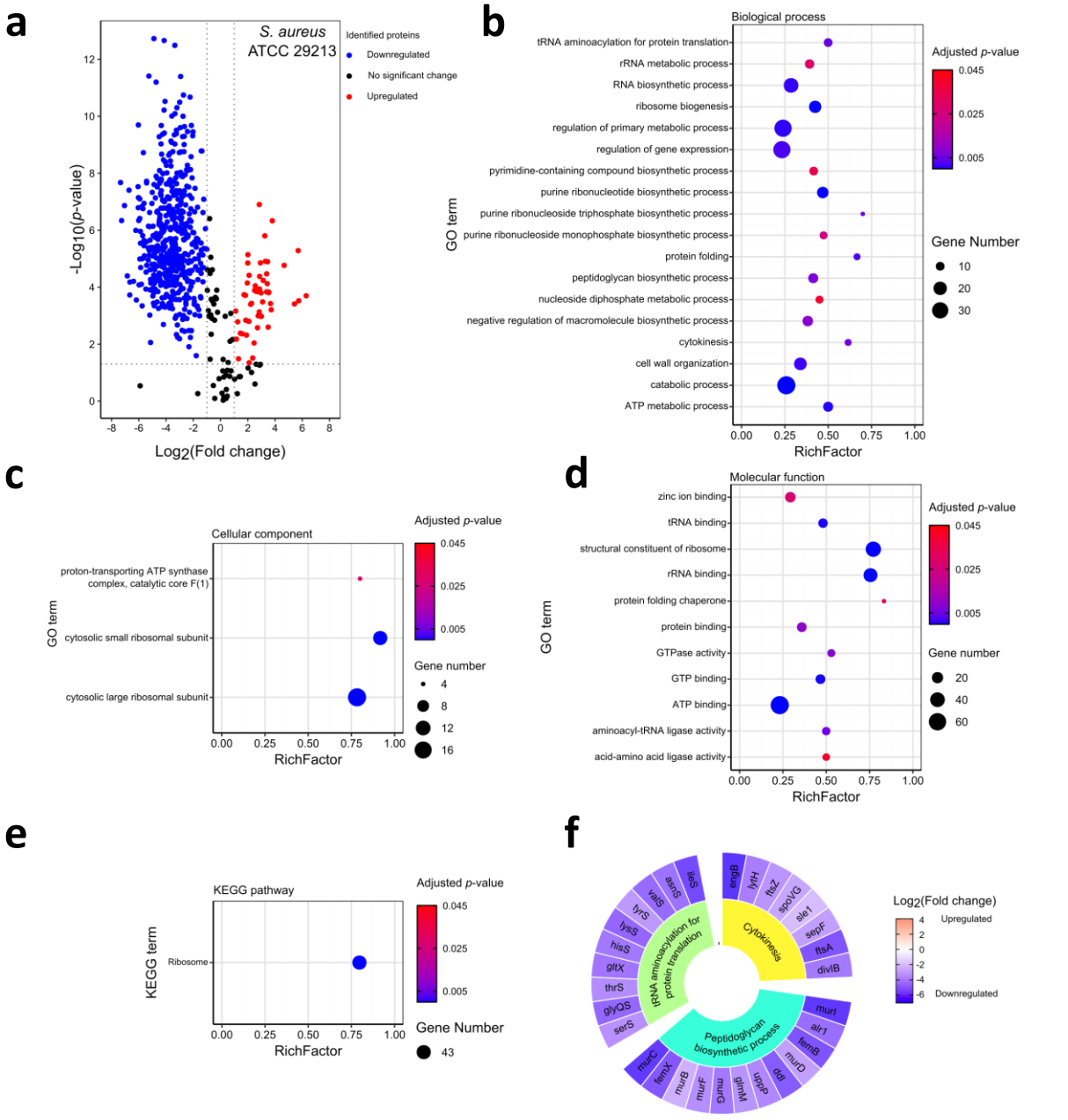

Figure 2.17 (a) Volcano plot showed the differentially expressed proteins (DEP)s in TPA-1 (2 × MIC, 6.25 μM)-treated *S. aureus* versus control *S. aureus* after an hour of incubation at 37℃ in the dark. (b) Biological function, (c) cellular component, (d) molecular function GO enrichment, and (e) KEGG pathway enrichment analysis of the corresponding genes of the DEPs in TPA-1-treated *S. aureus*. (f) Selected biological processes in *S. aureus* that were affected by TPA-1. Inner blocks are the names of the selected biological processes. Outer blocks show the fold change of the DEPs, which are represented by their gene names, in the corresponding biological processes. Three independent biological replicates were performed in this proteomic study.

2.3.5 Antiplanktonic Activities of TPA-1 with Light Irradiation

The PDT efficiency of TPA-1 on *S. aureus* and *P. aeruginosa* were assessed by irradiating the bacterial samples with a 300 W Xenon Lamp installed with a 420-780 nm UV-visible cut filter and a 600 nm band-pass filter (**Figure 2.18**). The final output light density was 50-60 mW/cm^2. The optimal therapeutic window for PDT is between 600 nm and 800 nm, as tissue absorption is lower in this range and it provides enough energy for PS to generate ROS.[149] Therefore, 600 nm light was chosen as the wavelength for conducting the antibacterial assays rather than 540 nm, which is the absorption maximum for TPA-1.

As shown in **Figure 2.19**, 2 μM of TPA-1, which was the sub-MIC of TPA-1 against *S. aureus*, was able to eradicate 99.2% ± 0.7% (2.2 ± 0.4 log CFU/mL reduction) of *S. aureus* and 99.96% ± 0.03% (3.4 ± 0.2 log CFU/mL reduction) of *P. aeruginosa* in 30 minutes of irradiation. If the irradiation was extended to 45 minutes, TPA-1 was capable of reducing over 99.99% (>5 log CFU/mL reduction) of *S. aureus* and *P. aeruginosa*. In contrast, irradiating bacteria with 600 nm light in PBS did not affect their viability. These results indicated that the PDT with TPA-1 could effectively eradicate both Gram-positive and Gram-negative bacteria.

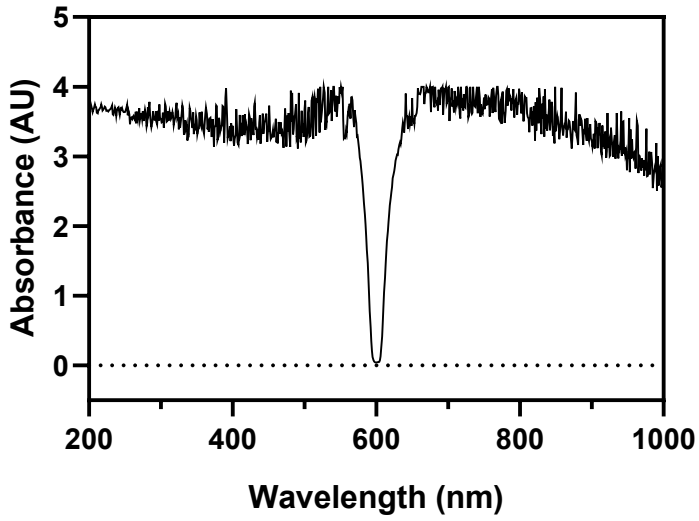

Figure 2.18. The absorption spectrum of the combined 420-780 nm UV-visible cut filter and the 600 nm band-pass filter.

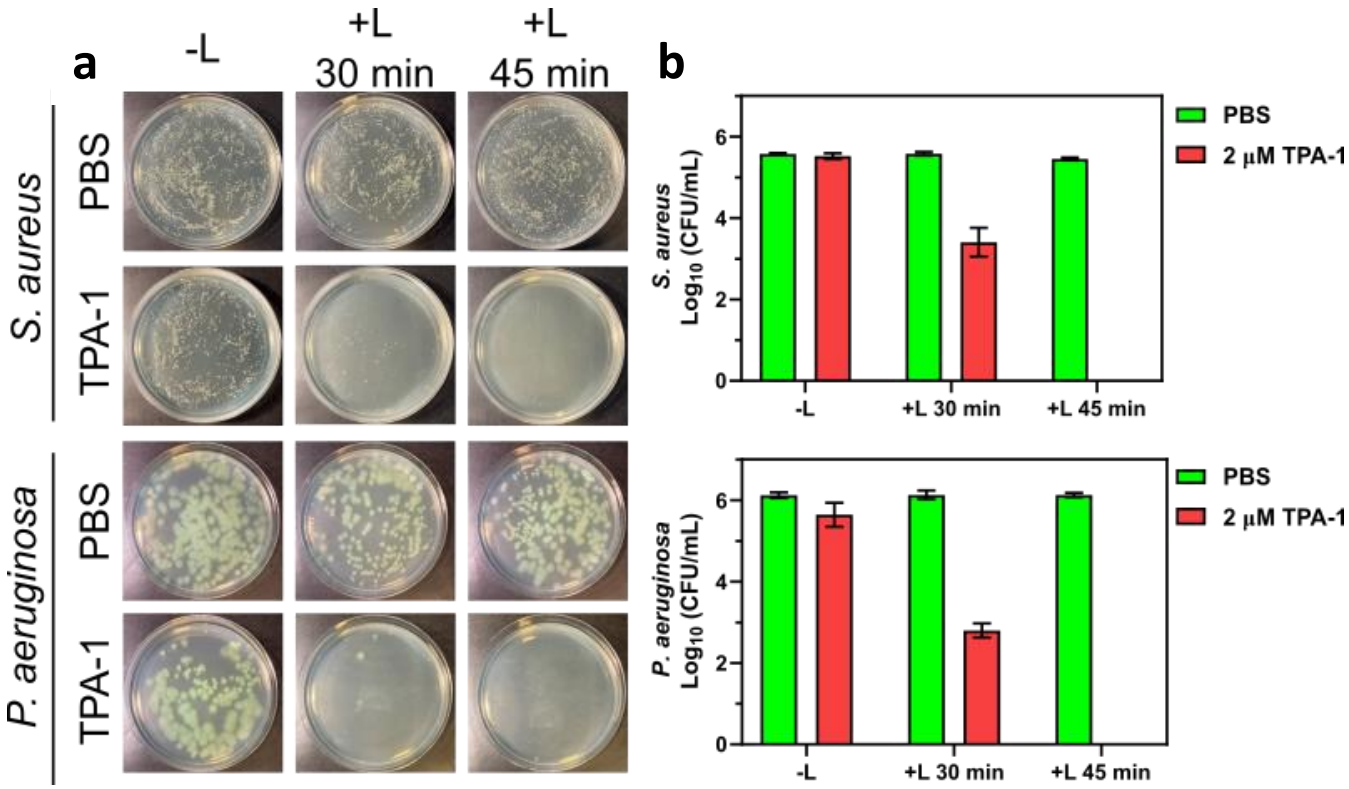

Figure 2.19. (a) Photographs of the LB agar plates and (b) the number of viable planktonic bacteria after PDT with TPA-1. -L: without light irradiation. +L: with 600 nm light irradiation (60 mW/cm2). Data are presented as the mean ± SD, n = 3 per group.

2.3.6 Antiplanktonic Mechanism of TPA-1 with Light Irradiation

The previous BTRC assays showed that TPA-1 could bind with LTA and LPS (**Figure 2.6b**), which are located on the respective bacterial membranes of *S. aureus* and *P. aeruginosa*. Therefore, the ROS generated by TPA-1 is expected to damage the bacterial membrane.

SEM images of *S. aureus* and *P. aeruginosa* were taken to investigate the PDT effect of TPA-1 on bacterial morphologies (**Figure 2.20)**. Intact surfaces were found on bacteria in the PBS control groups with and without irradiation, indicating that light irradiation alone did not affect bacterial morphology. In contrast, shrinkages and collapses were found on *S. aureus* and *P. aeruginosa* after PDT with TPA-1, suggesting damage to the cell envelope. Additionally, the changes in the DNA and protein contents in the supernatants from different treatments of *S. aureus* and *P. aeruginosa* were monitored by recording the absorbances at 260 nm (DNA) and 280 nm (Protein). As shown in **Figure 2.21**, the supernatants for *S. aureus* and *P. aeruginosa* after PDT with TPA-1 showed higher absorptions at 260 nm and 280 nm than the control groups, indicating that PDT with TPA-1 could cause DNA and protein leakage from the bacteria. Since the DNA and protein should be kept inside the cell by the bacterial membrane, these results, along with the SEM images, implied that the PDT with TPA-1 eradicated planktonic *S. aureus* and *P. aeruginosa* by causing bacterial membrane damage.

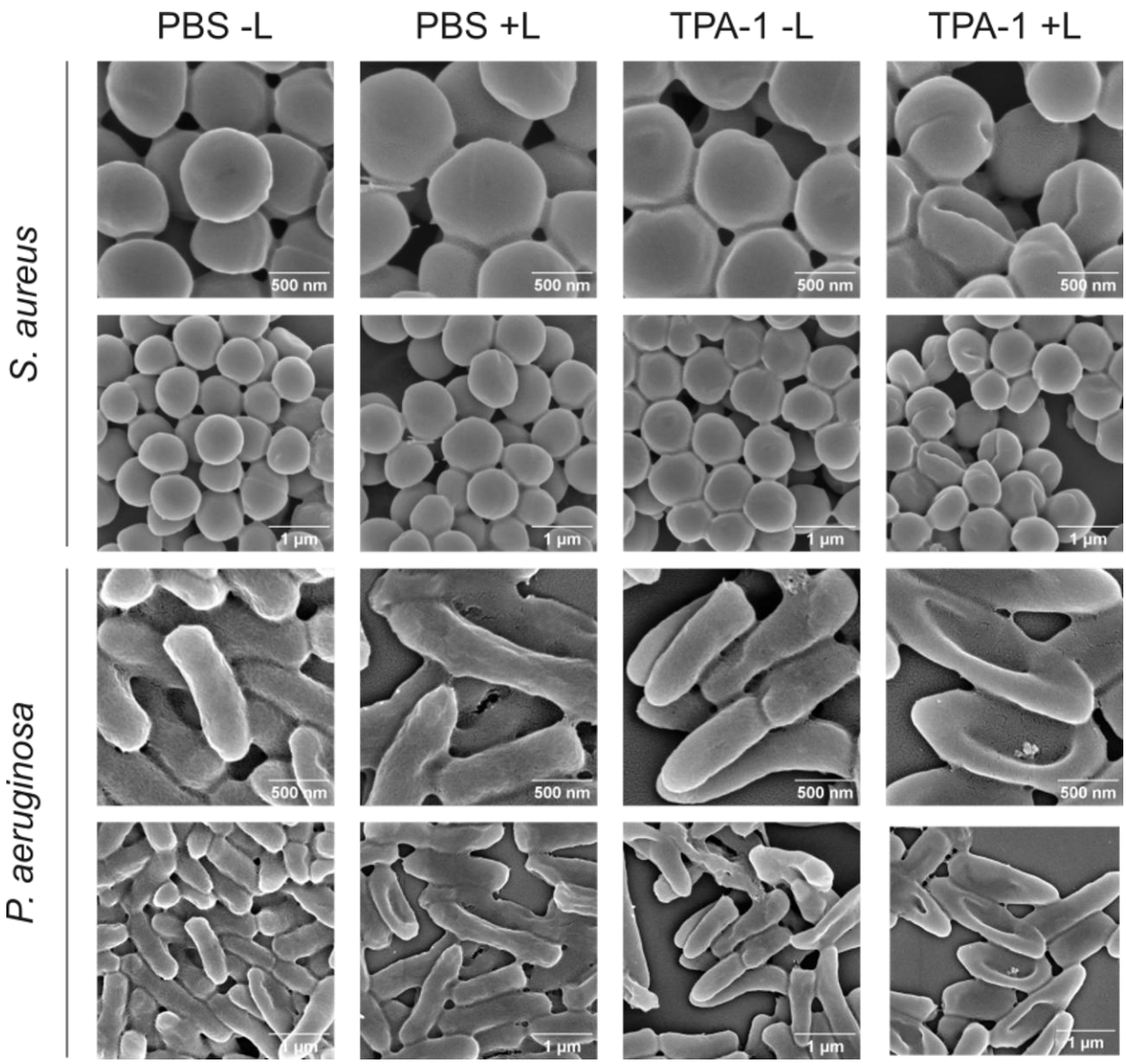

Figure 2.20. SEM images of *S. aureus* and *P. aeruginosa* after PDT with TPA-1 (10 µM). -L: without light irradiation. +L: with 600 nm light irradiation (60 mW/cm^2) for 45 minutes.

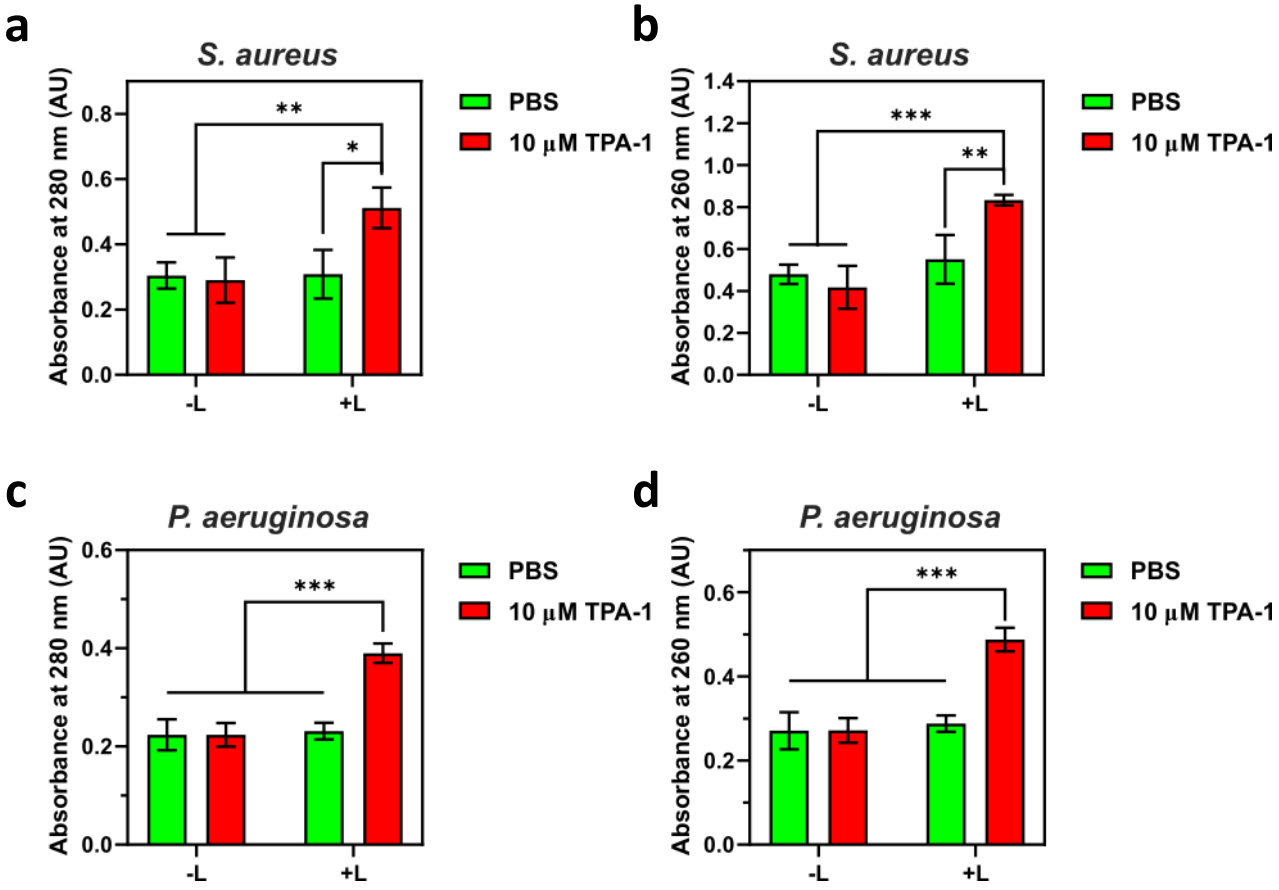

Figure 2.21. DNA/RNA and protein leakage after the PDT with TPA-1 were detected by the absorption at 260 nm and 280 nm, respectively. (a, b) Protein and DNA/RNA leakage from *S. aureus*. (c, d) Protein and DNA/RNA leakage from *P. aeruginosa*. -L: without light irradiation. +L: with 600 nm light irradiation (60 mW/cm^2) for 45 minutes. Data are presented as the mean ± SD, n = 3 per group. * p-value < 0.05, ** p-value < 0.01 and *** p-value < 0.001

2.4 Chapter II Summary

In summary, a novel antibacterial AIE PS, TPA-1, was synthesized. Compared to the previously reported TPA-NC-1, TPA-1 contains two quaternary ammonium groups, which help to improve the water solubility, enhance binding towards *S. aureus* LTA and *P. aeruginosa* LPS, and decrease the cytotoxicity against HFF-1 cells. Modifying the benzothiazolium group can further decrease cytotoxicity. Unlike conventional PSs, TPA-1 shows excellent antibacterial activity against *S. aureus* even without light irradiation. This property is due to the intrinsic antibacterial activity of TPA-1, which causes membrane damage and inhibits the DNA supercoiling activity of *S. aureus* DNA gyrase. Proteomic study also revealed that TPA-1 treatment could affect several biological processes in *S. aureus*, including cell division, cell wall synthesis, and translation. Upon light irradiation, TPA-1 shows broad-spectrum antibacterial activity against Gram-positive *S. aureus* and Gram-negative *P. aeruginosa* by causing damage to their bacterial cell membranes.

Chapter III

Assessments on the Antibiofilm Activity, Potential Off-Target Effects, and *In Vivo* Efficacy of TPA-1

3.1 Introduction

In biofilm-related infections, bacteria can encase themselves in self-produced extracellular polymeric substances (EPS) so that they are shielded from immune cells and antibiotics in the infected area.[6, 150] Apart from EPS, bacteria can alter their metabolic rate to adapt to the changes in environmental pressure, thereby enhancing their tolerance against antibiotics.[15, 151] Many reported antibacterial agents, including small molecules, peptides, and PSs, show antibacterial activities against planktonic bacteria, yet they often fail in antibiofilm performance. [114, 118, 120, 152, 153]

In this chapter, the antibiofilm activities of the designed PS, TPA-1, are reported. Without light irradiation, TPA-1 can inhibit the formation of *S. aureus* biofilm. Upon light irradiation, TPA-1 can eradicate mature biofilms formed by *S. aureus* and *P. aeruginosa*. Additionally, assays related to selectivity, haemolytic activity and light toxicity towards human cells were conducted to assess the potential off-target effects of TPA-1. Furthermore, *in vivo* wound infection models were designed to evaluate the therapeutic efficacy of TPA-1 in treating methicillin-resistant *S. aureus* (MRSA) and *P. aeruginosa* infections.

The work presented in this chapter was published in the Journal of Medicinal Chemistry, titled "A Water-Soluble Aggregation-Induced Emission Photosensitizer with Intrinsic Antibacterial Activity as an Antiplanktonic and Antibiofilm Therapeutic Agent" by **Hung, C. -H.**, et al.

3.2 Materials and Methods

3.2.1 Materials and Instruments

Crystal violet and D-(+)-glucose were purchased from Sigma-Aldrich. Calcein AM was purchased from Invitrogen™. Human erythrocytes were purchased from HaemoScan. All other materials used for bacterial growth and incubation were the same as in Chapter II (Section **2.2.1**).

3.2.2 Photographs and Fluorescence Imaging of Bacterial Biofilms

Overnight culture of *S. aureus* or *P. aeruginosa* was diluted to 1×10^5 CFU/mL in TSB (with 1% glucose). 200 μL of the diluted bacterial culture was added to an 8-well chamber slide (Nunc™ Lab-Tek™ Chamber). The slide was incubated at 37℃ for 24 hours for biofilm formation. After incubation, the planktonic bacteria were removed carefully by a micropipette. For photograph taking, the biofilm was incubated with PBS or 20 μM of TPA-1 at 30℃ for 20 minutes. Then, the biofilm was washed with PBS (3 times). The photographs were taken using a Nikon Ti2 DS-Ri2 high-speed color camera. For fluorescence images, the biofilm was first incubated with SYTO 9 (2.5 μM) at room temperature for 15 minutes. SYTO 9 solution was removed after incubation using a micropipette. 20 μM of TPA-1 or PBS was added to the biofilm and incubated at 30℃ for 20 minutes. The TPA-1 solution or PBS was removed using a micropipette right before taking the fluorescence images. The fluorescence images were taken with a Nikon Ti2 Eclipse DS-Qi2 CMOS camera. The excitation wavelengths for SYTO 9 and TPA-1 were 490 nm and 550 nm, respectively. Emission for SYTO 9 and TPA-1 were collected from 500 nm to 550 nm (ET525/50m filter) and 590 nm to 670 nm (ET630/75m filter), respectively.

3.2.3 Inhibition and Eradication of *S. aureus* Biofilm by TPA-1 without Light Irradiation

For the biofilm inhibition assay, an overnight culture of *S. aureus* in TSB was diluted to 1 × 10^7 CFU/mL with TSB (with 1% glucose). 10 μL of the diluted bacteria were added to a 96-well plate containing 90 μL of serially diluted TPA-1 in TSB (with 1% glucose). After overnight incubation at 37℃ in the dark, the medium in the well was removed using a micropipette. The remaining biofilm was washed with 200 μL PBS (3 times) and fixed with 100 μL methanol for 10 minutes. The methanol was then removed using a micropipette. After the remaining methanol had been completely evaporated, 150 μL of 0.1% crystal violet was added to the wells to stain the biofilm for 10 minutes. The liquid in the wells was removed using a micropipette, and the wells were washed with 200 μL PBS (3 times). The crystal violet adsorbed on the biofilm was dissolved in 100 μL of 95% ethanol with gentle shaking, and the absorbance at 570 nm was recorded. The biofilm inhibition % was calculated as $[1 - (OD_{TPA\text{-}1} - OD_{blank})/(OD_{medium} - OD_{blank})] \times 100\%$ where $OD_{TPA\text{-}1}$, OD_{medium} and OD_{blank} are the absorbances obtained from the wells with TPA-1-treated bacteria, with bacteria without treatment and with medium only, respectively. The experiments were carried out in triplicate.

For the biofilm eradication assay, an overnight culture of *S. aureus* in TSB was diluted to 1 × 10^5 CFU/mL in TSB (with 1% glucose). 100 μL of the diluted culture was transferred to a 96-well plate. The plate was incubated at 37℃ for 24 hours to allow the formation of mature biofilms. The medium was removed using a micropipette, and the biofilms were washed with 200 μL PBS (3 times). 100 μL of 2-fold diluted TPA-1 solutions in TSB (with 1% glucose) were added to the wells. The plate was further incubated for 24 hours in the dark. Crystal violet staining was then applied as above. The biofilm survival rate (%) was calculated as $(OD_{TPA\text{-}1} - OD_{blank})/(OD_{medium} - OD_{blank}) \times 100\%$ where $OD_{TPA\text{-}1}$, OD_{medium} and OD_{blank} are the absorbances

of the wells with TPA-1-treated bacteria, with bacteria without treatment and with medium only, respectively. The experiments were carried out in triplicate.

3.2.4 Photodynamic Eradication Assay on Bacterial Biofilms

Overnight culture of *S. aureus* or *P. aeruginosa* was diluted to 1×10^5 CFU/mL in TSB (with 1% glucose). 100 μL of the diluted bacterial culture was added to the wells of a 96-well plate. The plate was incubated in the dark for 24 hours at 37℃. Then, the planktonic bacterial suspensions were removed from the wells by a micropipette. The biofilms were washed with PBS (3 times) to remove any remaining planktonic bacteria. Different concentrations of TPA-1 were dissolved in PBS. TPA-1 solution was added to the biofilms (120 μL for *S. aureus*, 150 μL for *P. aeruginosa*). After 20 minutes of incubation in the dark at 30℃, the biofilms were kept in the dark or irradiated by 600 nm light (60 mW/cm2) for 45 minutes. After that, the TPA-1 solution was replaced by 120 μL of PBS. The biofilm was then suspended in PBS by scratching, followed by sonication (5 minutes, ⩽42 kHz) and vortexing (5 minutes, 950 rpm). The number of viable bacteria was determined by the plate counting method. All experiments were carried out in triplicate.

3.2.5 Change in Metabolic Rate of Bacterial Biofilms

Calcein-AM was used to study the metabolic rate of treated bacterial biofilms.[154] Mature *S. aureus* and *P. aeruginosa* biofilms were prepared as described above. The biofilms were treated with TPA-1 (10 μM) with or without light irradiation. After treatments, the biofilms were further incubated for an hour at 37℃ in darkness. Then, the TPA-1 solution was removed using a micropipette, and 2 μM of Calcein-AM in PBS was added to the biofilms. The biofilms were incubated for another hour at 37℃ in darkness. The Calcein-AM was removed and replaced with PBS using a micropipette. After 15 minutes of incubation at room temperature in darkness, the green fluorescence signal of Calcein-AM was captured by a Nikon Eclipse Ti2-E Live-cell

Fluorescence Imaging System with an excitation wavelength of 490 nm. The emission signal was collected from 500 nm to 550 nm. The experiments were duplicated.

3.2.6 Scanning Electron Microscope (SEM) Imaging of Biofilm Bacteria

Overnight cultures of *S. aureus* or *P. aeruginosa* were diluted to 1×10^5 CFU/mL in TSB (with 1 % glucose). 100 μL of diluted *S. aureus* was added to a 96-well plate and 200 μL of *P. aeruginosa* was added to an 8-well chamber. The plate and chamber were incubated at 37℃ for 24 hours to allow the formation of biofilms. After the biofilms were formed, the planktonic cells were carefully removed using a micropipette, and the remaining biofilms were washed with PBS (3 times). Then, TPA-1 (40 μM for *S. aureus* and 10 μM for *P. aeruginosa*) solution diluted in PBS or PBS (as control) was added to the biofilms and further incubated at 30℃ for 20 minutes. After incubation, the biofilms were irradiated with light at 600 nm (60 mW/cm^2) or kept in the dark for 45 minutes. 2.5% Glutaraldehyde was then added to the *S. aureus* biofilm for overnight fixation at 4℃ after PDT treatment. The *S. aureus* biofilm was then resuspended by scratching and centrifuged at 3900 × g for 5 minutes to collect the biofilm. The supernatant was removed, and the biofilm was gradually dehydrated with ethanol (30%, 50%, 70%, 90%, 100%). The dehydrated *S. aureus* biofilm was dropped on a silicon slide with absolute ethanol. After air drying, images of the biofilms on the silicon slide were taken using a Tescan MAIA3 SEM. For *P. aeruginosa,* the biofilm was first centrifuged at 3900 × g for 5 minutes. Then, 2.5% glutaraldehyde was added, and the biofilm was fixed overnight. The remaining steps for SEM sample preparation of *P. aeruginosa* biofilm were the same as those *S. aureus* biofilm.

3.2.7 Mass Spectrometry(MS)-Based Proteomic Analysis on Bacterial Biofilms

The bacterial biofilms for proteomic analysis were prepared using the same methods as described in the photodynamic eradication assay (**Section 3.2.4**). After PDT, the TPA-1 solution or PBS was removed. Then, the biofilm samples were prepared using an EasyPepTM

MS Sample Prep Kit. Mass spectrometry and data analysis were conducted in a similar manner as described in **Section 2.2.25**.

3.2.8 Selective Labelling of Bacteria over HFF-1 Cells

HFF-1 cells were seeded and cultured in confocal dishes at a density of 50,000 cells for 12 hours at 37℃ in darkness. The cells were washed with PBS (3 times) to remove the antibiotics from the medium. TPA-1 (10 μM) was first mixed with 1×10^8 CFU/mL *S. aureus* or *P. aeruginosa* in PBS. The mixture was then added to the cells and incubated for 20 minutes at 30℃ in darkness. The fluorescence signal from TPA-1 was observed using a Nikon Eclipse Ti2-E Live-cell Fluorescence Imaging System with an excitation wavelength of 550 nm and the emission was collected from 500 nm to 550 nm.

3.2.9 Light Toxicity of TPA-1 on HFF-1 Cells

HFF-1 cells were seeded in a 96-well plate with a density of 10,000 cells/well for 12 hours at 37℃ in the dark. Different concentrations of TPA-1 were added to the cell culture medium and incubated for 20 minutes at 37℃ in the dark. The cells were then incubated in the dark or irradiated by 600 nm light for 45 minutes. The cell viability was then evaluated using the MTT assay, which was described in the cytotoxicity assay (**Section 2.2.14**).

3.2.10 Haemolysis of TPA-1 on HFF-1 Cells

Human erythrocyte concentrate was prepared according to the kit manual from the Biomaterial Haemolytic Assay Kit (Haemoscan).[155] After the human erythrocytes had been washed and diluted with manufacturer's buffers, 100 μL of erythrocytes were added to 100 μL of various concentrations of compounds in PBS. 1% of Triton X was used as the positive control, while PBS was used as the negative control. The erythrocytes were then gently mixed with the TPA compounds and further incubated for an hour at 37℃. After that, the erythrocytes were centrifuged (1000 rpm, 5 minutes), and 20 μL of supernatant was added to 180 μL of PBS in a

96-well plate. The optical densities at 380 nm, 415 nm and 450 nm were measured using a plate reader. The final OD value of the compounds was calculated as $(2 \times OD_{415}) - (OD_{450} + OD_{380})$ where OD_{380}, OD_{415}, and OD_{450} are the optical densities of the solution at 380 nm, 415 nm, and 450 nm, respectively. The haemolysis rates of the compounds were calculated as $(OD_{compound} - OD_{PBS})/(OD_{TritonX}\text{-}OD_{PBS}) \times 100\%$ where $OD_{compound}$, OD_{PBS}, and $OD_{TritonX}$ are the final OD values of the erythrocytes mixed with TPA compounds, PBS and 1% Triton X, respectively. All experiments were triplicated.

3.2.11 *In vivo* Efficacy of TPA-1

All *in vivo* animal experiments were conducted by Hangzhou Yanqu Information Technology Co.,Ltd. and approved by the Department of Science and Technology of Zhejiang Province (SYXK(浙)2021-0043). Female BALB/c mice (10-12 weeks old) were kept in 12-hour light and 12-hour dark cycle with access to free food and water for 7 days before and throughout the experiment. The backs of the mice were shaved and disinfected with iodine. A full-thickness circular wound (7 mm in diameter) was then created at the back of the mice. The mice were allowed to recover for 24 hours after surgery to prevent sepsis.[156] 10 μL of 1×10^8 CFU/mL MRSA (ATCC 43300) or *P. aeruginosa* (ATCC 27853) in saline was added to the wound. The wound was covered with an adhesive dressing (3M Tegadarm, 1624w, 6 × 7 cm) for 24 hours of infection. Next, the mice were randomly divided into four groups: (1) 100 μL TPA-1 (90 μM) with 600 nm light irradiation (60 mW/cm^2) for 15 minutes, (2) 100 μL TPA-1 (90 μM) in the dark, (3) 100 μL saline with 600 nm light irradiation (60 mW/cm^2) for 15 minutes and (4) 100 μL saline in the dark. For light irradiation groups, TPA-1 and saline were incubated on the wound for 10 minutes before irradiation. The treatment was sustained for four days. The wound size and body weight of the mice were recorded every day. On day 6, the mice were euthanatized, and the wound tissue was collected. After that, the wound tissue was cut in half. Half of the tissue was used in hematoxylin and eosin (H&E) staining. The other half of the

tissue was homogenized, and the number of viable bacteria was measured using the plate counting method.

3.2.12 Statistical Analysis

Data in this chapter were reported as mean ± standard deviation (SD). Statistical analysis was conducted using GraphPad Prism 8. Multiple comparison tests were performed using Two-way ANOVA, followed by Tukey's tests, and p-value < 0.05 was defined as statistically significant.

3.3 Results and Discussion

3.3.1 Biofilm Labelling by TPA-1

The photographs of *S. aureus* and *P. aeruginosa* biofilms showed that TPA-1 stained the biofilms in blue color **(Figure 3.1**). PBS was used to wash the TPA-1-stained biofilms, but the blue color stayed on the biofilms, indicating that TPA-1 molecules can strongly bind to the *S. aureus* and *P. aeruginosa* biofilms.

A major challenge in eradicating bacterial biofilms is to overcome the penetration barrier of the EPS produced by bacteria. To investigate the penetration efficiency of TPA-1 in *S aureus* and *P. aeruginosa* biofilms, z-stacked fluorescence imaging was employed. As shown in **Figure 3.2**, TPA-1 could label the bacteria in the *S. aureus* and *P. aeruginosa* biofilms. Besides, the fluorescence signals of TPA-1 were found throughout the entire biofilms, suggesting that TPA-1 could penetrate and label the bacteria inside the *S. aureus* and *P. aeruginosa* biofilms.

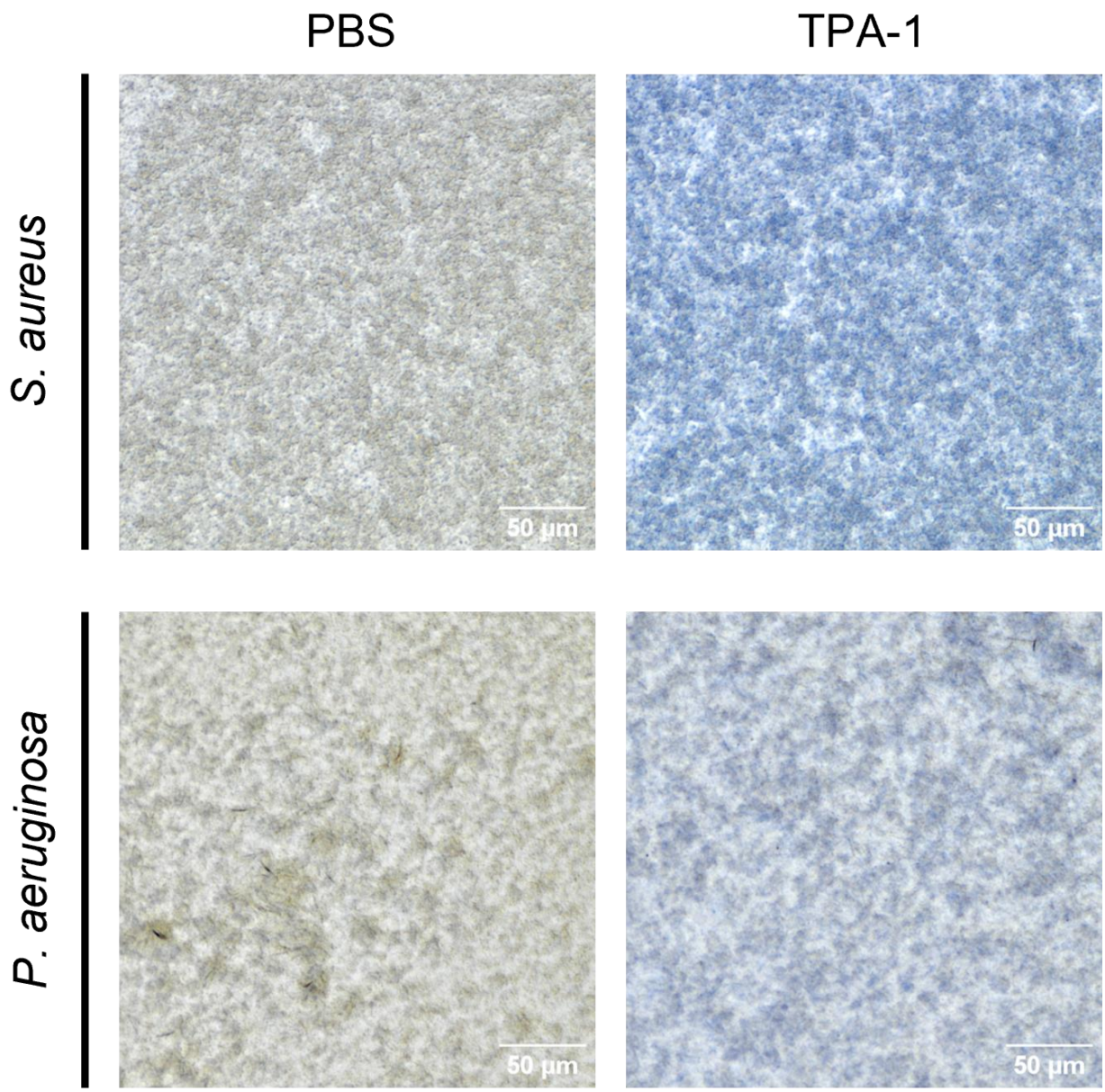

Figure 3.1. Photographs of *S. aureus* and *P. aeruginosa* biofilms with PBS or 20 μM TPA-1.

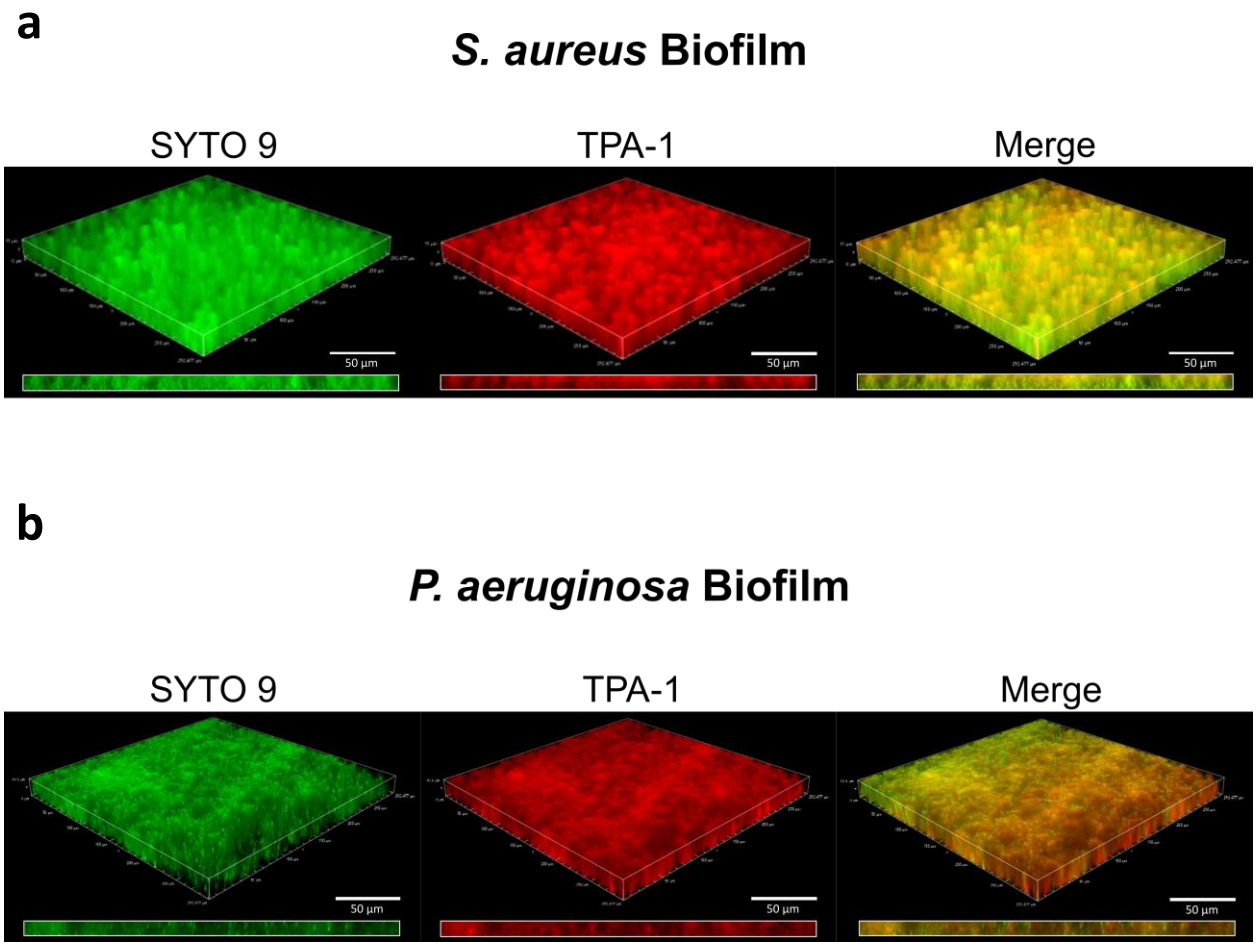

Figure 3.2. The fluorescence images of (a) *S. aureus* and (b) *P. aeruginosa* biofilms with SYTO 9 (2.5 µM, λex = 490 nm, λem = 500nm to 550 nm) and TPA-1 (20 µM, λex = 550 nm, λem = 590 nm to 670 nm). SYTO 9 is a commercial DNA stain that has been used to label biofilm bacteria.[157]

3.3.2 TPA-1 Against *S. aureus* Biofilm without Light Irradiation

As discussed in **Section 2.3.2**, TPA-1 can effectively kill *S. aureus* even without light irradiation. Hence, the antibiofilm activities of TPA-1 on *S. aureus* biofilm without light irradiation were also evaluated.

In **Figure 3.3a**, the biofilm inhibition percentage of TPA-1 on *S. aureus* increased from 0.781 μM to 3.13 μM and reached 100% at 6.25 μM. This result demonstrated that TPA-1 exhibited good biofilm inhibition ability against *S. aureus*. However, TPA-1 cannot eradicate preformed *S. aureus* biofilm. As shown in **Figure 3.3b**, even up to 100 μM of TPA-1, the *S. aureus* biofilm can still maintain a survival rate of over 90%. Therefore, without light irradiation, TPA-1 has good inhibition activity on the formation of *S. aureus* biofilm, but it has poor activity in eradicating mature *S. aureus* biofilm.

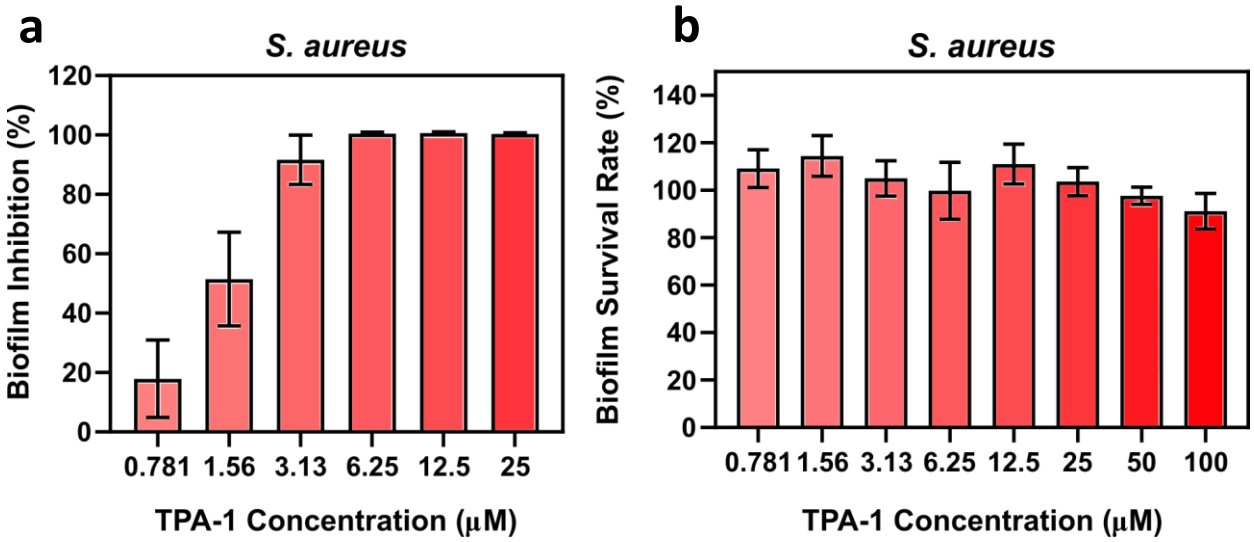

Figure 3.3. (a) The inhibition rate of the formation of *S. aureus* biofilm by TPA-1 without light irradiation. (b) The survival rate of mature *S. aureus* biofilm after incubation with TPA-1 without light irradiation. Data are presented as the mean ± SD, $n = 3$ per group.

3.3.3 Antibiofilm Activities of TPA-1 with Light Irradiation

Upon light irradiation at 600 nm, TPA-1 showed excellent antibiofilm activity against both *S. aureus* and *P. aeruginosa*. As shown in **Figure 3.4a** to **Figure 3.4d**, the biofilm eradication ability of TPA-1 is concentration and irradiation time dependent. The increase in TPA-1 concentration and irradiation time could enhance the antibiofilm activity of TPA-1. **Figure 3.4a** and **Figure 3.4c** demonstrated that 40 μM of TPA-1 was able to eradicate 92% ± 3% (1.18 ± 0.05 log CFU/mL reduction) of *S. aureus* in the biofilm and 99.8% ± 0.1 % (2.6 ± 0.2 log CFU/mL reduction) of *P. aeruginosa* in the biofilm in 45 minutes. The eradication ability of TPA-1 was better than that of vancomycin against *S. aureus* and meropenem against *P. aeruginosa*. Moreover, the PDT with TPA-1 was more effective than the commercial PS zinc phthalocyanine in eradicating bacterial biofilms at the same concentration (**Figure 3.5**).

The metabolic rates of the bacteria inside biofilms were also compared using Calcein-AM, a fluorescent dye that generates a green fluorescence signal within metabolically active cells. After PDT with TPA-1, both *S. aureus* and *P. aeruginosa* biofilms showed lower fluorescence signals than the PBS control groups (**Figure 3.6**), suggesting that the metabolic rate of *S. aureus* and *P. aeruginosa* inside the biofilms were decreased after PDT with TPA-1. This decrease in metabolic rates could be attributed to the eradication of bacteria in the biofilms during PDT. Additionally, *S. aureus* biofilm treated with TPA-1 in the dark (TPA-1 -L group) showed a lower fluorescence signal than the control groups but higher than that from TPA-1 PDT-treated *S. aureus* biofilm (TPA-1 +L group). These results suggested that the intrinsic antibacterial effect of TPA-1 eradicated some of the *S. aureus* in the biofilm, while light irradiation further enhanced the eradication ability of TPA-1.

In addition, SEM has been used to investigate the effects of TPA-1 on the morphology of bacteria in the biofilms (**Figure 3.4e**). Following PDT with TPA-1, the *S. aureus* and *P.*

aeruginosa in the biofilms showed shrinkages and collapses on the cell. In contrast, the bacteria treated with TPA-1 without light irradiation did not exhibit significant cell defects compared to the PBS control groups, indicating that TPA-1 had minimal effects on the cell envelope in the absence of light irradiation. Along with the results from fluorescence imaging, it is suggested that TPA-1 could penetrate the EPS barrier and target the bacteria inside the biofilms. Upon light irradiation, TPA-1 could eradicate bacteria in the biofilms by generating ROS that damage their cell membranes.

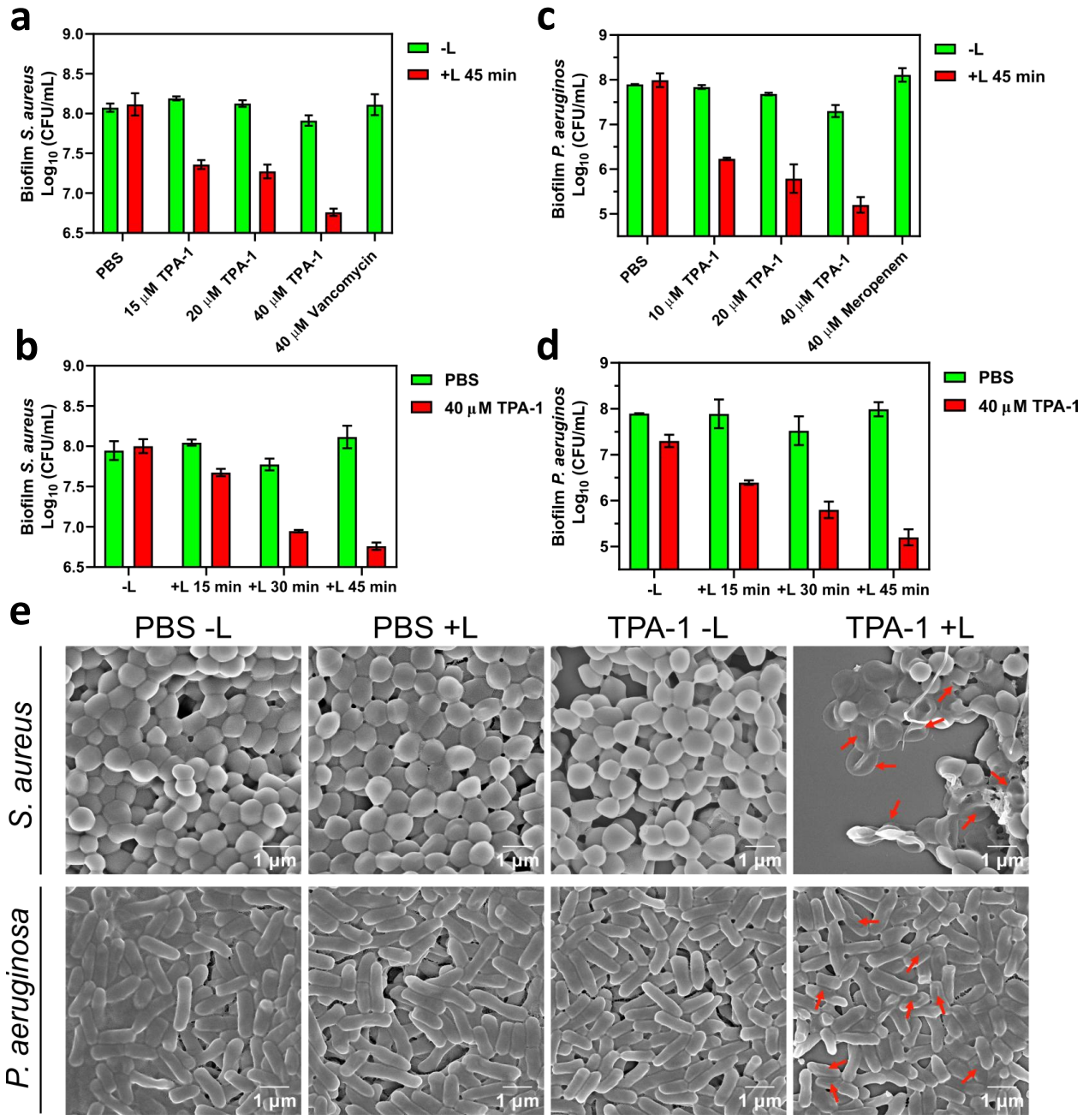

Figure 3.4. (a) Number of viable *S. aureus* in the biofilm after PDT with different concentrations of TPA-1 and (b) various irradiation times. (c) Number of viable *P. aeruginosa* in the biofilm after PDT with different concentrations of TPA-1 and (d) various irradiation times. (e) SEM images of *S. aureus* and *P. aeruginosa* biofilms with and without PDT with TPA-1. The red arrows indicate some of the shrinkages and collapses of the bacterial cells. -L: without light irradiation. +L: with 600 nm light (60 mW/cm^2) irradiation. Data are presented as the mean ± SD, n = 3 per group.

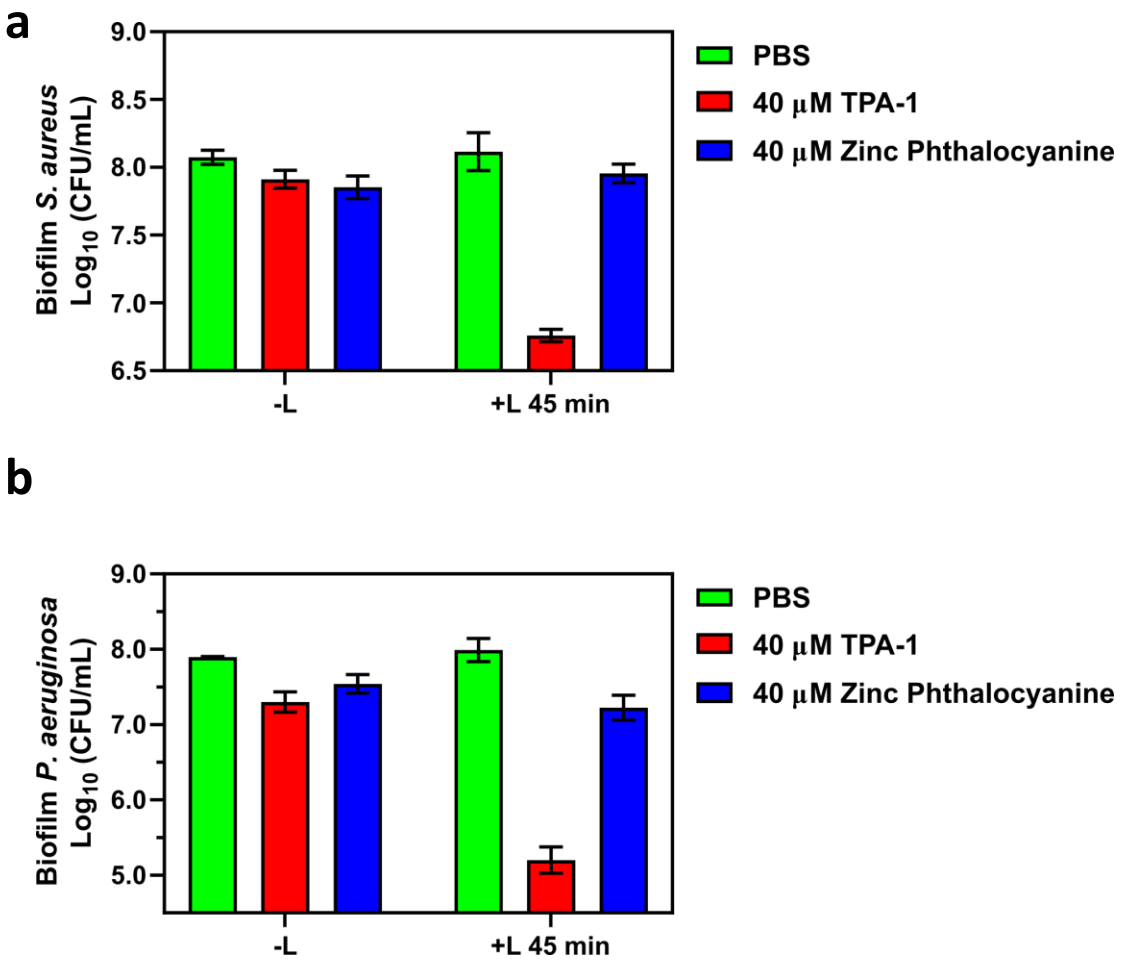

Figure 3.5. (a) Number of viable *S. aureus* and (b) *P. aeruginosa* in the biofilms after PDT with TPA-1 or zinc phthalocyanine. -L: without light irradiation. +L: with 600 nm light (60 mW/cm^2) irradiation. Data are presented as the mean ± SD, n = 3 per group.

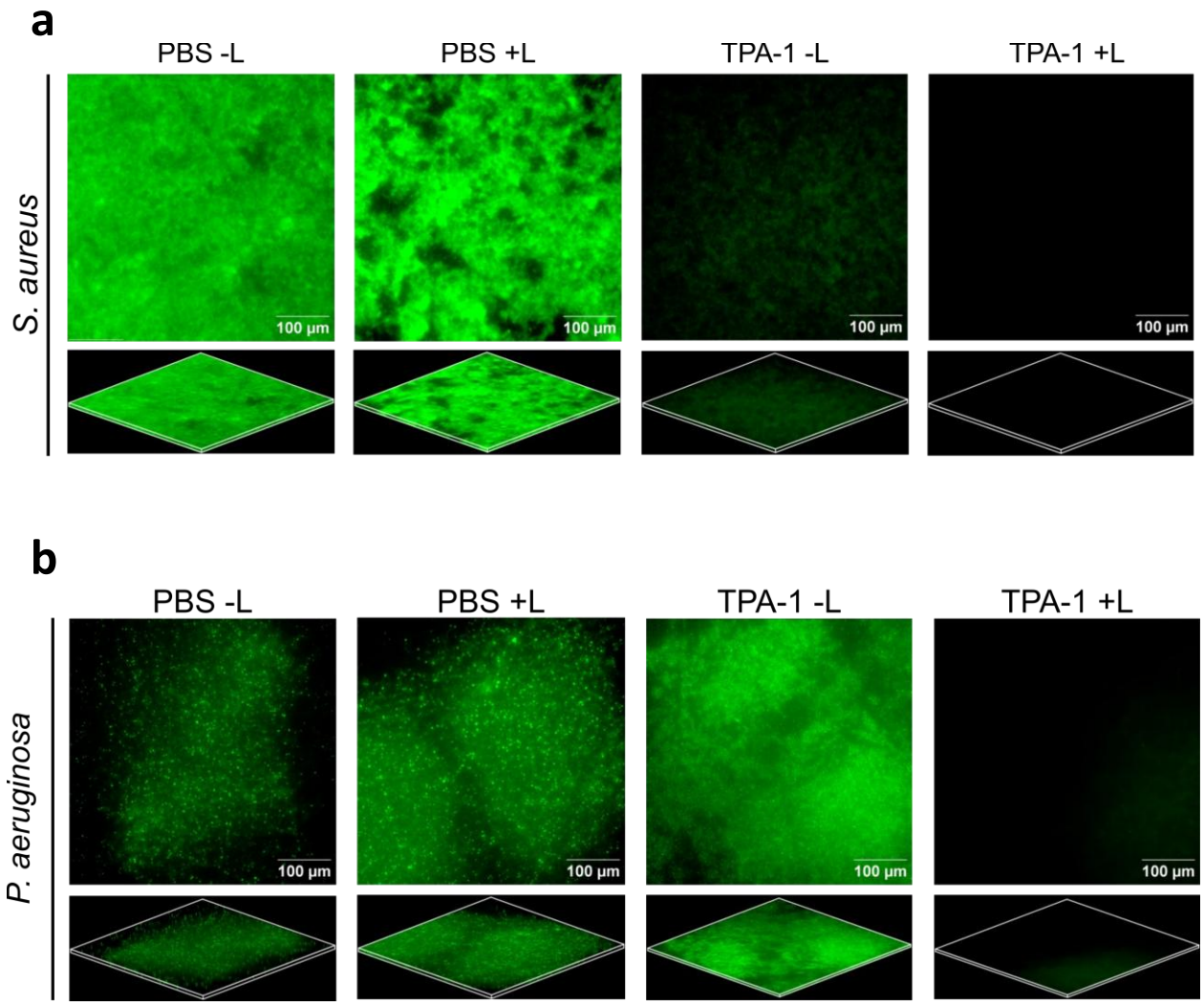

Figure 3.6. Fluorescence images of (a) *S. aureus* and (b) *P. aeruginosa* biofilms stained by Calcein-AM after various treatments with PBS or TPA-1. -L: without light irradiation. +L: with 600 nm light (60 mW/cm^2) irradiation. The excitation wavelength was 490 nm and the emission was collected from 500 nm to 550 nm.

3.3.4 MS-Based Proteomic Analysis on TPA-1 PDT-Treated *S. aureus* and *P. aeruginosa* Biofilm

To further investigate the antibacterial effects of TPA-1, MS-based proteomic analyses were performed on *S. aureus* and *P. aeruginosa* biofilm after PDT with TPA-1 (**Figure 3.7**). A total of 804 unique protein groups were identified in the *S. aureus* biofilm, while 56 were considered as DEPs. Within the DEPs, 44 were downregulated, and 12 were upregulated (**Figure 3.7a**). For *P. aeruginosa* biofilm, 1393 unique protein groups were identified. However, only 4 were DEPs, and all of them were downregulated (**Figure 3.7b**). GO and KEGG enrichment analyses were performed on the genes corresponding to the DEPs for *S. aureus* and *P. aeruginosa* biofilms. No significant enrichment was found in the *P. aeruginosa* biofilm. In contrast, enrichment analysis on *S. aureus* biofilm has classified the genes into three GO terms and one KEGG pathway (**Figure 3.7c - Figure 3.7f**). Based on the annotations, we focused on two terms, cell wall organization (GO) and *Staphylococcus aureus* infection (KEGG), as they are related to cell growth and virulence.

The expressions of cell wall organization-related proteins were decreased in *S. aureus* biofilm after PDT with TPA-1 (**Figure 3.7g**). Teichoic acid glycerol-phosphate primase (*tarB*) and lipoteichoic acid synthase (*ltaS*), which are proteins required in the synthesis of wall teichoic acid (WTA) and LTA, respectively, were downregulated.[158, 159] WTA and LTA are important components in *S. aureus* colonization and infection.[160, 161] The decrease in expression of these proteins might inhibit the synthesis of WTA and LTA, further reducing the virulence of *S. aureus* biofilm. Additionally, TPA-1 with light irradiation caused the downregulation of proteins related to *Staphylococcus aureus* infection. These proteins included γ-hemolysin components B, C (*hlgB*, *hlgC*) and staphylococcal superantigen-like 7 (*ssl7*), which are virulence factors released by *S. aureus* to evade the host immune system.[162, 163] The downregulation of these proteins could also reduce the virulence of *S. aureus* biofilm. Overall,

the proteomic data hinted that the PDT with TPA-1, apart from eradicating bacteria in the biofilm, could also reduce the virulence of *S. aureus* biofilm.

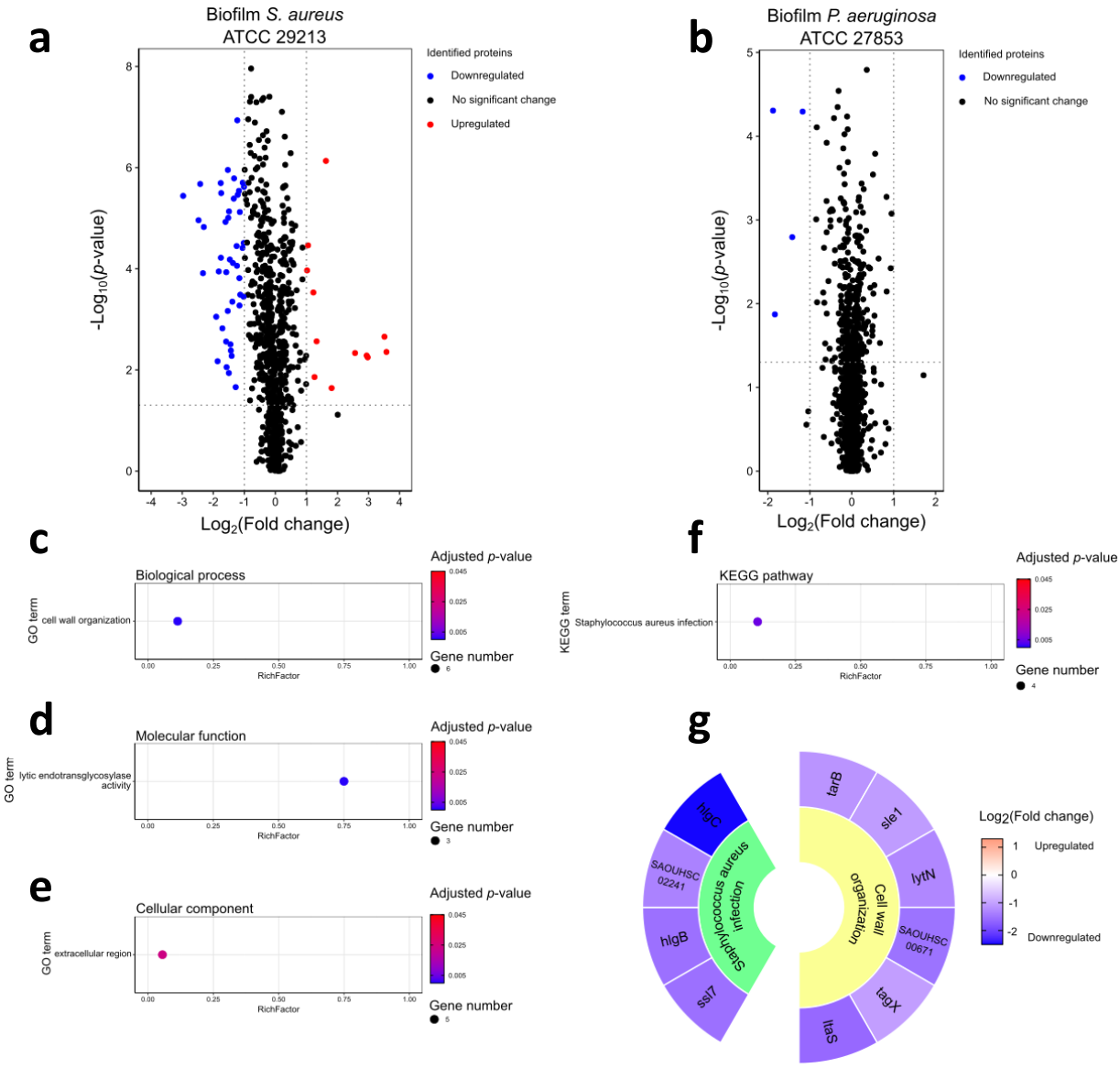

Figure 3.7 (a) Volcano plot showed the DEPs in TPA-1 (40 μM)-treated *S. aureus* biofilm versus PBS-treated *S. aureus* biofilm and (b) TPA-1 (40 μM)-treated *P. aeruginosa* biofilm versus PBS-treated *P. aeruginosa* biofilm after 45 minutes of 600 nm (60 mW/cm2) irradiation. (c) Biological process, (d) molecular function, (e) cellular component GO enrichment, and (f) KEGG pathway enrichment analysis of the corresponding genes of the DEPs in TPA-1-treated *S. aureus* biofilm after light irradiation. (g) Selected biological processes and KEGG pathway in *S. aureus* biofilm after PDT with TPA-1. Inner blocks are the names of the selected biological process and KEGG pathway. Outer blocks show the fold change of the DEPs, which are represented by their gene names, in the corresponding biological process and KEGG pathway. Three independent biological replicates were performed in this proteomic study.

3.3.5 Evaluation of Potential Off-Target Effects of TPA-1

Before conducting further *in vivo* studies, assessments were made on the potential off-target effects of TPA-1 to ensure its high biocompatibility.

To assess the selectivity of TPA-1, mixtures of HFF-1 cells (50000 cells/well) with 1×10^8 CFU/mL of *S. aureus* or *P. aeruginosa* were incubated with TPA-1. As shown in **Figure 3.8**, the fluorescence signal of TPA-1 was observed on *S. aureus* or *P. aeruginosa* but barely found on HFF-1 cells. This result demonstrated that TPA-1 is highly specific towards bacteria.

Moreover, TPA-1 showed minimal haemolysis on human erythrocytes. At concentrations as high as 200 μM, TPA-1 only induced less than 2% of the haemolysis rate (**Figure 3.9a**). The light toxicity of TPA-1 on HFF-1 cells was also investigated. The viability of HFF-1 cells still exceeded over 90% after PDT with 40 μM of TPA-1 for 45 minutes (**Figure 3.9b)**.

Collectively, these results indicated that TPA-1 could specifically target bacterial cells while maintaining low toxicity against human cells, both in the absence and presence of light. Therefore, it is suggested that TPA-1 could be safely and effectively applied in further *in vivo* studies.

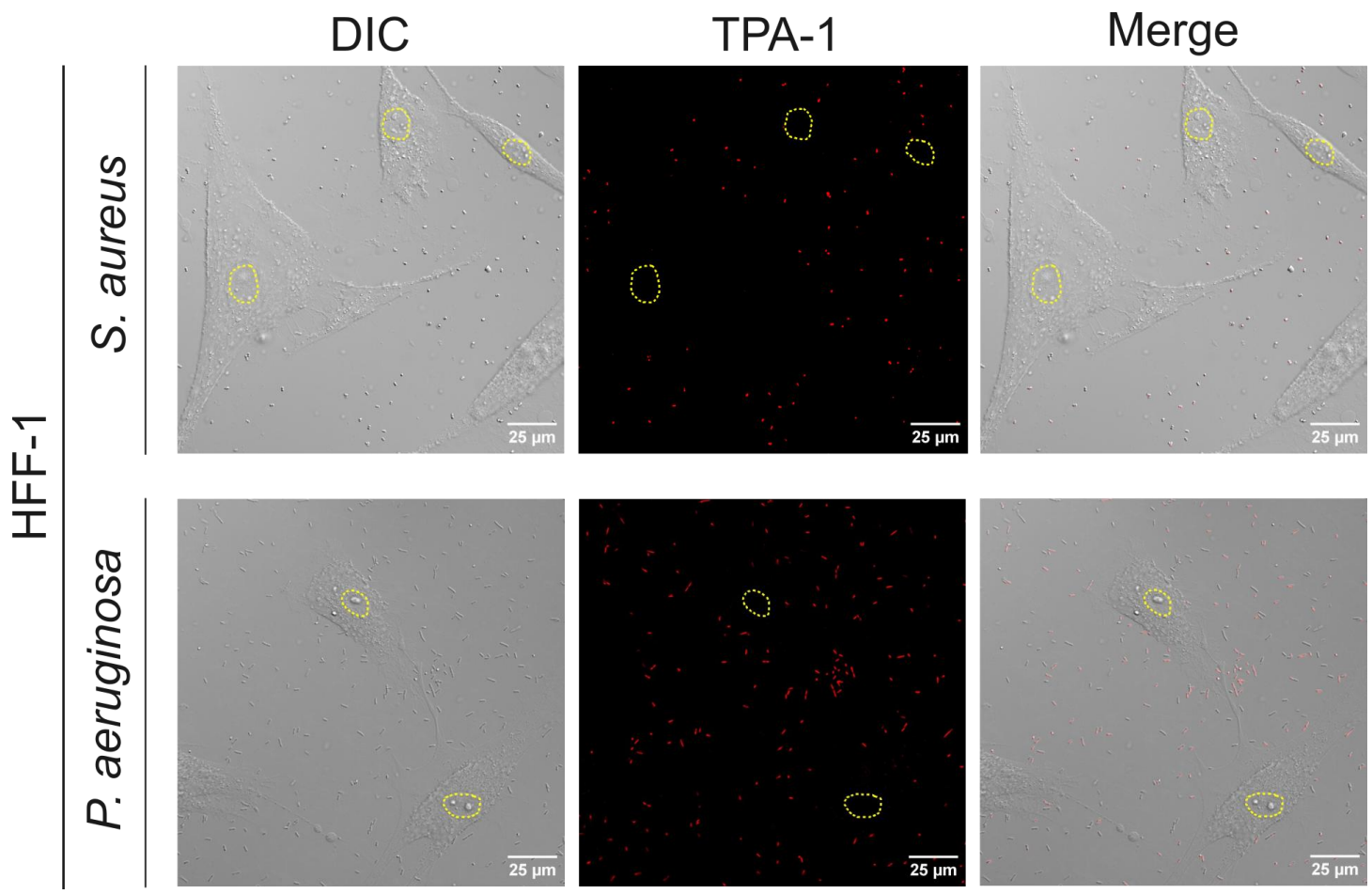

Figure 3.8. The fluorescence images of HFF-1 cells were mixed with *S. aureus* or *P. aeruginosa* and incubated with TPA-1 (10 μM). The yellow dotted circles were the nuclei of the HFF-1 cells.

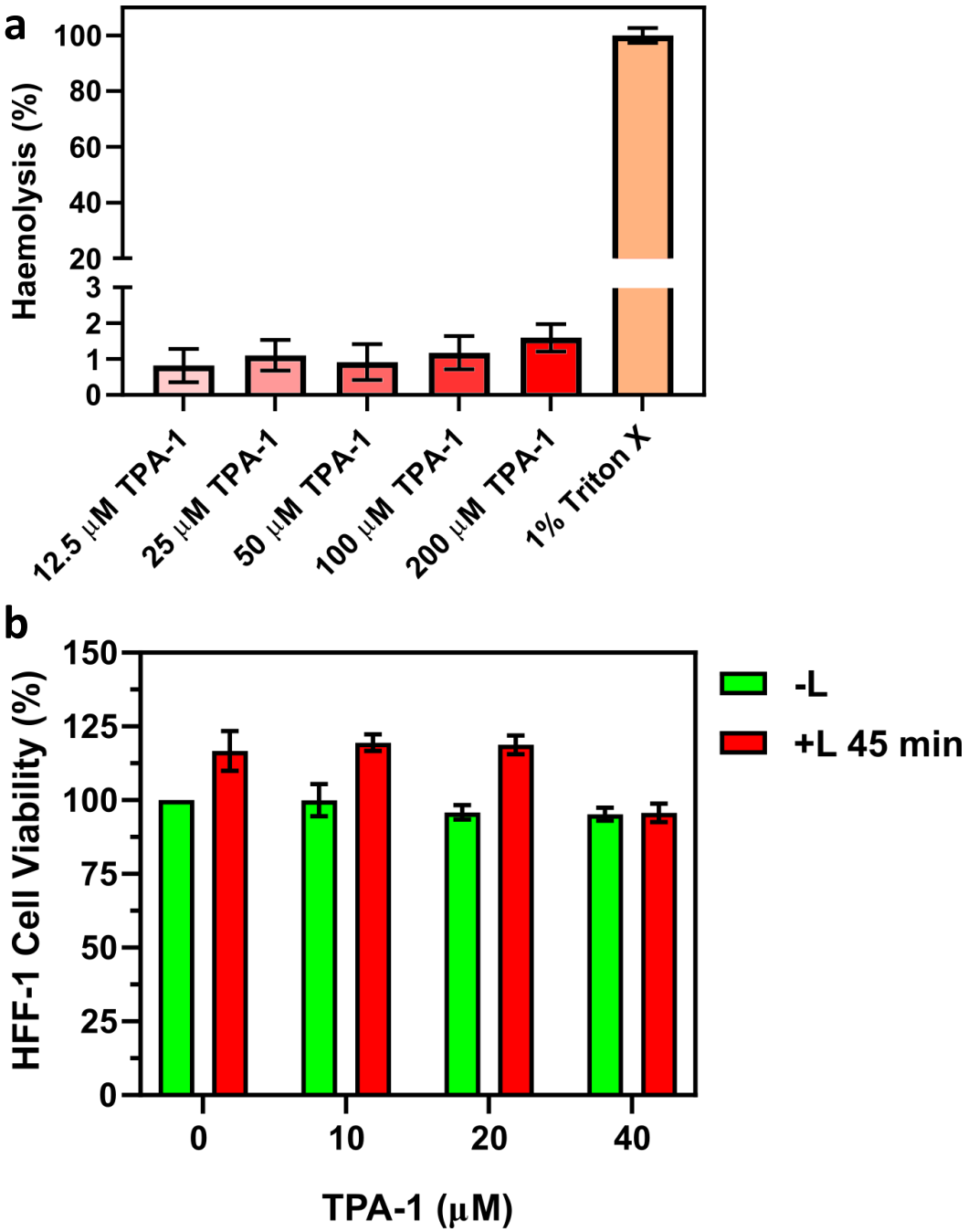

Figure 3.9. (a) The haemolysis rate of TPA-1 on human erythrocytes. (b) The viability of HFF-1 cells after PDT with TPA-1. Data are presented as the mean ± SD, n = 3 per group.

3.3.6 *In Vivo* Efficacy of TPA-1 on MRAS- or *P. aeruginosa*-Infected Mice

Wound infection models of MRSA and *P. aeruginosa* were designed to study the therapeutic efficacy of TPA-1. The experimental workflow is illustrated in **Figure 3.10a**. The detailed experimental procedures were reported in **Section 3.2.11**.

As shown in **Figure 3.10b** and **Figure 3.10c**, the MRSA- and *P. aeruginosa*-infected wounds after PDT with TPA-1 (TPA-1 +L) produced less pus than the rest of the groups. Besides, PDT with TPA-1 significantly reduced 96% ± 3 % (1.4 ± 0.6 log CFU/mg tissue reduction) of MRSA and 96% ± 4% (1.4 ± 0.4 log CFU/mg tissue reduction) of *P. aeruginosa* in the wound tissues (**Figure 3.11a, Figure 3.11c**). Additionally, the mice receiving 4 days of PDT treatment with TPA-1 had the smallest wound size compared to the other groups (**Figure 3.11b, Figure 3.11d)**.

To further assess the therapeutic efficacy of TPA-1, histological analysis on MRSA-infected wounds was conducted. Although all wounds showed signs of inflammation, the wounds after PDT with TPA-1 had fewer inflammatory cells infiltrated (**Figure 3.12a**). Masson's trichrome staining also showed that the TPA-1 +L group had a higher extent of collagen deposition than the other groups (**Figure 3.12b**). These results indicated that, with light irradiation, TPA-1 effectively eradicated MRSA and *P. aeruginosa in vivo* and promoted wound healing in bacteria-infected wounds. In contrast, the application of TPA-1 on wounds without light irradiation showed no therapeutic significance over the saline control groups, suggesting that light irradiation was essential for TPA-1 to deliver good therapeutic results *in vivo*.

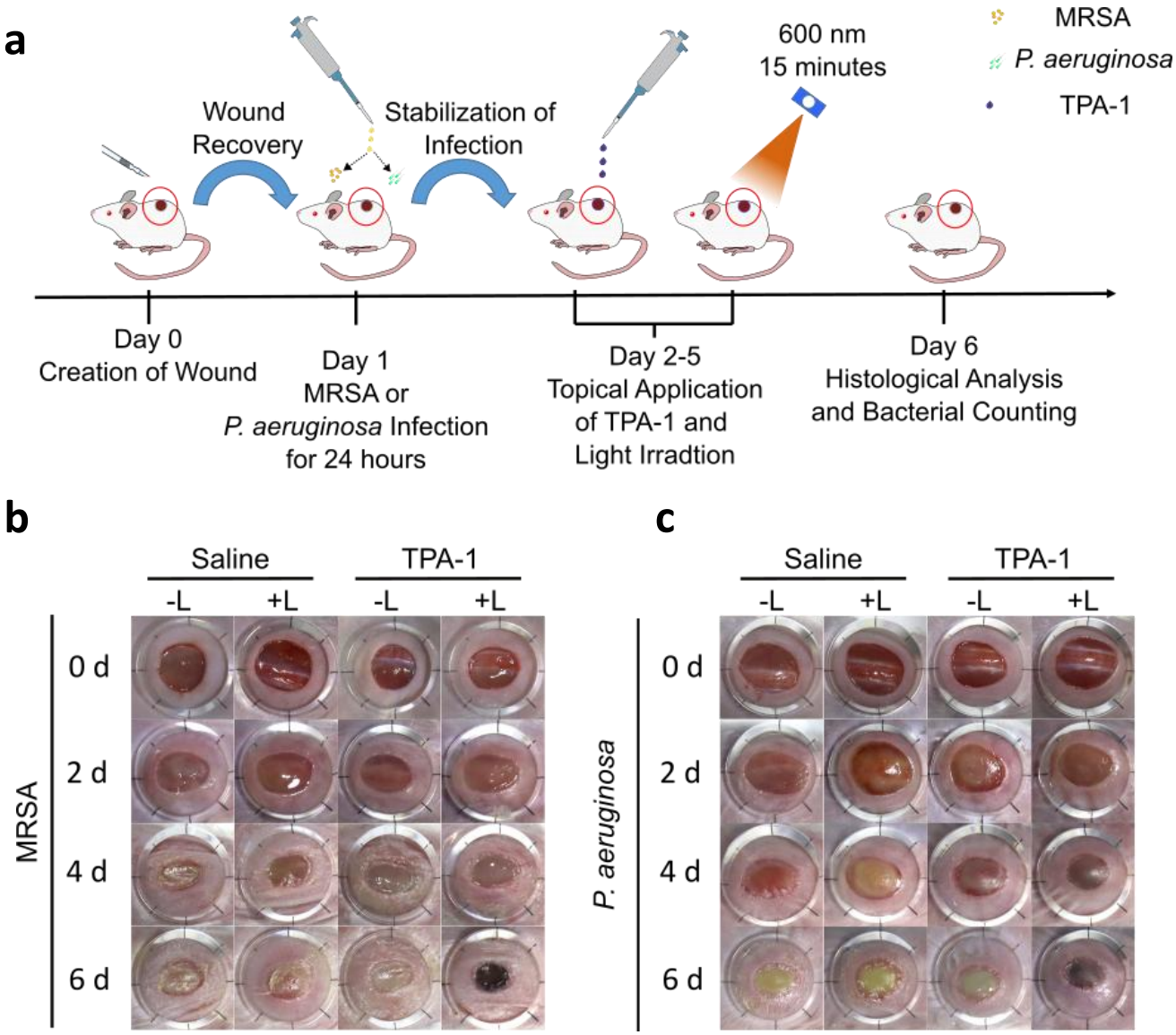

Figure 3.10. (a) An illustration shows the experimental workflow of the *in vivo* models. (b) Photographs of MRAS- and (c) *P. aeruginosa*-infected wounds after different treatments. -L: without light irradiation. +L: with 600 nm (60 mW/cm^2) light irradiation for 15 minutes.

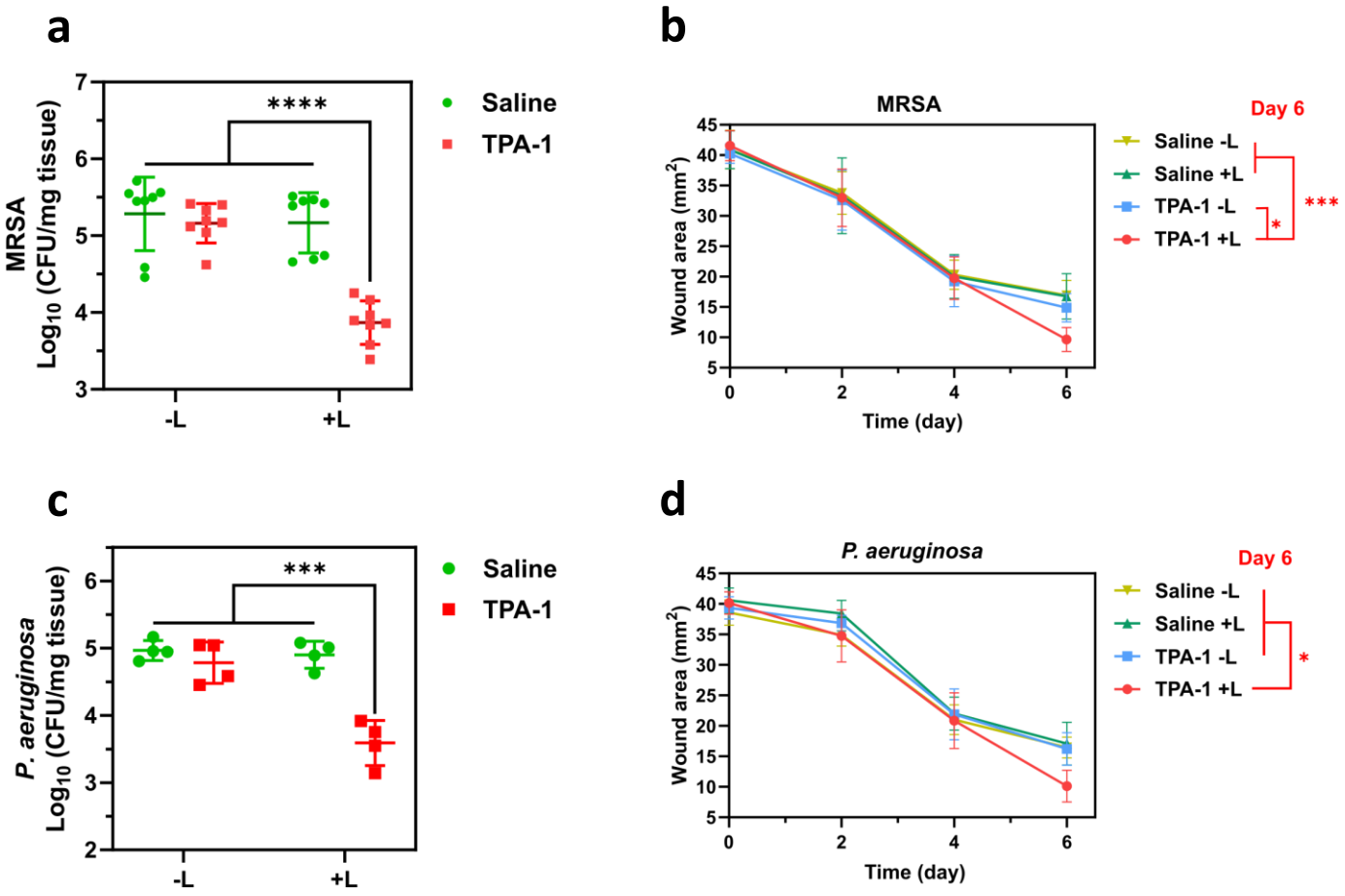

Figure 3.11. (a) Number of viable MRSA and (c) *P. aeruginosa* in the infected tissue after 4 days of treatments. (b) The wound area of MRSA- and (d) *P. aeruginosa*-infected wounds throughout the treatments. Data are presented as the mean ± SD. n = 8 per group for MRSA-infected mice. n = 4 per group for *P. aeruginosa*-infected mice. * p-value < 0.05; *** p-value < 0.001, **** p value-< 0.0001. -L: without light irradiation. +L: with 600 nm (60 mW/cm^2) light irradiation for 15 minutes.

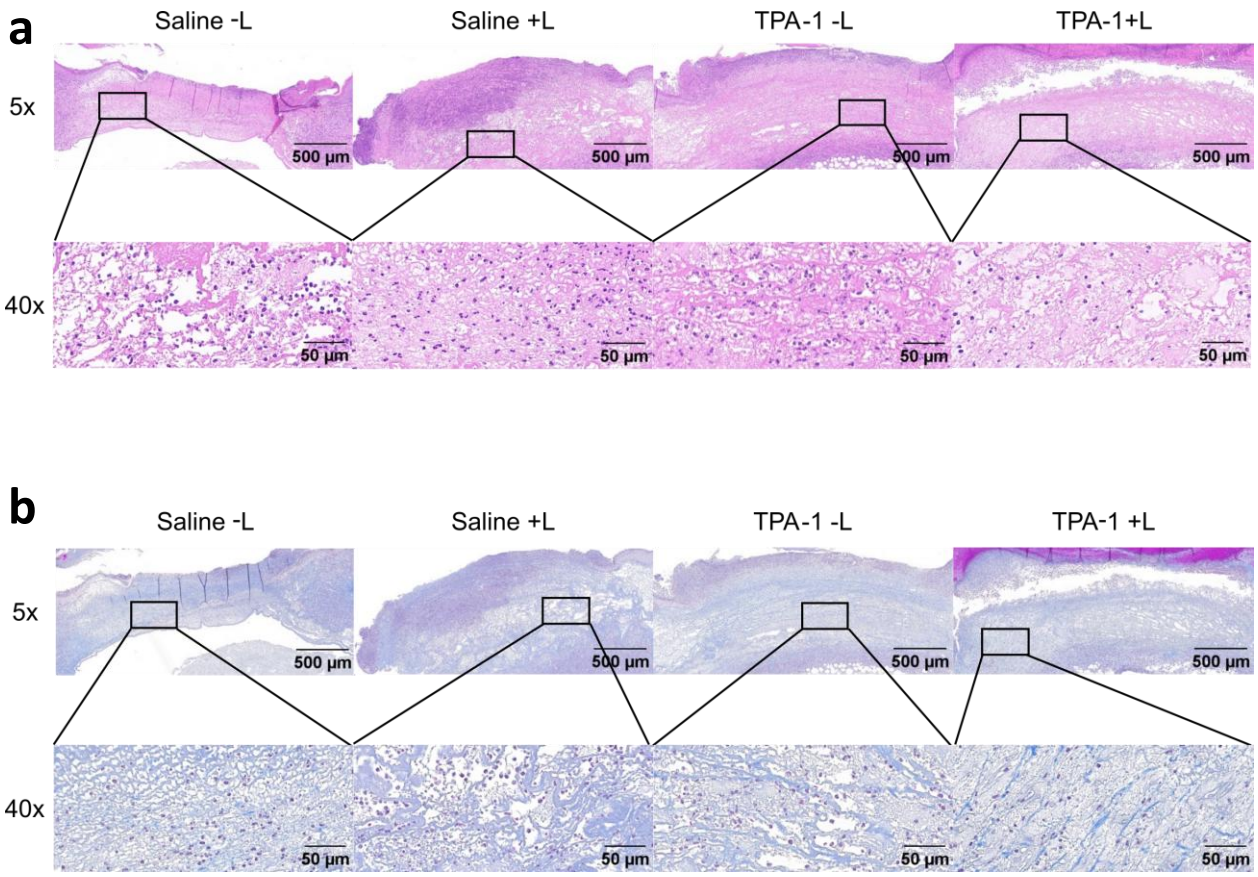

Figure 3.12. **(a)** Hematoxylin and eosin (H&E) and (b) Masson's trichrome staining of MRSA-infected tissue after 4 days of treatments. -L: without light irradiation. +L: with 600 nm (60 mW/cm^2) light irradiation for 15 minutes.

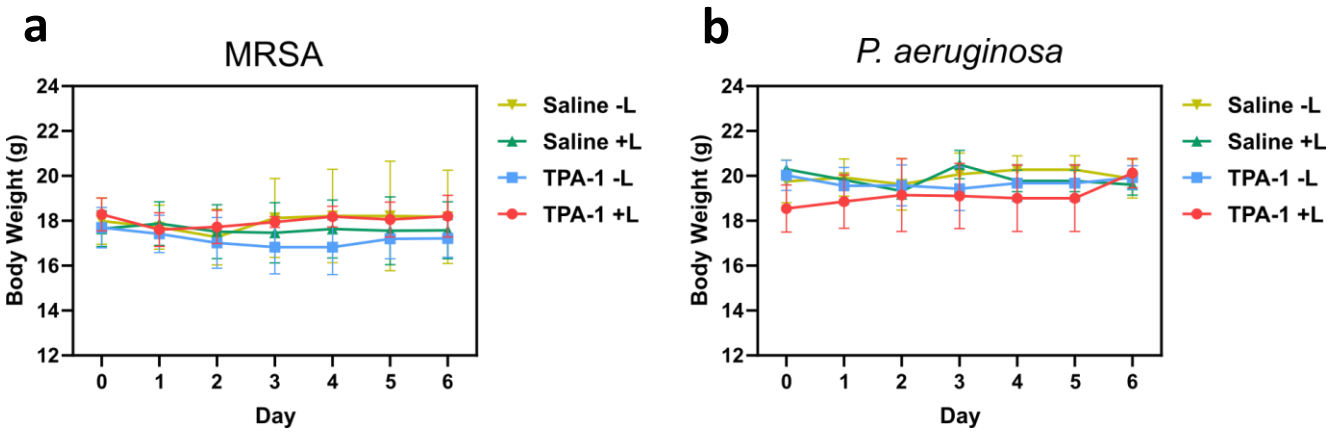

Figure 3.13. Body weight of (a) MRSA- and (b) *P. aeruginosa*-infected mice throughout the experiment. Data are presented as the mean ± SD. n = 8 per group for (a), n =4 per group for (b).

3.4 Chapter III Summary

In summary, TPA-1 can penetrate the EPS barrier and stain the bacteria inside bacterial biofilms. Without light irradiation, TPA-1 can inhibit the formation of *S. aureus* biofilm, but it has no significant antibacterial effect on mature biofilm. Upon light irradiation, TPA-1 can effectively eradicate *S. aureus* and *P. aeruginosa* in the biofilms. The proteomic results also showed that PDT with TPA-1 could reduce the virulence of *S. aureus* biofilm. Apart from great antibiofilm activity, TPA-1 also has minimal off-target effects. TPA-1 can selectively bind with *S. aureus* and *P. aeruginosa* in the presence of HFF-1 cells. Moreover, TPA-1 has minimal haemolytic activity against human erythrocytes, and the PDT with TPA-1 against HFF-1 cells induces minimal cell death. Furthermore, the therapeutic efficacy of TPA-1 was evaluated with *in vivo* MRSA- and *P. aeruginosa*-infected wound models. The PDT treatment of TPA-1 can significantly reduce the number of viable bacteria in wound tissue and promote wound healing. The good therapeutic efficacy and biocompatibility of TPA-1 make it a potential PS for treating clinical biofilm-related infections.

Chapter IV

Improving Antibiofilm Effects by Enhancing Intrinsic Antibacterial Activity

4.1 Introduction

PDT is an emerging technique for treating bacterial infections. The potential of TPA-1 as a photosensitizer (PS) in eradicating bacteria in planktonic and biofilm forms has been demonstrated in Chapter II and Chapter III. However, PDT has its weaknesses. One of the major flaws of the antibacterial PSs reported in the literature is that they will lose their antibacterial activity once the light source is removed.[69, 105, 164-167] Interestingly, as discussed in previous chapters, TPA-1 has good antibacterial activity against *S. aureus* even without light irradiation. Therefore, TPA-1 can serve as a new starting point for developing PSs that can extend the antibacterial effects in the dark.

In this chapter, based on the structure of TPA-1, several PSs that aim to achieve broad-spectrum antibacterial activity in the dark were designed and synthesized. Among these compounds, TPA-C3-C6 has the overall best MIC values against various bacteria. Studies related to cytotoxicity, antibiofilm activity and antibacterial mechanisms were also conducted. TPA-C3-C6 shows significant antibiofilm activities through the combined effect of photosensitizing and intrinsic antibacterial activity.

4.2 Materials and Methods

4.2.1 Materials and Instruments

2,3,3-Trimethylindolenine, 1,1,2-trimethyl-1H-benzo[e]indole and lepidine were purchased from TCI. 1,6-Dibromohexane, 1-bromohexane, *N,N,N′,N′*-tetramethylethylenediamine, polymyxin B sulfate, and ciprofloxacin were purchased from Sigma-Aldrich. SYTOX Green and TRIzol™ Plus RNA Purification Kit were purchased from Invitrogen™. Chlorin e6 was purchased from Santa Cruz Biotechnology. BeyoFast™ SYBR Green One-Step qRT-PCR Kit was purchased from Beyotime. *P. aeruginosa* DNA gyrase assay kit was purchased from Inspiralis. Quantitative polymerase chain reaction (qPCR) was conducted using a QuantStudio™ 7 Flex Real-Time PCR System with MicroAmp™ Fast 8-Tube Strip.

The other materials and instruments used in this chapter were the same as those reported in Chapter II (**Section 2.2.1**) and Chapter III (**Section 3.2.1**).

4.2.2 Synthesis of TPA-IN

The synthesis of membrane disruptor-like TPA derivatives was similar to that described in **Section 2.2.8.** TPA-IN was synthesized by replacing M1 with 1-ethyl-3,3-dimethyl-3H-indol-1-ium. TPA-IN was obtained as a deep blue solid (20 mg, 15% yield). ^{1}H NMR (400 MHz, CD_3OD) δ= 8.61 (d, *J* = 15.33 Hz, 1H), 7.97 (d, *J* = 4.14 Hz, 1H), 7.75-7.72 (m, 2H), 7.66-7.56 (m, 5H), 7.14-7.08 (m, 5H), 6.98 (d, *J* = 9.02 Hz, 4H), 6.87 (d, *J* = 8.89 Hz, 2H), 4.61-4.55 (m, 2H), 4.13 (t, *J* = 5.62 Hz, 4H), 3.62-3.58 (m, 4H), 3.21 (s, 18H), 2.35-2.28 (m, 4H), 1.83 (s, 6H), 1.55 ppm (t, *J* =7.28, 3H). ^{13}C NMR (100 MHz, CD_3OD) δ= 180.0, 157.3, 156.0, 150.9, 146.7, 143.5, 140.6, 140.0, 138.0, 129.1, 128.7, 127.4, 127.2, 124.4, 123.8, 122.7, 118.5, 115.4, 113.7, 107.2, 64.6, 64.1, 52.3, 52.23, 52.20, 51.8, 41.3, 25.3, 23.0. 12.3 ppm. HRMS (ESI) *m/z* calcd for $C_{48}H_{61}N_4O_2S^{3+}$ 252.4833 $[M-3Br]^{3+}$; found 252.4842.

4.2.3 Synthesis of TPA-BIN

TPA-BIN was synthesized by replacing M1 with 3-ethyl-1,1-dimethyl-1H-benzo[e]indol-3-ium. TPA-BIN was obtained as a deep blue solid (40 mg, 28.5% yield). ^{1}H NMR (400 MHz, CD_3OD) δ= 8.68 (d, *J* = 15.45 Hz, 1H), 8.38 (d, *J* = 8.46 Hz, 1H), 8.21 (d, *J* = 8.83 Hz, 1H), 8.13 (d, *J* = 8.09 Hz, 1H), 7.97 (d, *J* = 3.86 Hz, 1H), 7.92 (d, *J* = 8.83 Hz, 1H), 7.79 (t, *J* = 7.45 Hz, 1H), 7.69-7.64 (m, 3H), 7.57 (d, *J* = 4.23 Hz, 1H), 7.16-7.11 (m, 5H), 6.98 (d, *J* = 8.65 Hz, 4H), 6.87 (d, *J* = 8.46 Hz, 2H), 4.73-4.68 (m, 2H), 4.13 (t, *J* = 5.52 Hz, 4H), 3.63-3.58 (m, 4H), 3.21 (s, 18H), 2.35-2.28 (m, 4H), 2.08 (m, 6H), 1.61 ppm (t, *J* = 7.17 Hz, 3H). ^{13}C NMR (100 MHz, CD_3OD) δ= 180.9, 156.8, 155.8, 150.6, 145.3, 140.4, 140.0, 133.6, 131.3, 130.0, 128.1, 127.42, 127.36, 127.2, 126.8, 124.4, 124.0, 122.6, 118.6, 115.4, 1117.8, 106.9, 64.6, 64.1, 53.5, 52.3, 52.25, 52.22, 41.5, 25.2, 23.0, 12.5 ppm. HRMS (ESI) *m/z* calcd for $C_{52}H_{63}N_4O_2S^{3+}$ 269.1552 $[M\text{-}3Br]^{3+}$; found 269.1561.

4.2.4 Synthesis of TPA-C3-C6

TPA-C3-C6 was synthesized by replacing M1 with 3-hexyl-2-methylbenzo[d]thiazol-3-ium. TPA-C3-C6 was obtained as a dark purple solid (40 mg, 19% yield). ^{1}H NMR (600 MHz, CD_3OD) δ= 8.36 (d, *J* = 15.5 Hz, 1H), 8.20 (d, *J* = 7.96 Hz, 1H), 8.12 (d, *J* = 7.96 Hz, 1H), 7.86-7.83 (m, 1H), 7.76-7.73 (m, 2H), 7.58 (d, *J* = 8.80 Hz, 2H), 7.47 (d, *J* = 4.19 Hz, 1H), 7.43 (d, *J* = 14.65 Hz, 1H), 7.11 (d, *J* = 8.80 Hz, 4H), 6.97 (d, *J* = 8.80 Hz, 4H), 6.86 (d, *J* = 8.80 Hz, 2H), 4.83 (t, *J* = 7.96 Hz, 2H), 4.12 (t, *J* = 6.07 Hz, 4H), 3.61-3.59 (m, 4H), 3.21 (s, 18H), 2.33-2.29 (m, 4H), 1.99-1.94 (m, 2H), 1.54-1.49 (m, 2H), 1.43-1.33 (m, 4H), 0.92 ppm (t, *J* = 7.12 Hz, 3H). ^{13}C NMR (150 MHz, CD_3OD) δ= 172.4, 157.2, 155.8, 151.6, 143.5, 142.8, 141.6, 139.6, 138.3, 130.8, 129.6, 129.3, 128.6, 128.2, 125.6, 125.1, 124.9, 120.3, 117.2, 116.7, 109.6, 66.0, 65.6, 65.54, 65.51, 53.7, 53.63, 53.61, 32.5, 29.9, 27.2, 24.4, 23.6, 14.3 ppm. HRMS (ESI) *m/z* calcd for $C_{49}H_{63}N_4O_2S_2^{3+}$ 267.8125 $[M\text{-}3Br]^{3+}$; found 267.8134.

4.2.5 Synthesis of TPA-C3-C8

TPA-C3-C8 was synthesized by replacing M1 with 2-methyl-3-octylbenzo[d]thiazol-3-ium. TPA-C3-C8 was obtained as a dark purple solid (20 mg, 14% yield). ^{1}H NMR (600 MHz, CD_3OD) δ= 8.36 (d, *J* = 14.96 Hz, 1H), 8.20 (d, *J* = 8.35 Hz, 1H), 8.12 (d, *J* = 8.35 Hz, 1H), 7.84 (t, *J* = 7.95 Hz, 1H), 7.76-7.73 (m, 2H), 7.58 (d, *J* = 8.76 Hz, 2H), 7.47 (d, *J* = 3.91 Hz, 1H), 7.42 (d, *J* = 15.09 Hz, 1H), 7.11 (d, *J* = 8.89 Hz, 4H), 6.97 (d, *J* = 8.91 Hz, 4H), 6.86 (d, *J* = 8.91 Hz, 2H), 4.83 (t, *J* = 7.5 Hz, 2H), 4.12 (d, *J* = 5.63 Hz, 4H), 3.61-3.59 (m, 4H), 3.21 (s, 18H), 2.34-2.29 (m, 4H), 1.99-1.94 (m, 2H), 1.53-1.48 (m, 2H), 1.45-1.40 (m, 2H), 1.33-1.28 (m, 6H), 0.85 ppm (t, *J* = 6.80 Hz, 3H). ^{13}C NMR (150 MHz, CD_3OD) δ= 172.5, 157.2, 157.2, 155.8, 151.6, 143.5, 142.8, 141.6, 139.6, 138.4, 130.7, 129.6, 129.3, 128.6, 128.3, 125.6, 125.2, 124.9, 120.3, 117.3, 116.8, 109.7, 66.0, 65.6, 65.55, 65.53, 53.7, 53.65, 53.63, 33.0, 30.3, 30.2, 29.9, 27.5, 24.4, 23.7, 14.5 ppm. HRMS (ESI) *m/z* calcd for $C_{51}H_{67}N_4O_2S_2^{3+}$ 277.1563 $[M-3Br]^{3+}$; found 277.1573.

4.2.6 Synthesis of TPA-C6-C6

TPA-C6-C6 was synthesized by replacing dibromopropane with dibromohexane in compound 2 and M1 with 3-hexyl-2-methylbenzo[d]thiazol-3-ium. TPA-C6-C6 was obtained as a dark purple solid (40 mg, 18% yield). ^{1}H NMR (600 MHz, CD_3OD) δ= 8.35 (d, *J* = 15.06 Hz, 1H), 8.19 (d, *J* = 8.10 Hz, 1H), 8.11 (d, *J* = 8.58 Hz, 1H), 7.84 (t, *J* = 7.89 Hz, 1H), 7.75-7.73 (m, 2H), 7.57 (d, *J* = 8.64 Hz, 2H), 7.46 (d, *J* = 4.02 Hz, 1H), 7.41 (d, *J* = 15.12 Hz, 1H), 7.09 (d, *J* = 8.70 Hz, 4H), 6.92 (d, *J* = 8.76 Hz, 4H), 6.85 (d, *J* = 8.64 Hz, 2H), 4.82 (t, *J* = 7.53 Hz, 2H), 4.00 (t, *J* = 6.21 Hz, 4H), 3.37-3.34 (m, 4H), 3.31 (s, 18H), 1.99-1.94 (m, 2H), 1.83-1.82 (m, 8H), 1.64-1.59 (m, 4H), 1.53-1.45 (m, 6H), 1.43-1.33 (m, 4H), 0.92 ppm(t, *J* = 7.14 Hz, 3H). ^{13}C NMR (150 MHz, CD_3OD) δ= 172.4, 157.9, 156.0, 151.9, 143.5, 142.8, 141.0, 139.7, 138.2, 130.8, 129.6, 129.3, 128.7, 128.2, 125.2, 125.0, 124.9, 119.9, 116.6, 109.5, 69.0, 67.8,

53.5, 53.499, 53.474, 32.5, 30.2, 30.0, 27.3, 27.1, 26.8, 23.9, 23.6, 14.3 ppm. HRMS (ESI) *m/z* calcd for $C_{55}H_{75}N_4O_2S_2^{3+}$ 295.8438 $[M\text{-}3Br]^{3+}$; found 295.8449.

4.2.7 Synthesis of TPA-C6-C8

TPA-C6-C8 was synthesized by replacing dibromopropane with dibromohexane in compound 2 and M1 with 2-methyl-3-octylbenzo[d]thiazol-3-ium. TPA-C6-C8 was obtained as a dark purple solid (40 mg, 17% yield). ^{1}H NMR (600 MHz, CD_3OD) δ= 8.25 (d, *J* = 15.00 Hz, 1H), 8.14 (d, *J* = 7.98 Hz, 1H),8.06 (d, *J* = 8.58 Hz, 1H),7.81-7.79 (m, 1H), 7.70-7.68 (m, 2H), 7.47 (d, *J* = 8.82 Hz, 2H), 7.39 (d, *J* = 4.02 Hz, 1H), 7.30 (d, *J* = 15.12 Hz, 1H), 7.05 (d, *J* = 8.88 Hz, 4H), 6.91(d, *J* = 8.94 Hz, 4H), 6.75 (d, *J* = 8.76 Hz, 2H),4.75 (t, *J* = 7.53 Hz, 2H),4.00 (t, *J* = 6.21 Hz, 4H),3.37-3.34 (m, 4H), 3.14 (s, 18H), 1.95-1.89 (m, 2H), 1.86-1.81 (m, 8H), 1.63-1.58 (m, 4H), 1.50-1.46 (m, 6H), 1.42-1.38 (m, 2H), 1.33-1.26 (m, 6H), 0.85 ppm (t, *J* = 6.84 Hz, 3H). ^{13}C NMR (150 MHz, CD_3OD) δ= 172.1, 157.9, 156.0, 151.8, 143.4, 142.7, 140.8, 139.9, 138.2, 130.8, 129.5, 129.2, 128.7, 128.2, 125.0, 124.9, 119.6, 116.6, 109.3, 69.0, 67.8, 53.52, 53.50, 53.47, 33.0, 30.31, 30.27, 30.2, 29.9, 27.5, 27.1, 26.8, 23.9, 23.7, 14.5 ppm. HRMS (ESI) *m/z* calcd for $C_{57}H_{79}N_4O_2S_2^{3+}$ 305.1876 $[M\text{-}3Br]^{3+}$; found 305.1887.

4.2.8 Synthesis of TPA-C3-C6P

TPA-C3-C6P was synthesized by replacing M1 with 1-hexyl-4-methylquinolin-1-ium. TPA-C3-C6P was obtained as a dark purple solid (10 mg, 5% yield). ^{1}H NMR (600 MHz, CD_3OD) δ= 9.06 (d, *J* = 6.60 Hz, 1H), 8.81 (d, *J* = 8.22 Hz, 1H), 8.44 (d, *J* = 8.94 Hz, 1H), 8.30-8.27 (m, 2H), 8.25-8.22 (m, 1H), 8.02 (t, *J* = 7.74 Hz, 1H),7.86 (d, *J* = 15.48 Hz, 1H), 7.59-7.57 (m, 3H), 7.40 (d, *J* = 3.96 Hz, 1H), 7.10 (d, *J* = 8.94 Hz, 4H), 6.96 (d, *J* = 9.00 Hz, 4H), 6.89 (d, *J* = 8.82 Hz, 2H), 4.12 (t, *J* = 5.64 Hz, 4H), 3.61-3.58 (m, 4H), 3.21 (s, 18H), 2.34-2.29 (m, 4H), 2.09-2.03 (m, 2H), 1.52-1.47 (m, 2H), 1.42-1.35 (m, 6H), 0.92 ppm (t, *J* = 7.11 Hz, 3H). ^{13}C NMR (150 MHz, CD_3OD) δ= 156.9, 154.9, 151.8, 150.9, 147.6, 142.0, 140.4, 139.8, 137.9,

136.5, 136.2, 128.4, 127.9, 127.5, 126.5, 124.6, 120.9, 119.9, 117.8, 116.7, 116.4, 66.0, 65.6, 65.6, 65.6, 58.4, 53.7, 53.7, 53.6, 32.4, 30.9, 27.3, 24.4, 23.6, 14.3 ppm. HRMS (ESI) *m/z* calcd for $C_{51}H_{65}N_4O_2S^{3+}$ 265.8271 $[M-3Br]^{3+}$; found 265.8280.

4.2.9 Synthesis of TPA-N2-C3-C6

TPA-N2-C3-C6 was synthesized by replacing trimethylamine with N,N,N′,N′-Tetramethylethylenediamine in compound 4 and M1 with 3-hexyl-2-methylbenzo[d]thiazol-3-ium. TPA-N2-C3-C6 was obtained as a dark purple solid (100 mg, 50 % yield). ^{1}H NMR (600 MHz, CD_3OD) δ= 8.36 (d, *J* = 15.18 Hz, 1H), 8.20 (d, *J* = 8.04 Hz, 1H), 8.12 (d, *J* = 8.52 Hz, 1H), 7.86-7.83 (m, 1H), 7.76-7.73 (m, 2H), 7.59 (d, *J* = 8.16 Hz, 2H), 7.47 (d, *J* = 3.84 Hz, 1H), 7.43 (d, *J* = 15.06 Hz, 1H), 7.11 (d, *J* = 8.28 Hz, 4H), 6.97 (d, *J* = 8.34 Hz, 4H), 6.86 (d, *J* = 8.16 Hz, 2H), 4.83 (t, *J* = 7.44 Hz, 2H), 4.14-4.13 (m, 4H), 3.90-3.88 (m, 4H), 3.69-3.67 (m, 8H), 3.27 (s, 12H), 2.94 (s, 12H), 2.36-2.32 (m, 4H), 1.99-1.94 (m, 2H), 1.54-1.50 (m, 2H), 1.43-1.38 (m, 2H), 1.37-1.32 (m, 2H), 0.92 ppm (t, *J* = 7.05 Hz, 3H). ^{13}C NMR (150 MHz, CD_3OD) δ= 172.5, 157.1, 155.8, 151.6, 143.5, 142.8, 141.6, 139.6, 138.4, 130.9, 129.6, 129.3, 128.6, 128.3, 125.7, 125.2, 124.9, 120.3, 119.2, 117.3, 117.2, 116.8, 109.7, 65.9, 64.4, 58.9, 51.9, 51.1, 44.3, 32.5, 30.0, 27.3, 24.0, 23.6, 14.3 ppm. HRMS (ESI) *m/z* calcd for $C_{55}H_{77}N_6O_2S_2^{3+}$ 305.8511 $[M-3Br]^{3+}$; found 305.8522.

4.2.10 SYTOX Green Assay

Overnight cultures of *S. aureus* and *P. aeruginosa* were washed with PBS three times and diluted to OD = 0.2 with PBS. 4 μM of SYTOX Green was added to the bacterial suspension and incubated for 15 minutes in the dark at room temperature. 196 μL of bacteria suspension was transferred to the wells of a black 96-well plate. The fluorescence signals of the wells were monitored at 523 nm with an excitation at 504 nm. 4 μL of TPA-C3-C6 or PBS was added to

the solution after the fluorescence signals were stabilized (about an hour). The fluorescence signals were further recorded for 5 minutes. This experiment was conducted in triplicate.

4.2.11 Real-Time Quantitative Reverse Transcription PCR (RT-qPCR)

Overnight cultures of *S. aureus* and *P. aeruginosa* in TSB were diluted to 10^7 CFU/mL in MHB (1% glucose). 10 μL of the diluted cultures were added to a 96-well plate containing 90 μL of serially diluted TPA-C3-C6 in MHB (1% glucose). The plate was incubated at 37℃ for 24 hours. The wells without the addition of TPA-C3-C6 were used as a control. RNA extraction was performed on four independent wells of each TPA-C3-C6 concentration as well as the control without TPA-C3-C6, using a TRIzolTM Plus RNA Purification Kit. The extracted RNA was quantified by measuring the absorption at 260 nm. RT-qPCR reaction mixtures were prepared with a BeyoFast™ SYBR Green One-Step qRT-PCR Kit. qPCR reactions were conducted using a QuantStudio™ 7 Flex Real-Time PCR System. The PCR cycle was set up as follows: (a) 50℃ 30 minutes (reverse transcription) → (b) 95℃ 2 minutes (preheat for denaturation) → (c) 95℃ 15 seconds (denaturation) → (d) 60℃ 30 seconds (annealing & extension). (c) to (d) were repeated for 40 cycles. A melting curve analysis was conducted after the PCR reactions with the following settings: 95℃ 15 seconds → 60℃ 15 seconds → 95℃ 15 seconds.

4.2.12 Biofilm Recurrence Assay

After the *S. aureus* and *P. aeruginosa* were cultured in TSB for 16 to 20 hours, they were diluted to 10^6 CFU/mL in MHB (1% glucose). 100 μL of the diluted cultures was transferred to 96-well plates and incubated at 37℃ for 24 hours to form biofilms. The biofilms were then washed with PBS three times. 150 μL of serially diluted TPA-C3-C6 in PBS was added to the biofilms with blank PBS as a control and incubated for 20 minutes at 30℃. Vancomycin (*S. aureus*) and meropenem (*P. aeruginosa*) were used to compare the antibacterial effects of TPA-C3-C6.

After incubation, the biofilms were irradiated with 600 nm light (60 mW/cm^2) for 45 minutes. The solution in the wells was removed and replaced with corresponding compounds or PBS in MHB (1% glucose). The plates were incubated for another 16 to 20 hours. Finally, the number of viable bacterial cells inside the biofilm was quantified by plate colony counting, as described in **Section 3.2.4**.

4.2.13 Mass Spectrometry (MS)-Based Proteomic Study

Biofilms treated with TPA-C3-C6 or PBS with and without light irradiation were prepared in accordance with the procedures reported in **Section 4.2.12**. Then, the proteins in the biofilms were extracted and digested using an EasyPep™ MS Sample Prep Kit from Thermo Scientific™.

The tryptic digests (2 μL) were injected into a DIONEX UltiMate 3000 RSLCSnano UPLC system (Thermo Scientific, USA). A trap-and-elute method was adopted with a PepMap 5 mm x 300 μm C18 (Thermo Scientific, USA) and an Aurora 25 cm x 75 μm C18 column with CSI emitter (IonOpticks, Australia) with a trapping flow of 50 μL/min for 2 min in 50 °C. The elution gradient was applied with water (Solvent A) and acetonitrile (Solvent B) in 0.1% formic acid as follows: 2% B in 0-2 min, 5-35% B in 2-47 min, 35-90% B in 47-51 min, 90% B in 51-56 min, and 2% B from 56-60 min, in a constant 300 nL/min flow rate. Eluted samples were then introduced into a TimsTOF Pro 2 mass spectrometer (Bruker Daltonics, USA). The source parameters were 1400 V of capillary voltage and 3.0 L/min of dry gas at 180 °C. The inverse reduced ion mobility ($1/K_0$) of TIMS was set between 0.6-1.6 B_s/cm^2, and the ramp time was 100 ms. Data analysis was performed using the Spectronaut 19 proteomics software with factory settings to search against the reviewed *S. aureus* database (11,274 sequences; 8 December 2024) from UniProt.

Differentially expressed proteins (DEP)s were identified as p-value < 0.05 and Log_2(Fold Change) > 1 or < -1. Gene Ontology (GO) enrichment analysis was conducted using the PANTHER Overrepresentation Test (Released 20240807).[126, 127] The UniProt IDs of the identified proteins were used to search against the *Staphylococcus aureus* (all genes in database) and the *Pseudomonas aeruginosa* (all genes in database) reference database. Fisher's exact test and Bonferroni correction test were used as the statistical significance test and correction for multiple testing, respectively. Only GO terms with a Bonferroni-adjusted p-value less than 0.05 were considered significant. Kyoto Encyclopedia of Genes and Genomes (KEGG) pathway enrichment analysis was performed using the clusterprofiler package in RStudio.[128] The UniProt IDs of the identified proteins were searched against KEGG organisms code sao and pae for *S. aureus* and *P. aeruginosa*, respectively. The Bonferroni test was used as the correction test with an adjusted p-value cutoff of 0.05.

4.2.14 Other Assays in Chapter IV

Other assays discussed in this chapter were conducted in a similar manner as described in **Section 2.2** and **Section 3.2.**

4.3 Results and Discussions

4.3.1 Structural Design of New TPA Derivatives for Eradicating Bacteria in the Dark

As discussed in **Section 2.3.3**, the intrinsic antibacterial mechanisms of TPA-1 can be attributed to its interaction with the bacterial cell membrane. Damaging the bacterial membranes has been proven to be an effective antibacterial strategy.[168, 169] Many membrane-disruptive molecules have a detergent-like structure, which includes positively charged fragments for electrostatic interactions with the negatively charged bacterial membranes and a highly hydrophobic tail for membrane disruption.[125, 170, 171] Besides, modifications to the charged fragments and hydrophobic tails could alter the antibacterial activity of these molecules against both Gram-positive and Gram-negative bacteria. Based on the common structure of membrane disruptive molecules, several new TPA-1 derivatives that aim to maintain the photosensitizing ability and provide extra bacterial cell membrane disruptive activity on a broad-spectrum of bacteria have been designed and synthesized.

As shown in **Figure 4.1**, the newly synthesized TPA derivatives still maintain a donor-π-acceptor (D-π-A) structure, which promotes intramolecular charge transfer (**Section 2.3.1**). In order to keep the molecule as an AIE active PS, the triphenylamine core and thiophene bridge were retained as triphenylamine is important for AIE activity, and thiophene can extend the conjugate system while introducing sulphur atom into the system to promote intersystem crossing (**Section 2.3.1**). The major modifications are the quaternary ammonium side chains and the electron acceptors. The length and the polarity of the ammonium side chains were modified. Several electron acceptor groups with different hydrophobicity were also introduced into the structure for structure-activity relationship studies.

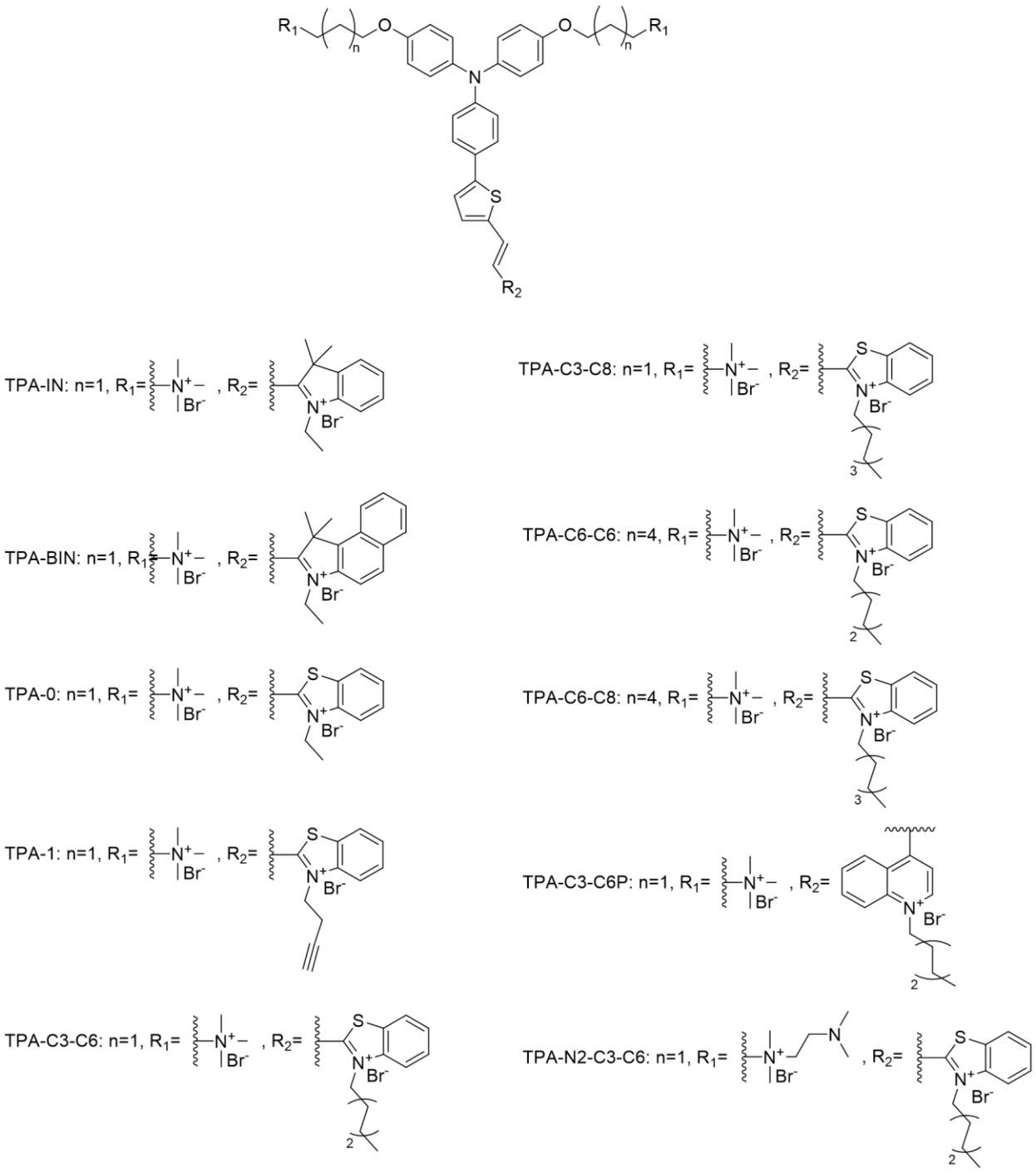

Figure 4.1. The structures of the membrane disruptor-like TPA derivatives.

4.3.2 Structure-Activity Relationship Studies of TPA Derivatives on Antiplanktonic Activities and Cytotoxicity without Light Irradiation

The antiplanktonic activities of different TPA derivatives against *S. aureus* and *P. aeruginosa* without light irradiation were assessed by MICs. The results are shown in **Table 4.1**.

The effect of different electron acceptor groups on the antibacterial activity was evaluated. Three electron acceptor groups were chosen, namely 3-ethyl-2-methylbenzo[d]thiazol-3-ium (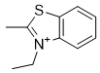), 1-ethyl-2,3,3-trimethyl-3H-indol-1-ium (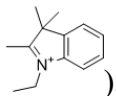), and 3-ethyl-1,1,2-trimethyl-1H-benzo[e]indol-3-ium (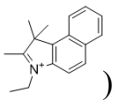). The hydrophobicity of the electron acceptor groups increases from 3-ethyl-2-methylbenzo[d]thiazol-3-ium to 3-ethyl-1,1,2-trimethyl-1H-benzo[e]indol-3-ium. The MIC results showed that the TPA derivative with the least hydrophobic electron acceptor, which is TPA-0 with 3-ethyl-2-methylbenzo[d]thiazol-3-ium, had the best overall MIC values (3.13 μM against *S. aureus* and 50 μM against *P. aeruginosa*). Therefore, the 2-methylbenzothiazol-3-ium derivative was selected for further modifications.

The effect of the length of the quaternary ammonium side chains on the triphenylamine core and the substituents of the benzothiazolium were investigated. From the MIC results, increasing the quaternary ammonium side chain length from three carbons to six carbons decreased the antibacterial activity. In addition, increasing the length of the substituents on the 2-methylbenzothiazol-3-ium moiety from two carbons to six carbons enhanced the antibacterial activity. However, a further increase from six carbons to eight carbons lowered the antibacterial effects. The optimal lengths are three carbons on quaternary ammonium side chains and six carbons on the substituents of the benzothiazolium moiety (TPA-C3-C6). TPA-C3-C6 showed good antiplanktonic activity against *S. aureus* (MIC: 3.13 μM) and moderate activity against *P. aeruginosa* (MIC: 20 μM).

Based on TPA-C3-C6, TPA-C3-C6P was synthesized to investigate the effect of molecular shape. TPA-C3-C6 has an L shape from the TPA core, whereas TPA-C3-C6P is linear in shape. For the MIC values, the shape did not affect the antibacterial activity. TPA-N2-C3-C6 was also synthesized from TPA-C3-C6 by increasing the number of polar groups on the quaternary ammonium side groups. This modification reduced the antibacterial effects of TPA-C3-C6. Overall, TPA-C3-C6 and TPA-C3-C6P have the best antibacterial activities against *S. aureus* and *P. aeruginosa*. Moreover, TPA-C3-C6 and TPA-C3-C6P are also active against a drug-resistant strain (MRSA) with a MIC of 3.13 μM, and three additional Gram-negative bacteria (*E. coli*, *K. pneumoniae*, and *A. baumannii*) ranged from 6.25 μM to 10 μM (**Table 4.2**).

Apart from antibacterial activity, it is also important for the compounds to have low cytotoxicity. Therefore, the cytotoxic effects of TPA-C3-C6 and TPA-C3-C6P against human cells were studied. As shown in **Figure 4.2a** and **Figure 4.2b**, TPA-C3-C6P showed high toxicity (CC_{50} = 29 ± 5 μM) against human fibroblast cells (HFF-1), indicating that TPA-C3-C6P may have low selectivity between the bacterial cell membrane and the human cell membrane. On the other hand, TPA-C3-C6 showed a low cytotoxicity against HFF-1 cells. The CC_{50} value of TPA-C3-C6 is 150 ± 10 μM, which is higher than the US FDA-approved PS Chlorin e6 (Ce6). The structure of TPA-C3-C6 and TPA-C3-C6P is very similar, except for the electron acceptor. The low cytotoxicity of TPA-C3-C6 may be due to the benzothiazolium group, which makes the overall structure bend into an L shape (**Figure 4.3**). This L-shaped structure may help to prevent the hydrophobic part of the molecule from inserting into the human cell membrane.

Furthermore, the haemolytic activity of TPA-C3-C6 was investigated (**Figure 4.2c**). At a concentration as high as 400 μM, TPA-C3-C6 only induced 10% ± 1% of haemolysis on human erythrocytes. As shown in **Figure 4.4**, TPA-C3-C6 is capable of generating ROS under light irradiation. Therefore, the light toxicity of TPA-C3-C6 against human cells was also assessed

(**Figure 4.2d)**. After irradiating HFF-1 cells with 80 μM TPA-C3-C6 for 45 minutes, the HFF-1 cell viability remained over 60%. This result indicated that PDT with TPA-C3-C6 caused limited toxicity to human cells. Along with its antibacterial activities, these results suggested that TPA-C3-C6 exhibited broad-spectrum antibacterial activity while maintaining relatively low cytotoxicity. Hence, TPA-C3-C6 is a promising candidate for further investigation into its antibacterial mechanisms and antibiofilm activity.

Table 4.1. The minimum inhibitory concentrations of TPA derivatives and control antibiotics against *S. aureus* and *P. aeruginosa*.

Compound	*S. aureus* (ATCC 29213)	*P. aeruginosa* (ATCC 27853)
TPA-IN	3.13 μM	100 μM
TPA-BIN	6.25 μM	50 μM
TPA-0	3.13 μM	50 μM
TPA-1	3.13 μM	>100 μM
TPA-C3-C6	3.13 μM	20 μM
TPA-C3-C8	3.13 μM	50 μM
TPA-C6-C6	6.25 μM	50 μM
TPA-C6-C8	6.25 μM	50 μM
TPA-C3-C6P	3.13 μM	20 μM
TPA-N2-C3-C6	6.25 μM	20 μM
Vancomycin	0.313 μM	-
Polymyxin B	-	1.56 μM
Ciprofloxacin	0.5 μM	0.25 μM

Table 4.2. The minimum inhibitory concentrations of TPA derivatives and control antibiotics against four additional Gram-positive and Gram-negative bacteria.

Compound	MRSA (BAA 41)	*K. pneumoniae* (BAA 1144)	*A. baumannii* (ATCC 19606)	*E. coli* (ATCC 25922)
TPA-C3-C6	3.13 μM	10 μM	10 μM	6.25 μM
TPA-C3-C6P	3.13 μM	10 μM	10 μM	6.25 μM
Vancomycin	0.625 μM	-	-	-
Polymyxin B	-	1.56 μM	1.56 μM	1.56 μM

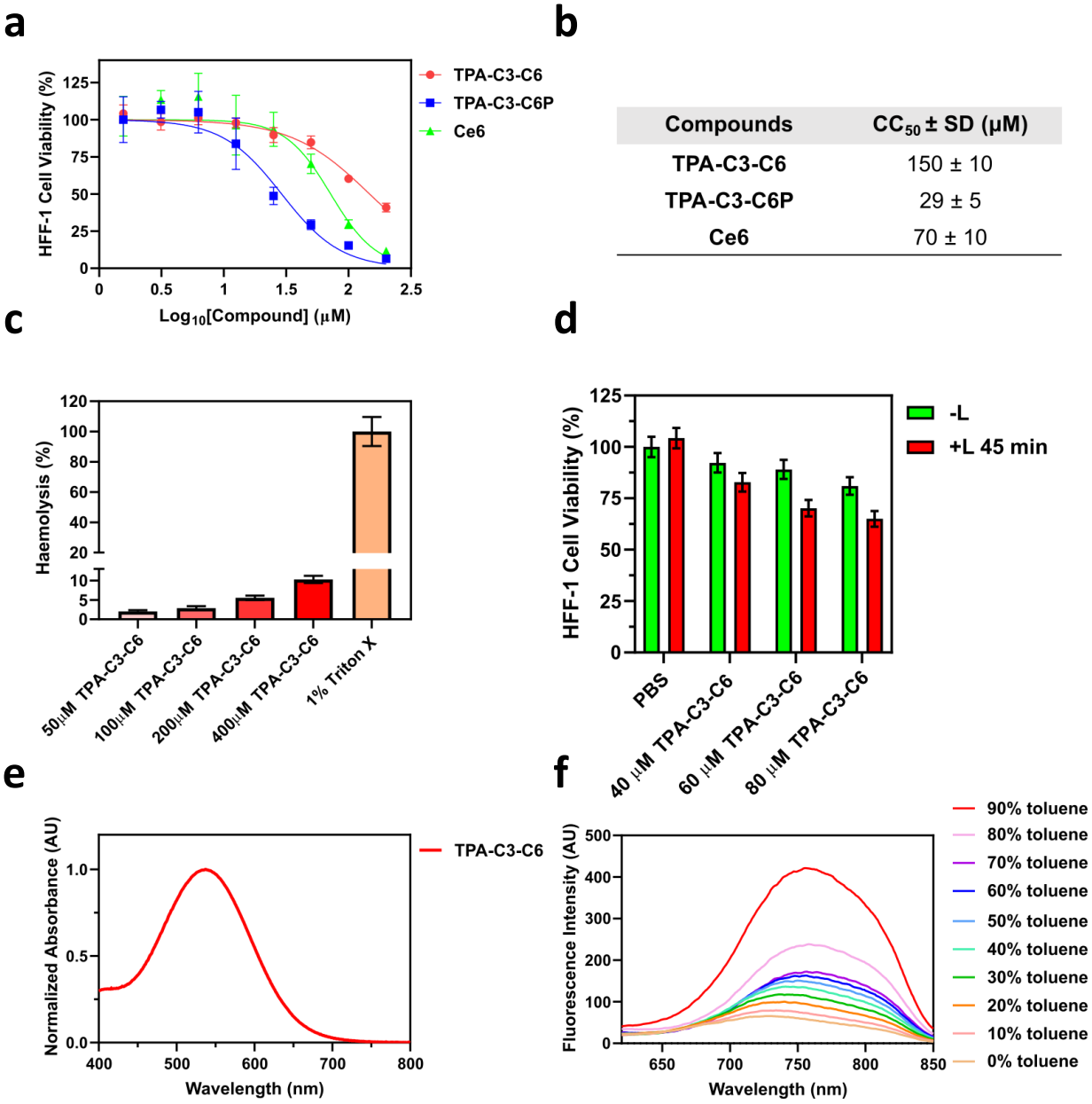

Figure 4.2. (a) The viability of HFF-1 cells after incubation with different compounds for 24 hours. (b) The CC_{50} values of different compounds on HFF-1. (c) The haemolysis rate of TPA-C3-C6 against human erythrocytes. (d) The viability of HFF-1 cells after PDT with different concentrations of TPA-C3-C6. (e) The normalized absorption spectrum of TPA-C3-C6 in water. (f) The fluorescence spectrum of TPA-C3-C6 in methanol with increasing percentages of toluene. TPA-C3-C6 is barely soluble in toluene. The fluorescence intensity increased with the toluene content, indicating the AIE effect of TPA-C3-C6. -L: without light irritation. +L: with 600 nm (60 mW/cm2) light irradiation for 45 minutes. Data are presented as the mean ± SD, n = 3 per group.

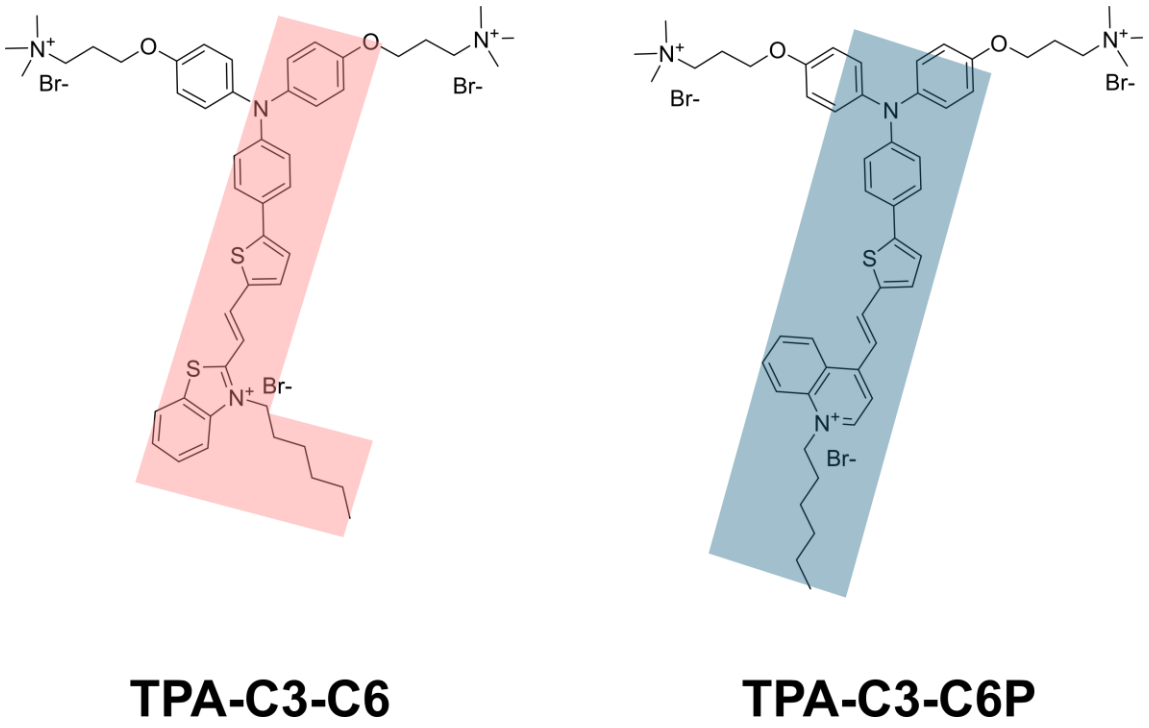

Figure 4.3. The chemical structures of TPA-C3-C6 and TPA-C3-C6P. TPA-C3-C6 has an L shape from the TPA core, while TPA-C3-C6P is linear.

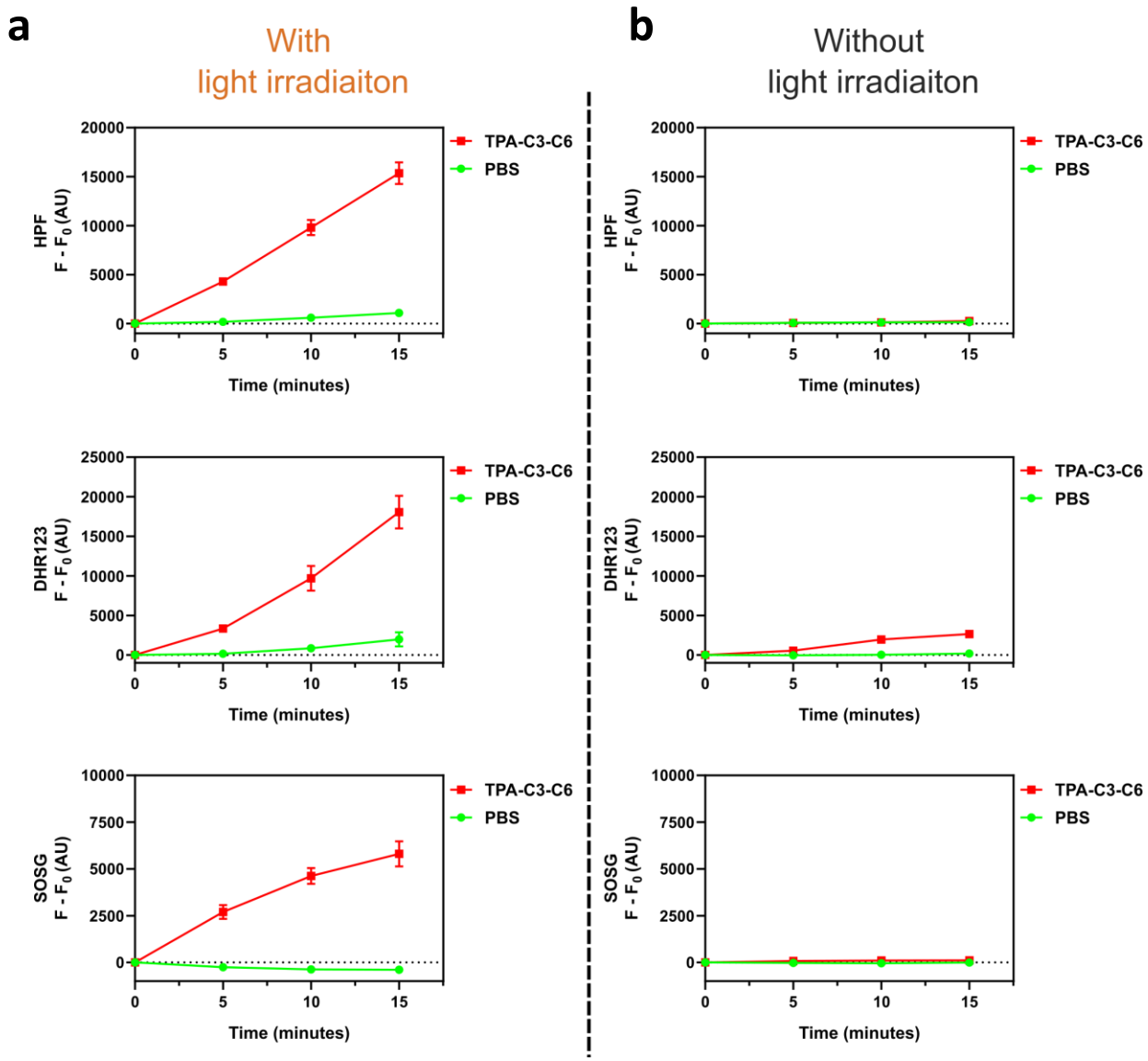

Figure 4.4. The ROS generation assay results of TPA-C3-C6 (10 μM) (a) with or (b) without 600 nm light irradiation (60 mW/cm^2) for 0 to 15 minutes. PBS was used as the negative control. HPF, DHR123, and SOSG were used to detect hydroxyl radical, non-specific ROS, and singlet oxygen, respectively. Data are presented as the mean ± SD, n = 3 per group.

4.3.3 Antibacterial Mechanisms of TPA-C3-C6 without Light Irradiation

The time-kill kinetics of TPA-C3-C6 on *S. aureus* and *P. aeruginosa* were conducted to study the antibacterial mechanisms of the compound. As shown in **Figure 4.5a**, 2 × MIC (6. 25 μM), 4 × MIC (12.5 μM) of TPA-C3-C6, and 4 × MIC (1.25 μM) of vancomycin were able to completely eradicate around 1×10^6 CFU/mL of *S. aureus* in 24 hours, indicating a bactericidal killing mode (> 3 log CFU/mL reduction). Moreover, 4 × MIC of TPA-C3-C6 eradicated all *S. aureus* in six hours, which was more rapid than 4 × MIC of vancomycin, demonstrating that TPA-C3-C6 can kill *S. aureus* more efficiently than vancomycin.

In **Figure 4.5b**, TPA-C3-C6 showed two different killing modes on *P. aeruginosa*. 4 × MIC (80 μM) of TPA-C3-C6 and 4 × MIC (6.25 μM) of polymyxin B could eradicate around 1×10^6 CFU/mL of *P. aeruginosa* within 30 minutes, indicating a strong bactericidal killing mode. However, 2 × MIC (40 μM) of TPA-C3-C6 could only suppress the growth of *P. aeruginosa* but cannot reduce the bacterial count by more than 3 log CFU/mL, suggesting a bacteriostatic mechanism.

Resistance development assays of TPA-C3-C6 against *S. aureus* and *P. aeruginosa* were also conducted to assess if the bacteria can easily generate resistance to TPA-C3-C6. *S. aureus* and *P. aeruginosa* at half MICs were continuously treated with TPA-C3-C6 and ciprofloxacin for 20 days, and the change in MIC of the two compounds was recorded. As shown in **Figure 4.6**, the MIC values of TPA-C3-C6 against *S. aureus* and *P. aeruginosa* were stable throughout the 20 days of treatment. No more than a 2-fold change in MIC was observed. However, the continuous treatment of ciprofloxacin on *S. aureus* and *P. aeruginosa* gave rise to a 16 to 32-fold increase in MIC values on the twentieth day, indicating a significant development of ciprofloxacin resistance. These results suggested that treatment with TPA-C3-C6 had a low tendency to generate resistance.

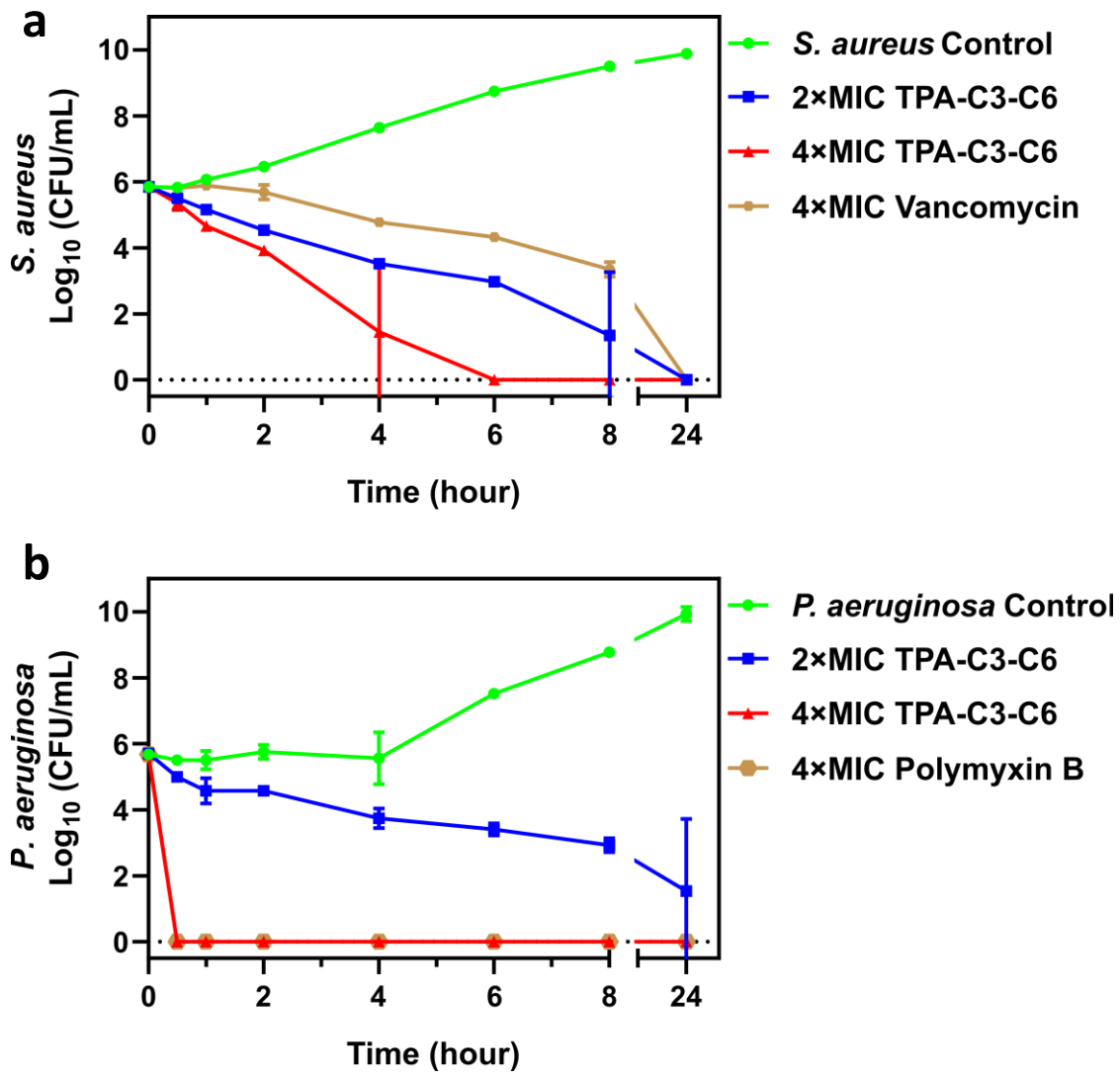

Figure 4.5. The time-kill kinetics assay results of TPA-C3-C6 against (a) *S. aureus* with vancomycin as positive control and (b) *P. aeruginosa* with polymyxin B as positive control. Data are presented as the mean ± SD, $n = 3$ per group.

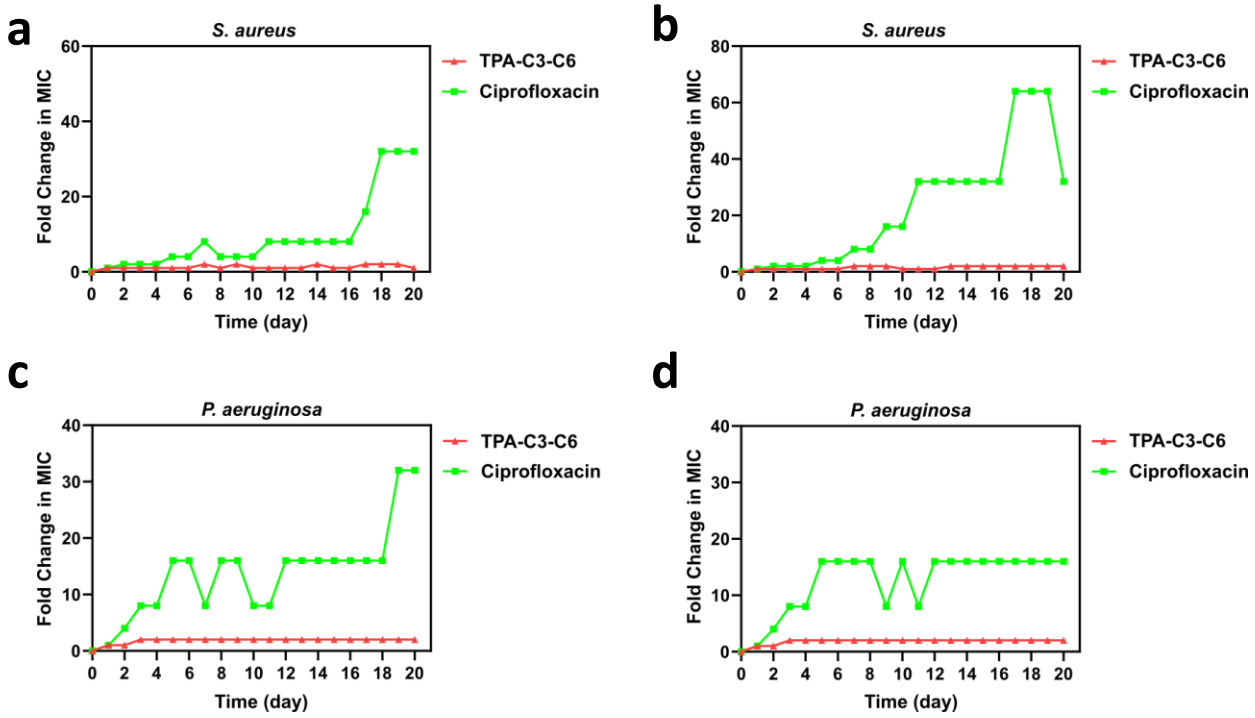

Figure 4.6. The resistance development assay results of TPA-C3-C6 and ciprofloxacin (positive control) against *S. aureus* and *P. aeruginosa*. (a) and (b) are the two independent replicates for *S. aureus*. (c) and (d) are the two independent replicates for *P. aeruginosa*.

Since the structure of TPA-C3-C6 still contains the quaternary ammonium groups, BODIPY™ TR Cadaverine (BTRC) was used to investigate the binding of TPA-C3-C6 with *S. aureus* lipoteichoic acid (LTA) and *P. aeruginosa* lipopolysaccharide (LPS). As shown in **Figure 4.7a** and **Figure 4.7b**, TPA-C3-C6 could displace the BTRC dye from LTA and LPS, indicating that TPA-C3-C6 could bind with LTA and LPS. Additionally, both MIC values of TPA-C3-C6 against *S. aureus* and *P. aeruginosa* increased after the addition of the corresponding LTA and LPS (**Figure 4.7c**, **Figure 4.7d**). This finding supported the hypothesis that binding of TPA-C3-C6 to LTA and LPS is necessary for its antibacterial activity.

TPA-C3-C6 was designed as a bacterial membrane-disruptive molecule. Therefore, assays related to membrane integrity were performed. The bacterial membrane permeability was assessed using SYTOX Green, which is a DNA-binding fluorescent probe. When the bacterial membrane is intact, it blocks SYTOX Green from entering the cell. However, if the bacterial membrane is damaged, SYTOX Green can penetrate the membrane and bind to the genomic DNA to generate a fluorescence signal (**Figure 4.8a**).[172] As shown in **Figure 4.8b** and **Figure 4.8c**, TPA-C3-C6 caused an increase in SYTOX Green signals in both *S. aureus* and *P. aeruginosa*. Meanwhile, the fluorescence signal for PBS control remained relatively stable. These suggested that TPA-C3-C6 could cause bacterial cell membrane damage in Gram-positive *S. aureus* and Gram-negative *P. aeruginosa*.

Apart from investigating the effects on membrane permeability, Disc3(5) was used to evaluate the change in bacterial membrane potential (**Figure 4.9**). Upon the addition of TPA-C3-C6 to *S. aureus* and *P. aeruginosa*, the Disc3(5) fluorescence signals of both bacteria increased, while the fluorescence signal for PBS control remained steady. These results show that TPA-C3-C6 can depolarize the bacterial membrane. Together with the SYTOX Green results, it implied that TPA-C3-C6 could affect the bacterial membrane integrity of both Gram-positive and Gram-negative bacteria.

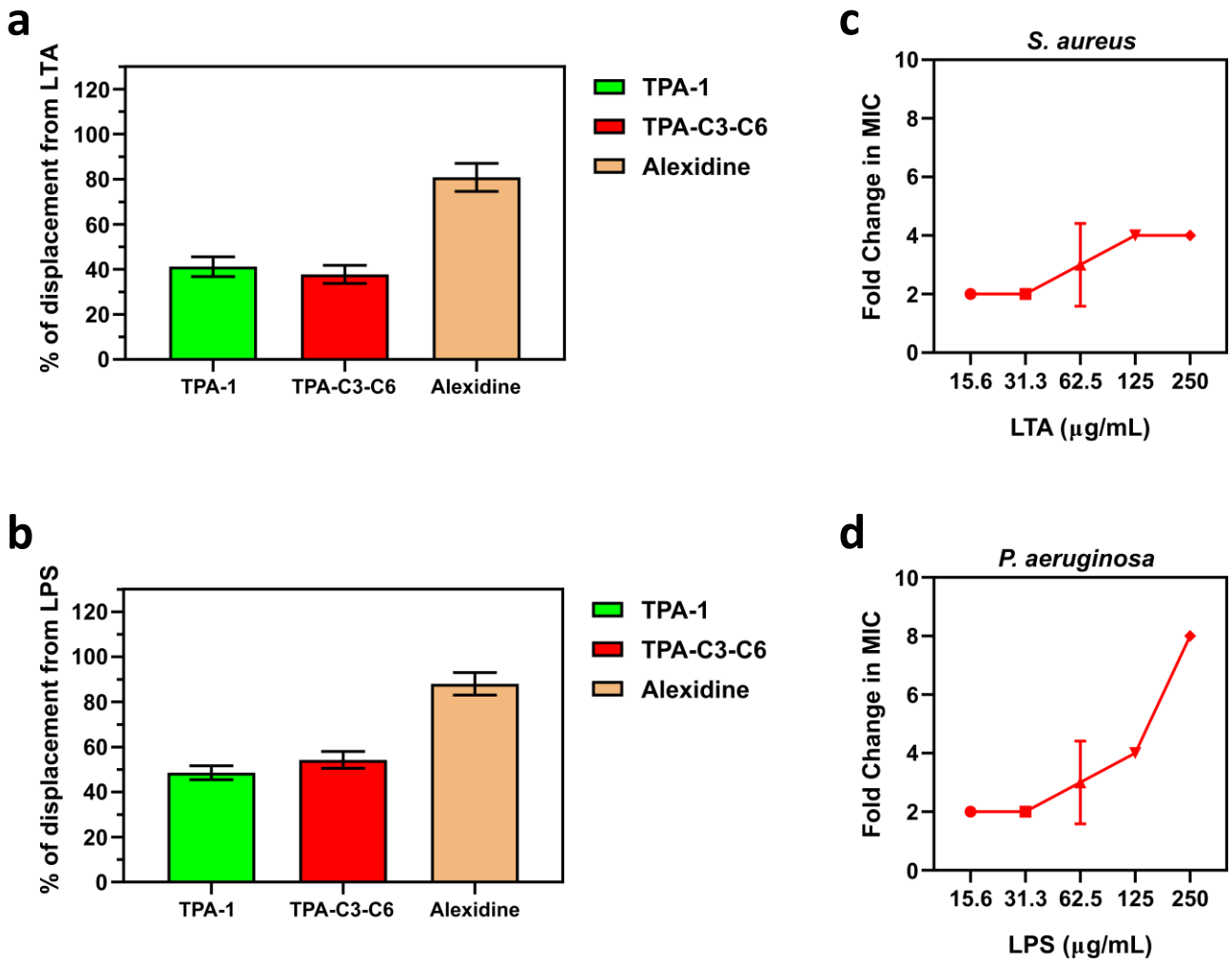

Figure 4.7. The (a) LTA and (b) LPS binding assay results of TPA compounds (10 µM) and alexidine (positive control, 10 µM) using BODIPY™ TR Cadaverine. Data are presented as the mean ± SD, n = 3 per group. (c) The fold change in MIC values of TPA-C3-C6 against *S. aureus* after the addition of LTA and (d) against *P. aeruginosa* after the addition of LPS. Data are presented as the mean ± SD, n = 2 per group.

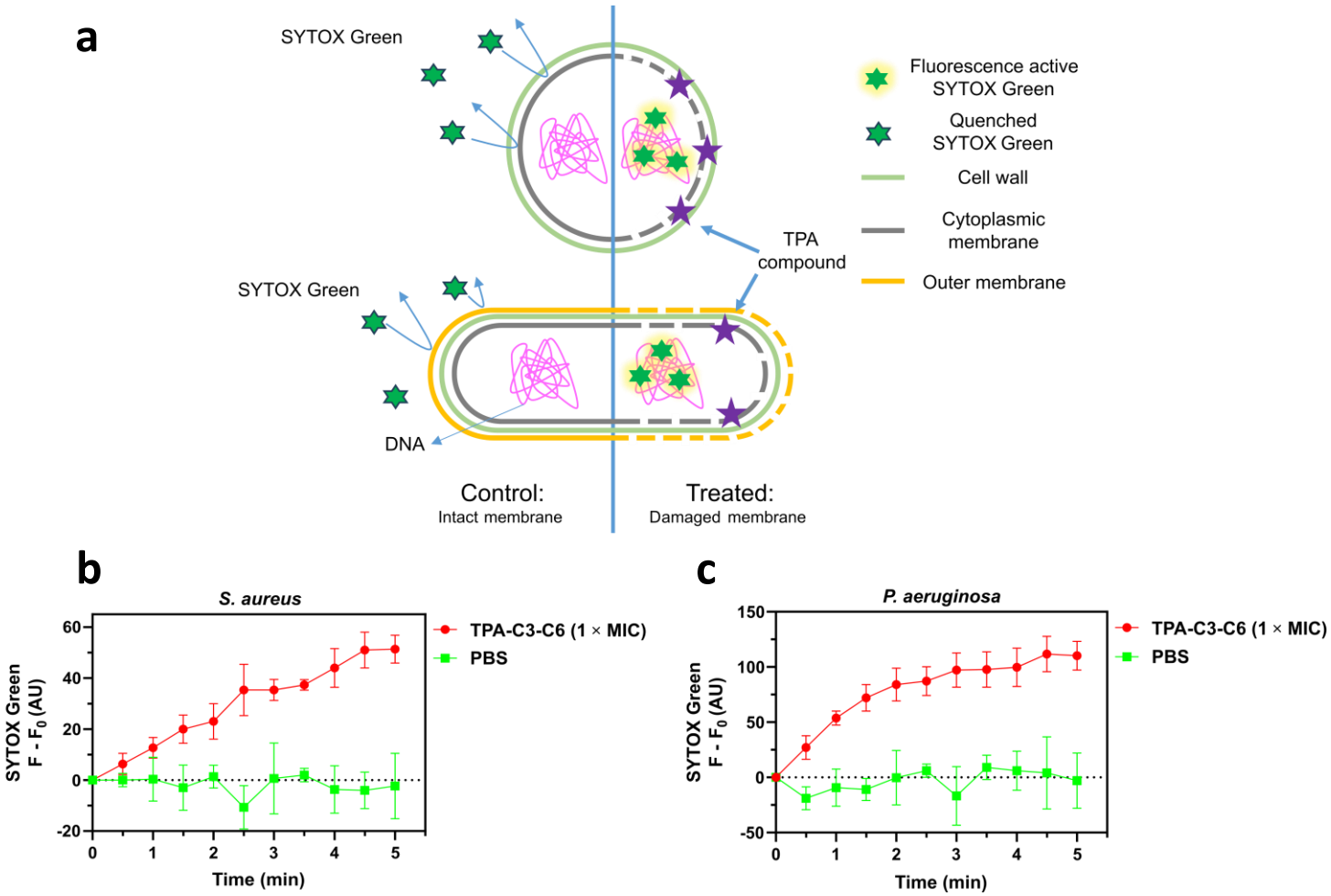

Figure 4.8. (a) An illustration shows the principle of SYTOX Green assay. (b) The SYTOX Green assay results of TPA-C3-C6 against *S. aureus* (1 × MIC, 3.13 μM) and (c) *P. aeruginosa*. (1 × MIC, 20 μM). Data are presented as the mean ± SD, $n = 3$ per group.

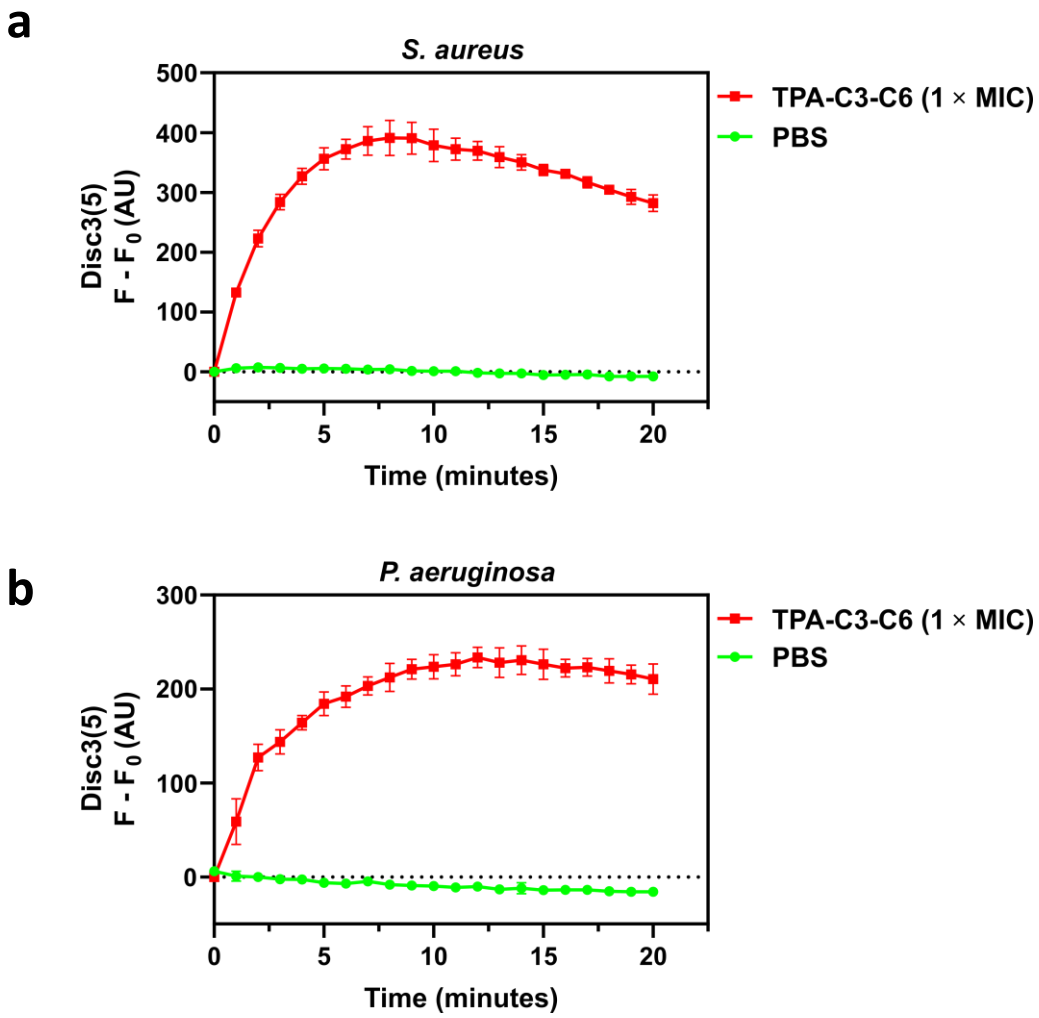

Figure 4.9. The Disc3(5) assay results of TPA-C3-C6 against (a) *S. aureus* (1 × MIC, 3.13 μM) and (b) *P. aeruginosa* (1 × MIC, 20 μM). Data are presented as the mean ± SD, $n = 3$ per group.

TPA-C3-C6 also exhibits binding ability towards *S. aureus* and *P. aeruginosa* genomic DNA. **Figure 4.10a** and **Figure 4.10b** showed that the *S. aureus* and *P. aeruginosa* DNA bands were slightly upshifted, and band intensities decreased after adding TPA-C3-C6. The upshift of the DNA band is probably due to the increase in molecular weight and decrease in negative charge upon binding with TPA-C3-C6. The binding of TPA-C3-C6 on DNA could also hinder the labelling by DNA stain (SYBR Safe), resulting in a decrease in band intensity.

Similar to TPA-1, TPA-C3-C6 interferes with the negative DNA supercoiling process carried out by bacterial DNA gyrases. As shown in **Figure 4.10c** and **Figure 4.10d**, *S. aureus* DNA gyrase and *P. aeruginosa* DNA gyrase could convert multiple bands of relaxed DNA (pBR322 plasmid) into a single supercoiled DNA band. The downshift of the DNA bands is due to the increase in charge density of the supercoiled DNA. For the *S. aureus* DNA gyrase, the addition of 20 μM of TPA-C3-C6 caused a decrease in the intensity of the supercoiled DNA band (**Figure 4.10c**). When the concentration of TPA-C3-C6 was increased to 40 μM, the supercoiled DNA band disappeared. For *P. aeruginosa* DNA gyrase, increasing the concentration of TPA-C3-C6 from 5 μM to 20 μM converted the single supercoiled DNA band into multiple DNA bands, indicating a decrease in supercoiling efficiency (**Figure 4.10d**). These results demonstrated that TPA-C3-C6 could interfere with the supercoiling activity of both *S. aureus* and *P. aeruginosa* DNA gyrases.

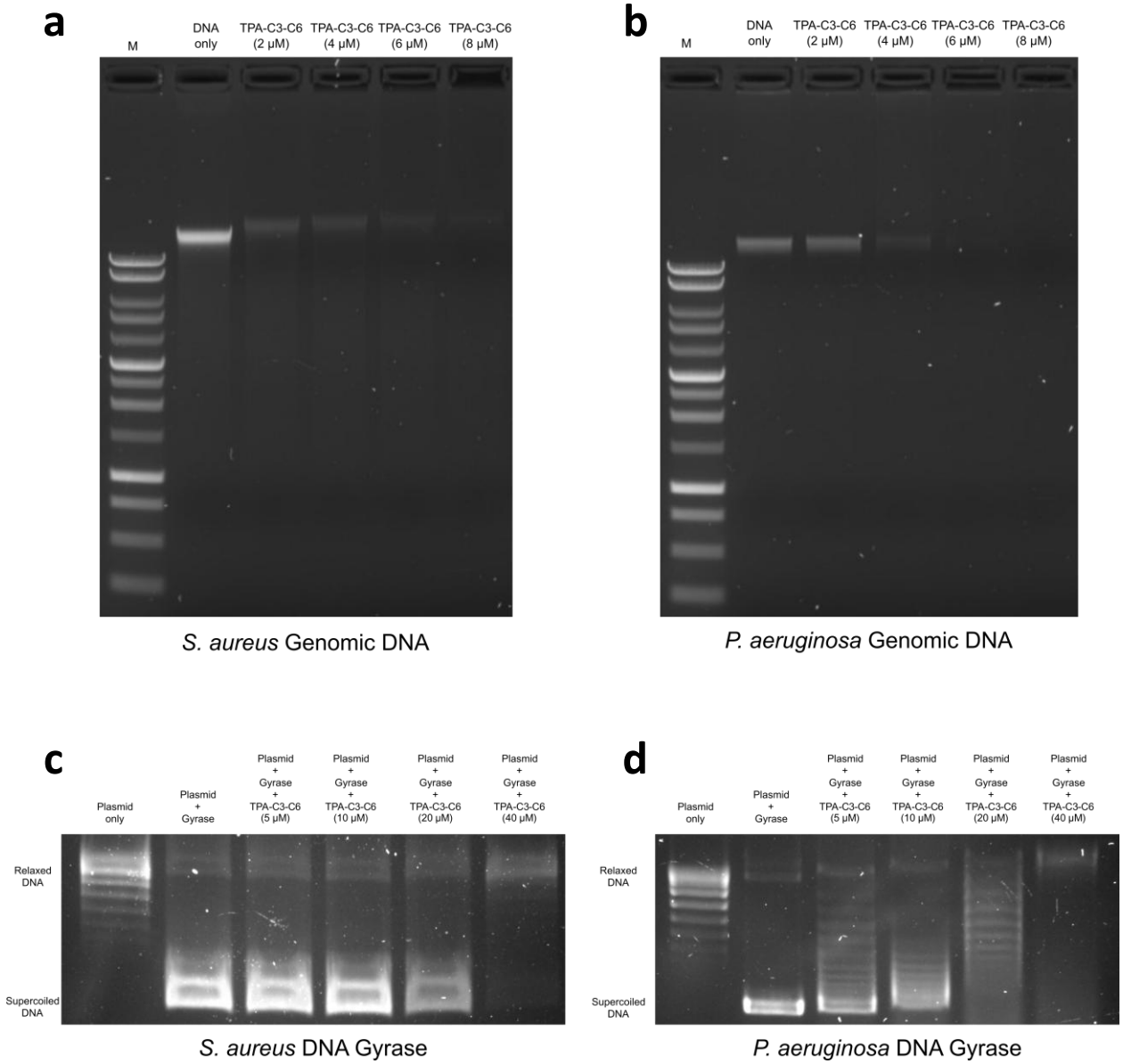

Figure 4.10. (a) The DNA gel (0.8% agarose) images of different concentrations of TPA-C3-C6 mixed with *S. aureus* genomic DNA or (b) *P. aeruginosa* genomic DNA. (c) The DNA gel image (1% agarose) showed the inhibition of the supercoiling activity on *S. aureus* DNA gyrase and (d) *P. aeruginosa* DNA gyrase with different concentrations of TPA-C3-C6.

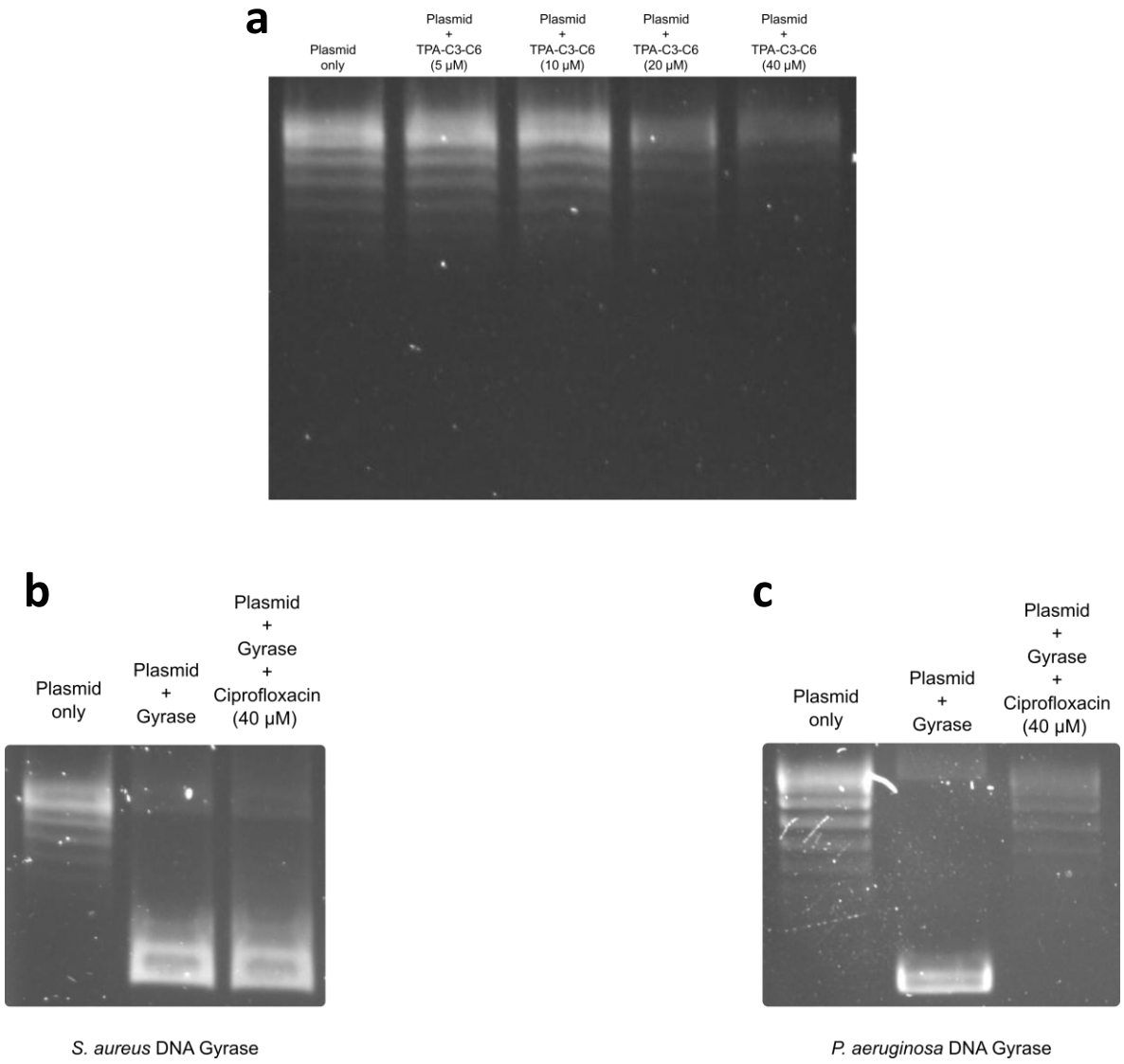

Figure 4.11. (a) The DNA gel image (1% agarose) of different concentrations of TPA-C3-C6 mixed with the substrate plasmid of the DNA supercoiling assay was used as the negative control. (b) The inhibition effect of ciprofloxacin on the supercoiling activity of *S. aureus* DNA gyrase and (c) *P. aeruginosa* DNA gyrase.

The effects of TPA-C3-C6 on the cell morphologies of *S. aureus* and *P. aeruginosa* were also studied using SEM (**Figure 4.12a**). After incubation with 2 × MIC of TPA-C3-C6 (6.25 μM) in the dark for 3 hours, the *S. aureus* cells showed shrinkages and collapses on the cell envelope, suggesting damage to the cell membrane. When the concentration of TPA-C3-C6 was increased to 4 × MIC (12.5 μM), intense cell lysis was observed on *S. aureus,* which is likely caused by the increase in the extent of cell membrane damage.

Additionally, the cell length of *P. aeruginosa* was elongated after incubation with 2 × MIC of TPA-C3-C6 (40 μM), while no significant damage was found on the cell envelope. This phenomenon was also found in 2 × MIC (0.5 μM) and 4 × MIC of ciprofloxacin (1 μM), which is an antibiotic that inhibits the activity of bacterial DNA gyrase (**Figure 4.12b**). The increase in cell length is a typical phenomenon observed in rod-shaped bacteria after treatment with β-lactams, DNA synthesis inhibitors, and FtsZ inhibitors due to their ability to interfere with proper cell division.[173-175] Therefore, 2 × MIC of TPA-C3-C6 could likely affect the cell division of *P. aeruginosa*. Moreover, instead of cell elongation, rough surfaces and spherical cell shapes were observed in *P. aeruginosa* that had been treated with 4 × MIC of TPA-C3-C6 (80 μM). This finding is similar to that of *P. aeruginosa* after treatment with β-lactams.[176-178] These results implied that different concentrations of TPA-C3-C6 could induce distinct changes in *P. aeruginosa* morphology.

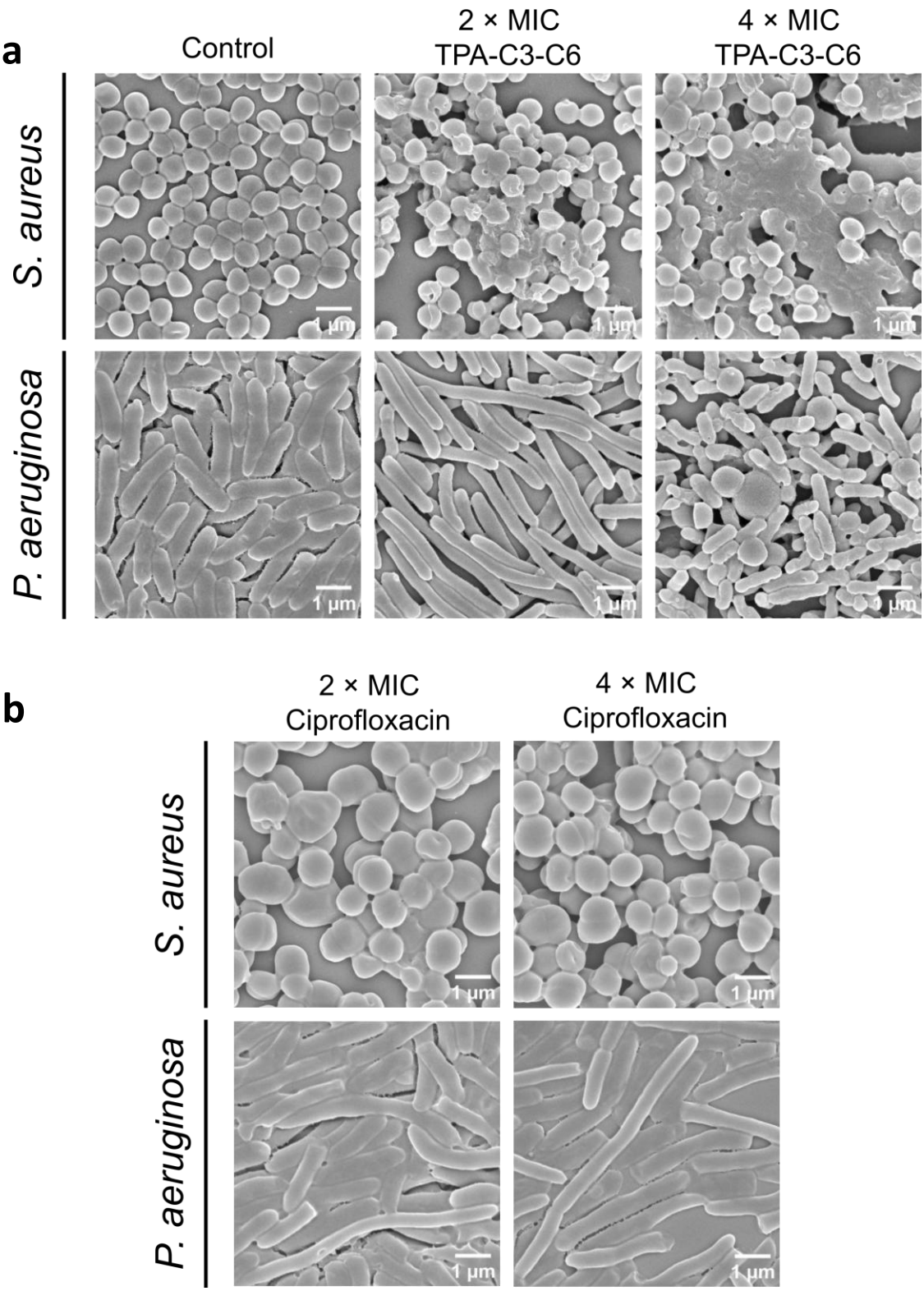

Figure 4.12. The SEM images of *S. aureus* and *P. aeruginosa* after incubation with different concentrations of (a) TPA-C3-C6 and (b) ciprofloxacin.

4.3.4 Biofilm Labelling and Biofilm Inhibitory Activity of TPA-C3-C6 without Light Irradiation

The penetration efficiency of TPA-C3-C6 in *S aureus* and *P. aeruginosa* biofilms was investigated using z-stacked fluorescence imaging (**Figure 4.13**). The fluorescence signals generated by TPA-C3-C6 can be observed throughout the entire bacterial biofilm, suggesting that TPA-C3-C6 could penetrate both *S. aureus* and *P. aeruginosa* biofilms.

TPA-C3-C6 also showed biofilm inhibition activity on both *S. aureus* and *P. aeruginosa*. As shown in **Figure 4.14a,** a 0.5 × MIC of TPA-C3-C6 (1.56 μM) can inhibit 70% ± 10% of *S. aureus* biofilm formation. The inhibition activity on *S. aureus* biofilm formation increased to over 95% at ≥ 3.13 μM of TPA-C3-C6. For *P. aeruginosa*, 1 × MIC of TPA-C3-C6 (20 μM) inhibited 30% ± 10% of *P. aeruginosa* biofilm formation. When the concentration of TPA-C3-C6 was increased to ≥ 30 μM, TPA-C3-C6 inhibited over 90% of *P. aeruginosa* biofilm formation (**Figure 4.14b**).

Since TPA-C3-C6 showed promising biofilm inhibitory activity, its biofilm inhibition mechanisms were further studied using real-time quantitative reverse transcription polymerase chain reaction (RT-qPCR), as shown in **Figure 4.14c** and **Figure 4.14d**. The detailed RT-qPCR results are summarized in **Table 4. 3** and **Table 4.4**.

For *S. aureus*, the accessory gene regulator (*agr*) quorum sensing system is essential in intercellular communication and initial biofilm attachment.[179] As shown in **Figure 4.14c**, the expression of *agrA* and *RNAIII,* which are involved in *agr* quorum sensing system, decreased with increasing concentration of TPA-C3-C6. This result indicated that TPA-C3-C6 could inhibit the quorum sensing system of *S. aureus* and might further affect the initial biofilm attachment. Additionally, *fnbB* and *clfB*, which translate into proteins that are involved in adhesion and binding with host fibronectin and fibrinogen during biofilm formation, were also

downregulated.[180-182] Apart from quorum sensing and cell adhesion, extracellular DNA (eDNA) is also an important component in *S. aureus* and other bacterial biofilms. eDNA has been reported to be crucial for the formation of a mature biofilm.[183] The release of eDNA for *S. aureus* biofilm formation is regulated by *cidA*, which translates into a holin-like protein that promotes cell autolysis.[184, 185] Upon addition of TPA-C3-C6, the transcription level of *cidA* in *S. aureus* was lowered, implying that TPA-C3-C6 could reduce the release of eDNA by inhibiting cell autolysis.

Regarding *P. aeruginosa*, Psl and Pel are two exopolysaccharides that maintain the structure and compactness of *P. aeruginosa* biofilm.[186] The qPCR results showed that genes related to Psl (*pslB*) and Pel (*pelB*) synthesis in TPA-C3-C6-treated *P. aeruginosa* were downregulated, suggesting that TPA-C3-C6 might inhibit the *P. aeruginosa* biofilm by affecting the structural stability of the biofilm. In addition, the expression of *alg44*, which is responsible for exopolysaccharide alginate synthesis, was decreased in TPA-C3-C6-treated *P. aeruginosa*.[186] Apart from affecting the production of exopolysaccharides, TPA-C3-C6 also affected the quorum sensing systems in *P. aeruginosa*. The quorum sensing systems in *P. aeruginosa* control the expression of multiple virulence factors and biofilm formation.[187] Inhibiting these systems has been reported to be effective in reducing *P. aeruginosa* biofilm formation.[188, 189] As shown in **Figure 4.14d**, the gene expressions related to the three major quorum sensing systems in *P. aeruginosa*, which include Las (*lasI*), Rhl (*rhlR*) and PQS (*pqsR*), were lowered after treatment with TPA-C3-C6. Las and Rhl quorum sensing systems are involved in the production of rhamnolipid.[190] Rhamnolipid is a biosurfactant that creates channels inside *P. aeruginosa* biofilm to maintain the biofilm structure.[191] The inhibition of TPA-C3-6 on the Las and Rhl quorum sensing system could affect *P. aeruginosa* biofilm integrity. Additionally, *pqsR* is a gene in the PQS quorum sensing system that positively regulates the expression of *pqsABCDE*.[192] It has been identified that *pqsA* is involved in the release of eDNA.[193] Therefore,

the decrease in the expression of *pqsR* could reduce the expression of *pqsA*, further inhibiting the release of eDNA.

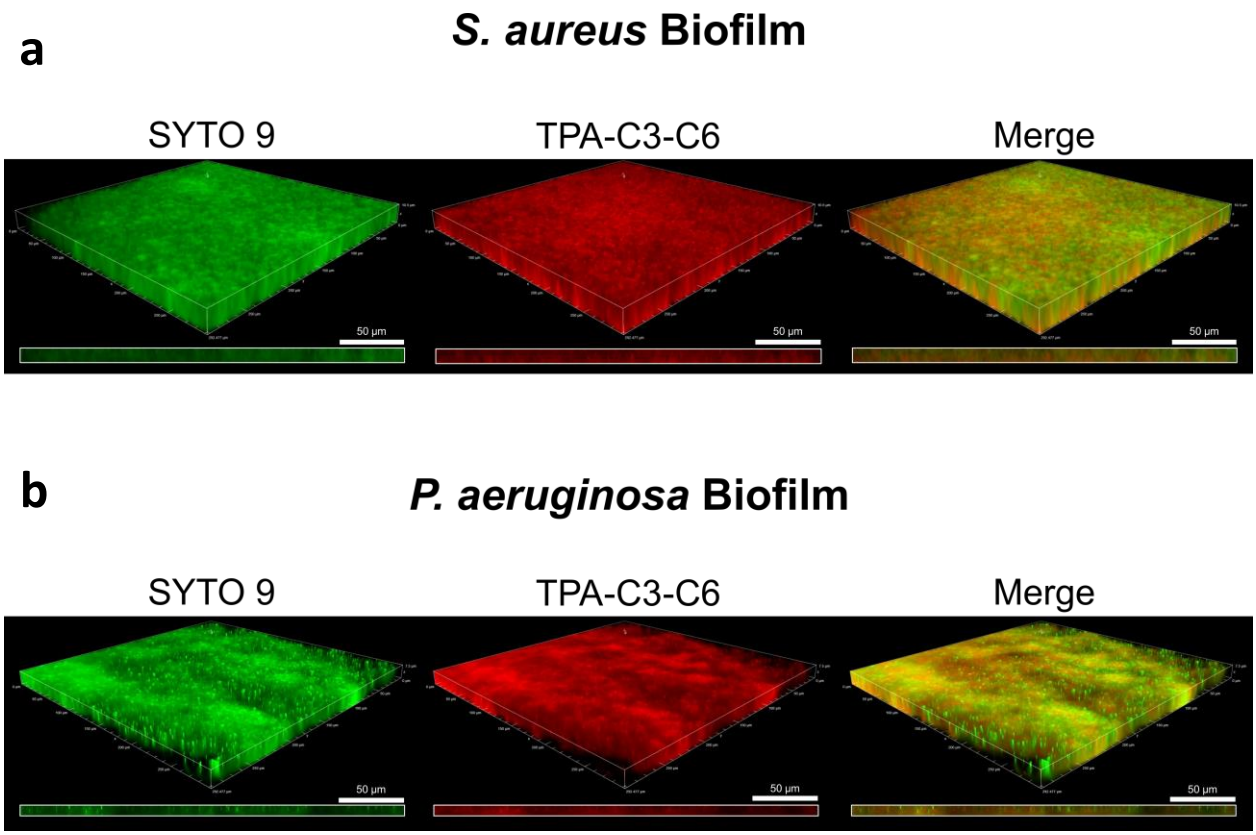

Figure 4.13. The fluorescence images of (a) *S. aureus* and (b) *P. aeruginosa* biofilms with SYTO 9 (2.5 μM, λex = 490 nm, λem = 500nm to 550 nm) and TPA-C3-C6 (20 μM, λex = 550 nm, λem = 590 nm to 670 nm).

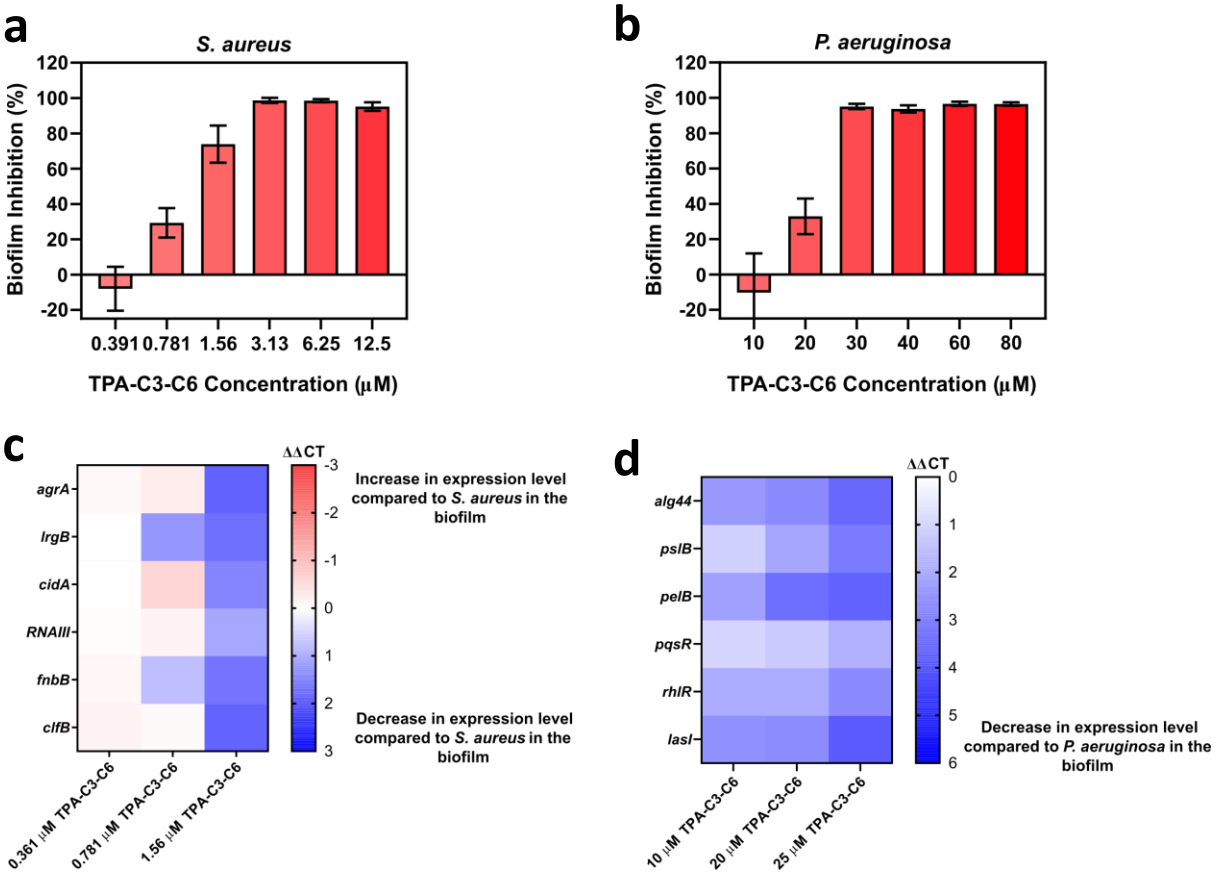

Figure 4.14. (a) The biofilm inhibition (%) of TPA-C3-C6 against *S. aureus* and (b) *P. aeruginosa*. Data are presented as the mean ± SD, $n = 3$ per group. (c) Real-time quantitative reverse transcription PCR (RT-qPCR) analysis results on several biofilm-related genes in *S. aureus* and (d) *P. aeruginosa* with different concentrations of TPA-C3-C6.

Table 4. 3. Summary table of the RT-qPCR results of *S. aureus* with different concentrations of TPA-C3-C6. $n = 4$ per group.

Samples	Genes	CT (mean ± SD)	ΔCT (mean ± SD)	ΔΔCT (mean ± SD)	*p*-value for ΔCT compared to *S. aureus* Biofilm
	rpoB (housekeeping)				
S. aureus Biofilm		22.2 ± 0.2			
0.316 µM TPA-C3-C6		22.2 ± 0.1			
0.781 µM TPA-C3-C6		20.8 ± 0.1			
1.56 µM TPA-C3-C6		20.0 ± 0.4			
	agrA				
S. aureus Biofilm		19.1 ± 0.1	-3.2 ± 0.2		
0.316 µM TPA-C3-C6		18.9 ± 0.1	-3.3 ± 0.2	-0.1 ± 0.3	0.48
0.781 µM TPA-C3-C6		17.3 ± 0.1	-3.4 ± 0.2	-0.3 ± 0.3	0.07
1.56 µM TPA-C3-C6		18.7 ± 0.3	-1.3 ± 0.5	1.8 ± 0.5	$P< 0.001$
	lrgB				
S. aureus Biofilm		25.28 ± 0.07	3.0 ± 0.2		
0.316 µM TPA-C3-C6		25.19 ± 0.2	3.0 ± 0.2	-0.0 ± 0.3	0.88
0.781 µM TPA-C3-C6		25.0 ± 0.1	4.3 ± 0.3	1.2 ± 0.2	$P< 0.001$
1.56 µM TPA-C3-C6		24. 7 ± 0.3	4.7 ± 0.4	1.7 ± 0.5	$P< 0.001$
	cidA				
S. aureus Biofilm		20.7 ± 0.2	-1.6 ± 0.2		
0.316 µM TPA-C3-C6		20.6 ± 0.2	-1.6 ± 0.3	-0.0 ± 0.4	0.98
0.781 µM TPA-C3-C6		18.5 ± 0.1	-2.2 ± 0.2	-0.6 ± 0.3	0.005
1.56 µM TPA-C3-C6		19.9 ± 0.4	-0.1 ± 0.5	1.4 ± 0.6	0.003
	RNAIII				
S. aureus Biofilm		15.0 ± 0.1	-7.2 ±0.2		
0.316 µM TPA-C3-C6		14.9 ± 0.1	-7.3 ± 0.2	-0.0 ± 0.3	0.67
0.781 µM TPA-C3-C6		13.30 ± 0.09	-7.4 ± 0.2	- 0.2 ± 0.2	0.13
1.56 µM TPA-C3-C6		13.7 ± 0.3	-6.2 ± 0.5	1.0 ± 0.6	0.01
	fnbB				
S. aureus Biofilm		25.6 ± 0.2	3.4 ± 0.2		
0.316 µM TPA-C3-C6		25.4 ± 0.4	3.2 ± 0.4	-0.1 ± 0.4	0.55
0.781 µM TPA-C3-C6		24.9 ± 0.1	4.1 ± 0.2	0.7 ± 0.3	0.003
1.56 µM TPA-C3-C6		24.9 ± 0.2	5.0 ± 0.5	1.6 ± 0.5	$P< 0.001$
	clfB				
S. aureus Biofilm		24.4 ± 0.1	2.1 ± 0.2		
0.316 µM TPA-C3-C6		24.1 ± 0.2	1.9 ± 0.2	-0.2 ± 0.3	0.23
0.781 µM TPA-C3-C6		22.7 ± 0.2	2.0 ± 0.2	-0.1 ± 0.3	0.51
1.56 µM TPA-C3-C6		23.9 ± 0.1	3.9 ± 0.5	1.8 ± 0.5	$P< 0.001$

Table 4.4. Summary table of the RT-qPCR results of *P. aeruginosa* with different concentrations of TPA-C3-C6. $n = 4$ per group.

Samples	Genes	CT (mean ± SD)	ΔCT (mean ± SD)	ΔΔCT (mean ± SD)	*p*-value for ΔCT compared to *P. aeruginosa* Biofilm
	rpoD (housekeeping)				
P. aeruginosa Biofilm		22.1 ± 0.1			
10 μM TPA-C3-C6		19.7 ± 0.1			
20 μM TPA-C3-C6		19.54 ± 0.09			
25 μM TPA-C3-C6		19.1 ± 0.1			
	alg44				
P. aeruginosa Biofilm		25.2 ± 0.2	3.0 ± 0.2		
10 μM TPA-C3-C6		25.15 ± 0.07	5.4 ± 0.1	2.4 ± 0.3	$p < 0.001$
20 μM TPA-C3-C6		25.29 ± 0.09	5.8 ± 0.1	2.7 ± 0.3	$p < 0.001$
25 μM TPA-C3-C6		25.7 ± 0.3	6.6 ± 0.4	3.5 ± 0.4	$p < 0.001$
	pslB				
P. aeruginosa Biofilm		23.76 ± 0.07	1.6 ± 0.1		
10 μM TPA-C3-C6		22.4 ± 0.1	2.7 ± 0.2	1.1 ± 0.2	$p < 0.001$
20 μM TPA-C3-C6		23.2 ± 0.1	3.7 ± 0.2	2.1 ± 0.2	$p < 0.001$
25 μM TPA-C3-C6		23.9 ± 0.7	4.7 ± 0.8	3.1 ± 0.8	$p < 0.001$
	pelB				
P. aeruginosa Biofilm		26.2 ± 0.2	4.1 ± 0.3		
10 μM TPA-C3-C6		26.0 ± 0.1	6.3 ± 0.2	2.2 ± 0.3	$p < 0.001$
20 μM TPA-C3-C6		27.0 ± 0.2	7.5 ± 0.2	3.4 ± 0.3	$p < 0.001$
25 μM TPA-C3-C6		26.95 ± 0.08	7.8 ± 0.2	3.7 ± 0.3	$p < 0.001$
	pqsR				
P. aeruginosa Biofilm		22.5 ± 0.2	0.5 ± 0.2		
10 μM TPA-C3-C6		21.20 ± 0.09	1.4 ± 0.2	1.0 ± 0.3	$p < 0.001$
20 μM TPA-C3-C6		21.3 ± 0.2	1.7 ± 0.2	1.2 ± 0.3	$p < 0.001$
25 μM TPA-C3-C6		21.4 ± 0.3	2.3 ± 0.3	1.8 ± 0.4	$p < 0.001$
	rhlR				
P. aeruginosa Biofilm		24.0 ± 0.1	1.9 ± 0.2		
10 μM TPA-C3-C6		23.61 ± 0.06	3.8 ± 0.1	2.0 ± 0.2	$p < 0.001$
20 μM TPA-C3-C6		23.4 ± 0.3	3.8 ± 0.3	1.9 ± 0.4	$p < 0.001$
25 μM TPA-C3-C6		23.7 ± 0.3	4.6 ± 0.3	2.7 ± 0.3	$p < 0.001$
	lasI				
P. aeruginosa Biofilm		22.99 ± 0.08	0.9 ± 0.2		
10 μM TPA-C3-C6		23.2 ± 0.1	3.6 ± 0.2	2.6 ± 0.2	$p < 0.001$
20 μM TPA-C3-C6		23.1 ± 0.4	3.6 ± 0.4	2.7 ± 0.4	$p < 0.001$
25 μM TPA-C3-C6		23.9 ± 0.4	4.8 ± 0.4	3.9 ± 0.4	$p < 0.001$

Table 4.5. The genes and their corresponding primers that were used in RT-qPCR of *S. aureus*.

Gene	Gene Description	Primer (5' – 3')	Reference
agrA	*agr* quorum sensing system	Forward: TGCGAAGACGATCCAAAAC Reverse: TTTAGCTTGCTCAAGCACCTC	**194**
lrgB	Negative control on peptidoglycan hydrolysis	Forward: TATTGCCCGAGGATTAGCAC Reverse: CAAAGACAGGCACAACTGCTAC	**194**
cidA	Promote cell lysis to release eDNA	Forward: CTTAGCCGGCAGTATTGTTG Reverse: GTTTGCACCGTCTTCTACCC	**194**
RNAIII	Posttranscriptional regulator, activated by *agr* quorum sensing system	Forward: AAGCCATCCCAACTTAATAACC Reverse: GCACTGAGTCCAAGGAAACTAAC	**194**
fnbB	Promote binding with fibronectin	Forward: GAACATGGTCAAGCACAAGG Reverse: ACGCCATAATTACCGTGACC	**194**
clfB	Promote binding with fibrinogen	Forward: TTATGGTGGTGGAAGTGCTG Reverse: ACGCCATAATTACCGTGACC	**194**
rpoB	β subunit of RNA polymerase (housekeeping gene)	Forward: ACAACCACTTGGCGGTAAAG Reverse: ATGCTTCAAGTGCCCATACC	**194**

Table 4.6. The genes and their corresponding primers that were used in RT-qPCR of *P. aeurginosa*.

Gene	Gene Description	Primer (5' – 3')	Reference
alg44	Synthesis of exopolysaccharide alginate	Forward: CCACCAGATGAAAGGGACC Reverse: AAGATCACCTGGCCCTTGTT	**195**
pslB	Synthesis of exopolysaccharide *psl*	Forward: CAACGAATCCACCTTCATCC Reverse: ACTCGCCGCTCTGTACCTC	**196**
pelB	Synthesis of exopolysaccharide *pel*	Forward: AGCGCTTGCAACAGATTCTC Reverse: AACAGGTTCCAGTGGGTTTC	**195**
pqsR	*pqs* quorum sensing system	Forward: GATAGCCTGGCGACGATCAA Reverse: CACTGGTTGAAGCGGGAGAT	**197**
rhlR	*rhl* quorum sensing system	Forward: GTTTGCGTAGCGAGATGCAG Reverse: GGCGTAGTAATCGAAGCCCA	**197**
lasI	*las* quorum sensing system	Forward: CTACAGCCTGCAGAACGACA Reverse: ATCTGGGTCTTGGCATTGAG	**198**
rpoD	RNA polymerase sigma factor (housekeeping gene)	Forward: GCGACGGTATTCGAACTTGT Reverse: CGAAGAAGGAAATGGTCGAG	**199**

4.3.5 Prevention of Biofilm Recurrence by TPA-C3-C6

One of the limitations of traditional PSs is that they lose their antibacterial effect once the light source is removed. Besides, most antibacterial PSs can rarely eradicate all bacteria in the biofilm within a single PDT treatment.[200, 201] Therefore, the bacteria that survive PDT can regrow and lead to recurrence of the biofilm. However, if a PS has potent antibacterial activity even without light irradiation, like TPA-C3-C6, it may be able to extend the antibacterial activity after PS and prevent biofilm recurrence.

To investigate the ability of TPA-C3-C6 to prevent biofilm recurrence, the number of viable biofilm bacteria right after treatments and with an additional overnight incubation in a nutrient-rich medium (MHB + 1% glucose) was compared.

The effects of TPA-C3-C6 on biofilms without light irradiation were first investigated. TPA-C3-C6 and vancomycin had a limited effect (< 0.3 log CFU/mL reduction) on the *S. aureus* in the biofilm after 45 minutes of treatment in the dark (**Figure 4.15a**). With further overnight incubation, the number of viable *S. aureus* in the biofilm treated with PBS and 80 μM vancomycin increased by 0.9 ± 0.3 log CFU/mL and 0.5 ± 0.3 log CFU/mL, respectively. On the other hand, those treated with 80 μM TPA-C3-C6 without light irradiation showed a decrease of 2 ± 1 log CFU/mL. These results suggested that extending the incubation time could allow TPA-C3-C6 to eradicate *S. aureus* in the biofilm without light irradiation. Meanwhile, 80 μM of vancomycin failed to inhibit the growth of *S. aureus* in the biofilm.

Similar antibacterial effects were observed against *P. aeruginosa* biofilm (**Figure 4.15b**). During the initial 45 minutes of incubation in the dark, the treatment with 80 μM of TPA-C3-C6 resulted in a decrease of 1.2 ± 0.1 log CFU/mL of *P. aeruginosa* in the biofilm. In contrast, 80 μM of meropenem only caused a decrease of 0.4 ± 0.1 log CFU/mL. Upon overnight incubation, 80 μM of TPA-C3-C6 caused a decrease of 2 ± 1 log CFU/mL of *P. aeruginosa* in

the biofilm, which was more efficient than 80 μM of meropenem (1.3 ± 0.4 log CFU/mL reduction).

The antibiofilm activity of TPA-C3-C6 was further investigated upon light irradiation. The PDT with 80 μM of TPA-C3-C6 resulted in a reduction of 1.5 ± 0.3 log CFU/ml for *S. aureus* and 1.3 ± 0.1 log CFU/mL for *P. aeruginosa* in the biofilms (**Figure 4.15a** and **Figure 4.15b**). After further overnight incubation, the antibacterial activity of TPA-C3-C6 was enhanced. 80 μM of TPA-C3-C6 led to a decrease of 3.3 ± 0.4 log CFU/mL for *S. aureus* and 3.0 ± 0.7 log CFU/mL for *P. aeruginosa* in the biofilms. These results suggested that the intrinsic antibacterial activity of TPA-C3-C6 could extend its antibiofilm effect and help prevent the recurrence of biofilms in the dark after PDT.

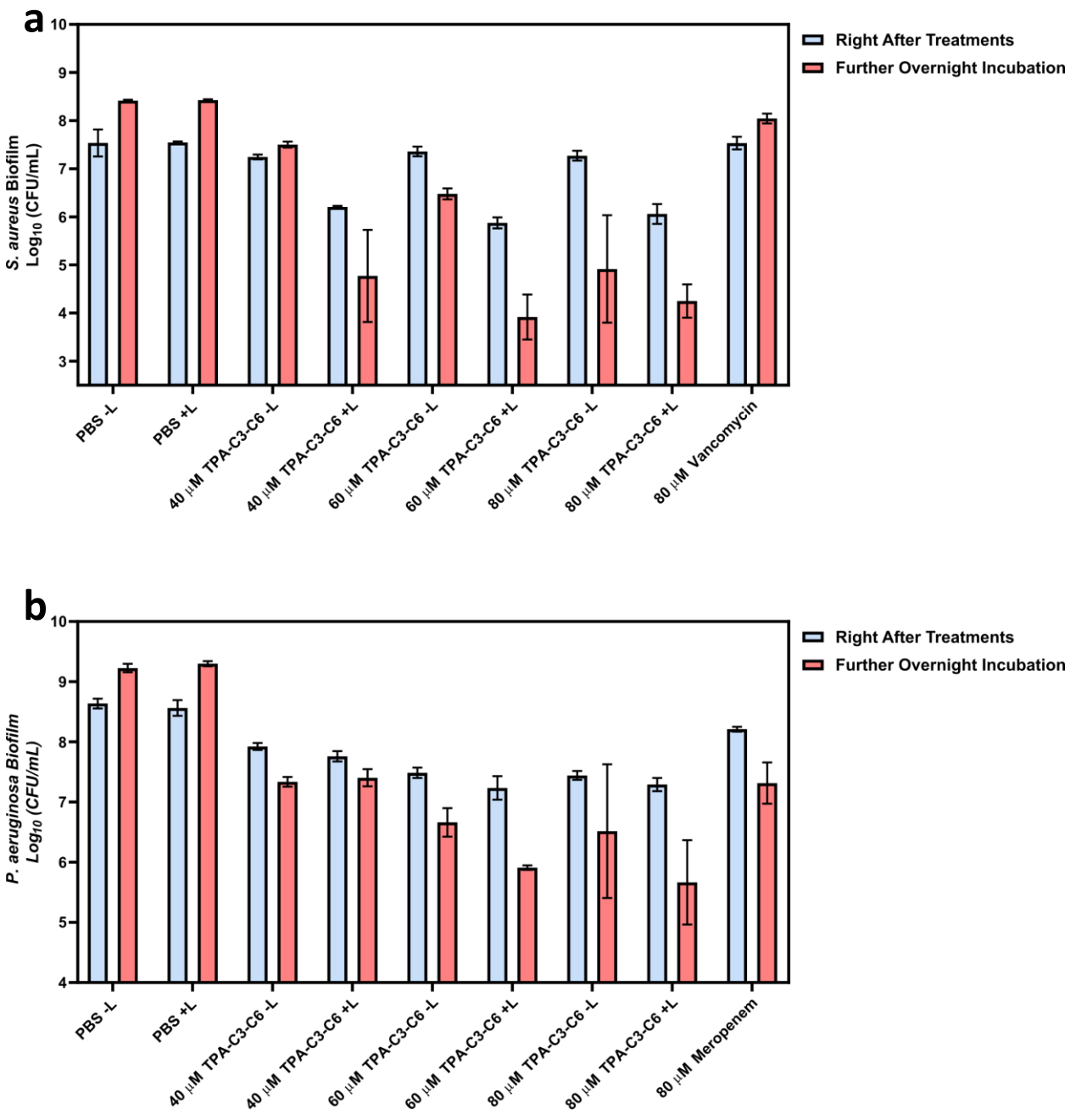

Figure 4.15. (a) The number of viable *S. aureus* in the biofilm right after treatment (blue bars) or with further overnight incubation (red bars) with TPA-C3-C6 and vancomycin. (b) The number of viable *P. aeruginosa* in the biofilm right after treatment or with further overnight incubation with TPA-C3-C6 and meropenem. -L: without light irritation. +L: with 600 nm (60 mW/cm^2) light irradiation. Data are presented as the mean ± SD, n = 3 per group.

4.3.6 Biofilm Eradication Mechanisms of TPA-C3-C6

Since TPA-C3-C6 can disrupt the planktonic bacteria membrane without light irradiation, the surface integrity of bacteria in the biofilms was investigated using SEM. As shown in **Figure 4.16a**, the morphology of *S. aureus* treated with TPA-C3-C6 without light irradiation (TPA-C3-C6 -L) right after the treatment showed smooth and intact cell surfaces, similar to those in the PBS control group. However, after overnight incubation, collapses and shrinkages were found on the *S. aureus* in the biofilm, suggesting that prolonged incubation is needed to induce damage to the cell envelope of the *S. aureus* in the biofilm. Moreover, a portion of *S. aureus* treated with TPA-C3-C6 with light irradiation (TPA-C3-C6 +L) showed signs of cell lysis right after the treatment, indicating that PDT with TPA-C3-C6 can immediately eradicate some of the *S. aureus* inside the biofilm by causing structural damage. Following overnight incubation, the majority of *S. aureus* in the TPA-C3-C6 with light irradiation (TPA-C3-C6 +L) group were found to be damaged and lysed, which was more severe than the damage observed in the group of TPA-C3-C6 without light irradiation (TPA-C3-C6 -L).

For the *P. aeruginosa* biofilm, TPA-C3-C6 treatments, both with (TPA-C3-C6 +L) and without light irradiation (TPA-C3-C6 -L), caused rough cell surfaces and signs of cell lysis right after the treatment (**Figure 4.16b**). These findings indicated that TPA-C3-C6 could damage the cell envelope regardless of ROS generation, which is consistent with the similar eradication effects seen in both groups, as shown in **Figure 4.15b**. The TPA-C3-C6 without light irradiation (TPA-C3-C6 -L) group showed similar cell damage on *P. aeruginosa* with and without overnight incubation. However, some *P. aeruginosa* in the TPA-C3-C6 with light irradiation (TPA-C3-C6 +L) group failed to maintain the rod-like structure after overnight incubation. This phenomenon was also observed in the planktonic *P. aeruginosa* that were treated with the same concentration (4 × MIC, 80 μM) of TPA-C3-C6 in the dark for three hours (**Figure 4.12a**). Since the morphology of *S. aureus* and *P. aeruginosa* from the TPA-C3-C6 with light

irradiation (TPA-C3-C6 +L) groups after overnight incubation resembled that of planktonic *S. aureus* and *P. aeruginosa* treated with TPA-C3-C6, it is proposed that, besides causing bacterial membrane damage, the ROS generated during PDT may also cause damage to the extracellular polymeric substances (EPS), allowing TPA-C3-C6 to penetrate the biofilm more effectively and eradicate the bacteria by inducing additional membrane damage.

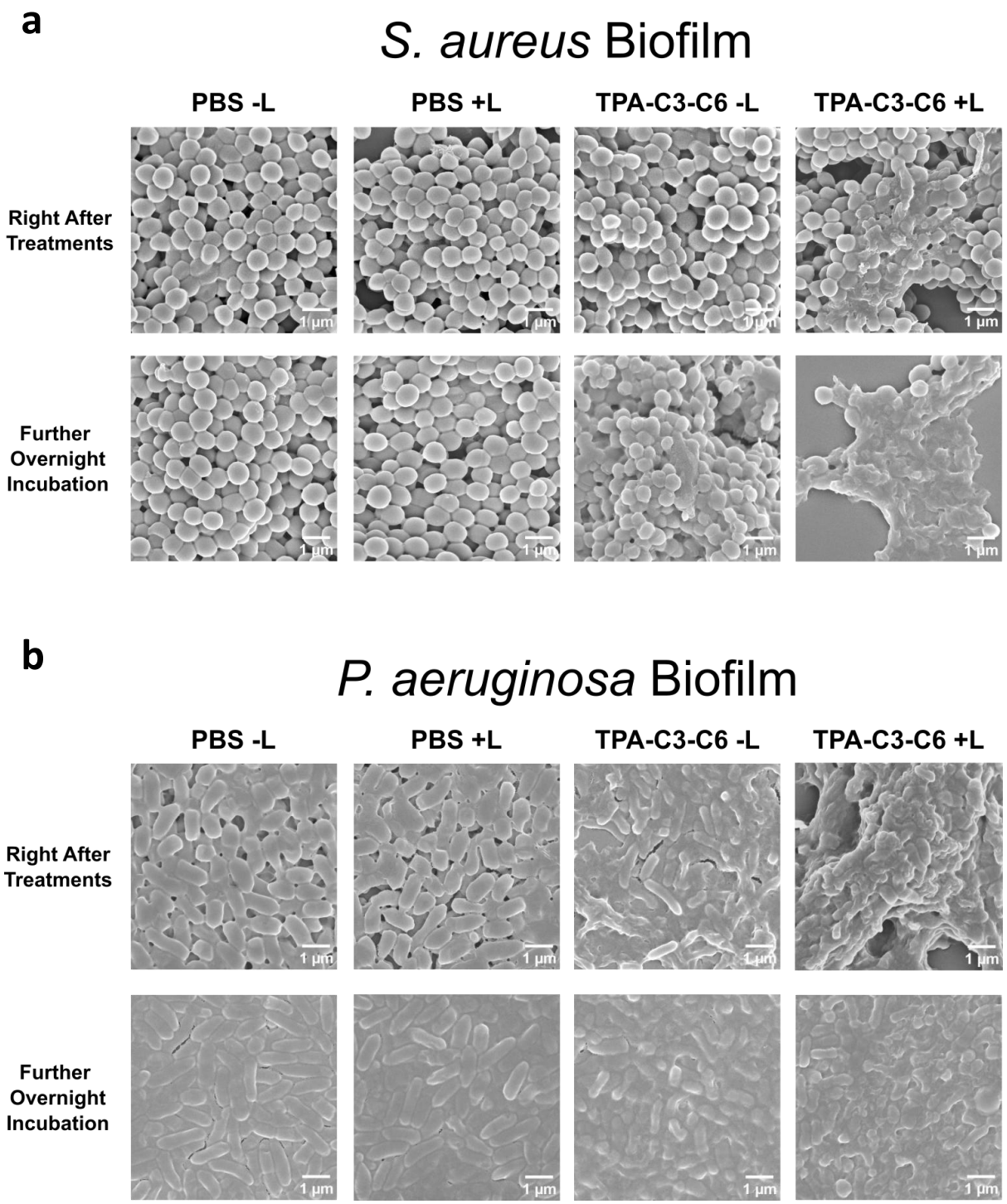

Figure 4.16. (a) The SEM images of *S. aureus* biofilm right after the treatments or with further overnight incubation in MHB (1% glucose) with PBS or 80 μM TPA-C3-C6. (b) The SEM images of *P. aeruginosa* biofilm right after the treatments or with further overnight incubation in MHB (1% glucose) with PBS or 80 μM TPA-C3-C6. -L: without light irritation. +L: with 600 nm (60 mW/cm^2) light irradiation.

To further validate the effect of TPA-C3-C6 on the bacteria inside the biofilm, mass spectrometry (MS)-based proteomic analysis was performed on TPA-C3-C6 PDT-treated and overnight incubated *S. aureus* and *P. aeruginosa* biofilms. A total of 1000 unique protein groups were identified in biofilm *S. aureus*, and 186 of them are considered as differentially expressed proteins (DEPs) based on p-value < 0.05 and $\log_2$(Fold change) >1 or <-1. Among the DEPs, 153 were downregulated, and 33 were upregulated (**Figure 4.17a**). Gene ontology (GO) and Kyoto Encyclopedia of Genes and Genomes (KEGG) pathway enrichment analysis on the genes corresponding to the DEPs were conducted using the PANTHER Classification System and the clusterprofiler package in RStudio.[126-128] The GO enrichment analysis categorized the DEPs into biological processes, molecular functions, and cellular components (**Figure 4.17b - Figure 4.17d)**. In addition, KEGG pathway analysis identified two major KEGG pathways (**Figure 4.17e**). Within the identified GO and KEGG pathway, one biological process and one KEGG pathway, namely translation (GO) and *Staphylococcus aureus* infection (KEGG), were selected for investigation as they are related to bacterial growth and virulence (**Figure 4.17f**).

Regarding translation, all the DEPs identified in this GO term were downregulated. These proteins include large ribosomal subunit proteins bL27, uL18, bL36, uL30, bL33B, uL14, bL9, and bL33A (*rpmA*, *rplR*, *rpmJ*, *rpmD*, *rpmG2*, *rplN*, *rplI*, *rpmG1*) and small ribosomal subunit proteins bS20, uS9, uS19, and bS21 (*rpsT*, *rpsI*, *rpsS*, *rpsU*). The bacterial ribosome (70S) is constructed by a large ribosomal subunit (50S) and a small ribosomal subunit (30S).[202] The downregulation of these subunits could inhibit the assembly of ribosomes, subsequently reducing the translation efficiency in *S. aureus*. Moreover, the TPA-C3-C6 treatment also caused the downregulation of proteins in the *Staphylococcus aureus* infection KEGG pathway. For example, clumping factor B (*clfB*), which facilitates the binding of *S. aureus* towards human cells, was downregulated.[182] γ-hemolysin component B, C (*hlgB*, *hlgC*)[162], FPRL1 inhibitory protein (*flr*)[203], and leucotoxin LukDv (*lukDv*)[204], which are proteins produced by *S.*

aureus to counteract the immune system, were also downregulated. This finding suggested that TPA-C3-C6 could reduce the virulence of *S. aureus* biofilm.

As discussed in **Section 4.3.4**, the quorum sensing system, especially *agr* system, controls *S. aureus* biofilm formation and expression of virulence factors.[179] Therefore, all DEPs that are involved in the quorum sensing system of *S. aureus* were manually selected for investigation. As shown in **Figure 4.17g,** most of the DEPs that are related to quorum sensing, such as accessory gene regulator protein A and B (*agrA*, *agrB*) and delta-hemolysin (*hld*), were downregulated, indicating that PDT with TPA-C3-C6, followed by overnight incubation, could inhibit the quorum sensing system in *S. aureus* biofilm.

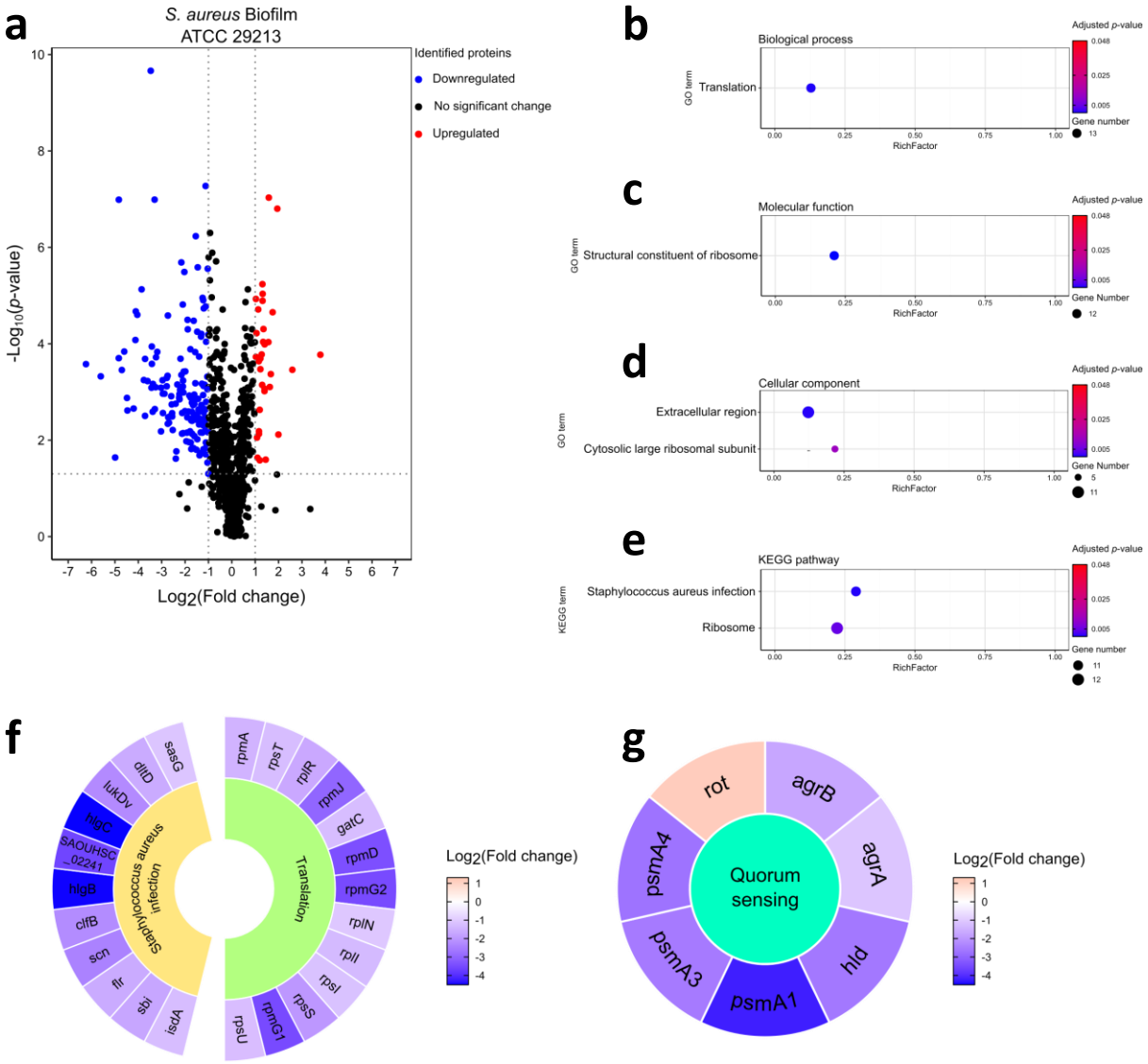

Figure 4.17. (a) Volcano plot showed the differentially expressed proteins (DEP)s in TPA-C3-C6 (80 μM)-treated *S. aureus* biofilm versus control *S. aureus* biofilm after PDT and overnight incubation. (b) Biological function, (c) molecular function, (d) cellular component GO enrichment, and (e) KEGG pathway enrichment analysis of the corresponding genes of the DEPs in TPA-C3-C6-treated *S. aureus* biofilm. (f) Selected biological process, KEGG pathway, and (g) quorum sensing proteins in *S. aureus* biofilm that were affected by TPA-C3-C6. Inner blocks were the names of the selected biological process or pathway. Outer blocks show the fold change of the DEPs, which are represented by their gene names, in the corresponding biological process or pathway. Three independent biological replicates were performed in this proteomic study.

For TPA-C3-C6-treated *P. aeruginosa* biofilm, 1262 unique protein groups were identified, and 118 of them were considered DEPs. Within the DEPs, 87 were downregulated, and 31 were upregulated (**Figure 4.18a**). GO and KEGG pathway enrichment analyses were then conducted. Three GO terms and 2 KEGG pathways showed statistically significant enrichment (**Figure 4.18b - Figure 4.18d**). Among these terms and pathways, translation (GO) and phenazine biosynthesis (KEGG) were selected for investigation as they are also related to bacterial growth and virulence (**Figure 4.18e**).

Similar to the TPA-C3-C6-treated *S. aureus* biofilm, the majority of the DEPs related to the GO term, translation, were downregulated, which include large ribosomal subunits uL29, bL33, uL15, bL32, and bL27 (*rpmC*, *rpmG*, *rplO*, *rpmF*, *rpmA*) and small ribosomal subunits uS15 and bS20 (*rpsO*, *rpsT*). Therefore, it is also suggested that TPA-C3-C6 can cause a decrease in translation efficiency, which may inhibit the growth of *P. aeruginosa* in the biofilm. Additionally, TPA-C3-C6 reduced the expression of proteins involved in phenazine biosynthesis (KEGG). For instance, phenazine biosynthesis proteins PhzB1, PhzB2, and PhzD1 (*phzB1*, *phzB2*, *phzD1*) were downregulated, potentially inhibiting the synthesis of phenazines in *P. aeruginosa* biofilm. Phenazines are pigmented metabolites produced by various bacteria, including *P. aeruginosa*.[205] According to reported literature, phenazines contribute to *P. aeruginosa* virulence.[206] For example, phenazine produced by *P. aeruginosa* can downregulate the transcription and directly inhibit the catalase activity in human lung epithelial cells, which can cause damage to the epithelial cells due to oxidative stress.[207] Therefore, the inhibition in phenazine synthesis caused by TPA-C3-C6 treatment may reduce the virulence of *P. aeruginosa* biofilm.

The DEPs related to quorum sensing of *P. aeruginosa* have also been studied. As shown in **Figure 4.18f**, all quorum-sensing related DEPs, such as HTH-type quorum-sensing regulator RhlR (*rhlR*) and 2-heptyl-3-hydroxy-4(1H)-quinolone synthase (*pqsH*), were downregulated,

suggesting that treatment of TPA-C3-C6 could inhibit the quorum sensing system of the *P. aeruginosa* inside the biofilm.

Collectively, SEM images showed that TPA-C3-C6 could eradicate *S. aureus* and *P. aeruginosa* in the biofilms by PDT-caused cell membrane damage and intrinsic membrane disruption activity. The MS-based proteomic studies further revealed that the combined effects of intrinsic antibacterial activity and PDT with TPA-C3-C6 could affect translation efficiency, virulence and quorum sensing systems in *S. aureus* and *P. aeruginosa* biofilms.

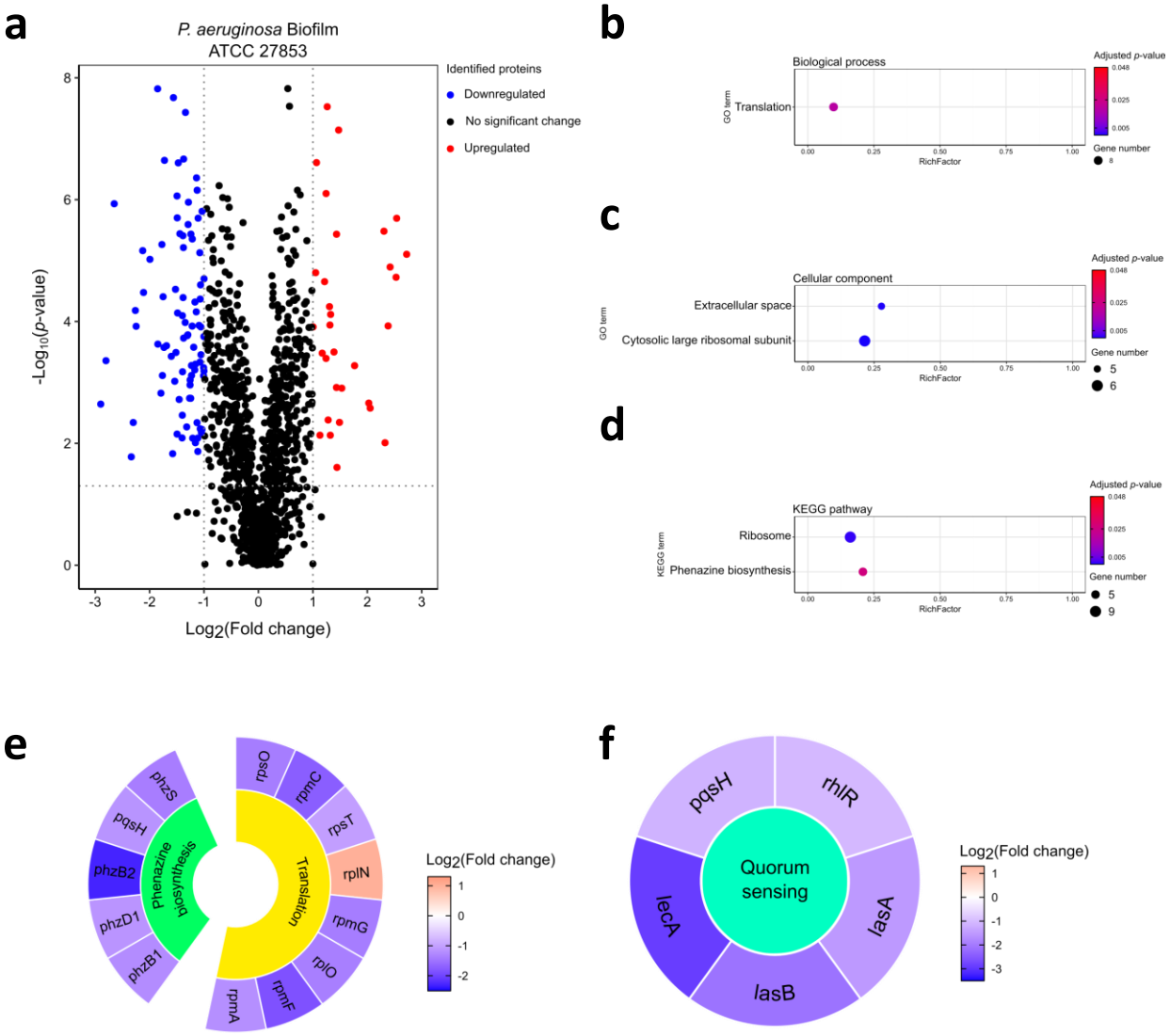

Figure 4.18. (a) Volcano plot showed the differentially expressed proteins (DEP)s in TPA-C3-C6 (80 μM)-treated *P. aeruginosa* biofilm versus control *P. aeruginosa* biofilm after PDT and overnight incubation. (b) Biological function, (c) cellular component GO enrichment, and (d) KEGG pathway enrichment analysis of the corresponding genes of the DEPs in TPA-C3-C6-treated *P. aeruginosa* biofilm. (e) Selected biological process, KEGG pathway, and (f) quorum sensing proteins in *P. aeruginosa* biofilm that were affected by TPA-C3-C6. Inner blocks were the names of the selected biological process or pathway. Outer blocks show the fold change of the DEPs, which are represented by their gene names, in the corresponding biological process or pathway. Three independent biological replicates were performed in this proteomic study.

4.4 Chapter IV Summary

To improve the intrinsic antibacterial activity and preserve the PDT ability, eight new PSs based on the structure of TPA-1 were synthesized. Among these, TPA-C3-C6 showed the best intrinsic antiplanktonic activity without light irradiation and good compatibility with human cells, as demonstrated by the cytotoxicity and haemolysis assays. The antibacterial mechanism studies show that TPA-C3-C6 targets bacterial membranes and interferes with the negative supercoiling activity of bacterial DNA gyrases. TPA-C3-C6 also inhibits *S. aureus* and *P. aeruginosa* biofilm formation by inducing downregulation of biofilm-related genes. Besides, the combined effects of PDT and intrinsic antibacterial activities provide TPA-C3-C6 with good activity against mature biofilms and prevent biofilm recurrence. Proteomic analysis suggested that the intrinsic antibacterial activity of TPA-C3-C6, along with PDT, could reduce translation efficiency and virulence in *S. aureus* and *P. aeruginosa* biofilms. Overall, TPA-C3-C6 can serve as an example for developing antibacterial PSs that retain their antibacterial activity even without light irradiation.

Chapter V

Conclusions

5.1 General Conclusions

Bacterial infections have always been a threat to human health. With the ability to form bacterial biofilms and the emergence of AMR, traditional antibiotics that were discovered decades ago are losing their effectiveness against bacteria. This urgency has driven the development of new antibacterial agents to treat bacterial infections, including PDT, which requires a PS to generate ROS upon light irradiation. Despite efforts invested in developing efficient PS, only a limited number of compounds show low cytotoxicity and good antibiofilm activity. Besides, most of the antibacterial PSs lose their activity once the light source is removed. This property can result in biofilm recurrence if some bacteria have survived in PDT.

In this thesis, PSs with AIE properties have been developed as antiplanktonic and antibiofilm agents. Various designs and structural modifications have been made to improve the water solubility, antibacterial activity, and biocompatibility of the AIE PSs. Additionally, intrinsic antibacterial activities have also been incorporated into the PSs, which help extend the antibacterial effects even without light irradiation.

In the work as reported in this thesis, a water-soluble and bacteria-targeting AIE PS, TPA-1, has been designed. TPA-1 exhibits minimal toxicity towards human cells with and without light irradiation. Unlike traditional PS, TPA-1 acts as a narrow-spectrum antibacterial agent, killing planktonic *S. aureus* and inhibiting their biofilm formation even without light irradiation. The mechanism study reveals that TPA-1 can depolarize the *S. aureus* membrane and inhibit the negative supercoiling activity of the *S. aureus* DNA gyrase. Mass spectrometry (MS)-based proteomic analysis further shows that TPA-1 can cause downregulation of multiple essential proteins in *S. aureus*, including proteins related to cell division, cell wall synthesis and translation. With light irradiation, TPA-1 can eradicate *S. aureus* and *P. aeruginosa* in their planktonic and biofilm forms by generating ROS that cause cell membrane damage. Besides, TPA-1 with light irradiation can significantly reduce the bacterial burden and promote wound

healing in MRSA- and *P. aeruginosa*-infected mice models, indicating that TPA-1 has good *in vivo* therapeutic efficacy.

Inspired by the intrinsic antibacterial properties of TPA-1, several membrane disruptor-like AIE PSs that aim to achieve broad-spectrum antibacterial effects without light irradiation were also designed. Among these AIE PSs, TPA-C3-C6 has the best intrinsic antibacterial activity while exhibiting relatively low cytotoxicity. Without light irritation, TPA-C3-C6 shows good antiplanktonic activity against *S. aureus* and moderate activity against *P. aeruginosa*. The intrinsic antibacterial activity of TPA-C3-C6 is attributed to its ability to disrupt bacterial membranes and interfere with the negative supercoiling activity of *S. aureus* and *P. aeruginosa* DNA gyrases. In addition, TPA-C3-C6 can inhibit the biofilm formation of *S. aureus* and *P. aeruginosa* by downregulating quorum sensing and biofilm-related genes. Furthermore, TPA-C3-C6 can prevent biofilm recurrence through the combined effects of PDT and intrinsic antibacterial activity, which can also reduce translation and virulence in *S. aureus* and *P. aeruginosa* biofilms.

5.2 Future Perspectives

The work presented in this thesis has demonstrated the incorporation of intrinsic antibacterial properties as well as biocompatibility into a PS. It is believed that the examples shown here can drive the development of PSs with extended activity in the dark. Meanwhile, some other weaknesses of the currently developed PSs have yet to be addressed. For example, biofilm-infected wounds are hypoxic, which greatly limits the effectiveness of PDT. To improve *in vivo* PDT efficiency, it is suggested that oxygen-carrying or oxygen-generating materials can be introduced with PSs into the wounds. Perfluorocarbons are commonly used to develop artificial blood due to their ability to dissolve substantial amounts of oxygen.[208] Perfluorocarbon-based oxygen carriers, such as Perftoran, can be used as mediums to dissolve PSs or crafted into nanocarriers that deliver both PSs and oxygen.[208, 209] These mixtures or nanocarriers can

increase the oxygen content in the infected area, thereby further enhancing the efficacy of PDT. Moreover, antibacterial PSs often rely on cationization to target negatively charged bacteria. Although human cells carry less negatively charged than bacteria, a small portion of positively charged PSs can still be internalized by human cells, potentially causing cytotoxicity. Therefore, there is a need to develop alternative targeting strategies. One possible approach could be designing low molecular weight PSs that can passively diffuse into bacterial cells and target specific proteins or cellular components without requiring cationization. For instance, small and neutral PSs, such as thiocarbonyl-substituted naphthalimides, could be coupled with a D-alanine moiety, allowing them to enter the bacterial cells and metabolically incorporate into the bacterial cell wall. Hopefully, these proposed strategies can overcome some of the shortcomings of currently developed PSs and lead to the development of a safe and effective antibacterial PS that can enter clinical trials.

References

(1) Ran, B.; Wang, Z.; Cai, W.; Ran, L.; Xia, W.; Liu, W.; Peng, X. Organic Photo-antimicrobials: Principles, Molecule Design, and Applications. *J. Am. Chem. Soc.* **2021**, *143* (43), 17891-17909.

(2) Kohanski, M. A.; Dwyer, D. J.; Collins, J. J. How antibiotics kill bacteria: from targets to networks. *Nat. Rev. Microbiol.* **2010**, *8* (6), 423-435.

(3) Wellington, E. M. H.; Boxall, A. B. A.; Cross, P.; Feil, E. J.; Gaze, W. H.; Hawkey, P. M.; Johnson-Rollings, A. S.; Jones, D. L.; Lee, N. M.; Otten, W.; et al. The role of the natural environment in the emergence of antibiotic resistance in Gram-negative bacteria. *The Lancet Infect. Dis.* **2013**, *13* (2), 155-165.

(4) Naghavi, M.; Vollset, S. E.; Ikuta, K. S.; Swetschinski, L. R.; Gray, A. P.; Wool, E. E.; Robles Aguilar, G.; Mestrovic, T.; Smith, G.; Han, C.; et al. Global burden of bacterial antimicrobial resistance 1990-2021: a systematic analysis with forecasts to 2050. *The Lancet* **2024**, *404* (10459), 1199-1226.

(5) Jonas, O. B. I., Alec; Berthe,Franck Cesar Jean; Le Gall,Francois G.; Marquez,Patricio V.. *Drug-resistant infections: a threat to our economic future (vol 2): final report*; HNP/Agriculture Global Antimicrobial Resistance Initiative Washington, D.C. : World Bank Group., 2017.

(6) Hall, C. W.; Mah, T.-F. Molecular mechanisms of biofilm-based antibiotic resistance and tolerance in pathogenic bacteria. *FEMS Microbiol. Rev.* **2017**, *41* (3), 276-301.

(7) Flemming, H.-C.; Wingender, J. The biofilm matrix. *Nat. Rev. Microbiol.* **2010**, *8* (9), 623-633.

(8) Anwar, H.; Dasgupta, M.; Costerton, J. Testing the susceptibility of bacteria in biofilms to antibacterial agents. *Antimicrob. Agents Chemother.* **1990**, *34* (11), 2043-2046.

(9) Rasmussen, T. B.; Givskov, M. Quorum-sensing inhibitors as anti-pathogenic drugs. *Int. J. Med. Microbiol.* **2006**, *296* (2), 149-161.

(10) Ciofu, O.; Moser, C.; Jensen, P. Ø.; Høiby, N. Tolerance and resistance of microbial biofilms. *Nat. Rev. Microbiol.* **2022**, *20* (10), 621-635.

(11) Sauer, K.; Stoodley, P.; Goeres, D. M.; Hall-Stoodley, L.; Burmølle, M.; Stewart, P. S.; Bjarnsholt, T. The biofilm life cycle: expanding the conceptual model of biofilm formation. *Nat. Rev. Microbiol.* **2022**, *20* (10), 608-620.

(12) Pestrak, M. J.; Gupta, T. T.; Dusane, D. H.; Guzior, D. V.; Staats, A.; Harro, J.; Horswill, A. R.; Stoodley, P. Investigation of synovial fluid induced *Staphylococcus aureus* aggregate development and its impact on surface attachment and biofilm formation. *PLOS ONE* **2020**, *15* (4), e0231791.

(13) Hall-Stoodley, L.; Stoodley, P.; Kathju, S.; Høiby, N.; Moser, C.; Costerton, J. W.; Moter, A.; Bjarnsholt, T. Towards diagnostic guidelines for biofilm-associated infections. *FEMS Immunol. Med. Microbiol.* **2012**, *65* (2), 127-145.

(14) Crabbé, A.; Jensen, P.; Bjarnsholt, T.; Coenye, T. Antimicrobial Tolerance and Metabolic Adaptations in Microbial Biofilms. *Trends Microbiol.* **2019**, *27* (10), 850-863.

(15) Stewart, P. S.; Franklin, M. J. Physiological heterogeneity in biofilms. *Nat. Rev. Microbiol.* **2008**, *6* (3), 199-210.

(16) Pamp, S. J.; Gjermansen, M.; Johansen, H. K.; Tolker-Nielsen, T. Tolerance to the antimicrobial peptide colistin in *Pseudomonas aeruginosa* biofilms is linked to metabolically active cells, and depends on the pmr and mexAB-oprM genes. *Mol. Microbiol.* **2008**, *68* (1), 223-240.

(17) Anderl, J. N.; Zahller, J.; Roe, F.; Stewart, P. S. Role of Nutrient Limitation and Stationary-Phase Existence in *Klebsiella pneumoniae* Biofilm Resistance to Ampicillin and Ciprofloxacin. *Antimicrob. Agents Chemother.* **2003**, *47* (4), 1251-1256.

(18) Cao, B.; Christophersen, L.; Thomsen, K.; Sønderholm, M.; Bjarnsholt, T.; Jensen, P.; Høiby, N.; Moser, C. Antibiotic penetration and bacterial killing in a *Pseudomonas aeruginosa* biofilm model. *J. Antimicrob. Chemother.* **2015**, *70* (7), 2057-2063.

(19) Cao, B.; Christophersen, L.; Kolpen, M.; Jensen, P.; Sneppen, K.; Høiby, N.; Moser, C.; Sams, T. Diffusion Retardation by Binding of Tobramycin in an Alginate Biofilm Model. *PLoS One* **2016**, *11* (4), e0153616.

(20) Singh, R.; Sahore, S.; Kaur, P.; Rani, A.; Ray, P. Penetration barrier contributes to bacterial biofilm-associated resistance against only select antibiotics, and exhibits genus-, strain- and antibiotic-specific differences. *Pathog. Dis.* **2016**, *74* (6).

(21) Bagge, N.; Schuster, M.; Hentzer, M.; Ciofu, O.; Givskov, M.; Greenberg, E. P.; Høiby, N. *Pseudomonas aeruginosa* biofilms exposed to imipenem exhibit changes in global gene expression and beta-lactamase and alginate production. *Antimicrob. Agents Chemother.* **2004**, *48* (4), 1175-1187.

(22) Nguyen, D.; Joshi-Datar, A.; Lepine, F.; Bauerle, E.; Olakanmi, O.; Beer, K.; McKay, G.; Siehnel, R.; Schafhauser, J.; Wang, Y.; et al. Active starvation responses mediate antibiotic tolerance in biofilms and nutrient-limited bacteria. *Science* **2011**, *334* (6058), 982-986.

(23) Khakimova, M.; Ahlgren, H. G.; Harrison, J. J.; English, A. M.; Nguyen, D. The stringent response controls catalases in *Pseudomonas aeruginosa* and is required for hydrogen peroxide and antibiotic tolerance. *J. Bacteriol.* **2013**, *195* (9), 2011-2020.

(24) Žgur Bertok, D.; Podlesek, Z. The *Escherichia coli* SOS Response: Much More than DNA Damage Repair. In *Escherichia coli Old and New Insights*, Starčič Erjavec, M. Ed.; IntechOpen, 2021.

(25) Niu, H.; Gu, J.; Zhang, Y. Bacterial persisters: molecular mechanisms and therapeutic development. *Signal Transduct. Target. Ther.* **2024**, *9* (1), 174.

(26) Zhang, Y. Persisters, persistent infections and the Yin–Yang model. *Emerg. Microbes Infect.* **2014**, *3* (1), 1-10.

(27) Van Acker, H.; Sass, A.; Bazzini, S.; De Roy, K.; Udine, C.; Messiaen, T.; Riccardi, G.; Boon, N.; Nelis, H. J.; Mahenthiralingam, E.; Coenye, T. Biofilm-Grown Burkholderia cepacia Complex Cells Survive Antibiotic Treatment by Avoiding Production of Reactive Oxygen Species. *PLOS ONE* **2013**, *8* (3), e58943.

(28) Vázquez-Laslop, N.; Lee, H.; Neyfakh Alexander, A. Increased Persistence in Escherichia coli Caused by Controlled Expression of Toxins or Other Unrelated Proteins. *J. Bacteriol.* **2006**, *188* (10), 3494-3497.

(29) Gerdes, K.; Maisonneuve, E. Bacterial Persistence and Toxin-Antitoxin Loci. *Annu. Rev. Microbiol.* **2012**, *66* (Volume 66, 2012), 103-123.

(30) Van Acker, H.; Van Dijck, P.; Coenye, T. Molecular mechanisms of antimicrobial tolerance and resistance in bacterial and fungal biofilms. *Trends Microbiol.* **2014**, *22* (6), 326-333.

(31) Sharma, D.; Misba, L.; Khan, A. U. Antibiotics versus biofilm: an emerging battleground in microbial communities. *Antimicrob. Resist. Infect. Control* **2019**, *8*, 76.

(32) Sen, C. K.; Gordillo, G. M.; Roy, S.; Kirsner, R.; Lambert, L.; Hunt, T. K.; Gottrup, F.; Gurtner, G. C.; Longaker, M. T. Human skin wounds: a major and snowballing threat to public health and the economy. *Wound Repair Regen.* **2009**, *17* (6), 763-771.

(33) Bjarnsholt, T. The role of bacterial biofilms in chronic infections. *APMIS* **2013**, *121* (s136), 1-58.

(34) Broxton, C. N.; Culotta, V. C. SOD Enzymes and Microbial Pathogens: Surviving the Oxidative Storm of Infection. *PLoS Pathog.* **2016**, *12* (1), e1005295.

(35) Hamblin, M. R. Antimicrobial photodynamic inactivation: a bright new technique to kill resistant microbes. *Curr. Opin. Microbiol.* **2016**, *33*, 67-73.

(36) Wainwright, M.; Phoenix, D. A.; Laycock, S. L.; Wareing, D. R.; Wright, P. A. Photobactericidal activity of phenothiazinium dyes against methicillin-resistant strains of *Staphylococcus aureus*. *FEMS Microbiol Lett* **1998**, *160* (2), 177-181.

(37) Wainwright, M.; Maisch, T.; Nonell, S.; Plaetzer, K.; Almeida, A.; Tegos, G. P.; Hamblin, M. R. Photoantimicrobials-are we afraid of the light? *Lancet Infect. Dis.* **2017**, *17* (2), e49-e55.

(38) Hamblin, M. R.; Hasan, T. Photodynamic therapy: a new antimicrobial approach to infectious disease? *Photochem. Photobiol. Sci.* **2004**, *3* (5), 436-450.

(39) Alves, E.; Faustino, M. A.; Neves, M. G.; Cunha, A.; Tome, J.; Almeida, A. An insight on bacterial cellular targets of photodynamic inactivation. *Future Med. Chem.* **2014**, *6* (2), 141-164.

(40) Laxminarayan, R.; Duse, A.; Wattal, C.; Zaidi, A. K. M.; Wertheim, H. F. L.; Sumpradit, N.; Vlieghe, E.; Hara, G. L.; Gould, I. M.; Goossens, H.; et al. Antibiotic resistance 2014;the need for global solutions. *Lancet Infect. Dis.* **2013**, *13* (12), 1057-1098.

(41) Giuliani, F.; Martinelli, M.; Cocchi, A.; Arbia, D.; Fantetti, L.; Roncucci, G. In Vitro Resistance Selection Studies of RLP068/Cl, a New Zn(II) Phthalocyanine Suitable for Antimicrobial Photodynamic Therapy. *Antimicrob. Agents Chemother.* **2010**, *54* (2), 637-642.

(42) Cassidy, C. M.; Donnelly, R. F.; Tunney, M. M. Effect of sub-lethal challenge with Photodynamic Antimicrobial Chemotherapy (PACT) on the antibiotic susceptibility of clinical bacterial isolates. *J. Photochem. and Photobiol. B.* **2010**, *99* (1), 62-66.

(43) Zhou, W.; Jiang, X.; Zhen, X. Development of organic photosensitizers for antimicrobial photodynamic therapy. *Biomater. Sci.* **2023**, *11* (15), 5108-5128.

(44) Nguyen, V.-N.; Zhao, Z.; Tang, B. Z.; Yoon, J. Organic photosensitizers for antimicrobial phototherapy. *Chem. Soc. Rev.* **2022**, *51* (9), 3324-3340.

(45) Foote, C. S. DEFINITION OF TYPE I and TYPE II PHOTOSENSITIZED OXIDATION. *Photochem. Photobiol.* **1991**, *54* (5), 659-659.

(46) Ni, J.; Wang, Y.; Zhang, H.; Sun, J. Z.; Tang, B. Z. Aggregation-Induced Generation of Reactive Oxygen Species: Mechanism and Photosensitizer Construction. *Molecules* **2021**, *26* (2), 268.

(47) Dąbrowski, J. M. Chapter Nine - Reactive Oxygen Species in Photodynamic Therapy: Mechanisms of Their Generation and Potentiation. In *Advances in Inorganic Chemistry*, van Eldik, R., Hubbard, C. D. Eds.; Vol. 70; Academic Press, 2017; pp 343-394.

(48) Silva, E. F. F.; Serpa, C.; Dąbrowski, J. M.; Monteiro, C. J. P.; Formosinho, S. J.; Stochel, G.; Urbanska, K.; Simões, S.; Pereira, M. M.; Arnaut, L. G. Mechanisms of Singlet-Oxygen and Superoxide-Ion Generation by Porphyrins and Bacteriochlorins and their Implications in Photodynamic Therapy. *Chem. Eur. J.* **2010**, *16* (30), 9273-9286.

(49) Awad, M. M.; Tovmasyan, A.; Craik, J. D.; Batinic-Haberle, I.; Benov, L. T. Important cellular targets for antimicrobial photodynamic therapy. *Appl. Microbiol. Biotechnol.* **2016**, *100* (17), 7679-7688.

(50) Sobotta, L.; Skupin-Mrugalska, P.; Piskorz, J.; Mielcarek, J. Porphyrinoid photosensitizers mediated photodynamic inactivation against bacteria. *Eur. J. Med. Chem.* **2019**, *175*, 72-106.

(51) Agnez-Lima, L. F.; Mascio, P. D.; Napolitano, R. L.; Fuchs, R. P.; Menck, C. F. M. Mutation Spectrum Induced by Singlet Oxygen in *Escherichia coli* Deficient in Exonuclease III. *Photochem. Photobiol.* **1999**, *70* (4), 505-511.

(52) Geng, Z.; Cao, Z.; Liu, J. Recent advances in targeted antibacterial therapy basing on nanomaterials. *Exploration* **2023**, *3* (1), 20210117.

(53) Xie, J.; Wang, Y.; Choi, W.; Jangili, P.; Ge, Y.; Xu, Y.; Kang, J.; Liu, L.; Zhang, B.; Xie, Z.; et al. Overcoming barriers in photodynamic therapy harnessing nano-formulation strategies. *Chem. Soc. Rev.* **2021**, *50* (16), 9152-9201.

(54) Silva, A. F.; dos Santos, A. R.; Trevisan, D. A. C.; Bonin, E.; Freitas, C. F.; Batista, A. F. P.; Hioka, N.; Simões, M.; Graton Mikcha, J. M. Xanthene Dyes and Green LED for the Inactivation of Foodborne Pathogens in Planktonic and Biofilm States. *Photochem. Photobiol.* **2019**, *95* (5), 1230-1238.

(55) Macia, N.; Bresoli-Obach, R.; Nonell, S.; Heyne, B. Hybrid Silver Nanocubes for Improved Plasmon-Enhanced Singlet Oxygen Production and Inactivation of Bacteria. *J. Am. Chem. Soc.* **2019**, *141* (1), 684-692.

(56) Zhu, Y.; Wu, S.; Sun, Y.; Zou, X.; Zheng, L.; Duan, S.; Wang, J.; Yu, B.; Sui, R.; Xu, F.-J. Bacteria-Targeting Photodynamic Nanoassemblies for Efficient Treatment of Multidrug-Resistant Biofilm Infected Keratitis. *Adv. Funct. Mater.* **2022**, *32* (14), 2111066.

(57) Wu, S.; Xu, C.; Zhu, Y.; Zheng, L.; Zhang, L.; Hu, Y.; Yu, B.; Wang, Y.; Xu, F.-J. Biofilm-Sensitive Photodynamic Nanoparticles for Enhanced Penetration and Antibacterial Efficiency. *Adv. Funct. Mate.* **2021**, *31* (33), 2103591.

(58) Ebaston, T. M.; Nakonechny, F.; Talalai, E.; Gellerman, G.; Patsenker, L. Iodinated xanthene-cyanine NIR dyes as potential photosensitizers for antimicrobial photodynamic therapy. *Dyes Pigments* **2021**, *184*, 108854.

(59) Guan, Y.; Yu, B.; Ding, J.; Sun, T.; Xie, Z. BODIPY photosensitizers for antibacterial photodynamic therapy. *Chin. Chem. Lett.* **2024**, 110645..

(60) Liu, H.; Li, H.; Li, W.; Zhang, J.; Ye, J.; Liao, S.; Li, Y.; Yin, S. Chalcogen modification: one-step strategy for tuning the photophysical properties and NIR phototherapy of iodinated BODIPY. *Mater. Chem. Front.* **2024**, *8* (20), 3308-3320.

(61) Dai, X.; Chen, X.; Zhao, Y.; Yu, Y.; Wei, X.; Zhang, X.; Li, C. A Water-Soluble Galactose-Decorated Cationic Photodynamic Therapy Agent Based on BODIPY to Selectively Eliminate Biofilm. *Biomacromolecules* **2018**, *19* (1), 141-149.

(62) Li, C.; Li, Y.; Wu, Q.; Sun, T.; Xie, Z. Multifunctional BODIPY for effective inactivation of Gram-positive bacteria and promotion of wound healing. *Biomater. Sci.* **2021**, *9* (22), 7648-7654.

(63) Scatena, R.; Bottoni, P.; Pontoglio, A.; Giardina, B. Pharmacological Modulation of Nitric Oxide Release: New Pharmacological Perspectives, Potential Benefits and Risks. *Curr. Med. Chem.* **2010**, *17* (1), 61-73.

(64) Lin, G.; Hu, M.; Zhang, R.; Zhu, Y.; Gu, K.; Bai, J.; Li, J.; Dong, X.; Zhao, W. Discovery of Meso-(meta-Pyridinium) BODIPY Photosensitizers: In Vitro and In Vivo Evaluations for Antimicrobial Photodynamic Therapy. *J. Med. Chem.* **2021**, *64* (24), 18143-18157.

(65) Wen, H.; Wu, Q.; Liu, L.; Li, Y.; Sun, T.; Xie, Z. Structural optimization of BODIPY photosensitizers for enhanced photodynamic antibacterial activities. *Biomater. Sci.* **2023**, *11* (8), 2870-2876.

(66) Egawa, Y.; Miki, R.; Seki, T. Colorimetric Sugar Sensing Using Boronic Acid-Substituted Azobenzenes. *Materials (Basel)* **2014**, *7* (2), 1201-1220.

(67) Merchat, M.; Bertolini, G.; Giacomini, P.; Villaneuva, A.; Jori, G. Meso-substituted cationic porphyrins as efficient photosensitizers of gram-positive and gram-negative bacteria. *J. Photochem. Photobiol. B.* **1996**, *32* (3), 153-157.

(68) Hu, H.; Wang, H.; Yang, Y.; Xu, J.-F.; Zhang, X. A Bacteria-Responsive Porphyrin for Adaptable Photodynamic/Photothermal Therapy. *Angew. Chem. Int. Ed.* **2022**, *61* (23), e202200799.

(69) Zhang, H.; Zhu, Y.; Li, Y.; Qi, X.; Yang, J.; Qi, H.; Li, Q.; Ma, Y.; Zhang, Y.; Zhang, X.; Zhang, L. A Bifunctional Zwitterion-Modified Porphyrin for Photodynamic Nondestructive Tooth Whitening and Biofilm Eradication. *Adv. Funct. Mater.* **2021**, *31* (42), 2104799.

(70) Zhang, H.; Li, Q.; Qi, X.; Li, Y.; Ma, H.; Grinholc, M.; Nakonieczna, J.; Yu, B.; Wang, X.; Zhang, L. Iron-blocking antibacterial therapy with cationic heme-mimetic gallium

porphyrin photosensitizer for combating antibiotic resistance and enhancing photodynamic antibacterial activity. *Chem. Eng. J.* **2023**, *451*, 138261.

(71) Chitambar, C. R. The therapeutic potential of iron-targeting gallium compounds in human disease: From basic research to clinical application. *Pharmacol. Res.* **2017**, *115*, 56-64.

(72) Mondal, D.; Bera, S. Porphyrins and phthalocyanines: promising molecules for light-triggered antibacterial nanoparticles. *Adv. Nat. Sci. Nanosci. Nanotechnol.* **2014**, *5* (3), 033002.

(73) Langerreiter, D.; Kostiainen, M. A.; Kaabel, S.; Anaya-Plaza, E. A Greener Route to Blue: Solid-State Synthesis of Phthalocyanines. *Angew. Chem. Int. Ed.* **2022**, *61* (42), e202209033.

(74) Galstyan, A. Turning Photons into Drugs: Phthalocyanine-Based Photosensitizers as Efficient Photoantimicrobials. *Chem. Eur. J.* **2021**, *27* (6), 1903-1920.

(75) Fan, P.-P.; Li, S.-L.; Zheng, B.-Y.; Zheng, B.-D.; Lv, L.-L.; Ke, M.-R.; Huang, J.-D. Synthesis and photothermal/photodynamic antimicrobial activities of phthalocyanines tetra-substituted by morpholinyl moieties. *Dyes Pigments* **2023**, *212*, 111122.

(76) Chu, J. C. H.; Chin, M. L.; Wong, C. T. T.; Hui, M.; Lo, P.-C.; Ng, D. K. P. One-Pot Synthesis of a Cyclic Antimicrobial Peptide-Conjugated Phthalocyanine for Synergistic Chemo-Photodynamic Killing of Multidrug-Resistant Bacteria. *Adv. Ther.* **2021**, *4* (3), 2000204.

(77) Wang, R.; Kim, D.; Yang, M.; Li, X.; Yoon, J. Phthalocyanine-Assembled "One-For-Two" Nanoparticles for Combined Photodynamic–Photothermal Therapy of Multidrug-Resistant Bacteria. *ACS Appl. Mater. Interfaces* **2022**, *14* (6), 7609-7616.

(78) Xu, Z.; Li, H.; Zhou, S.; Sun, H.; Zhang, P.; Zheng, K.; Ding, C. Boric acid-substituted phthalocyanine/ciprofloxacin co-assembled nanoparticles for constructing bacteria-responsive intelligent wound dressings with synergistic therapy and recognition of bacterial infections. *Int. J. Biol. Macromol.* **2025**, *301*, 140333.

(79) Luo, J.; Xie, Z.; Lam, J. W. Y.; Cheng, L.; Chen, H.; Qiu, C.; Kwok, H. S.; Zhan, X.; Liu, Y.; Zhu, D.; Tang, B. Z. Aggregation-induced emission of 1-methyl-1,2,3,4,5-pentaphenylsilole. *Chem. Commun.* **2001**, (18), 1740-1741.

(80) Mei, J.; Leung, N. L. C.; Kwok, R. T. K.; Lam, J. W. Y.; Tang, B. Z. Aggregation-Induced Emission: Together We Shine, United We Soar! *Chem. Rev.* **2015**, *115* (21), 11718-11940.

(81) Gu, B.; Wu, W.; Xu, G.; Feng, G.; Yin, F.; Chong, P. H. J.; Qu, J.; Yong, K.-T.; Liu, B. Precise Two-Photon Photodynamic Therapy using an Efficient Photosensitizer with Aggregation-Induced Emission Characteristics. *Adv. Mater.* **2017**, *29* (28), 1701076.

(82) Liu, Z.; Zou, H.; Zhao, Z.; Zhang, P.; Shan, G.-G.; Kwok, R. T. K.; Lam, J. W. Y.; Zheng, L.; Tang, B. Z. Tuning Organelle Specificity and Photodynamic Therapy Efficiency by Molecular Function Design. *ACS Nano* **2019**, *13* (10), 11283-11293.

(83) Hu, F.; Qi, G.; Kenry; Mao, D.; Zhou, S.; Wu, M.; Wu, W.; Liu, B. Visualization and In Situ Ablation of Intracellular Bacterial Pathogens through Metabolic Labeling. *Angew. Chem. Int. Ed.* **2020**, *59* (24), 9288-9292.

(84) Liu, S.; Wang, B.; Yu, Y.; Liu, Y.; Zhuang, Z.; Zhao, Z.; Feng, G.; Qin, A.; Tang, B. Z. Cationization-Enhanced Type I and Type II ROS Generation for Photodynamic Treatment of Drug-Resistant Bacteria. *ACS Nano* **2022**, *16* (6), 9130-9141.

(85) Ma, K.; Dong, J.; Yan, D.; Wang, D.; Wang, Y.; Wang, J.; Wang, D.; Tan, H.; Tang, B. Z. Molecular Engineering of AIE-Active Photosensitizers with High Biosafety for Effect Extracellular Antibacteria. *Small* **2025**, *21* (4), 2403937.

(86) Lee, M. M. S.; Yu, E. Y.; Yan, D.; Chau, J. H. C.; Wu, Q.; Lam, J. W. Y.; Ding, D.; Kwok, R. T. K.; Wang, D.; Tang, B. Z. The Role of Structural Hydrophobicity on Cationic Amphiphilic Aggregation-Induced Emission Photosensitizer-Bacterial Interaction and Photodynamic Efficiency. *ACS Nano* **2023**, *17* (17), 17004-17020.

(87) Liu, S.; Feng, G.; Tang, B. Z.; Liu, B. Recent advances of AIE light-up probes for photodynamic therapy. *Chem. Sci.* **2021**, *12* (19), 6488-6506.

(88) Feng, G.; Liu, B. Aggregation-Induced Emission (AIE) Dots: Emerging Theranostic Nanolights. *Acc. Chem. Res.* **2018**, *51* (6), 1404-1414.

(89) Hu, F.; Xu, S.; Liu, B. Photosensitizers with Aggregation-Induced Emission: Materials and Biomedical Applications. *Adv. Mater.* **2018**, *30* (45), 1801350.

(90) Mei, J.; Hong, Y.; Lam, J. W. Y.; Qin, A.; Tang, Y.; Tang, B. Z. Aggregation-Induced Emission: The Whole Is More Brilliant than the Parts. *Adv. Mater.* **2014**, *26* (31), 5429-5479.

(91) Liu, C.; Ding, Q.; Liu, Y.; Wang, Z.; Xu, Y.; Lu, Q.; Chen, X.; Liu, J.; Sun, Y.; Li, R.; et al. An NIR Type I Photosensitizer Based on a Cyclometalated Ir(III)-Rhodamine Complex for a Photodynamic Antibacterial Effect toward Both Gram-Positive and Gram-Negative Bacteria. *Inorg. Chem.* **2024**, *63* (28), 13059-13067.

(92) Chen, H.; Yan, S.; Zhang, L.; Zhao, B.; Zhu, C.; Deng, G.; Liu, J. A Self-degrading and NIR-II emissive type I/II photosensitizer with synergistic photodynamic and photothermal properties for antibacterial and anticancer. *Sens. Actuators, B-Chem.* **2024**, *405*, 135346.

(93) Kong, L.; Zhang, R.; Gong, J.; Wang, H.; Zhai, L.; Dang, D.; Liu, Q.; Zhao, Z.; Tang, B. Z. Aggregation-induced emission photosensitizer for antibacterial therapy of methicillin-resistant *Staphylococcus aureus*. *Chem. Commun.* **2024**, *60* (46), 5960-5963.

(94) Macià, M. D.; del Pozo, J. L.; Díez-Aguilar, M.; Guinea, J. Microbiological diagnosis of biofilm-related infections. *Enferm. Infecc. Microbiol. Clin.* **2018**, *36* (6), 375-381.

(95) Otvagin, V. F.; Kuzmina, N. S.; Krylova, L. V.; Volovetsky, A. B.; Nyuchev, A. V.; Gavryushin, A. E.; Meshkov, I. N.; Gorbunova, Y. G.; Romanenko, Y. V.; Koifman, O. I.; et al. Water-Soluble Chlorin/Arylaminoquinazoline Conjugate for Photodynamic and Targeted Therapy. *J. Med. Chem.* **2019**, *62* (24), 11182-11193.

(96) Xia, F.-W.; Guo, B.-W.; Zhao, Y.; Wang, J.-L.; Chen, Y.; Pan, X.; Li, X.; Song, J.-X.; Wan, Y.; Feng, S.; Wu, M.-Y. Type I Photosensitizer Targeting Glycans: Overcoming Biofilm Resistance by Inhibiting the Two-Component System, Quorum Sensing, and Multidrug Efflux. *Adv. Mater.* **2023**, *35* (52), 2309797.

(97) Mei, J.; Hong, Y.; Lam, J. W.; Qin, A.; Tang, Y.; Tang, B. Z. Aggregation-induced emission: the whole is more brilliant than the parts. *Adv. Mater.* **2014**, *26* (31), 5429-5479.

(98) Hong, Y.; Lam, J. W. Y.; Tang, B. Z. Aggregation-induced emission: phenomenon, mechanism and applications. *Chem. Commun.* **2009**, (29), 4332.

(99) Xue, B.; Hou, A.; Du, Y.; Qi, Y.; Jiang, H.; Zhou, H.; Zhou, Z.; Chen, H. AIE donor-dependent photosensitizer for enhance photodynamic antibacterial interface. *Surf. Interfaces* **2023**, *39*, 102996.

(100) Wang, H.; Pan, X.; Wang, Y.; Liu, W.; Dai, T.; Yuan, B.; Chen, X.; Chen, Z. A new class of nitrobenzoic acid-based AIE photosensitizers for highly efficient photodynamic antibacterial therapy. *Sci. China Mater.* **2021**, *64* (10), 2601-2612.

(101) Shi, H.; Pan, X.; Wang, Y.; Wang, H.; Liu, W.; Wang, L.; Chen, Z. Restricting Bond Rotations by Ring Fusion: A Novel Molecular Design Strategy to Improve Photodynamic Antibacterial Efficacy of AIE Photosensitizers. *ACS Appl. Mater. Interfaces* **2022**, *14* (15), 17055-17064.

(102) Wang, J.-L.; Xia, F.-W.; Wang, Y.; Shi, H.-Z.; Wang, L.-J.; Zhao, Y.; Song, J.-X.; Wu, M.-Y.; Feng, S. Molecular Charge and Antibacterial Performance Relationships of Aggregation-Induced Emission Photosensitizers. *ACS Appl. Mater. Interfaces* **2023**, *15* (14), 17433-17443.

(103) Gong, J.; Liu, L.; Li, C.; He, Y.; Yu, J.; Zhang, Y.; Feng, L.; Jiang, G.; Wang, J.; Tang, B. Z. Oxidization enhances type I ROS generation of AIE-active zwitterionic photosensitizers for photodynamic killing of drug-resistant bacteria. *Chem. Sci.* **2023**, *14* (18), 4863-4871.

(104) Shi, X.; Sung, S. H. P.; Chau, J. H. C.; Li, Y.; Liu, Z.; Kwok, R. T. K.; Liu, J.; Xiao, P.; Zhang, J.; Liu, B.; et al. Killing G(+) or G(−) Bacteria? The Important Role of Molecular Charge in AIE-Active Photosensitizers. *Small Methods* **2020**, *4* (7), 2000046.

(105) Shi, J.; Wang, Y.; He, W.; Ye, Z.; Liu, M.; Zhao, Z.; Lam, J. W. Y.; Zhang, P.; Kwok, R. T. K.; Tang, B. Z. Precise Molecular Engineering of Type I Photosensitizer with Aggregation-Induced Emission for Image-Guided Photodynamic Eradication of Biofilm. *Molecules* **2023**, *28* (14), 5368.

(106) Goodman, C. M.; McCusker, C. D.; Yilmaz, T.; Rotello, V. M. Toxicity of Gold Nanoparticles Functionalized with Cationic and Anionic Side Chains. *Bioconjug. Chem.* **2004**, *15* (4), 897-900.

(107) Wu, S.; Xu, C.; Zhu, Y.; Zheng, L.; Zhang, L.; Hu, Y.; Yu, B.; Wang, Y.; Xu, F. J. Biofilm-Sensitive Photodynamic Nanoparticles for Enhanced Penetration and Antibacterial Efficiency. *Adv. Funct. Mater.* **2021**, *31* (33), 2103591.

(108) Zhu, C.; Yang, Q.; Liu, L.; Lv, F.; Li, S.; Yang, G.; Wang, S. Multifunctional Cationic Poly(p-phenylene vinylene) Polyelectrolytes for Selective Recognition, Imaging, and Killing of Bacteria Over Mammalian Cells. *Adv. Mater.* **2011**, *23* (41), 4805-4810.

(109) Shen, H.; Xu, C.; Ye, R.; Liu, T.-M.; Zhang, J.; Kwok, R. T. K.; Lam, J. W. Y.; Guo, Z.; Sun, J.; Tang, B. Z. Water-Soluble Aggregation-Induced Emission Luminogens with Near-Infrared Emission for Advanced Phototheranostics. *Small Sci.* **2023**, *3* (9), 2300052.

(110) Chen, L.; Chen, S.-L.; Yuan, Y.; Leng, X.; Xu, X.; Chen, J.; Shi, J.; Qian, K.; Xie, Y.; Ding, Q.; et al. Complexity made easy: Aggregation-induced emission small molecules for cancer diagnosis and phototherapies. *Aggregate* **2024**, *5* (6), e657.

(111) Bai, H.; He, W.; Chau, J. H. C.; Zheng, Z.; Kwok, R. T. K.; Lam, J. W. Y.; Tang, B. Z. AIEgens for microbial detection and antimicrobial therapy. *Biomaterials* **2021**, *268*, 120598.

(112) Li, N. N.; Li, J. Z.; Liu, P.; Pranantyo, D.; Luo, L.; Chen, J. C.; Kang, E.-T.; Hu, X. F.; Li, C. M.; Xu, L. Q. An antimicrobial peptide with an aggregation-induced emission (AIE) luminogen for studying bacterial membrane interactions and antibacterial actions. *Chem. Commun.* **2017**, *53* (23), 3315-3318.

(113) Wang, C.; Wang, J.; Xue, K.; Xiao, M.; Sun, Z.; Zhu, C. A receptor-targeting AIE photosensitizer for selective bacterial killing and real-time monitoring of photodynamic therapy outcome. *Chem. Commun.* **2022**, *58* (50), 7058-7061.

(114) Yu, Y.; Liu, Y.; Chen, Y.; Chen, J.; Feng, G.; Tang, B. Z. Cationic AIE-active photosensitizers for highly efficient photodynamic eradication of drug-resistant bacteria. *Mater. Chem. Front.* **2023**, *7* (1), 96-105.

(115) Zhang, J.; He, X.; Tang, B. Z. Aggregation-Induced Emission-Armored Living Bacteriophage-DNA Nanobioconjugates for Targeting, Imaging, and Efficient Elimination of Intracellular Bacterial Infection. *ACS Nano* **2024**, *18* (4), 3199-3213.

(116) Cai, W.; Shen, T.; Wang, D.; Li, T.; Yu, J.; Peng, C.; Tang, B. Z. Efficient antibacterial AIEgens induced ROS for selective photodynamic treatment of bacterial keratitis. *Front. Chem.* **2023**, *10*.

(117) Zhuang, Z.; Meng, Z.; Li, J.; Shen, P.; Dai, J.; Lou, X.; Xia, F.; Tang, B. Z.; Zhao, Z. Antibacterial Theranostic Agents with Negligible Living Cell Invasiveness: AIE-Active Cationic Amphiphiles Regulated by Alkyl Chain Engineering. *ACS Nano* **2022**, *16* (8), 11912-11930.

(118) Zhang, H.; He, C.; Shen, L.; Tao, W.; Zhu, J.; Song, J.; Li, Z.; Yin, J. Membrane-targeting amphiphilic AIE photosensitizer for broad-spectrum bacteria imaging and photodynamic killing of bacteria. *Chin. Chem. Lett.* **2023**, *34* (9), 108160.

(119) Yang, P.; Huang, H.; Xie, X. Removal of antibiotic resistant bacteria in wastewater by aggregation-induced emission photosensitizer. *Environ. Pollut.* **2023**, *334*, 121738.

(120) Liu, M.; Song, W.; Deng, P.; Nong, S.; Zhang, X.; Yu, Y.; Li, G.; Xu, L. Specific discrimination and efficient elimination of gram-positive bacteria by an aggregation-induced emission-active ruthenium (II) photosensitizer. *Eur. J. Med. Chem.* **2023**, *251*, 115249.

(121) Liu, L.; Li, C.; Gong, J.; Zhang, Y.; Ji, W.; Feng, L.; Jiang, G.; Wang, J.; Tang, B. Z. A Highly Water-Soluble Aggregation-Induced Emission Luminogen with Anion-π+ Interactions for Targeted NIR Imaging of Cancer Cells and Type I Photodynamic Therapy. *Angew. Chem. Int. Ed.* **2023**, *62* (33), e202307776.

(122) Zorko, M.; Jerala, R. Alexidine and chlorhexidine bind to lipopolysaccharide and lipoteichoic acid and prevent cell activation by antibiotics. *J. Antimicrob. Chemother.* **2008**, *62* (4), 730-737.

(123) Wood, S. J.; Miller, K. A.; David, S. A. Anti-endotoxin agents. 1. Development of a fluorescent probe displacement method optimized for the rapid identification of lipopolysaccharide-binding agents. *Comb. Chem. High Throughput Screen.* **2004**, *7* (3), 239-249.

(124) Institute, C. a. L. S. *Methods for Dilution Antimicrobial Susceptibility Tests for Bacteria That Grow Aerobically; Approved Standard—Ninth Edition*; 2012.

(125) Cai, Q.; Yu, Q.; Liang, W.; Li, H.; Liu, J.; Li, H.; Chen, Y.; Fang, S.; Zhong, R.; Liu, S.; Lin, S. Membrane-Active Nonivamide Derivatives as Effective Broad-Spectrum Antimicrobials: Rational Design, Synthesis, and Biological Evaluation. *J. Med. Chem.* **2022**, *65* (24), 16754-16773.

(126) Thomas, P. D.; Ebert, D.; Muruganujan, A.; Mushayahama, T.; Albou, L.-P.; Mi, H. PANTHER: Making genome-scale phylogenetics accessible to all. *Protein Sci.* **2022**, *31* (1), 8-22.

(127) Mi, H.; Muruganujan, A.; Huang, X.; Ebert, D.; Mills, C.; Guo, X.; Thomas, P. D. Protocol Update for large-scale genome and gene function analysis with the PANTHER classification system (v.14.0). *Nat. Protoc.* **2019**, *14* (3), 703-721.

(128) Yu, G.; Wang, L. G.; Han, Y.; He, Q. Y. clusterProfiler: an R package for comparing biological themes among gene clusters. *Omics* **2012**, *16* (5), 284-287.

(129) Wen, H.; Zhang, Z.; Kang, M.; Li, H.; Xu, W.; Guo, H.; Li, Y.; Tan, Y.; Wen, Z.; Wu, Q.; et al. One-for-all phototheranostics: Single component AIE dots as multi-modality theranostic agent for fluorescence-photoacoustic imaging-guided synergistic cancer therapy. *Biomaterials* **2021**, *274*, 120892.

(130) Misra, R.; Bhattacharyya, S. P. Introduction. In *Intramolecular Charge Transfer*, 2018; pp 1-27.

(131) Zhang, L.; Huang, Z.; Dai, D.; Xiao, Y.; Lei, K.; Tan, S.; Cheng, J.; Xu, Y.; Liu, J.; Qian, X. Thio-bisnaphthalimides as Heavy-Atom-Free Photosensitizers with Efficient Singlet Oxygen Generation and Large Stokes Shifts: Synthesis and Properties. *Org. Lett.* **2016**, *18* (21), 5664-5667.

(132) Marian, C. M. Spin–orbit coupling and intersystem crossing in molecules. *Wiley Interdiscip. Rev. Comput. Mol. Sci.* **2012**, *2* (2), 187-203.

(133) Wood, S. J.; Miller, K. A.; David, S. A. Anti-endotoxin agents. 2. Pilot high-throughput screening for novel lipopolysaccharide-recognizing motifs in small molecules. *Comb. Chem. High Throughput Screen.* **2004**, *7* (8), 733-747.

(134) Adams, P. G.; Lamoureux, L.; Swingle, K. L.; Mukundan, H.; Montaño, G. A. Lipopolysaccharide-induced dynamic lipid membrane reorganization: tubules, perforations, and stacks. *Biophys. J.* **2014**, *106* (11), 2395-2407.

(135) Waggoner, A. Optical probes of membrane potential. *J. Membr. Biol.* **1976**, *27* (1), 317-334.

(136) Te Winkel, J. D.; Gray, D. A.; Seistrup, K. H.; Hamoen, L. W.; Strahl, H. Analysis of Antimicrobial-Triggered Membrane Depolarization Using Voltage Sensitive Dyes. *Front. Cell Dev. Biol.* **2016**, *4*, 29.

(137) Gellert, M.; Mizuuchi, K.; O'Dea, M. H.; Nash, H. A. DNA gyrase: an enzyme that introduces superhelical turns into DNA. *Proc. Natl. Acad. Sci. U.S.A.* **1976**, *73* (11), 3872-3876.

(138) Fogg, J. M.; Judge, A. K.; Stricker, E.; Chan, H. L.; Zechiedrich, L. Supercoiling and looping promote DNA base accessibility and coordination among distant sites. *Nat. Commun.* **2021**, *12* (1), 5683.

(139) Naughton, C.; Avlonitis, N.; Corless, S.; Prendergast, J. G.; Mati, I. K.; Eijk, P. P.; Cockroft, S. L.; Bradley, M.; Ylstra, B.; Gilbert, N. Transcription forms and remodels supercoiling domains unfolding large-scale chromatin structures. *Nat. Struct. Mol. Biol.* **2013**, *20* (3), 387-395.

(140) Drew, H. R.; Weeks, J. R.; Travers, A. A. Negative supercoiling induces spontaneous unwinding of a bacterial promoter. *EMBO J.* **1985**, *4* (4), 1025-1032.

(141) Magnan, D.; Bates, D. Regulation of DNA Replication Initiation by Chromosome Structure. *J. Bacteriol.* **2015**, *197* (21), 3370-3377.

(142) de Boer, P. A. J. Advances in understanding *E. coli* cell fission. *Curr. Opin. Microbiol.* **2010**, *13* (6), 730-737.

(143) Gong, H.; Yan, D.; Cui, Y.; Li, Y.; Yang, J.; Yang, W.; Zhan, R.; Wan, Q.; Wang, X.; He, H.; et al. The divisome is a self-enhancing machine in *Escherichia coli* and *Caulobacter crescentus*. *Nat. Commun.* **2024**, *15* (1), 8198.

(144) den Blaauwen, T.; Hamoen, L. W.; Levin, P. A. The divisome at 25: the road ahead. *Curr. Opin. Microbiol.* **2017**, *36*, 85-94.

(145) Pichoff, S.; Lutkenhaus, J. Tethering the Z ring to the membrane through a conserved membrane targeting sequence in FtsA. *Mol. Microbiol.* **2005**, *55* (6), 1722-1734.

(146) Duman, R.; Ishikawa, S.; Celik, I.; Strahl, H.; Ogasawara, N.; Troc, P.; Löwe, J.; Hamoen, L. W. Structural and genetic analyses reveal the protein SepF as a new membrane anchor for the Z ring. *Proc. Natl. Acad. Sci.* **2013**, *110* (48), E4601-E4610.

(147) Schäper, S.; Brito, A. D.; Saraiva, B. M.; Squyres, G. R.; Holmes, M. J.; Garner, E. C.; Hensel, Z.; Henriques, R.; Pinho, M. G. Cell constriction requires processive septal peptidoglycan synthase movement independent of FtsZ treadmilling in *Staphylococcus aureus*. *Nat. Microbiol.* **2024**, *9* (4), 1049-1063.

(148) Smith, C. A. Structure, Function and Dynamics in the mur Family of Bacterial Cell Wall Ligases. *J. Mol. Biol.* **2006**, *362* (4), 640-655.

(149) Kim, M. M.; Darafsheh, A. Light Sources and Dosimetry Techniques for Photodynamic Therapy. *Photochem. Photobiol.* **2020**, *96* (2), 280-294.

(150) Costerton, J. W.; Stewart, P. S.; Greenberg, E. P. Bacterial biofilms: a common cause of persistent infections. *Science* **1999**, *284* (5418), 1318-1322.

(151) Lewis, K. Persister cells, dormancy and infectious disease. *Nat. Rev. Microbiol.* **2007**, *5* (1), 48-56.

(152) Eloïse, L.; Petit, L.; Nominé, Y.; Heurtault, B.; Ben Hadj Kaddour, I.; Senger, B.; Rodon Fores, J.; Vrana, N. E.; Barbault, F.; Lavalle, P. The antibacterial properties of branched peptides based on poly(l-arginine): In vitro antibacterial evaluation and molecular dynamic simulations. *Eur. J. Med. Chem.* **2024**, *268*, 116224.

(153) Yang, R.; Xue, Z.; Li, X.; Xu, T.; Zhong, Y.; Hu, S.; Qin, S.; Guo, Y. Novel natural osthole-inspired amphiphiles as membrane targeting antibacterials against methicillin-resistant *Staphylococcus aureus* (MRSA). *Eur. J. Med. Chem.* **2024**, *271*, 116449.

(154) Xiu, W.; Wan, L.; Yang, K.; Li, X.; Yuwen, L.; Dong, H.; Mou, Y.; Yang, D.; Wang, L. Potentiating hypoxic microenvironment for antibiotic activation by photodynamic therapy to combat bacterial biofilm infections. *Nat. Commun.* **2022**, *13* (1), 3875.

(155) Hemolysis Assay for Biomaterials_Manual. HaemoScan: 2024.

(156) Thorn, C. R.; Wignall, A.; Kopecki, Z.; Kral, A.; Prestidge, C. A.; Thomas, N. Liquid Crystal Nanoparticles Enhance Tobramycin Efficacy in a Murine Model of *Pseudomonas aeruginosa* Biofilm Wound Infection. *ACS Infect. Dis.* **2022**, *8* (4), 841-854.

(157) Müsken, M.; Di Fiore, S.; Römling, U.; Häussler, S. A 96-well-plate–based optical method for the quantitative and qualitative evaluation of *Pseudomonas aeruginosa* biofilm formation and its application to susceptibility testing. *Nat. Protoc.* **2010**, *5* (8), 1460-1469.

(158) Gründling, A.; Schneewind, O. Synthesis of glycerol phosphate lipoteichoic acid in *Staphylococcus aureus*. *Proc. Natl. Acad. Sci.* **2007**, *104* (20), 8478-8483.

(159) Brown, S.; Zhang, Y.-H.; Walker, S. A Revised Pathway Proposed for *Staphylococcus aureus* Wall Teichoic Acid Biosynthesis Based on In Vitro Reconstitution of the Intracellular Steps. *Chem. Biol.* **2008**, *15* (1), 12-21.

(160) Weidenmaier, C.; Kokai-Kun, J. F.; Kristian, S. A.; Chanturiya, T.; Kalbacher, H.; Gross, M.; Nicholson, G.; Neumeister, B.; Mond, J. J.; Peschel, A. Role of teichoic acids in *Staphylococcus aureus* nasal colonization, a major risk factor in nosocomial infections. *Nat. Med.* **2004**, *10* (3), 243-245.

(161) Sheen, T. R.; Ebrahimi, C. M.; Hiemstra, I. H.; Barlow, S. B.; Peschel, A.; Doran, K. S. Penetration of the blood-brain barrier by *Staphylococcus aureus*: contribution of membrane-anchored lipoteichoic acid. *J. Mol. Med. (Berl)* **2010**, *88* (6), 633-639.

(162) Spaan, A. N.; Vrieling, M.; Wallet, P.; Badiou, C.; Reyes-Robles, T.; Ohneck, E. A.; Benito, Y.; de Haas, C. J. C.; Day, C. J.; Jennings, M. P.; et al. The staphylococcal toxins γ-haemolysin AB and CB differentially target phagocytes by employing specific chemokine receptors. *Nat. Commun.* **2014**, *5* (1), 5438.

(163) Bestebroer, J.; Aerts, P. C.; Rooijakkers, S. H. M.; Pandey, M. K.; Köhl, J.; Van Strijp, J. A. G.; De Haas, C. J. C. Functional basis for complement evasion by staphylococcal superantigen-like 7. *Cell. Microbiol.* **2010**, *12* (10), 1506-1516.

(164) Wang, Y.; Ren, M.; Li, Y.; Liu, F.; Wang, Y.; Wang, Z.; Feng, L. Bioactive AIEgens Tailored for Specific and Sensitive Theranostics of Gram-Positive Bacterial Infection. *ACS Appl. Mater. Interfaces* **2022**, *14* (41), 46340-46350.

(165) Wang, Y.; Liao, J.; Lyu, Y.; Guo, Q.; Zhu, Z.; Wu, X.; Yu, J.; Wang, Q.; Zhu, W.-H. An AIE Photosensitizer with Simultaneous Type I and Type II ROS Generation: Efficient Bacterial Elimination and Hypoxic Tumor Ablation. *Adv. Funct. Mater.* **2023**, *33* (33), 2301692.

(166) Zhou, T.; Hu, R.; Wang, L.; Qiu, Y.; Zhang, G.; Deng, Q.; Zhang, H.; Yin, P.; Situ, B.; Zhan, C.; et al. An AIE-Active Conjugated Polymer with High ROS-Generation Ability and Biocompatibility for Efficient Photodynamic Therapy of Bacterial Infections. *Angew. Chem. Int. Ed.* **2020**, *59* (25), 9952-9956.

(167) Li, T.; Wu, Y.; Cai, W.; Wang, D.; Ren, C.; Shen, T.; Yu, D.; Qiang, S.; Hu, C.; Zhao, Z.; et al. Vision Defense: Efficient Antibacterial AIEgens Induced Early Immune Response for Bacterial Endophthalmitis. *Adv. Sci.* **2022**, *9* (25), 2202485.

(168) Liu, J.; Li, H.; He, Q.; Chen, K.; Chen, Y.; Zhong, R.; Li, H.; Fang, S.; Liu, S.; Lin, S. Design, synthesis, and biological evaluation of tetrahydroquinoline amphiphiles as membrane-targeting antimicrobials against pathogenic bacteria and fungi. *Eur. J. Med. Chem.* **2022**, *243*, 114734.

(169) Yu, Q.; Cai, Q.; Liang, W.; Zhong, K.; Liu, J.; Li, H.; Chen, Y.; Li, H.; Fang, S.; Zhong, R.; et al. Design of phenothiazine-based cationic amphiphilic derivatives incorporating arginine residues: Potential membrane-active broad-spectrum antimicrobials combating pathogenic bacteria in vitro and in vivo. *Eur. J. Med. Chem.* **2023**, *260*, 115733.

(170) Chen, Y.; Li, H.; Liu, J.; Zhong, R.; Li, H.; Fang, S.; Liu, S.; Lin, S. Synthesis and biological evaluation of indole-based peptidomimetics as antibacterial agents against Gram-positive bacteria. *Eur. J. Med. Chem.* **2021**, *226*, 113813.

(171) Fang, S.; Kang, W.-T.; Li, H.; Cai, Q.; Liang, W.; Zeng, M.; Yu, Q.; Zhong, R.; Tao, Y.; Liu, S.; Lin, S. Development of cannabidiol derivatives as potent broad-spectrum antibacterial agents with membrane-disruptive mechanism. *Eur. J. Med. Chem.* **2024**, *266*, 116149.

(172) Dumpati, S.; Dutta, D. Bacterial Dye Release Measures in Response to Antimicrobial Peptides. In *Membrane Lipids: Methods and Protocols*, Cranfield, C. G. Ed.; Springer US, 2022; pp 285-290.

(173) Chung, C.-C.; Cheng, I. F.; Chen, H.-M.; Kan, H.-C.; Yang, W.-H.; Chang, H.-C. Screening of Antibiotic Susceptibility to β-Lactam-Induced Elongation of Gram-Negative Bacteria Based on Dielectrophoresis. *Anal. Chem.* **2012**, *84* (7), 3347-3354.

(174) Kumar, K.; Divya, A.; T., B. W.; J., T. P.; A., S. R.; and Ojima, I. Discovery of Anti-TB Agents that Target the Cell-Division Protein FtsZ. *Future Med. Chem.* **2010**, *2* (8), 1305-1323.

(175) Nonejuie, P.; Burkart, M.; Pogliano, K.; Pogliano, J. Bacterial cytological profiling rapidly identifies the cellular pathways targeted by antibacterial molecules. *Proc. Natl. Acad. Sci.* **2013**, *110* (40), 16169-16174.

(176) Monahan Leigh, G.; Turnbull, L.; Osvath Sarah, R.; Birch, D.; Charles Ian, G.; Whitchurch Cynthia, B. Rapid Conversion of *Pseudomonas aeruginosa* to a Spherical Cell Morphotype Facilitates Tolerance to Carbapenems and Penicillins but Increases Susceptibility to Antimicrobial Peptides. *Antimicrob. Agents Chemother.* **2014**, *58* (4), 1956-1962.

(177) Trautmann, M.; Heinemann, M.; Zick, R.; Möricke, A.; Seidelmann, M.; Berger, D. Antibacterial Activity of Meropenem against *Pseudomonas aeruginosa*, Including Antibiotic-Induced Morphological Changes and Endotoxin-Liberating Effects. *Eur. J. Clin. Microbiol. Infect. Dis.* **1998**, *17* (11), 754-760.

(178) Horii, T.; Kobayashi, M.; Sato, K.; Ichiyama, S.; Ohta, M. An in-vitro study of carbapenem-induced morphological changes and endotoxin release in clinical isolates of gram-negative bacilli. *J. Antimicrob. Chemother.* **1998**, *41* (4), 435-442.

(179) Kong, K.-F.; Vuong, C.; Otto, M. *Staphylococcus* quorum sensing in biofilm formation and infection. *Int. J. Med. Microb.* **2006**, *296* (2), 133-139.

(180) O'Neill, E.; Humphreys, H.; O'Gara, J. P. Carriage of both the fnbA and fnbB genes and growth at 37 degrees C promote FnBP-mediated biofilm development in meticillin-resistant *Staphylococcus aureus* clinical isolates. *J. Med. Microbiol.* **2009**, *58* (Pt 4), 399-402.

(181) Abraham, N. M.; Jefferson, K. K. *Staphylococcus aureus* clumping factor B mediates biofilm formation in the absence of calcium. *Microbiology* **2012**, *158* (6), 1504-1512.

(182) O'Brien, L. M.; Walsh, E. J.; Massey, R. C.; Peacock, S. J.; Foster, T. J. *Staphylococcus aureus* clumping factor B (ClfB) promotes adherence to human type I cytokeratin 10: implications for nasal colonization. *Cell. Microbiol.* **2002**, *4* (11), 759-770.

(183) Whitchurch, C. B.; Tolker-Nielsen, T.; Ragas, P. C.; Mattick, J. S. Extracellular DNA Required for Bacterial Biofilm Formation. *Science* **2002**, *295* (5559), 1487-1487.

(184) Okshevsky, M.; Meyer, R. L. The role of extracellular DNA in the establishment, maintenance and perpetuation of bacterial biofilms. *Crit. Rev. Microbiol.* **2015**, *41* (3), 341-352.

(185) Ranjit, D. K.; Endres, J. L.; Bayles, K. W. *Staphylococcus aureus* CidA and LrgA proteins exhibit holin-like properties. *J. Bacteriol.* **2011**, *193* (10), 2468-2476.

(186) Ghafoor, A.; Hay, I. D.; Rehm, B. H. Role of exopolysaccharides in *Pseudomonas aeruginosa* biofilm formation and architecture. *Appl. Environ. Microbiol.* **2011**, *77* (15), 5238-5246.

(187) Yong, Y.-C.; Wu, X.-Y.; Sun, J.-Z.; Cao, Y.-X.; Song, H. Engineering quorum sensing signaling of *Pseudomonas* for enhanced wastewater treatment and electricity harvest: A review. *Chemosphere* **2015**, *140*, 18-25.

(188) Soukarieh, F.; Gurnani, P.; Romero, M.; Halliday, N.; Stocks, M.; Alexander, C.; Cámara, M. Design of Quorum Sensing Inhibitor–Polymer Conjugates to Penetrate *Pseudomonas aeruginosa* Biofilms. *ACS Macro Lett.* **2023**, *12* (3), 314-319.

(189) Liu, J.; Hou, J.-S.; Chang, Y.-Q.; Peng, L.-J.; Zhang, X.-Y.; Miao, Z.-Y.; Sun, P.-H.; Lin, J.; Chen, W.-M. New Pqs Quorum Sensing System Inhibitor as an Antibacterial Synergist against Multidrug-Resistant *Pseudomonas aeruginosa*. *J. Med. Chem.* **2022**, *65* (1), 688-709.

(190) Pearson, J. P.; Pesci, E. C.; Iglewski, B. H. Roles of *Pseudomonas aeruginosa* las and rhl quorum-sensing systems in control of elastase and rhamnolipid biosynthesis genes. *J. Bacteriol.* **1997**, *179* (18), 5756-5767.

(191) Davey, M. E.; Caiazza, N. C.; O'Toole, G. A. Rhamnolipid surfactant production affects biofilm architecture in *Pseudomonas aeruginosa* PAO1. *J. Bacteriol.* **2003**, *185* (3), 1027-1036.

(192) Gallagher, L. A.; McKnight, S. L.; Kuznetsova, M. S.; Pesci, E. C.; Manoil, C. Functions Required for Extracellular Quinolone Signaling by *Pseudomonas aeruginosa*. *J. Bacteriol.* **2002**, *184* (23), 6472-6480.

(193) Allesen-Holm, M.; Barken, K. B.; Yang, L.; Klausen, M.; Webb, J. S.; Kjelleberg, S.; Molin, S.; Givskov, M.; Tolker-Nielsen, T. A characterization of DNA release in *Pseudomonas aeruginosa* cultures and biofilms. *Mol. Microb.* **2006**, *59* (4), 1114-1128.

(194) Vollaro, A.; Esposito, A.; Esposito, E. P.; Zarrilli, R.; Guaragna, A.; De Gregorio, E. PYED-1 Inhibits Biofilm Formation and Disrupts the Preformed Biofilm of *Staphylococcus aureus*. *Antibiotics* **2020**, *9* (5), 240.

(195) Song, Y.-Q.; Kyung, S. M.; Kim, S.; Kim, G.; Lee, S. Y.; Yoo, H. S. Effects of synthetic peptide RP557 and its origin, LL-37, on carbapenem-resistant *Pseudomonas aeruginosa*. *Microbiol. Spectr.* **2023**, *11* (5), e00430-00423.

(196) Li, W.-R.; Ma, Y.-K.; Shi, Q.-S.; Xie, X.-B.; Sun, T.-L.; Peng, H.; Huang, X.-M. Diallyl disulfide from garlic oil inhibits *Pseudomonas aeruginosa* virulence factors by inactivating key quorum sensing genes. *Appl. Microbiol. and Biotechnol.* **2018**, *102* (17), 7555-7564.

(197) Birmes, F. S.; Säring, R.; Hauke, M. C.; Ritzmann, N. H.; Drees, S. L.; Daniel, J.; Treffon, J.; Liebau, E.; Kahl, B. C.; Fetzner, S. Interference with *Pseudomonas aeruginosa* Quorum Sensing and Virulence by the Mycobacterial *Pseudomonas* Quinolone Signal Dioxygenase AqdC in Combination with the *N*-Acylhomoserine Lactone Lactonase QsdA. *Infect. Immun.* **2019**, *87* (10), 10.1128/iai.00278-00219.

(198) Fusco, A.; Savio, V.; Stelitano, D.; Baroni, A.; Donnarumma, G. The Intestinal Biofilm of *Pseudomonas aeruginosa* and *Staphylococcus aureus* Is Inhibited by Antimicrobial Peptides HBD-2 and HBD-3. *Appl. Sci.* **2021**, *11* (14), 6595.

(199) Roberts, A. E. L.; Maddocks, S. E.; Cooper, R. A. Manuka honey is bactericidal against *Pseudomonas aeruginosa* and results in differential expression of oprF and algD. *Microbiology* **2012**, *158* (12), 3005-3013.

(200) Li, H.; Zheng, X.; Gao, Z.; Mu, T.; Liu, M.; Li, J.; Wu, J.; Zhang, W.; Lee, C.-S.; Liu, W.; Wang, P. ROS-Responsive Core-Shell Microneedles Based on Simultaneous Efficient Type I/II Photosensitizers for Photodynamic Against Bacterial Biofilm Infections. *Adv. Funct. Mater.* **2024**, *35* (21), 2401477.

(201) Chen, S.; Xie, J.; Weng, S.; Meng, W.; Zheng, J.; Huang, B.; Zhan, R.; Zhang, W.; Tian, J. A supramolecular photosensitizer for combating multiple antibiotic resistance via photodynamic biofilm dispersion. *Chem. Eng. J.* **2024**, *496*, 153951.

(202) Byrgazov, K.; Vesper, O.; Moll, I. Ribosome heterogeneity: another level of complexity in bacterial translation regulation. *Curr. Opin. Microbiol.* **2013**, *16* (2), 133-139.

(203) Prat, C.; Bestebroer, J.; de Haas, C. J.; van Strijp, J. A.; van Kessel, K. P. A new *staphylococcal* anti-inflammatory protein that antagonizes the formyl peptide receptor-like 1. *J. Immunol.* **2006**, *177* (11), 8017-8026.

(204) Morinaga, N.; Kaihou, Y.; Noda, M. Purification, cloning and characterization of variant LukE-LukD with strong leukocidal activity of *staphylococcal* bi-component leukotoxin family. *Microbiol. Immunol.* **2003**, *47* (1), 81-90.

(205) Vilaplana, L.; Marco, M. P. Phenazines as potential biomarkers of *Pseudomonas aeruginosa* infections: synthesis regulation, pathogenesis and analytical methods for their detection. *Anal. Bioanal. Chem.* **2020**, *412* (24), 5897-5912.

(206) Hall, S.; McDermott, C.; Anoopkumar-Dukie, S.; McFarland, A. J.; Forbes, A.; Perkins, A. V.; Davey, A. K.; Chess-Williams, R.; Kiefel, M. J.; Arora, D.; Grant, G. D. Cellular Effects of Pyocyanin, a Secreted Virulence Factor of *Pseudomonas aeruginosa*. *Toxins* **2016**, *8* (8), 236.

(207) O'Malley, Y. Q.; Reszka, K. J.; Rasmussen, G. T.; Abdalla, M. Y.; Denning, G. M.; Britigan, B. E. The *Pseudomonas* secretory product pyocyanin inhibits catalase activity in human lung epithelial cells. *Am. J. Physiol. Lung Cell. Mol. Physiol.* **2003**, *285* (5), L1077-1086.

(208) Kim, J.-H.; Jung, E.-A.; Kim, J.-E. Perfluorocarbon-based artificial oxygen carriers for red blood cell substitutes: considerations and direction of technology. *J. Pharm. Investig.* **2024**, *54* (3), 267-282.

(209) Hu, D.; Zou, L.; Yu, W.; Jia, F.; Han, H.; Yao, K.; Jin, Q.; Ji, J. Relief of Biofilm Hypoxia Using an Oxygen Nanocarrier: A New Paradigm for Enhanced Antibiotic Therapy. *Adv. Sci.* **2020**, *7* (12), 2000398.

Appendices

1. Characterizations for Compounds Synthesized in Chapter II

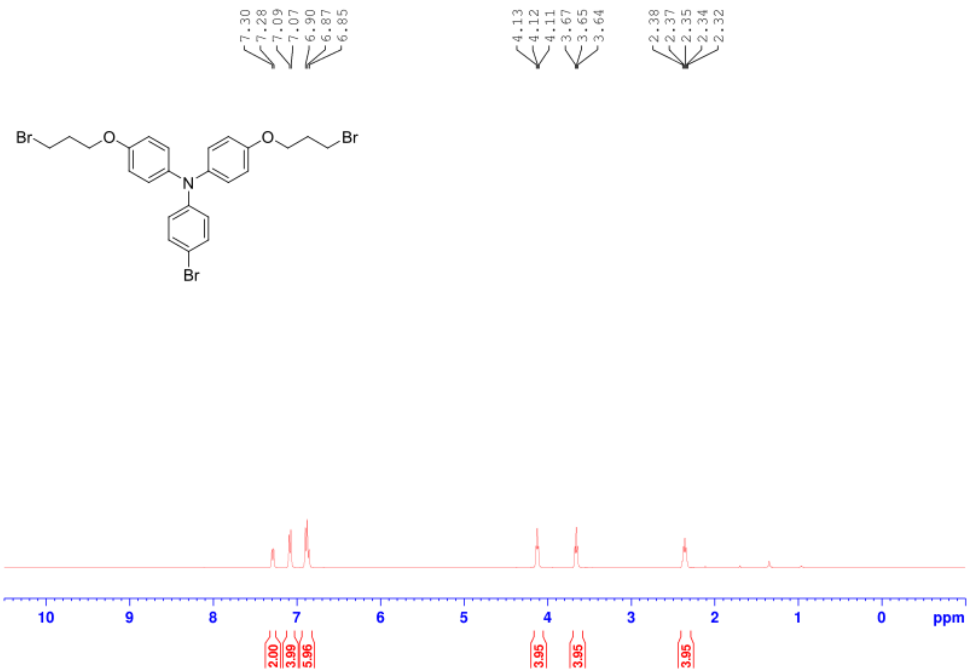

Figure S1. ^{1}H NMR spectrum (400 MHz, $CDCl_3$) of compound 2.

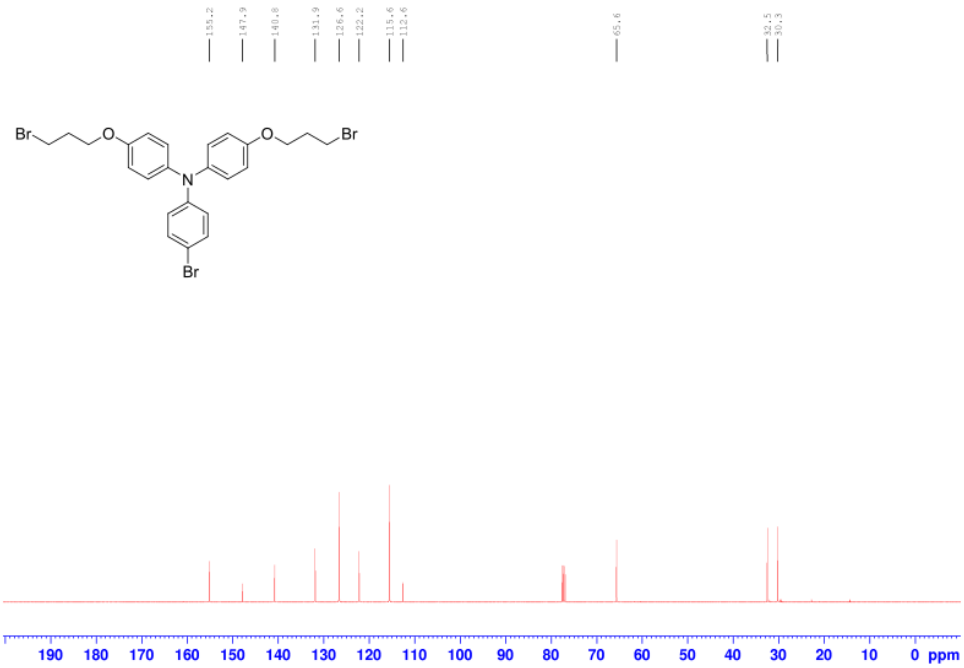

Figure S2. ^{13}C NMR spectrum (101 MHz, $CDCl_3$) of compound 2.

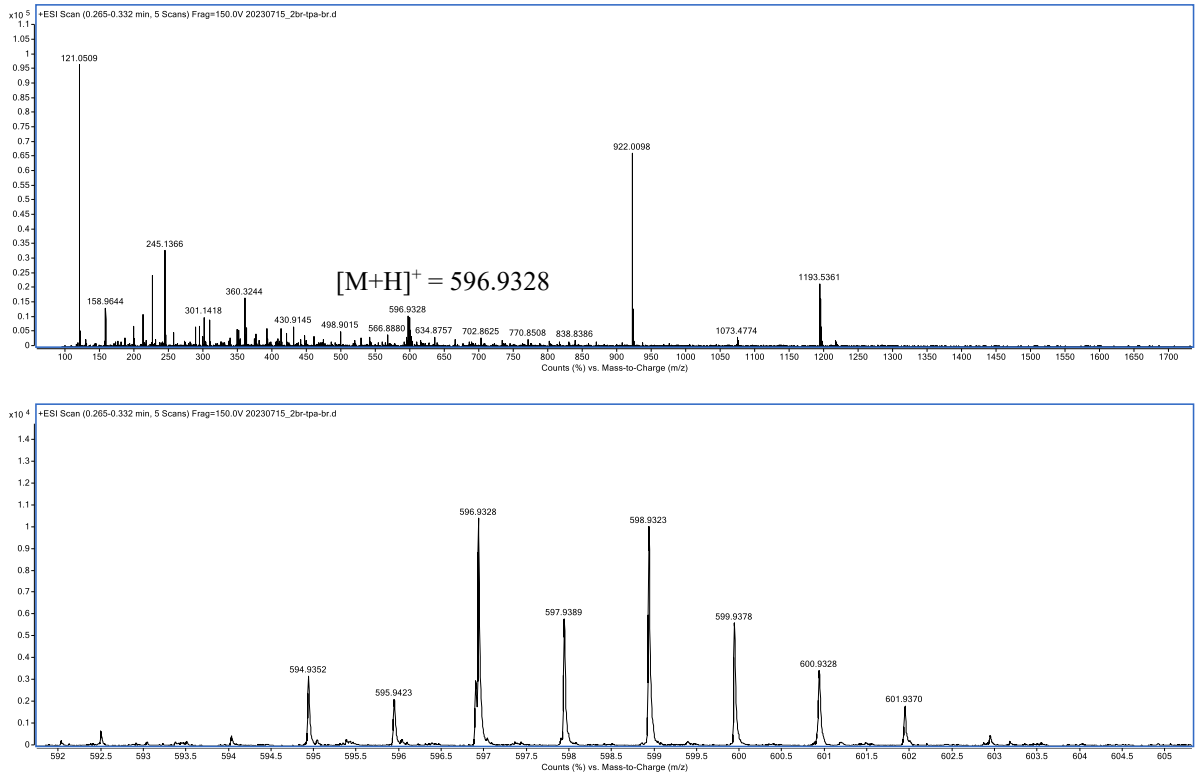

Figure S3. High-resolution mass spectrum (ESI) of compound 2.

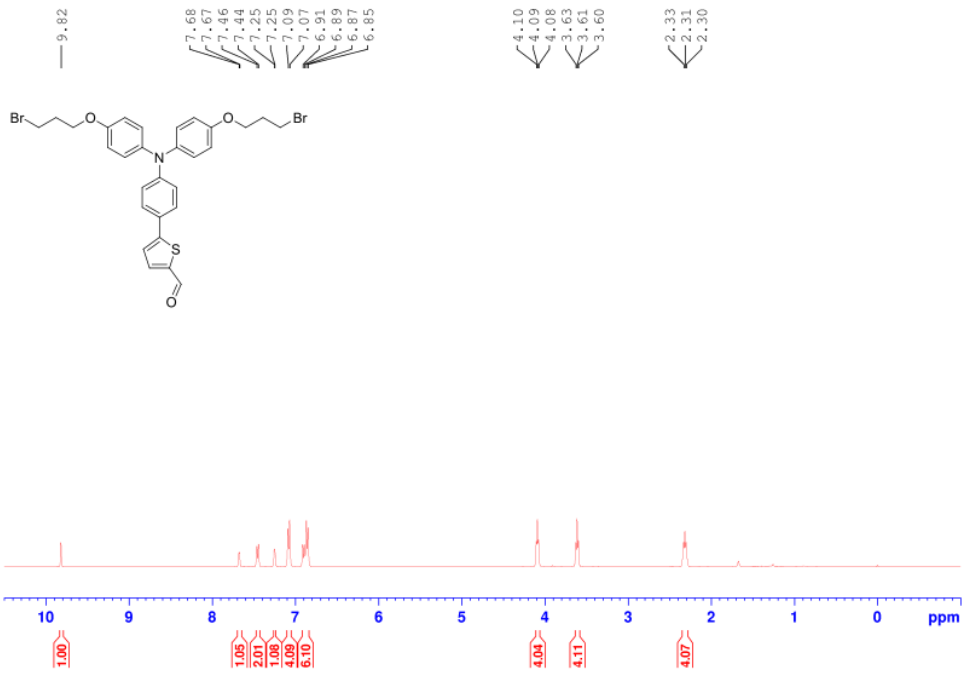

Figure S4. ^{1}H NMR spectrum (400 MHz, $CDCl_3$) of compound 3.

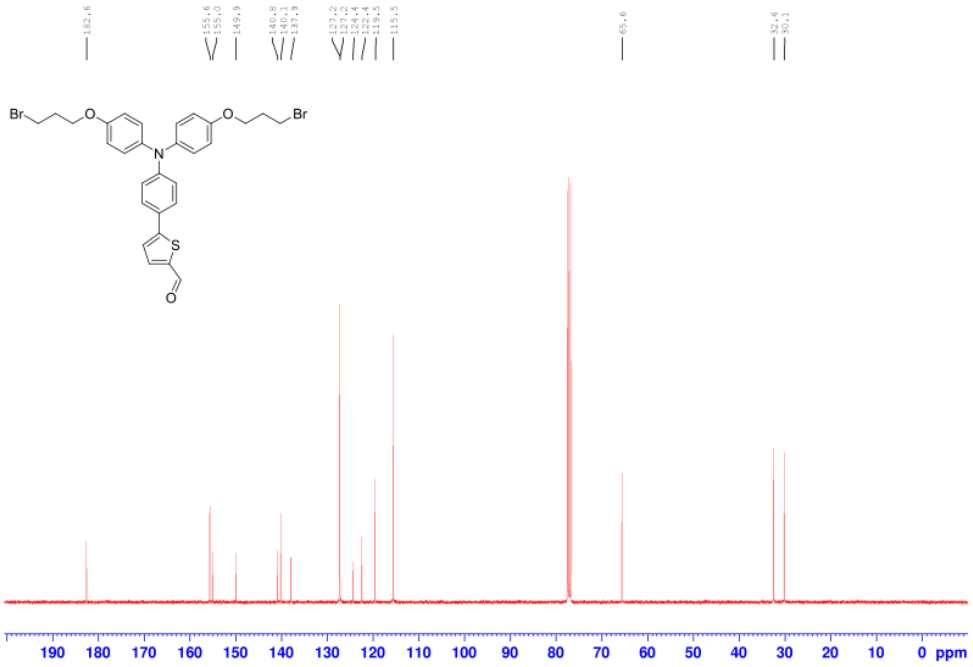

Figure S5. ^{13}C NMR spectrum (101 MHz, $CDCl_3$) of compound 3.

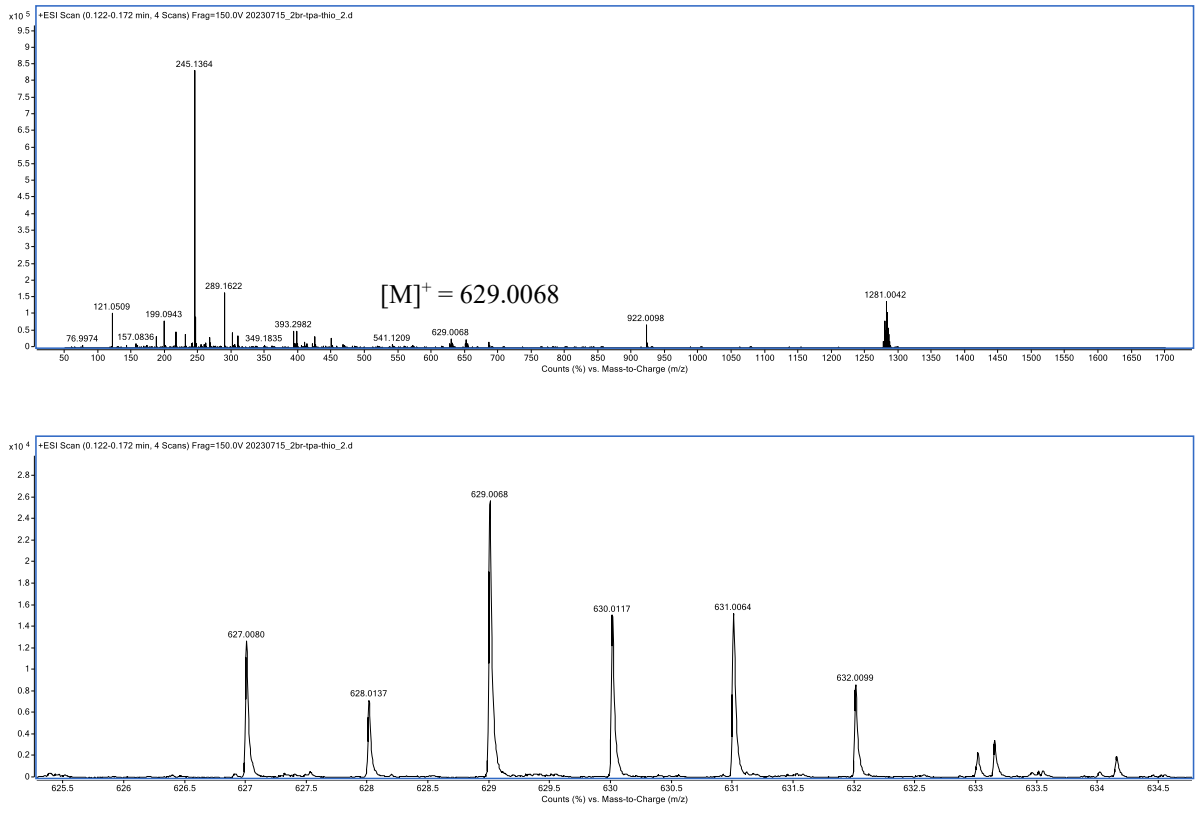

Figure S6. High-resolution mass spectrum (ESI) of compound 3.

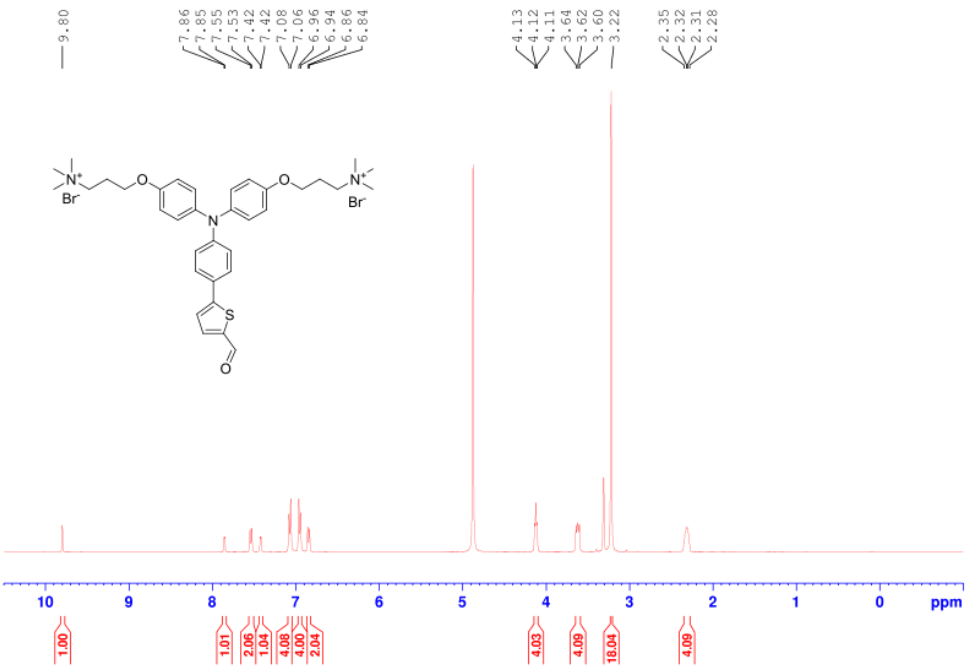

Figure S7. ^{1}H NMR spectrum (400 MHz, CD_3OD) of compound 4.

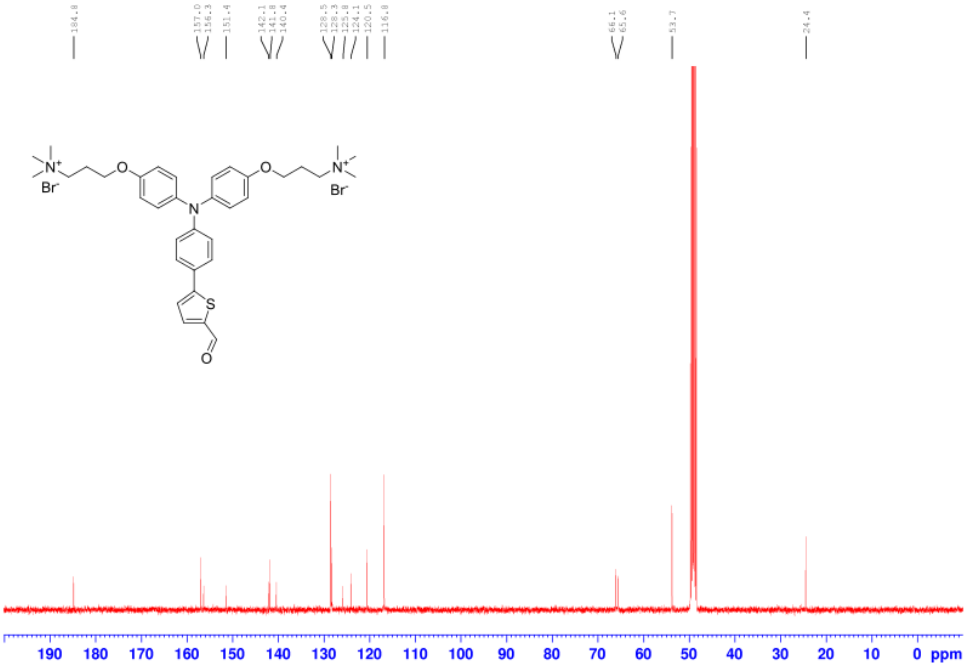

Figure S8. ^{13}C NMR spectrum (101 MHz, CD_3OD) of compound 4.

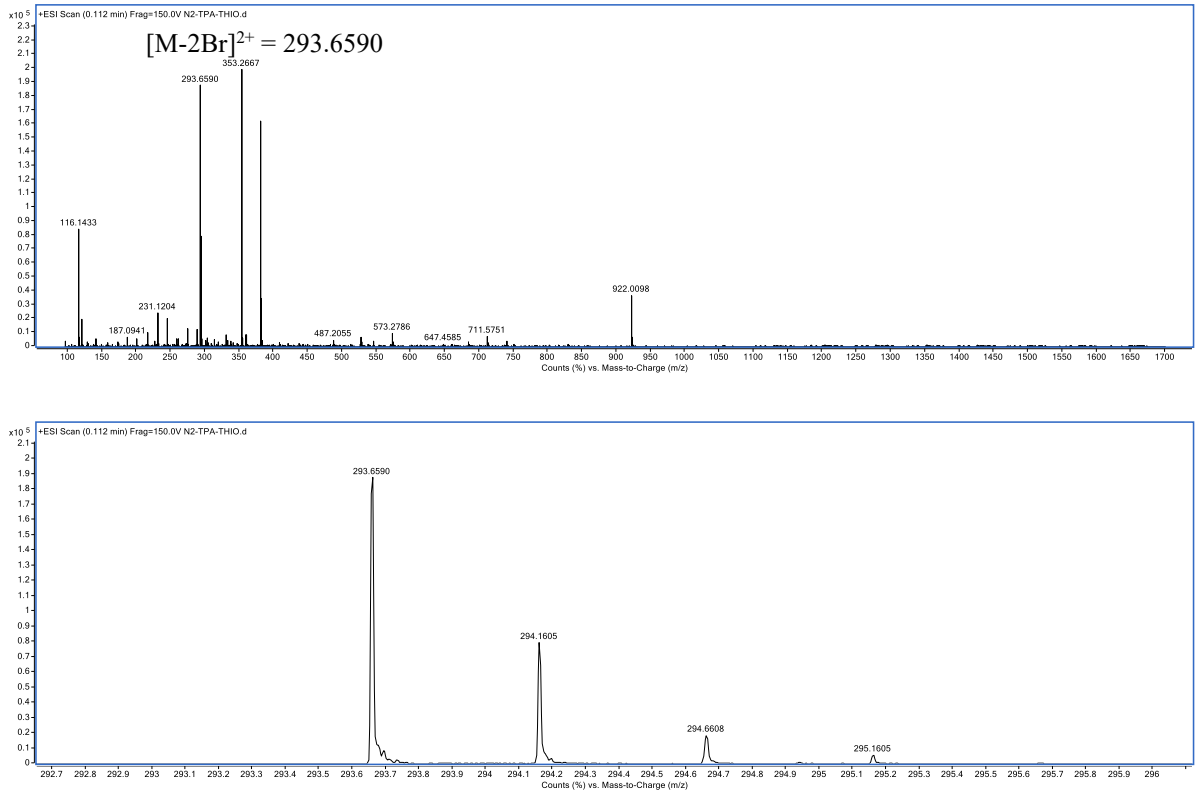

Figure S9. High-resolution mass spectrum (ESI) of compound 4.

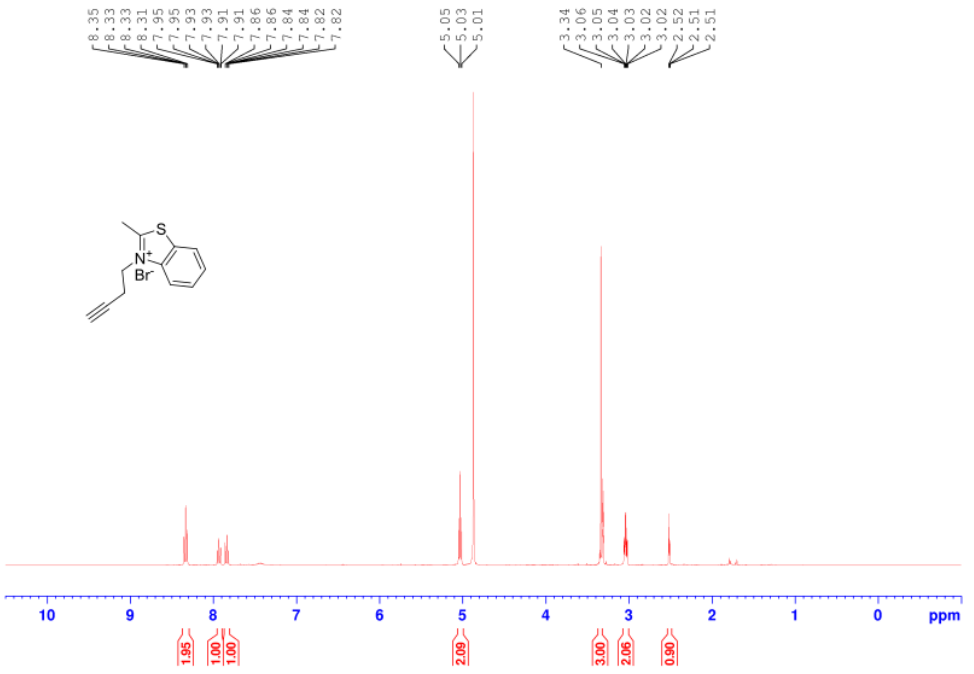

Figure S10. ^{1}H NMR spectrum (400 MHz, CD_3OD) of M1.

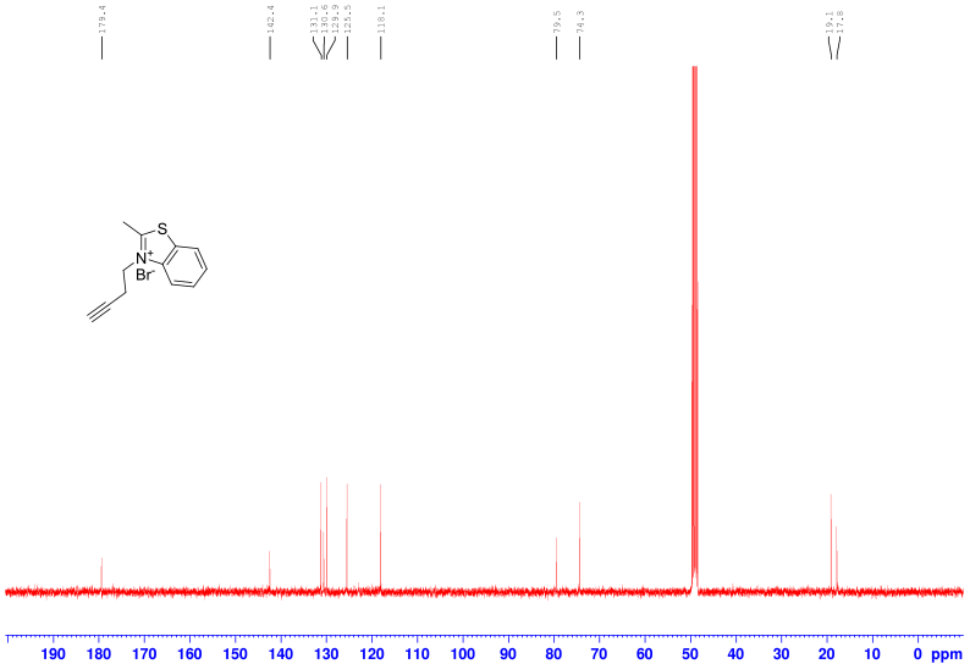

Figure S11. ^{13}C NMR spectrum (101 MHz, CD_3OD) of compound M1.

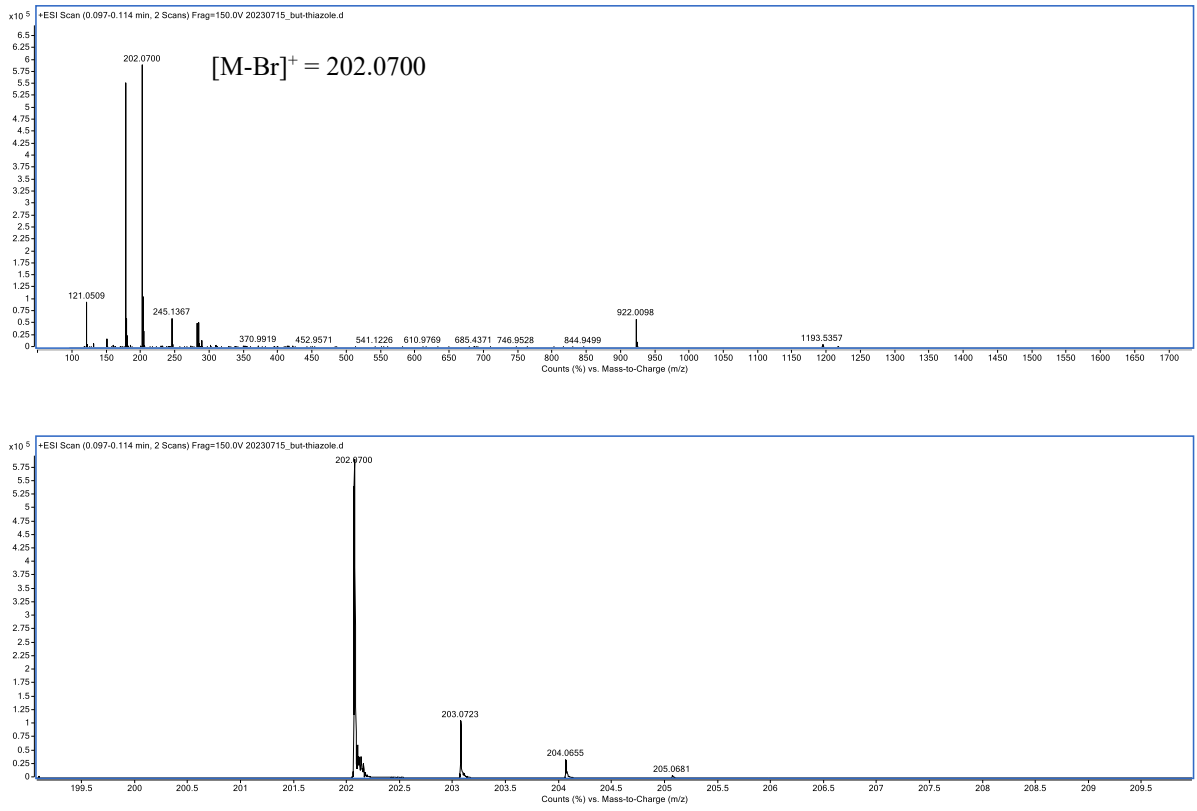

Figure S12. High-resolution mass spectrum (ESI) of compound M1

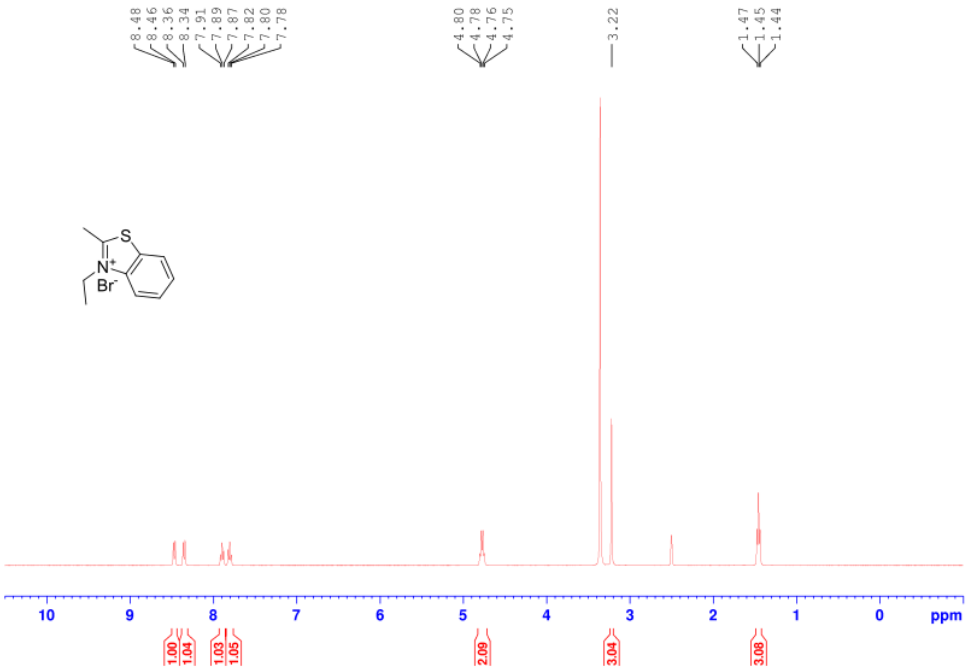

Figure S13. ^{1}H NMR spectrum (400 MHz, DMSO-d_6) of M2.

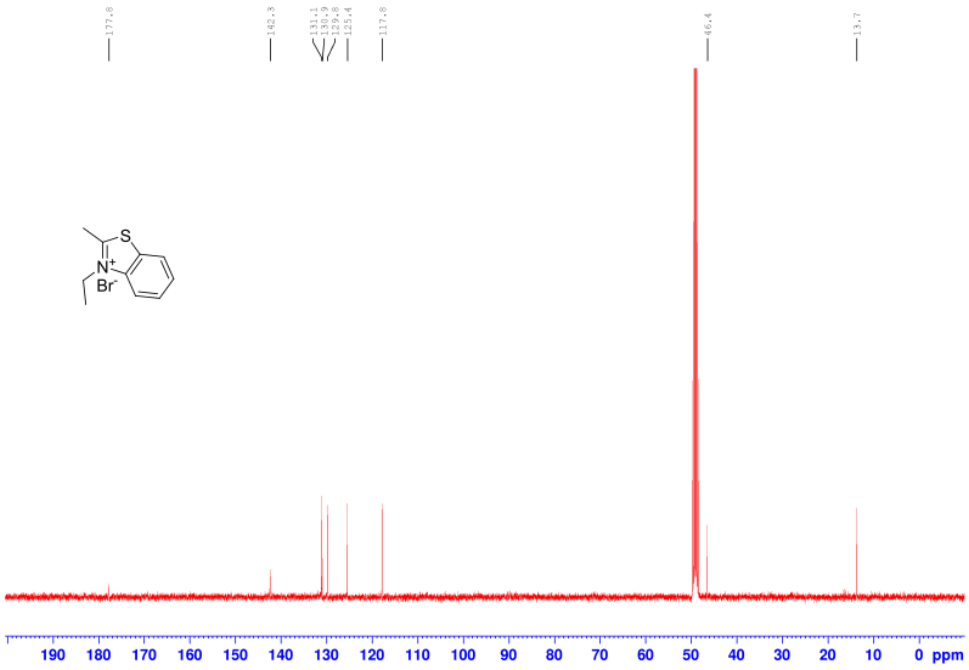

Figure S14. ^{13}C NMR spectrum (101 MHz, CD_3OD) of M2.

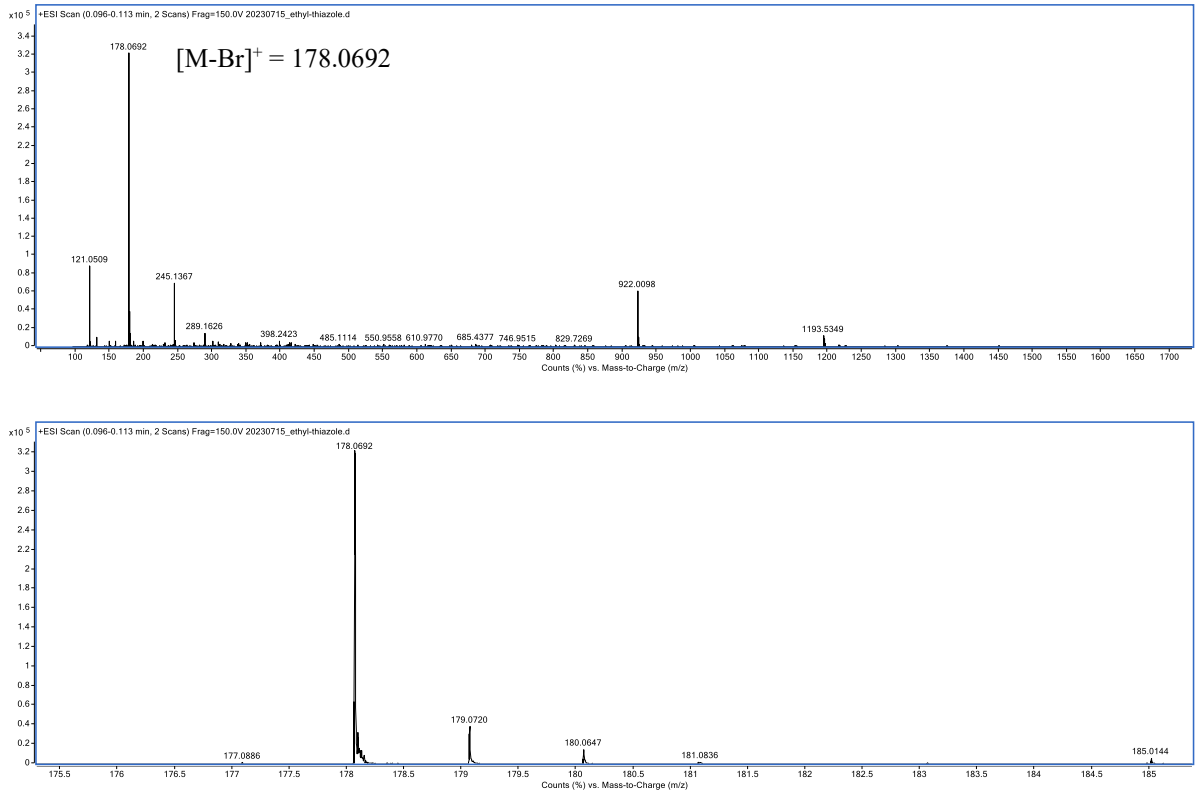

Figure S15. High-resolution mass spectrum (ESI) of M2.

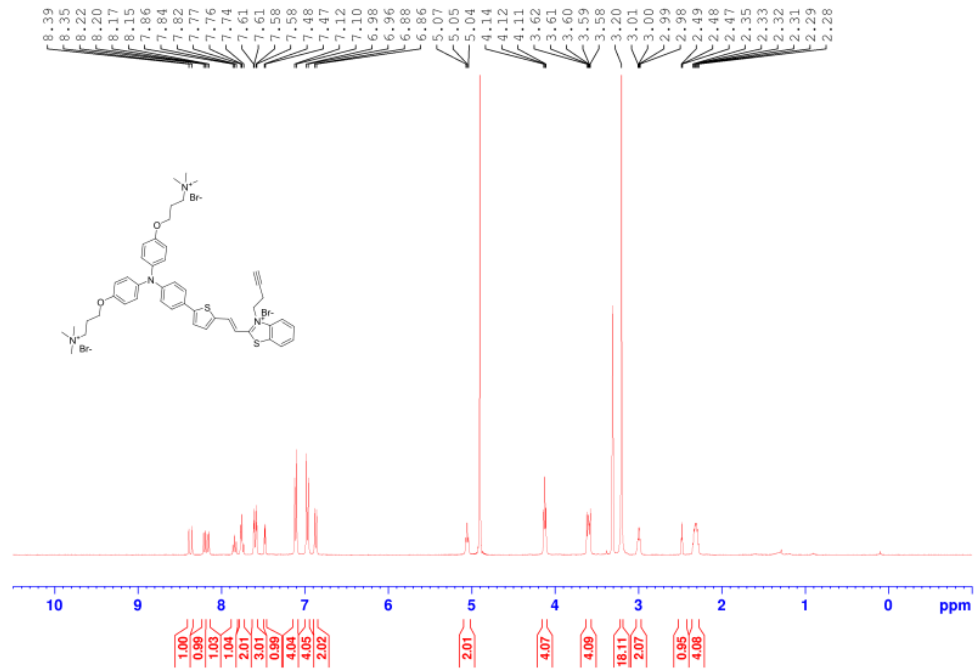

Figure S16. ^{1}H NMR spectrum (400 MHz, CD_3OD) of TPA-1.

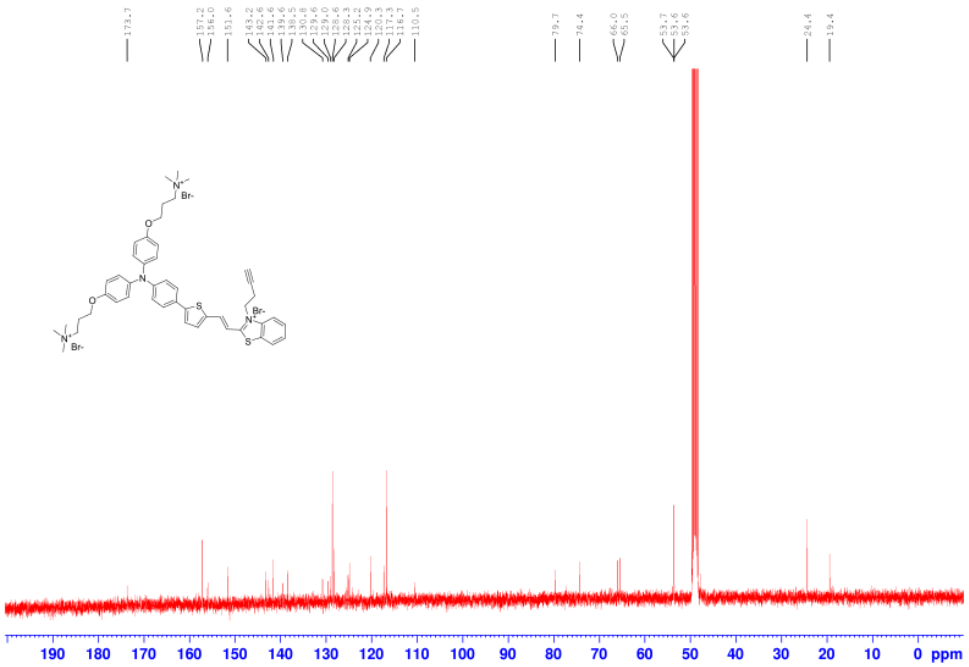

Figure S17. ^{13}C NMR spectrum (101 MHz, CD_3OD) of TPA-1.

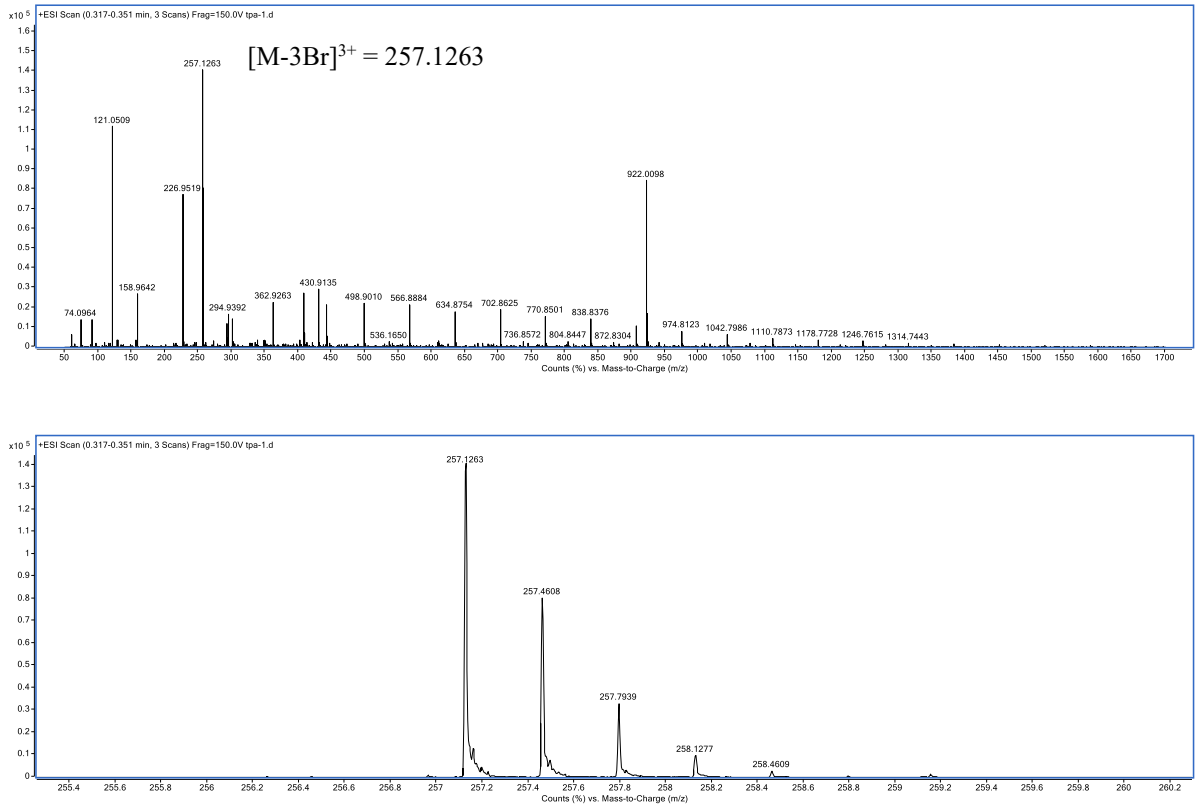

Figure S18. High-resolution mass spectrum (ESI) of TPA-1.

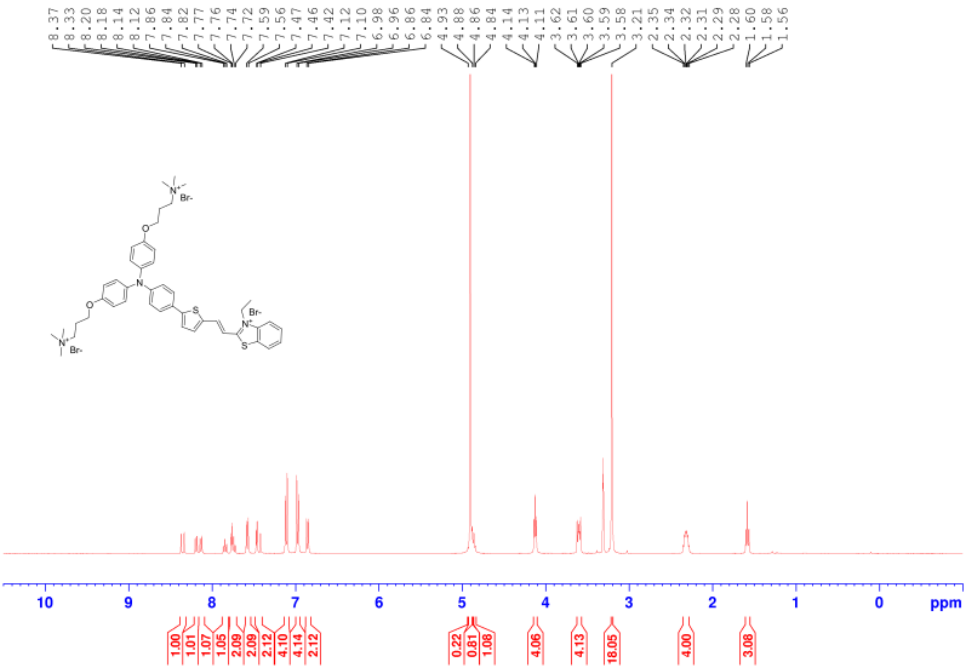

Figure S19. ^{1}H NMR spectrum (400 MHz, CD_3OD) of TPA-0.

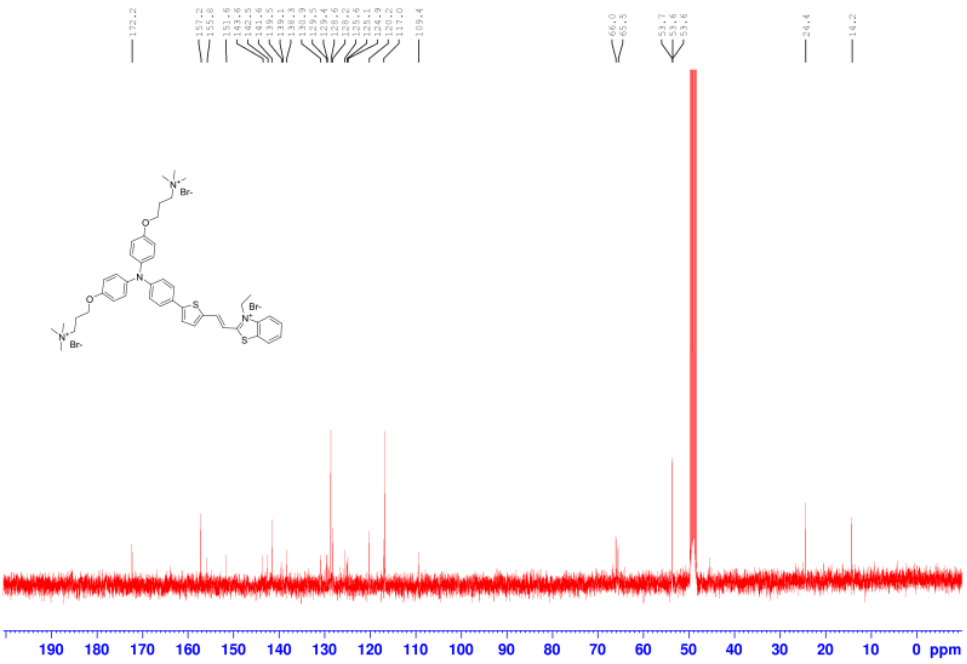

Figure S20. ^{13}C NMR spectrum (101 MHz, CD_3OD) of TPA-0.

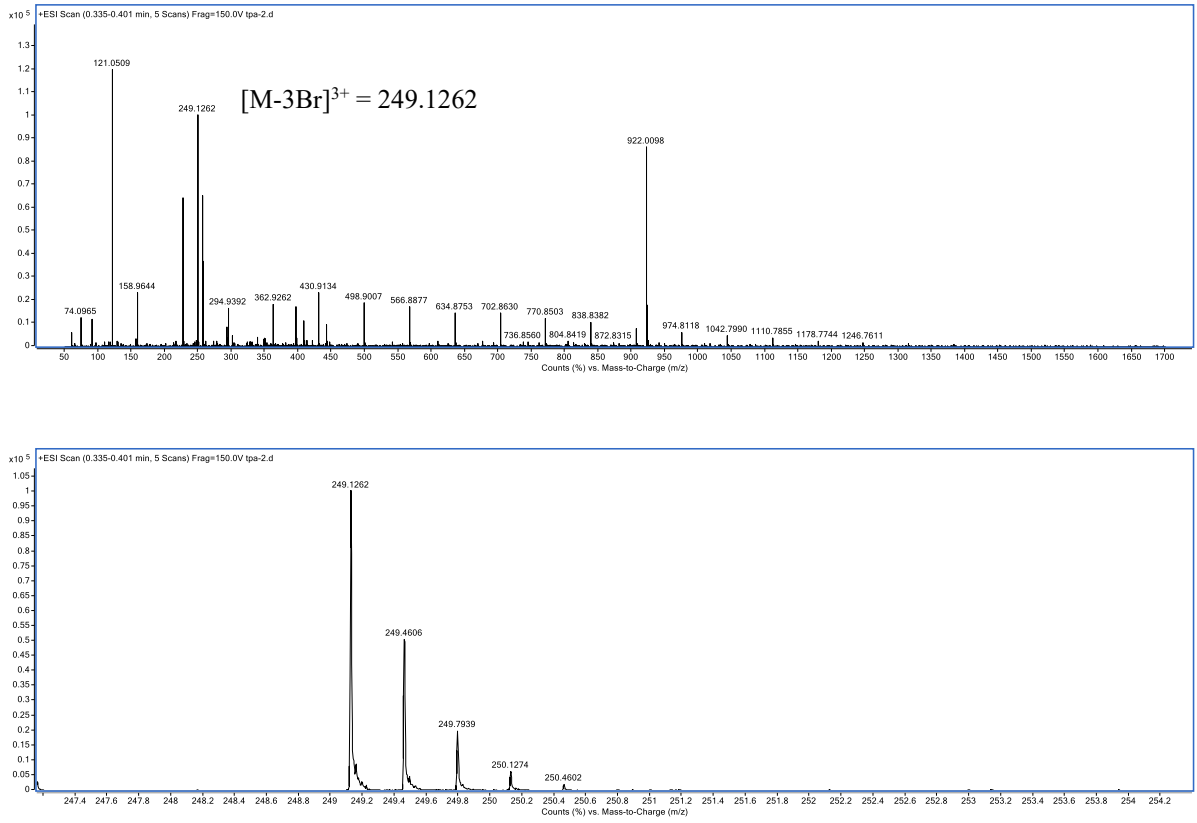

Figure S21. High-resolution mass spectrum (ESI) of TPA-0.

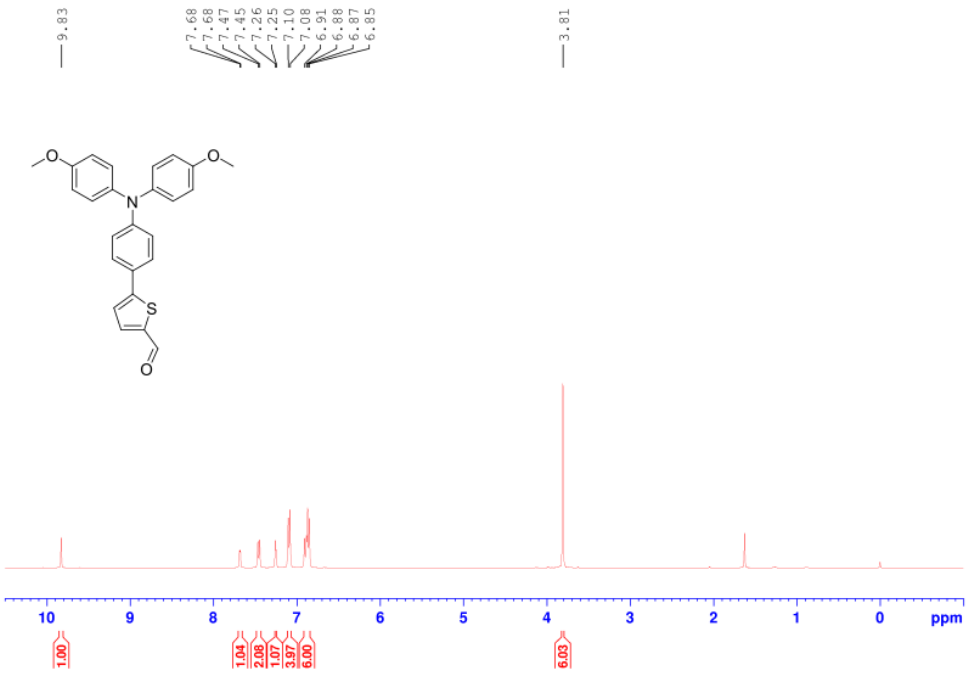

Figure S22. ^{1}H NMR spectrum (400 MHz, $CDCl_3$) of Compound 5.

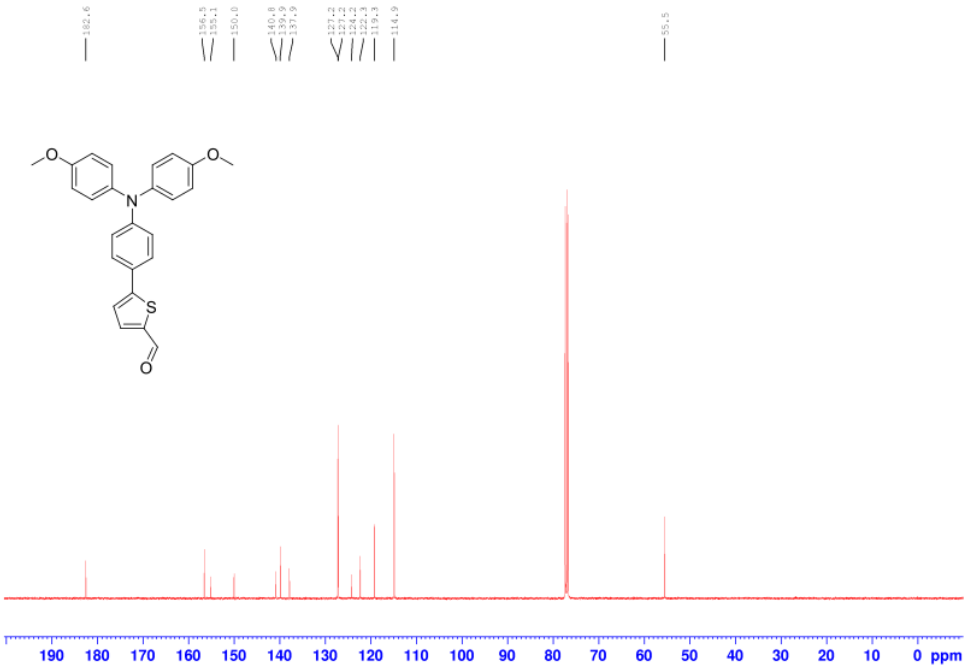

Figure S23. ^{13}C NMR spectrum (101 MHz, $CDCl_3$) of Compound 5.

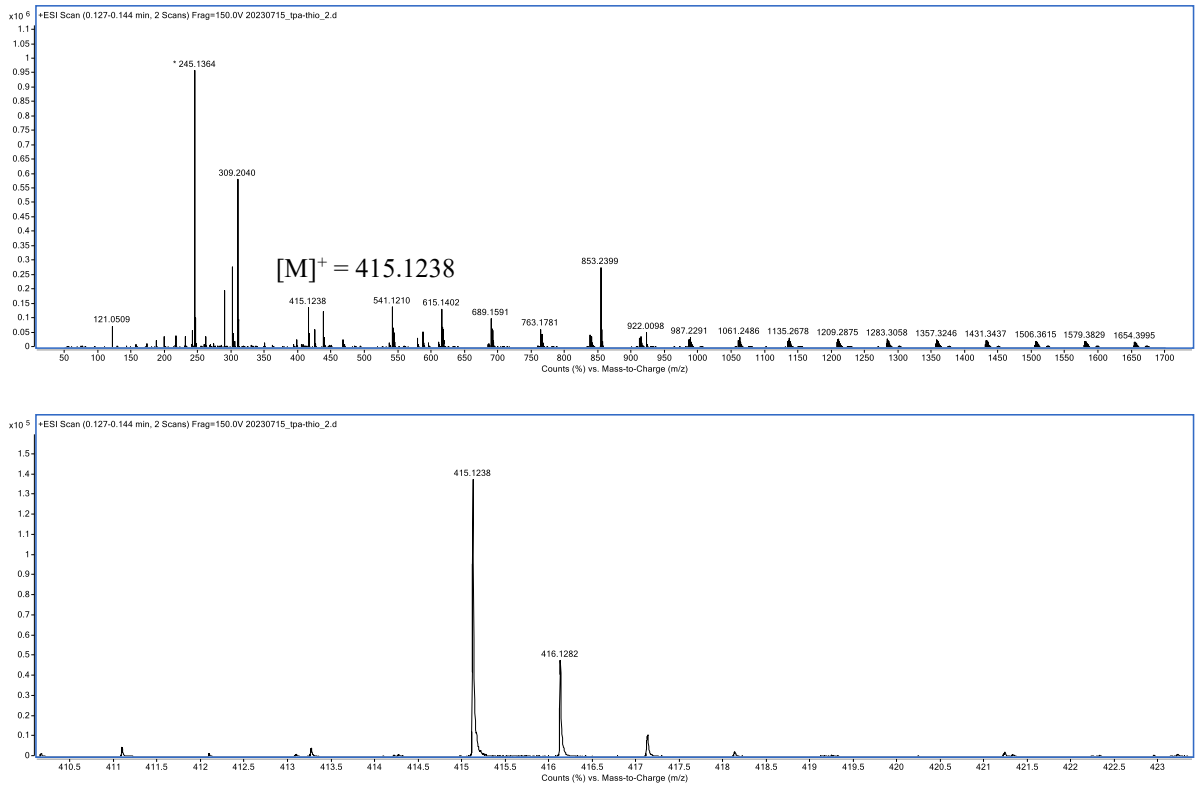

Figure S24. High-resolution mass spectrum (ESI) of Compound 5.

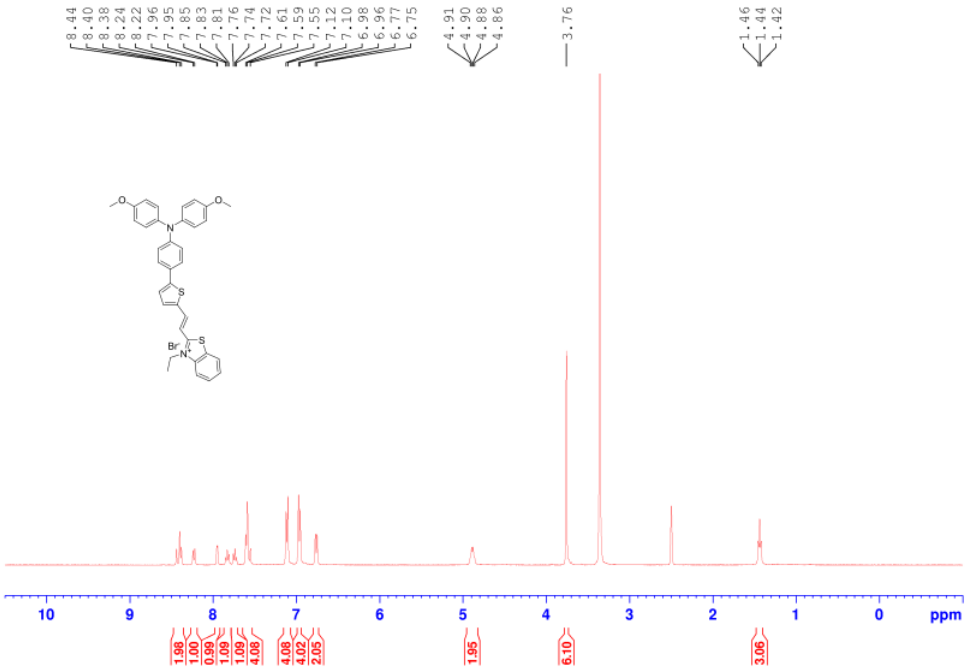

Figure S25. ^{1}H NMR spectrum (400 MHz, DMSO-d_6) of TPA-NC-1.

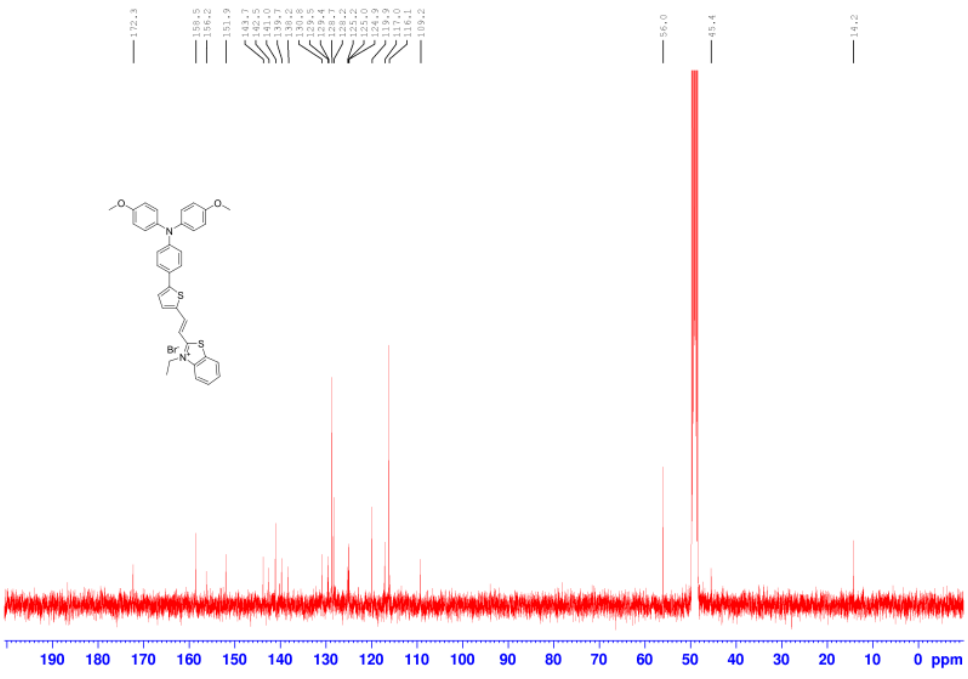

Figure S26. ^{13}C NMR spectrum (101 MHz, CD_3OD) of TPA-NC-1.

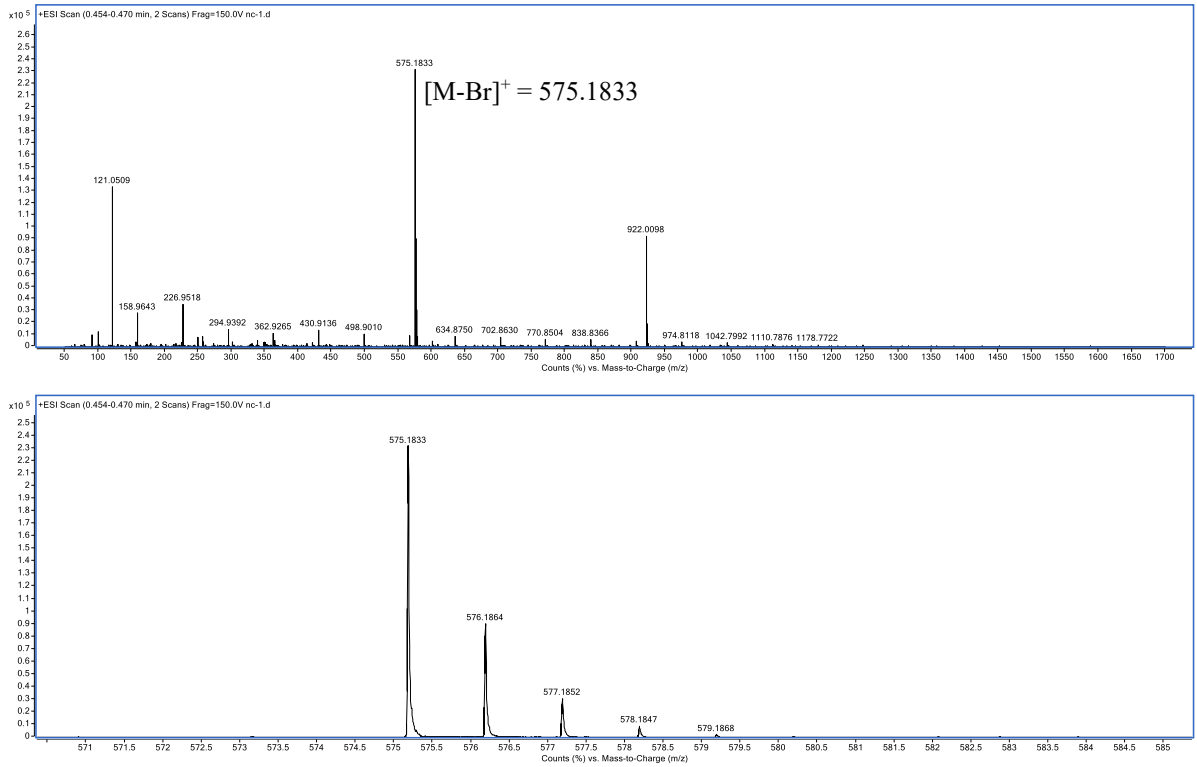

Figure S27. High-resolution mass spectrum (ESI) of TPA-NC-1.

2. Characterizations for compounds synthesized in Chapter IV

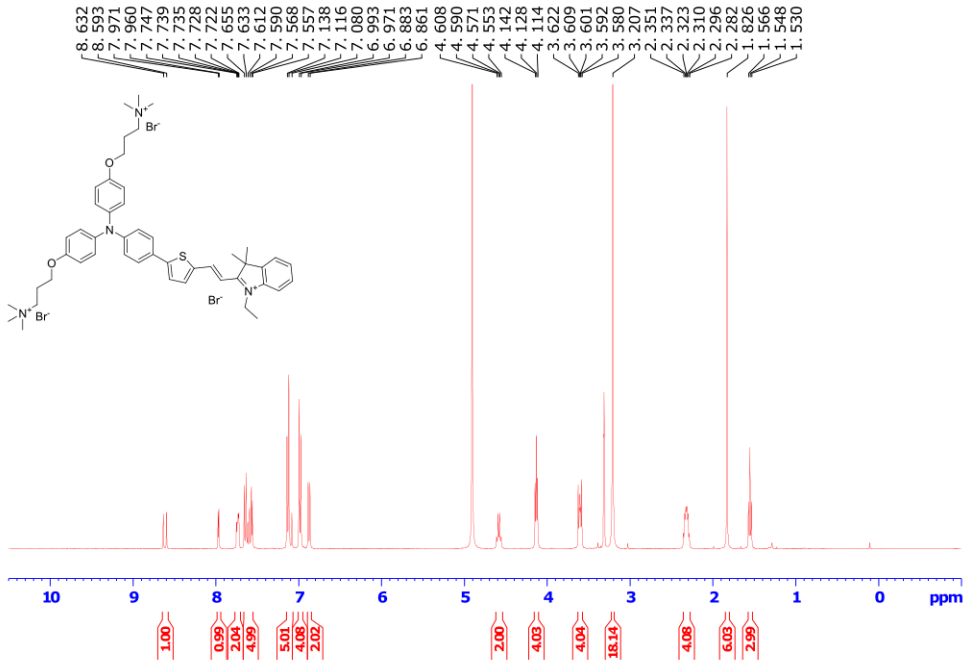

Figure S28. ^{1}H NMR spectrum (400 MHz, CD_3OD) of TPA-IN.

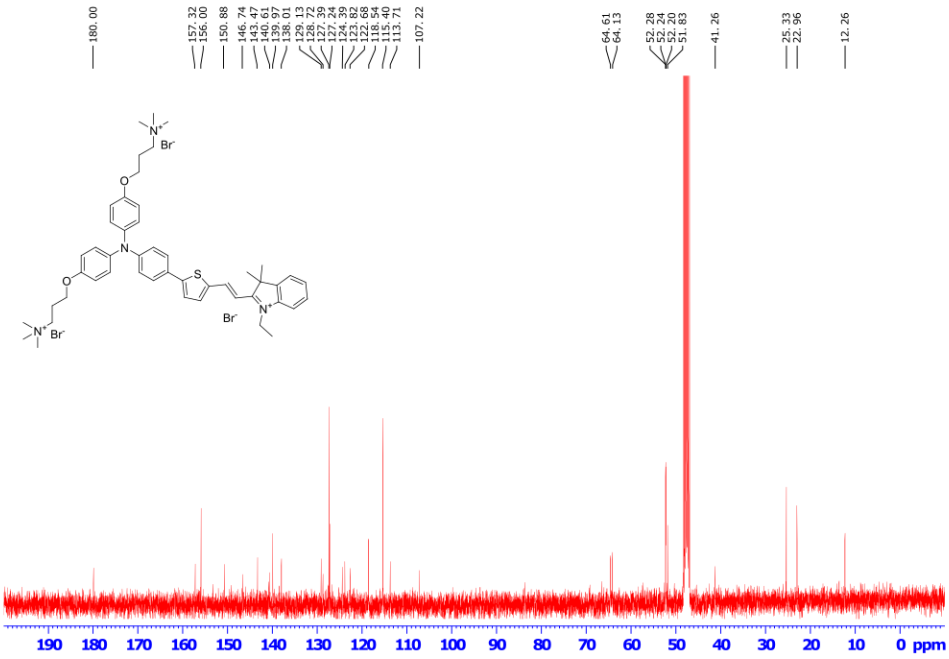

Figure S29. ^{13}C NMR spectrum (101 MHz, CD_3OD) of TPA-IN.

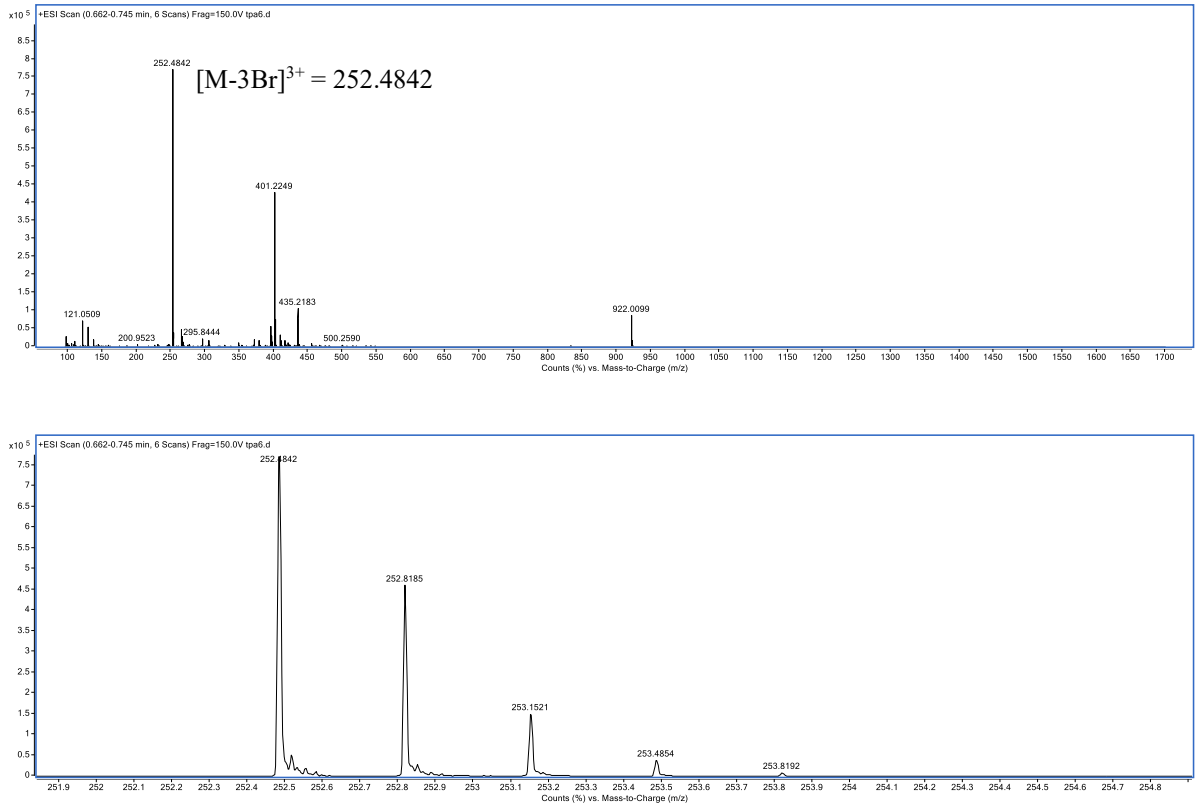

Figure S30. High-resolution mass spectrum (ESI) of TPA-IN.

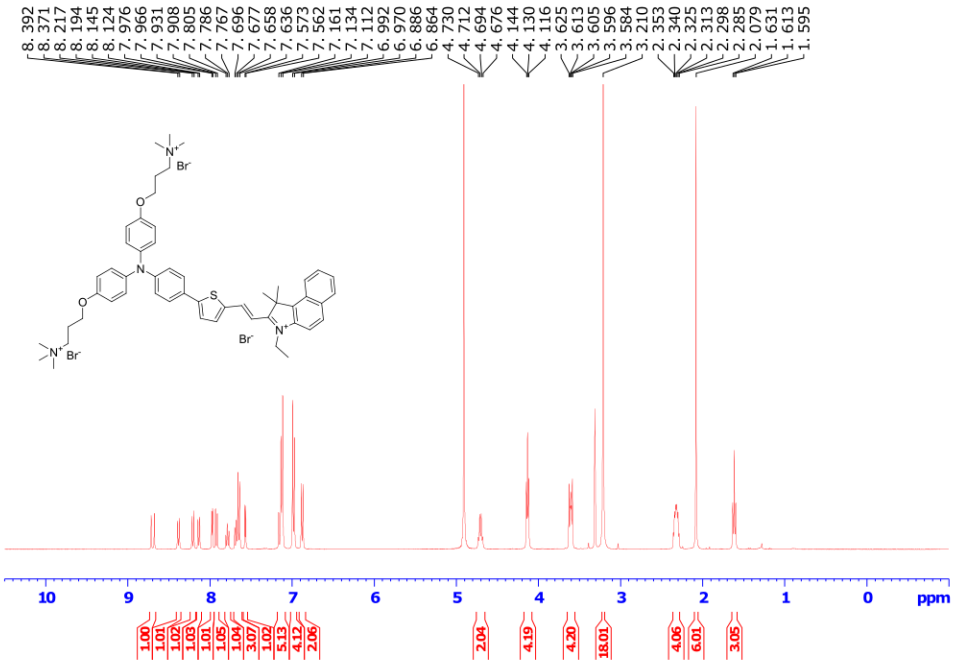

Figure S31. ^{1}H NMR spectrum (400 MHz, CD_3OD) of TPA-BIN.

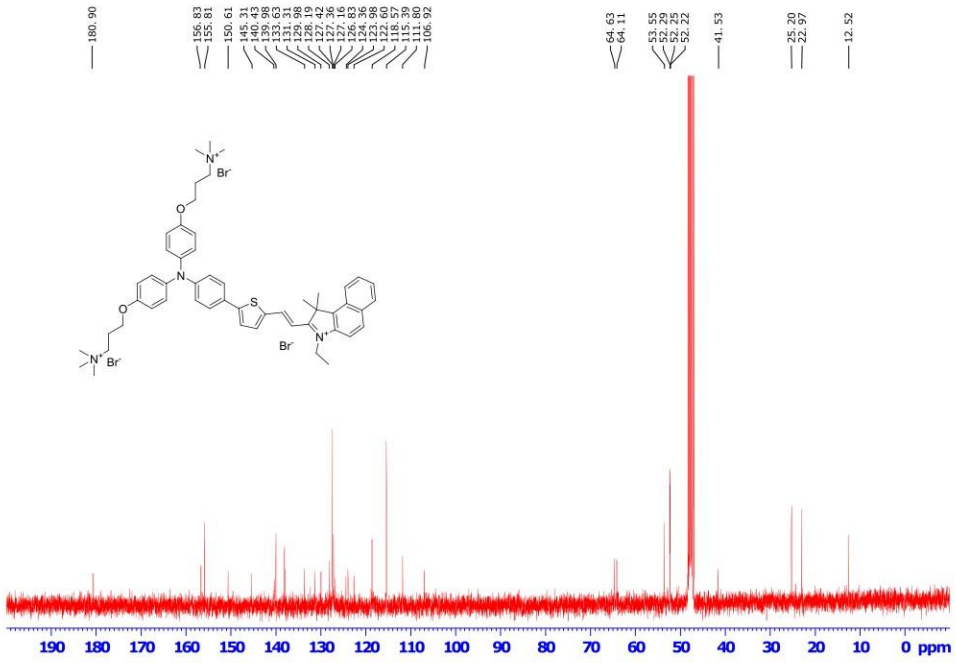

Figure S32. ^{13}C NMR spectrum (101 MHz, CD_3OD) of TPA-BIN.

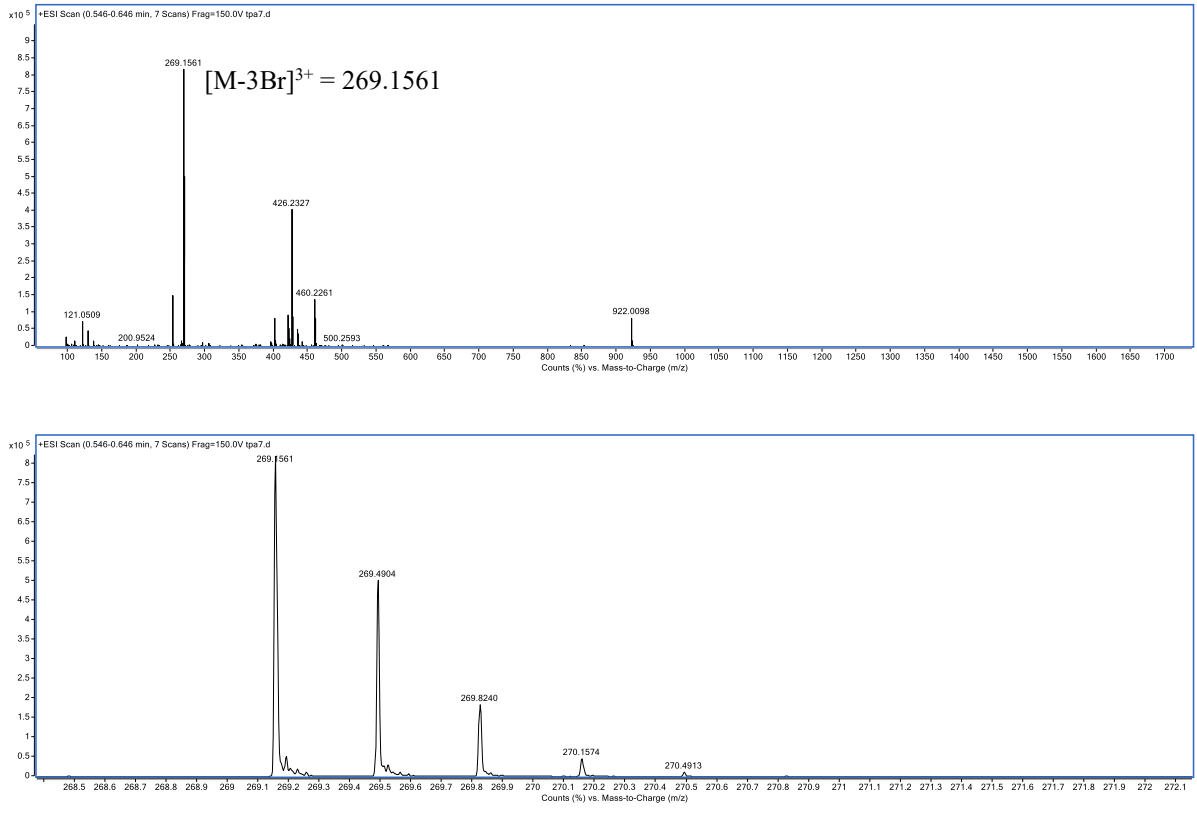

Figure S33. High-resolution mass spectrum (ESI) of TPA-BIN.

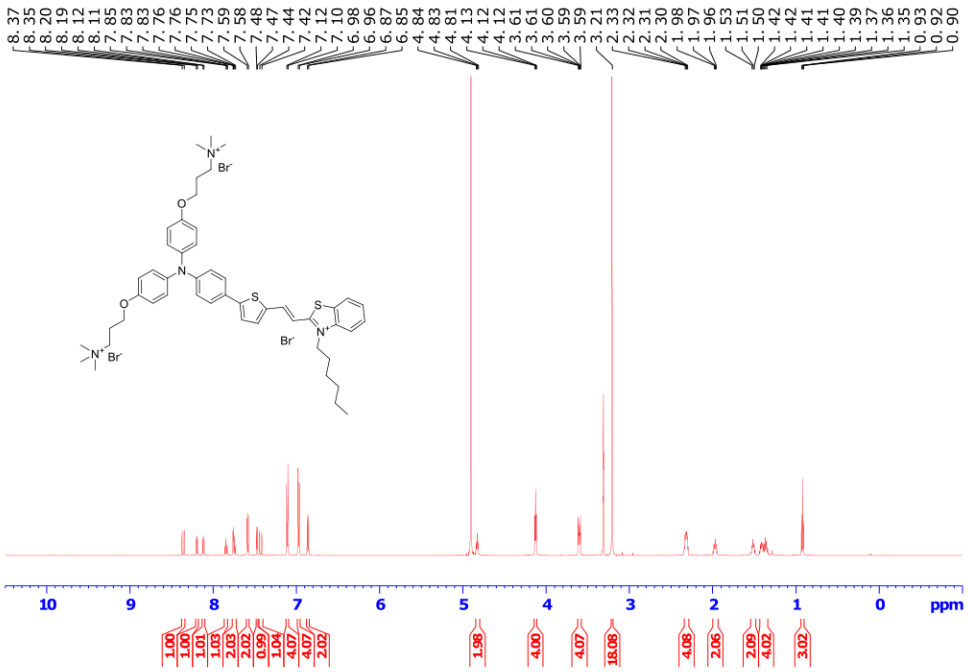

Figure S34. ^{1}H NMR spectrum (600 MHz, CD_3OD) of TPA-C3-C6.

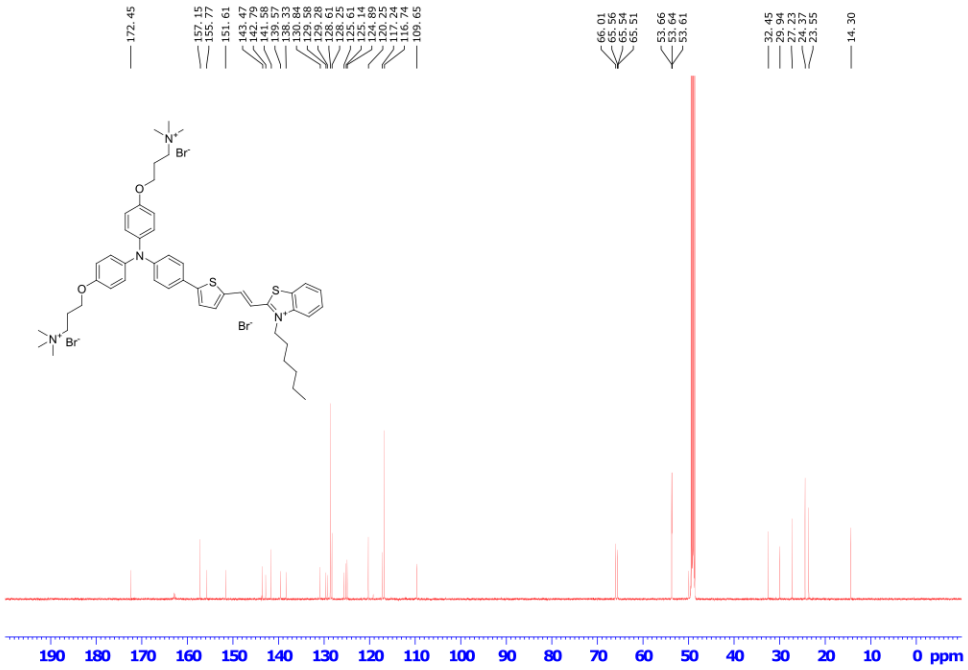

Figure S35. ^{13}C NMR spectrum (151 MHz, CD_3OD) of TPA-C3-C6.

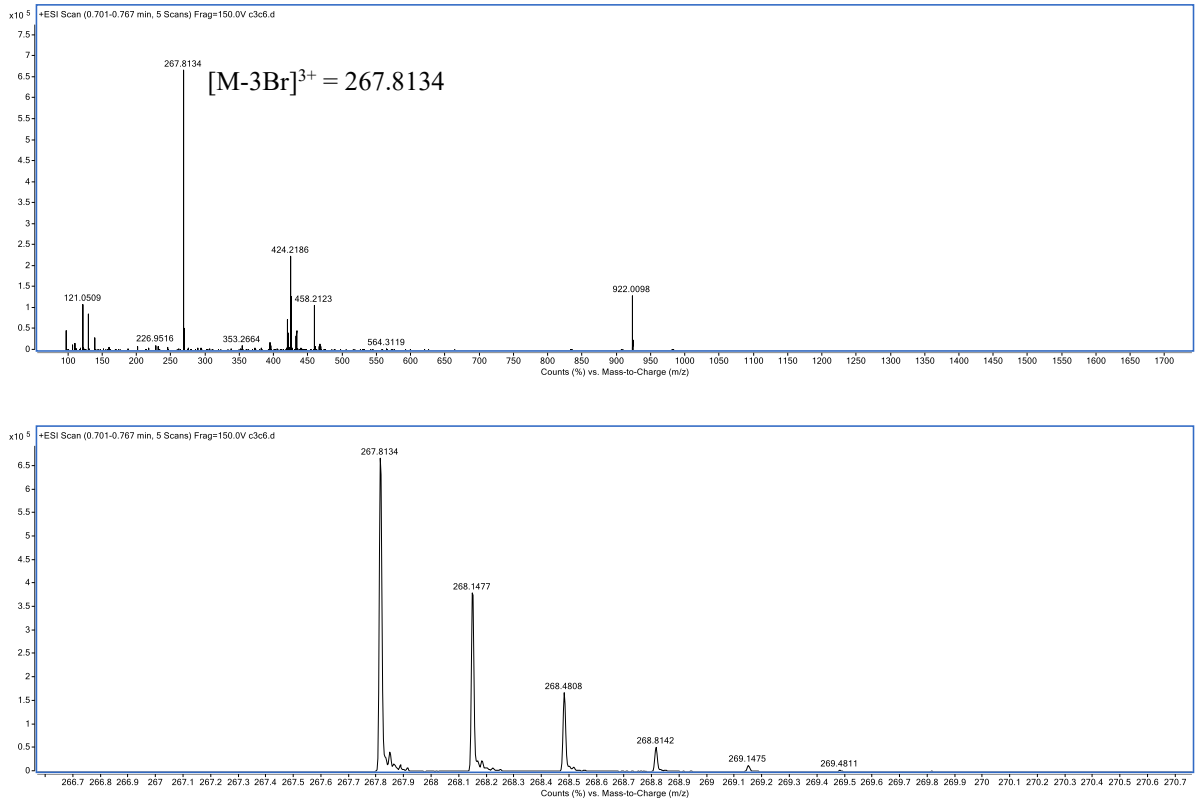

Figure S36. High-resolution mass spectrum (ESI) of TPA-C3-C6.

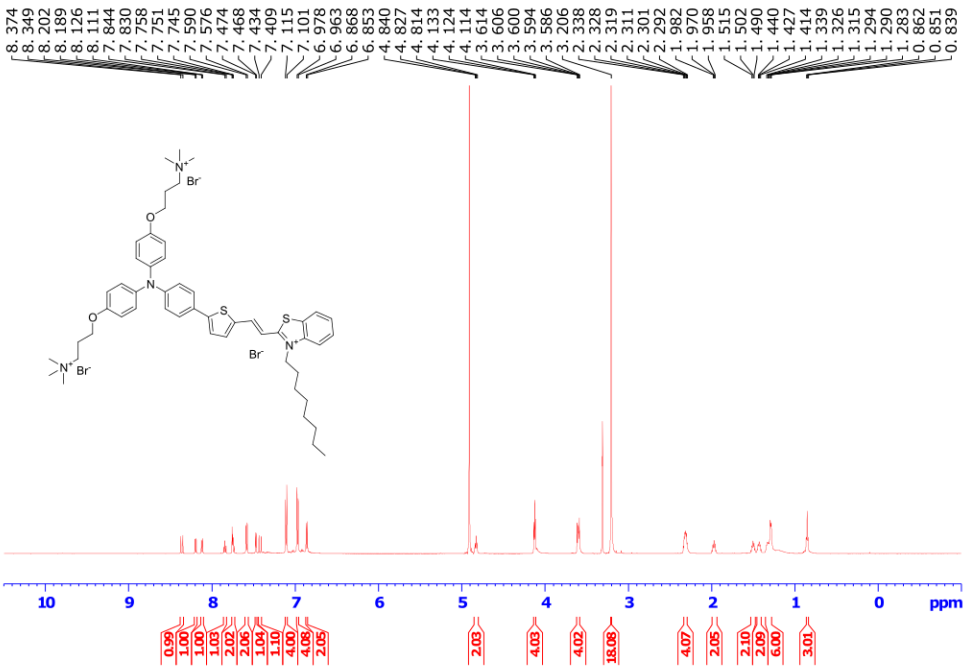

Figure S37. ^{1}H NMR spectrum (600 MHz, CD_3OD) of TPA-C3-C8.

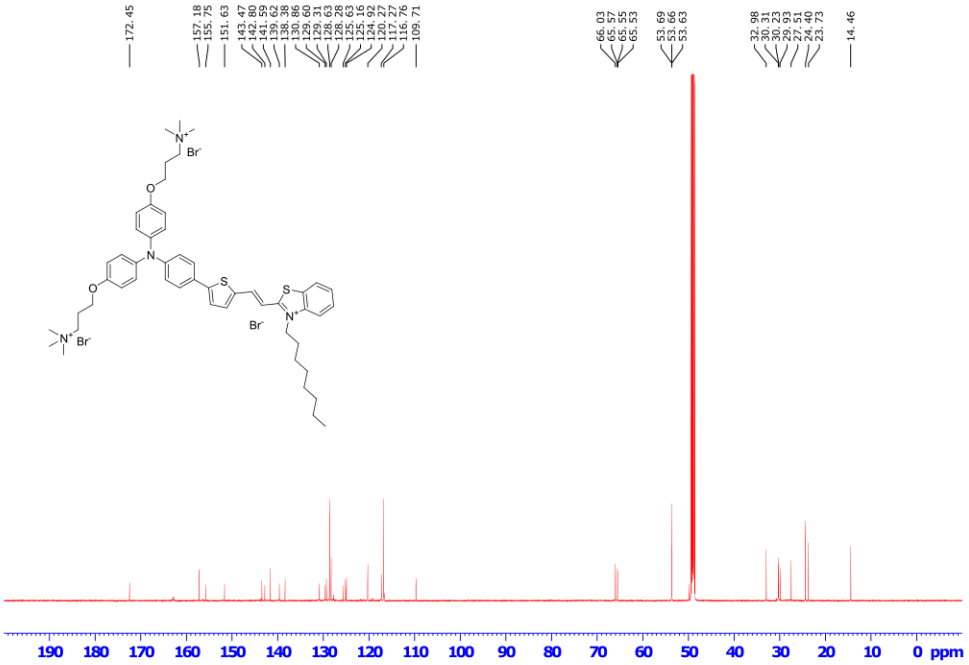

Figure S38. ^{13}C NMR spectrum (151 MHz, CD_3OD) of TPA-C3-C8.

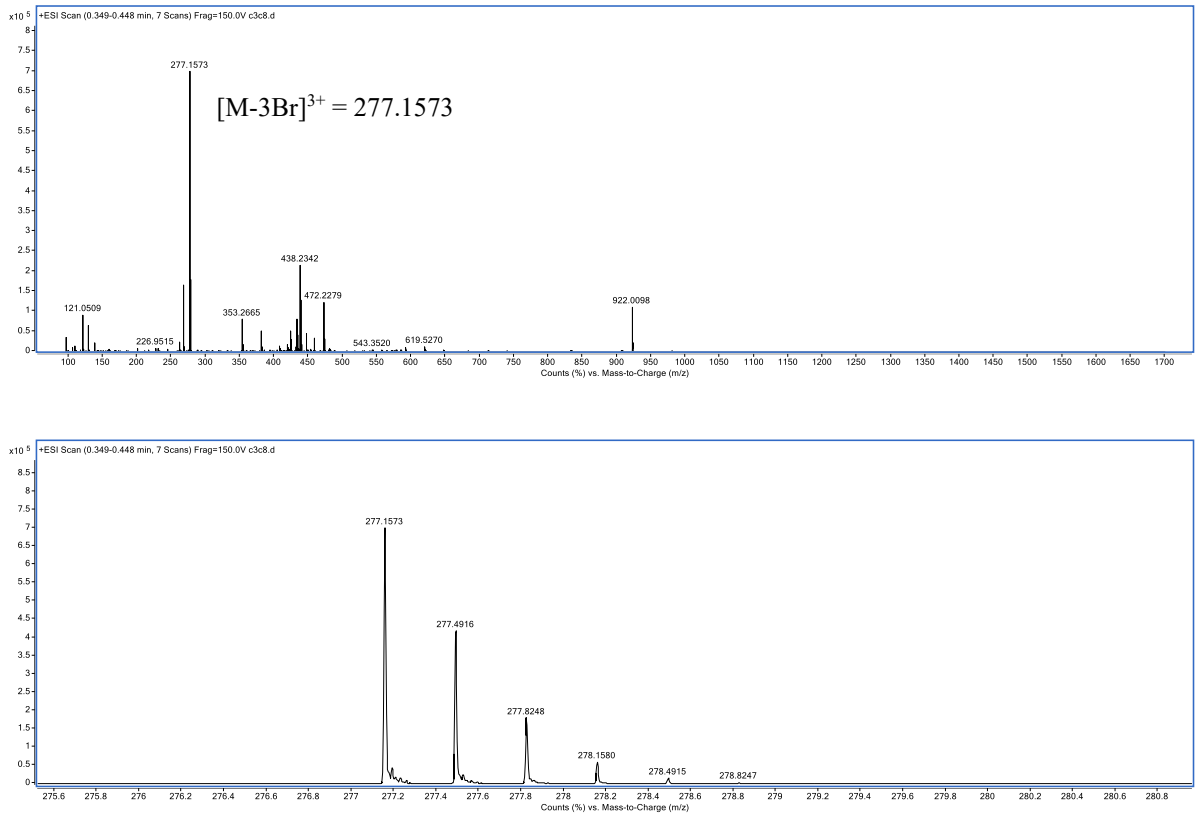

Figure S39. High-resolution mass spectrum (ESI) of TPA-C3-C8.

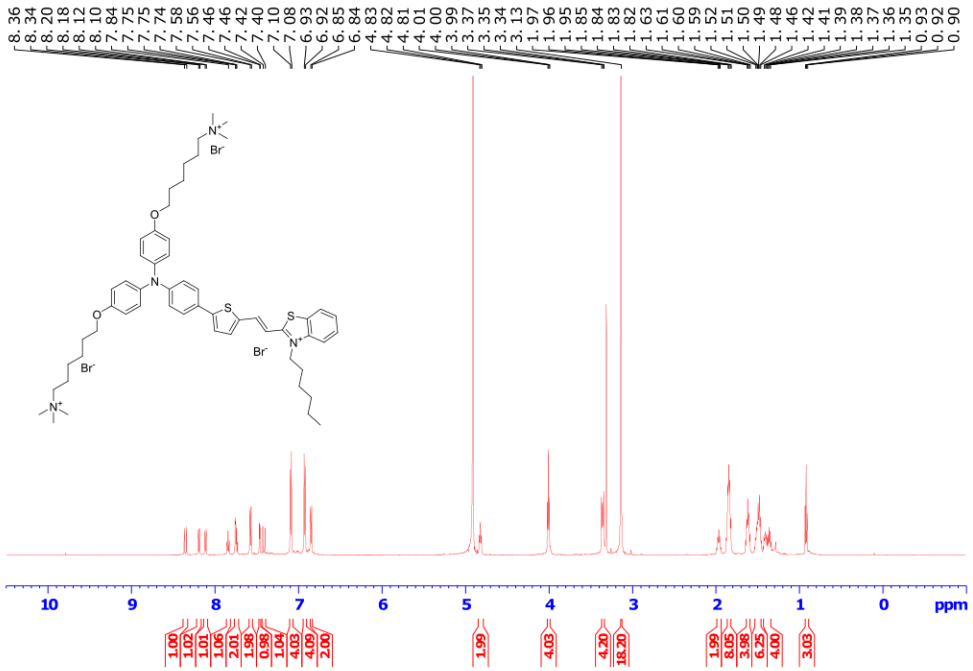

Figure S40. ^{1}H NMR spectrum (600 MHz, CD_3OD) of TPA-C6-C6.

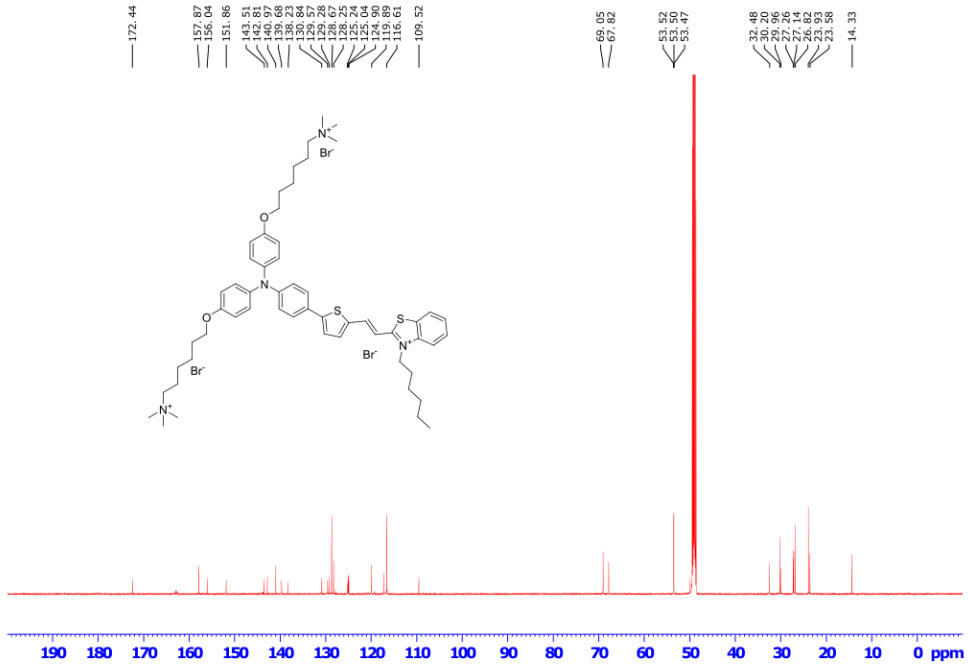

Figure S41. ^{13}C NMR spectrum (151 MHz, CD_3OD) of TPA-C6-C6.

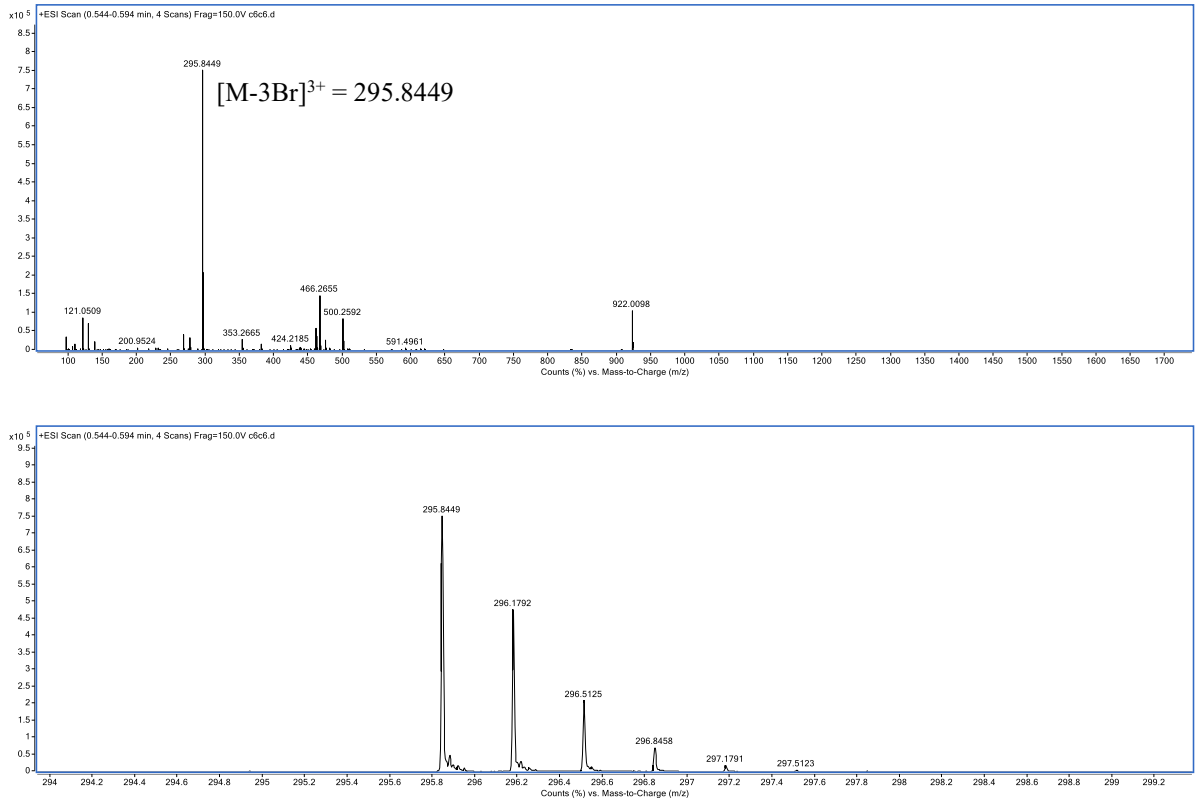

Figure S42. High-resolution mass spectrum (ESI) of TPA-C6-C6.

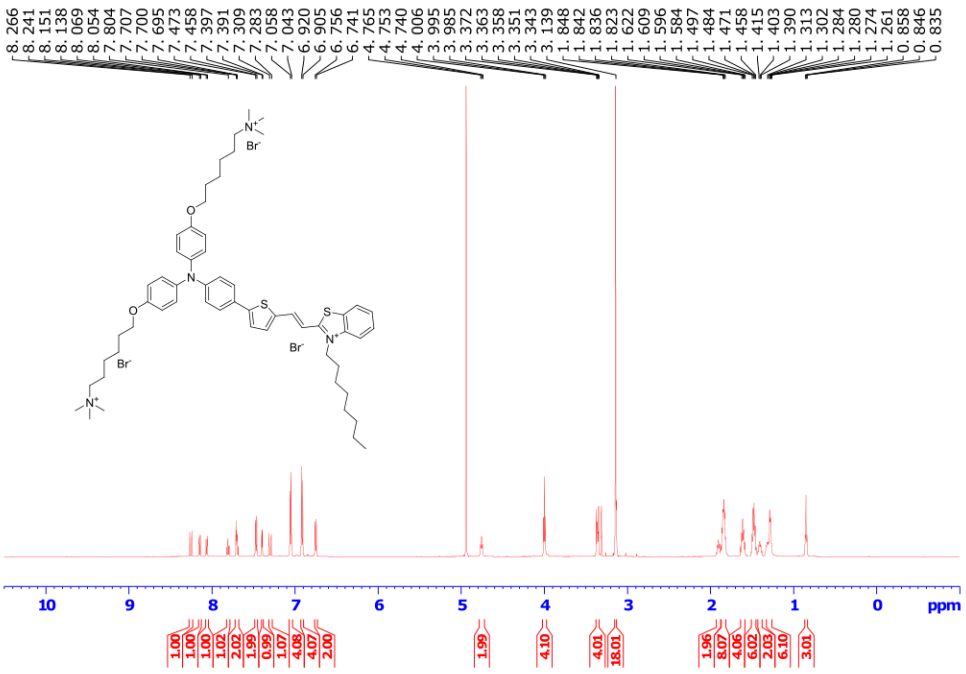

Figure S43. ^{1}H NMR spectrum (600 MHz, CD_3OD) of TPA-C6-C8.

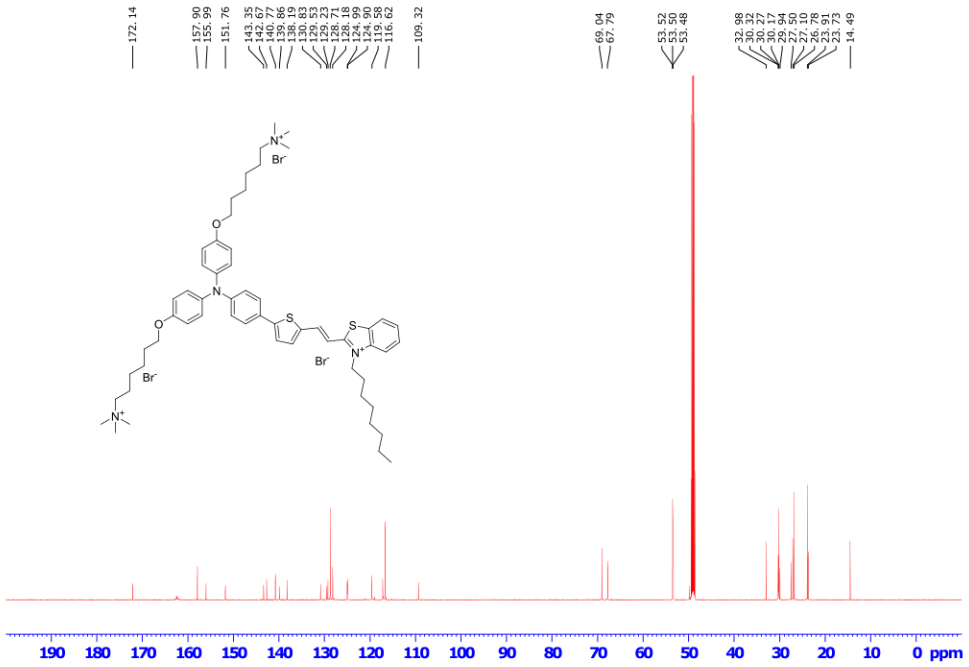

Figure S44. ^{13}C NMR spectrum (151 MHz, CD_3OD) of TPA-C6-C8.

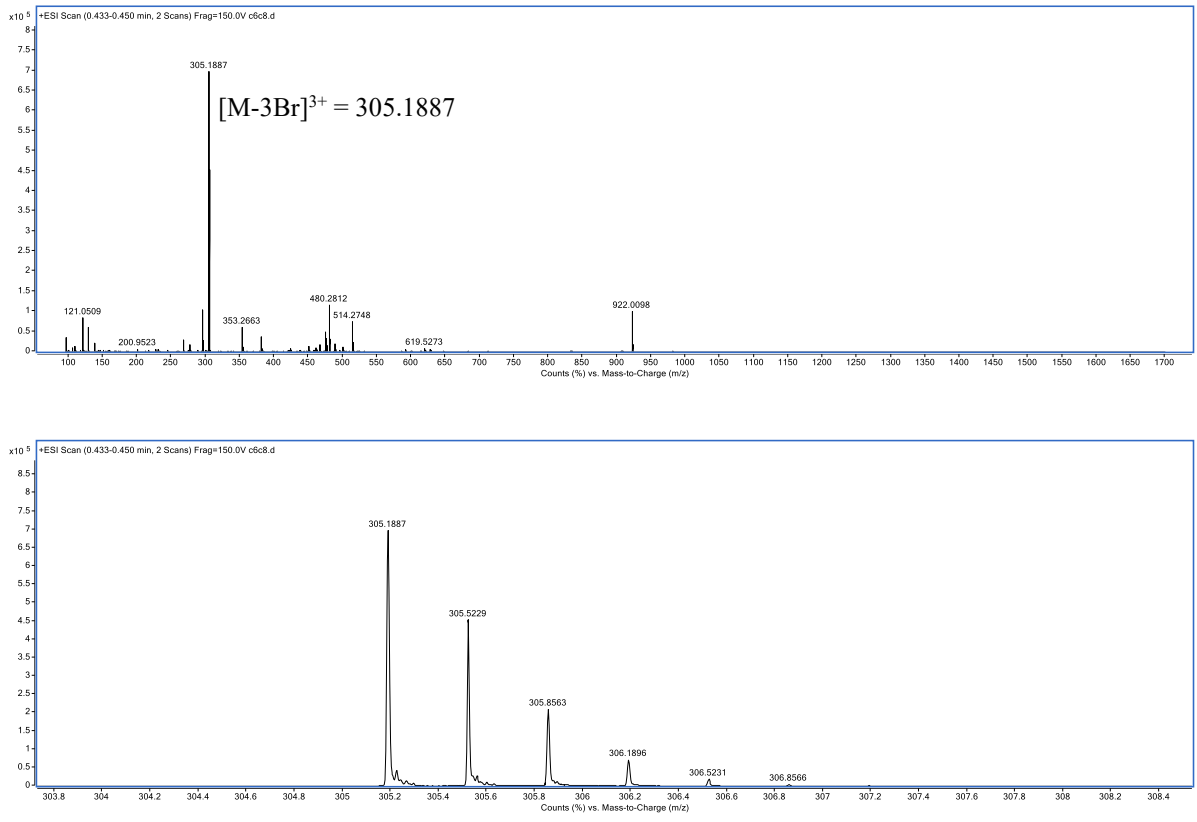

Figure S45. High-resolution mass spectrum (ESI) of TPA-C6-C8.

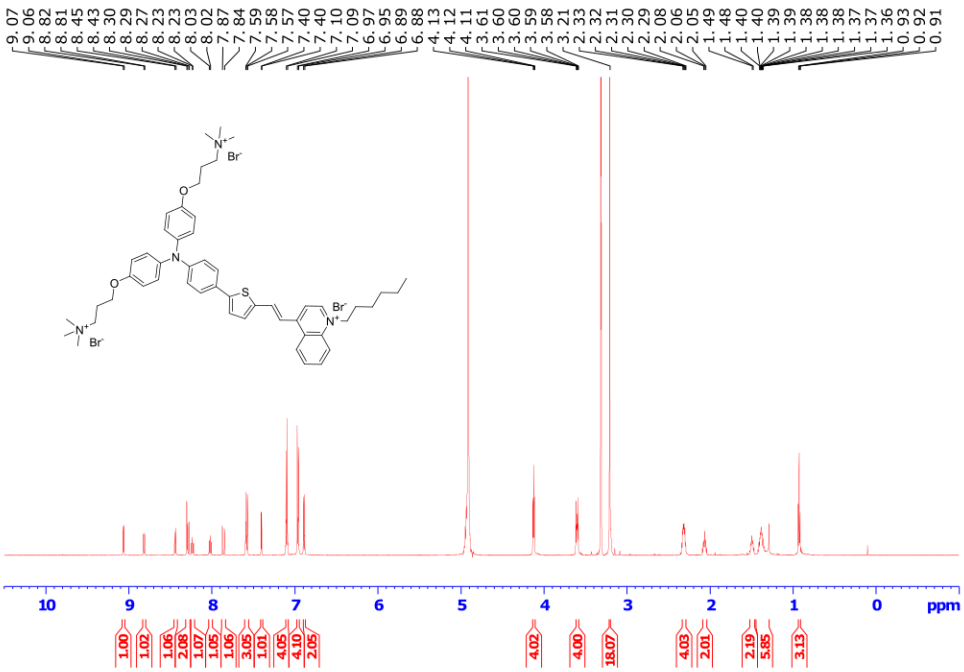

Figure S46. ^{1}H NMR spectrum (600 MHz, CD_3OD) of TPA-C3-C6P.

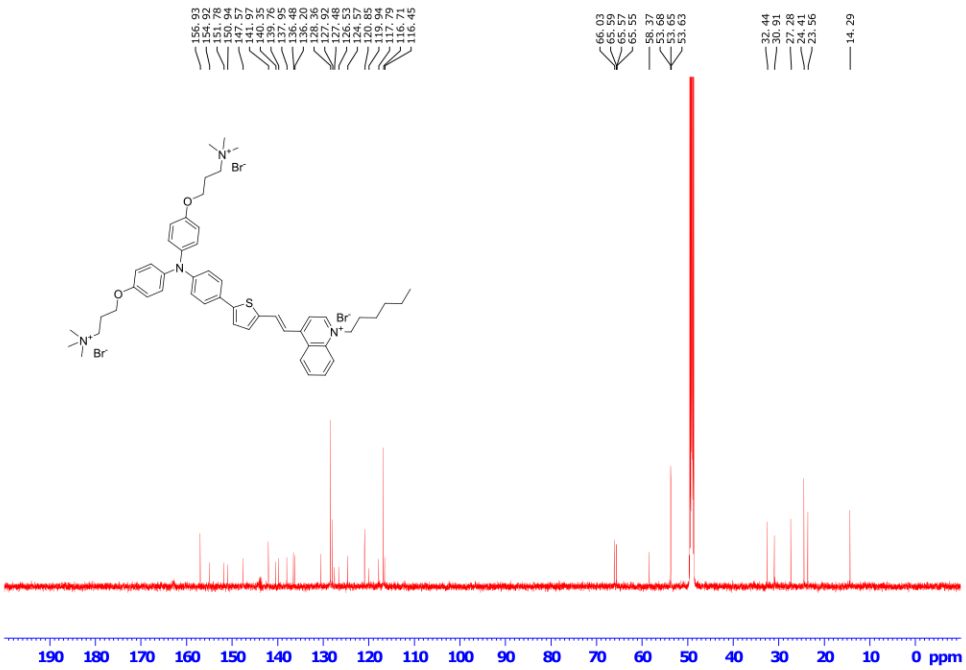

Figure S47. ^{13}C NMR spectrum (151 MHz, CD_3OD) of TPA-C3-C6P.

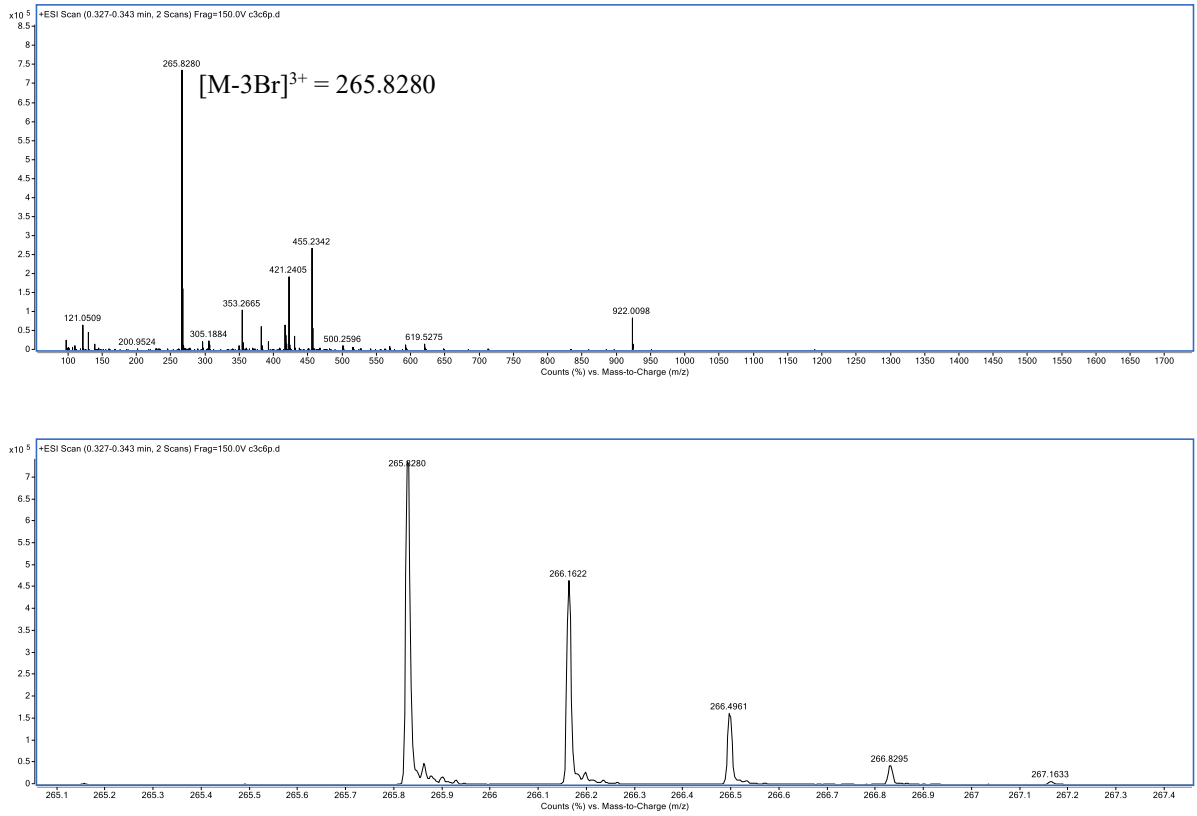

Figure S48. High-resolution mass spectrum (ESI) of TPA-C3-C6P.

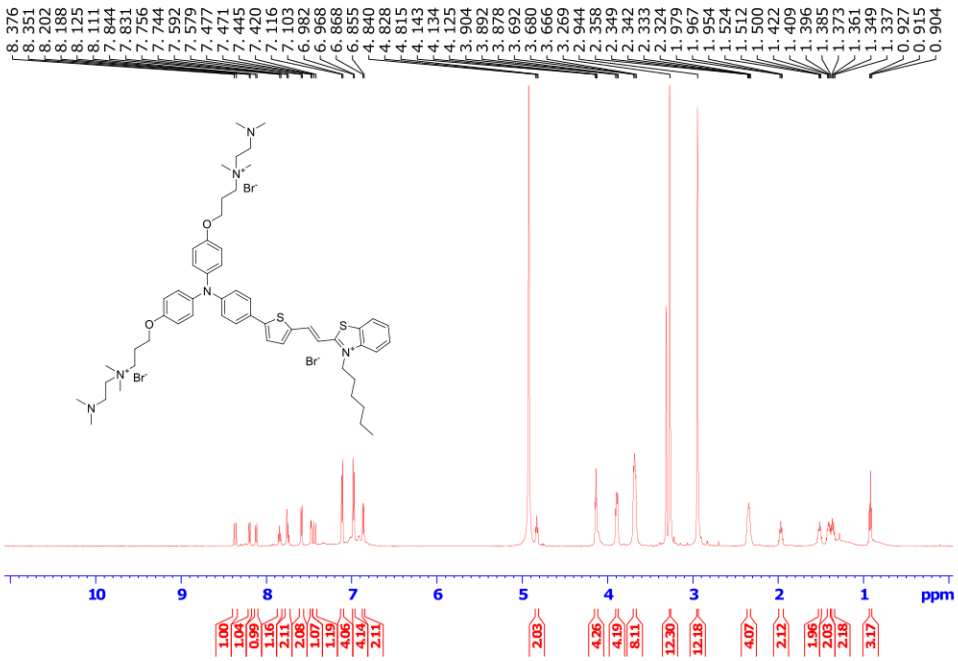

Figure S49. ^{1}H NMR spectrum (600 MHz, CD_3OD) of TPA-N2-C3-C6.

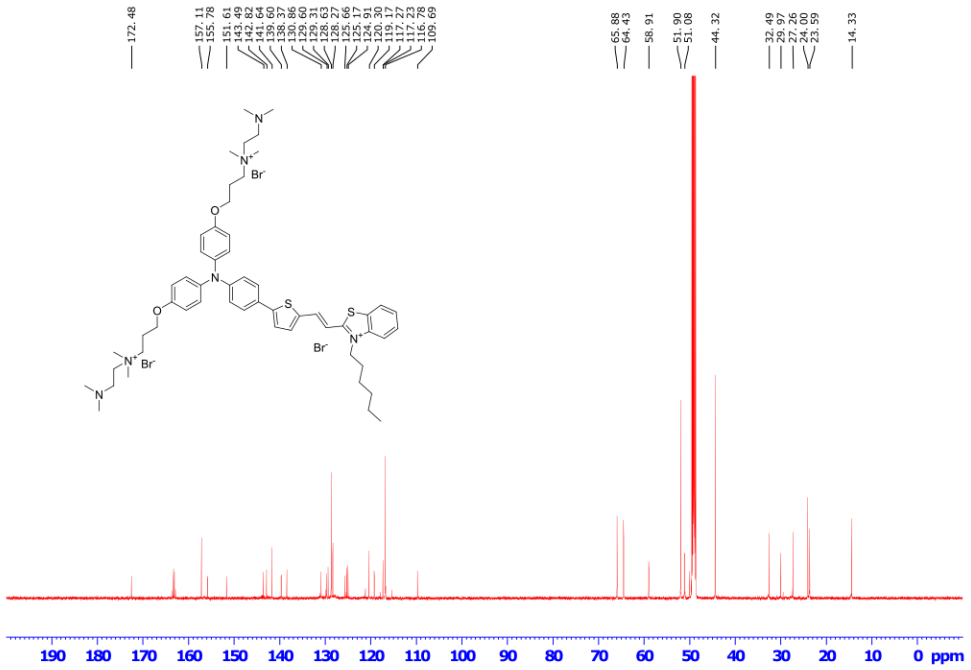

Figure S50. ^{13}C NMR spectrum (151 MHz, CD_3OD) of TPA-N2-C3-C6.

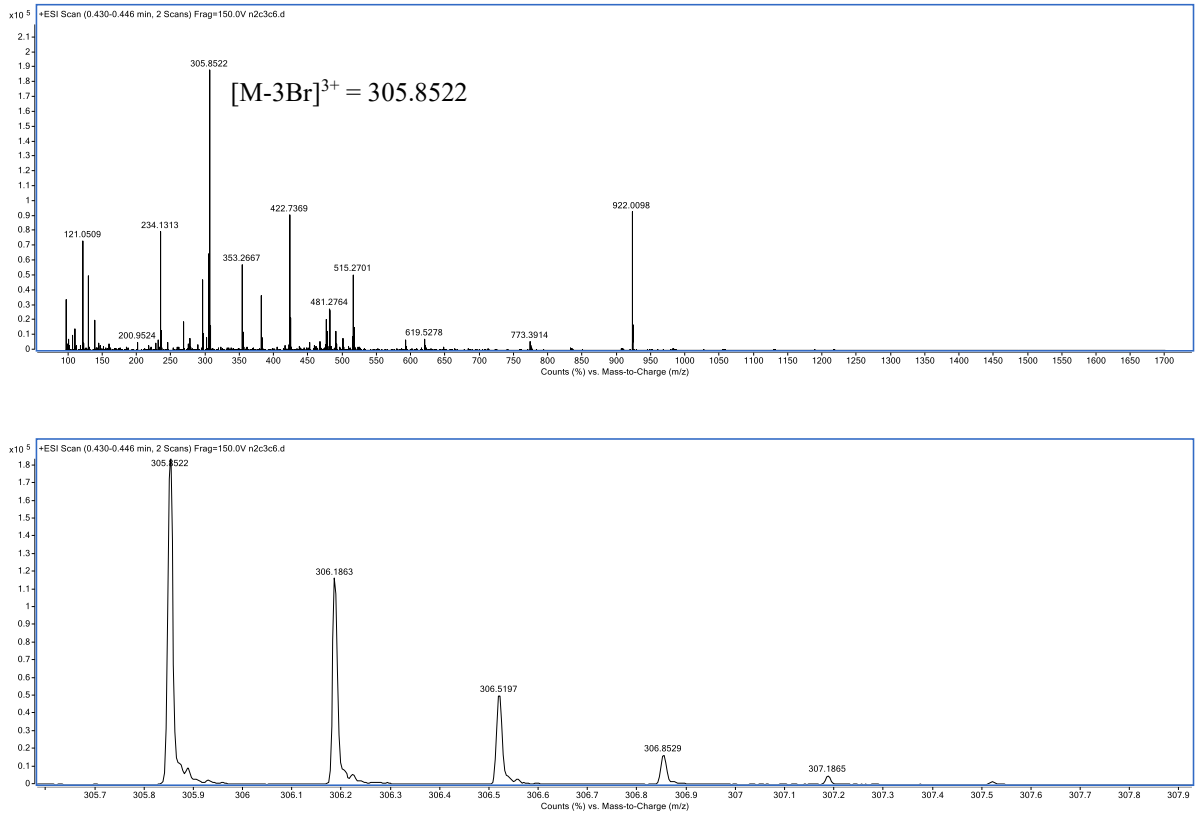

Figure S51. High-resolution mass spectrum (ESI) of TPA-N2-C3-C6.